Title: **Studies of Some Volatile Compounds of Main Group Elements.**

Author: **Simon Aldridge, Jesus College, Oxford.**

Degree: **Doctor of Philosophy.**

Date: **Hilary Term, 1996.**

Abstract:

Methylzinc tetrahydroborate, [$MeZnBH_4$], has been prepared by two routes and the structure of the solid determined by X-ray crystallography to reveal helical polymers in which MeZn and BH_4 units alternate. The latter functions as a bidentate ligand with respect to each of the adjacent metal atoms. Investigation by mass spectrometry and matrix isolation shows that the vapour consists of an equilibrium mixture of monomeric and dimeric species. The pattern of infrared bands for the monomer is characteristic of a bidentate BH_4 group, a finding consistent with the results of DFT calculations. Disproportionation into [Me_2Zn] and [$Zn(BH_4)_2$] is a common feature of the chemistry of methylzinc tetrahydroborate, although it has been possible to isolate and characterize the adduct [$MeZnBH_4{\cdot}SMe_2$].

The reaction between [B_4H_{10}] and [Me_2Zn] in the gas phase affords colourless acicular crystals of [$(MeZn)_2B_3H_7$] in yields of *ca.* 10%. This compound has been characterized by chemical analysis and by NMR and vibrational spectroscopy. X-ray crystallography reveals that the product is a dimer, [$(MeZn)_2B_3H_7]_2$, featuring two distinct zinc environments. Two B_3H_7ZnMe ligands, formally derived from B_3H_8 by replacement of a μ_2-H by a μ_2-ZnMe unit, each function in a *bis*(bidentate) manner linking together two other MeZn centres through pairs of Zn–H–B bridges.

The structures of several aluminium tetrahydroborates in the solid phase have been investigated by X-ray diffraction. The structure of dimethylaluminum tetrahydroborate has been shown to consist of helical polymeric chains in which Me_2Al and BH_4 units alternate. Here, too, the BH_4 groups exhibit bidentate ligation with respect to each of the adjacent metal atoms, although the degree of interaction between the metal centre and the BH_4 group is somewhat less than in [$MeZnBH_4$]. Solid aluminium *tris*(tetrahydroborate) exhibits two phases with a transition temperature in the range 180-195 K. Each phase is made up of discrete $Al(BH_4)_3$ units, the principal differences relating to the packing of the individual molecules. In the α phase the $Al(BH_4)_3$ molecules display an angle of 78.2° between the AlB_3 and $Al(\mu\text{-}H)_2B$ planes and are disposed about a 2_1 crystallographic screw axis; in the β phase the molecular units conform to D_{3h} symmetry.

Dimethylindium octahydrotriborate, [$Me_2InB_3H_8$], has been synthesized by the reaction between trimethylindium and tetraborane(10) and characterized by chemical analysis and by NMR and vibrational spectroscopy. X-ray diffraction of a single crystal reveals that the solid consists of [$Me_2InB_3H_8$] units, although there is evidence of charge separation in the sense $[Me_2In]^+[B_3H_8]^-$ and of secondary interaction between terminal hydrogen atoms and adjacent indium centres. The infrared spectrum of the matrix-isolated vapour is consistent with a monomeric structure similar to that of [$Me_2AlB_3H_8$].

Studies of Some Volatile Compounds of Main Group Elements

A thesis submitted in partial fulfilment of the
requirements for the degree of Doctor of Philosophy

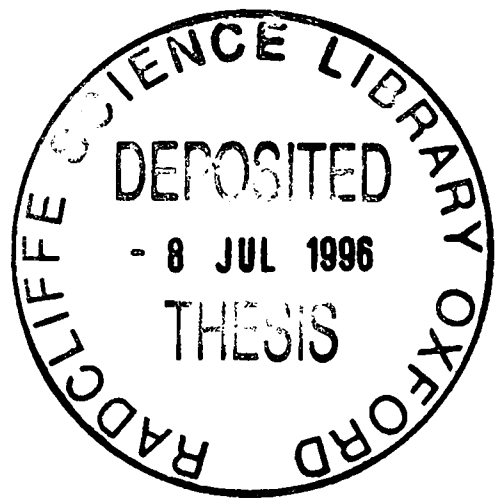

Simon Aldridge

Jesus College, Oxford

Hilary Term, 1996

Acknowledgements

It is with a great deal of thanks that I wish to acknowledge the contributions made by the following people to the work carried out over the last three and a half years.

My supervisor, Dr. Tony Downs, for much helpful advice and encouragement, for his unfailing good humour and for numerous extensive meals, not least with Hampshire County Cricket Club. Many thanks also to Mary for cookery *par excellence* and for never forgetting a birthday.

Drs. Simon Parsons and Sandy Blake for carrying out the crystallography described in this thesis. Special thanks to Simon for perseverance above and beyond the call of duty, for his hospitality in Edinburgh and for much amusement during his time in Oxford.

Matthias Hofmann for carrying out the calculations on the Zn/B systems and Dr. Paul Brain for helping instigate them.

Dr. Tim Greene for never being too busy to help, for many good ideas and for (nominally) sharing a lab with me for the past three and a half years.

Dr. Colin Pulham for carrying out some of the mass spectrometry experiments and for much assistance in earlier years.

Phil Souter for help with the FT-Raman measurements in Southampton, for the odd beer or two (not least in Chamonix and Dublin) and for keeping up the "moral" in T13 and T14.

Dr. Sean McGrady for providing me with the sample of $(CHD_2)_2Zn$ and for his (hopefully) unique sense of humour.

Dr. Nils Metzler for many a helping hand coming to grips with the new NMR machine.

Members of the Downs' Group past and present for their unswerving dedication (to tea at 11 am and 4 pm) and in particular Dean Brown for much amusement and his ever liberal opinions and Drs. Loos and Limberg for their contrasting views on post-doctoral life. Further thanks to Tim, Phil, Sean and Leigh Morris for their help in proof reading this thesis.

Cath, for immeasurable support throughout virtually the entire course of this work, especially when things weren't going so well, and for putting up with untold evenings in the lab.

Notes

1 Torr = 1 mmHg = 133.3 Pa

The following abbreviations are used in the text and in the tabulation of spectra:

Me = $-CH_3$

Et = $-CH_2CH_3$

^{n}Pr = $-CH_2CH_2CH_3$

^{n}Bu = $-CH_2CH_2CH_2CH_3$

^{i}Bu = $-CH_2CH(CH_3)_2$

^{t}Bu = $-C(CH_3)_3$

Ph = $-C_6H_5$

Cp = C_5H_5

Cp* = C_5Me_5

dmpe = $Me_2PCH_2CH_2PMe_2$

tmen = $Me_2NCH_2CH_2NMe_2$

triphos = *tripod* = $MeC(CH_2PPh_2)_3$

tsi = $-C(SiMe_3)_3$

THF = tetrahydrofuran

NMR = nuclear magnetic resonance

IR = infrared

FT = Fourier transform

DFT = density functional theory

SCF = self-consistent field

tz = triple zeta

HF = Hartree-Foch

sv = split valence

ν = stretching mode

δ = deformation mode

ρ = rocking mode

s = symmetric

a = antisymmetric

t = terminal

b = bridging

c = bonded to carbon

RMS = root mean square

s = strong

m = medium

w = weak

br = broad

sh = shoulder

v = very

ν_i = anharmonic frequency

ω_i = harmonic frequency

x_i = anharmonicity constant

NMR spectra are expressed in accordance with the chemical shift convention outlined by IUPAC; *i.e.* a positive chemical shift denotes a positive frequency and *vice versa* with respect to the designated reference substance.

^{1}H NMR spectra are referenced to Me_4Si

^{11}B NMR spectra are referenced to $Et_2O{\cdot}BF_3$

The following representations are used in diagrams:

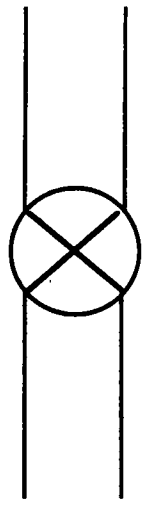

Young's greaseless valve

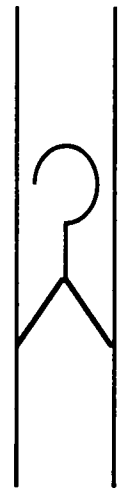

break-seal

constriction

Contents

Chapter One
Introduction

1.1 Preamble

The hydrides of the Group 13 elements have attracted much interest since the pioneering work of Stock during the 1930's.[1] On the other hand, compounds in which a metal atom is directly bonded to a boron hydride group were first synthesized as late as the 1960's.[2-7] Both types of compound have subsequently had a major influence on theories of structure and bonding,[8-12] ideas such as multi-centre bonding being formulated initially to explain the electron deficiency of molecules such as B_2H_6 and B_4H_{10}.[9] More recently, the electron-counting "rules" which govern cluster chemistry, collectively known as "Polyhedral Skeleton Electron Pair Theory", have been formulated in order to explain structure and bonding in metallaborane and metallacarborane cluster compounds.[10,11,13-21] Metal-containing clusters have also attracted a great deal of interest as a result of a growing mass of evidence supporting their use as catalysts and reaction centres in both industrial and biochemical systems. The use of boron hydrides and carboranes and of their metal derivatives as precursors or intermediates in the synthesis of larger molecules has provided unique access to the study of metals in clusters.[3,7]

The original research described in this thesis was concerned with the synthesis, manipulation, and structural, spectroscopic and chemical characterization of compounds in which a metal atom is covalently bound to a tetrahydroborate group or to a boron hydride fragment containing three boron atoms. The following four sections of this chapter give brief outlines of the chemistry relevant to the present studies, while the final section introduces the aims of the research.

1.2 Tetrahydroborate Derivatives

Several detailed reviews of compounds containing the tetrahydroborate group

already exist,[6,22,23] and only a brief overview of the chemistry relevant to the current investigations will be presented here. In addition, a discussion of relevant spectroscopic properties of tetrahydroborate derivatives can be found in Sections 2.2.1 and 2.2.2.

1.2.1 Occurrence and Synthesis of Tetrahydroborate Derivatives

The tetrahydroborate ion, BH_4^-, is the simplest known anionic boron hydride and numerous metallic elements have been shown to form tetrahydroborate derivatives.[6,22,23] The stability of such compounds is dependent, crucially, upon the electronegativity of the metal, M; those elements with electronegativities greater than that of boron do not, as a rule, form tetrahydroborates but compete instead for the hydride ion to form an M–H bond and diborane. Thus, for example, relatively few tetrahydroborates of the more electronegative metals, such as nickel and copper, are known, and these are stable under normal conditions only when the electronegativity of the metal is reduced by coordination to a soft ligand such as triphenylphosphine.[24] The oxidizing power of the metal also has considerable bearing on the stability of the tetrahydroborate derivative. Thus, for example, the reaction of $[Cp_2HfCl_2]$ with $[LiBH_4]$ generates $[Cp_2Hf(BH_4)_2]$,[25] whereas the analogous reaction with $[Cp_2TiCl_2]$ yields the titanium(III) compound $[Cp_2Ti(BH_4)]$.[26]

Tetrahydroborate derivatives range from the essentially ionic structures containing more-or-less discrete BH_4^- ions formed by the metals of Groups 1 and 2, through the vast range of transition-metal derivatives, in which a variety of modes of coordination is in evidence, to the more covalent derivatives of aluminium and the post-transition metals. Within this last category known compounds are confined to the Group 12 metals zinc and cadmium and the Group 13 metals aluminium, gallium, indium and thallium.

There are three commonly used preparative routes to tetrahydroborate derivatives.

(i) Reaction of a metal halide with an alkali-metal tetrahydroborate, as exemplified by reaction (1), for which the principal thermodynamic driving force is the formation of

$$ZrCl_4 + 4LiBH_4 \longrightarrow Zr(BH_4)_4 + 4LiCl \qquad (1)$$

the alkali metal halide.[27]

(ii) Reaction of the methyl derivative of a metal with the easily synthesized aluminium *tris*(tetrahydroborate), $Al(BH_4)_3$, *e.g.*[28,29]

$$Me_6Al_2 + Al(BH_4)_3 \longrightarrow 3Me_2Al(BH_4) \quad (2)$$

$$Me_6Al_2 + 4Al(BH_4)_3 \longrightarrow 6MeAl(BH_4)_2 \quad (3)$$

(iii) Reaction of diborane with a suitable substrate, frequently an alkyl or alkoxy derivative of the metal, *e.g.*[30]

$$Me_3M + B_2H_6 \longrightarrow Me_2MBH_4 + 1/2[MeBH_2]_2 \ (M = Ga \text{ or } In) \quad (4)$$

1.2.2 Coordination of the Tetrahydroborate Group

The most notable feature of the tetrahydroborate ligand is the variety of its mode of coordination to a metal centre. In addition to the unique "side-on" mode of coordination exhibited by two of the BH_4 groups in $[Ti(BH_4)_3(PMe_3)_2]$[31] at least four such modes of coordination have been clearly established for a mononuclear complex.[6] These are shown in Figure 1.1.

The ionic form (type **I**) is essentially confined to the tetrahydroborates of the Group 1 and 2 metals and a few of the post-transition metals. Some of these compounds find extensive use as hydride-transfer and reducing agents, as well as in the synthesis of the more overtly molecular tetrahydroborates of types **II, III** and **IV**.[23]

The copper complexes, $[(Ph_2PMe)_3CuBH_4]$[32] and $[(triphos)CuBH_4]$,[33] the vanadium complex $[(dmpe)_2V(BH_4)]$,[34] and the anion $[H_3B{-}H{-}BH_3]^-$ [35] are the only species for which monodentate coordination has been convincingly established. In $[(triphos)CuBH_4]$ the Cu–H–B angle is significantly bent [121(3)°], with the implication that either the boron atom or a second bridging hydrogen atom is involved to some extent in bonding to the metal centre.[33] Interestingly, the complex $[(Ph_2PMe)_3CuBH_4]$ loses a phosphine ligand in benzene solution, forming $[(Ph_2PMe)_2CuBH_4]$ in which the BH_4

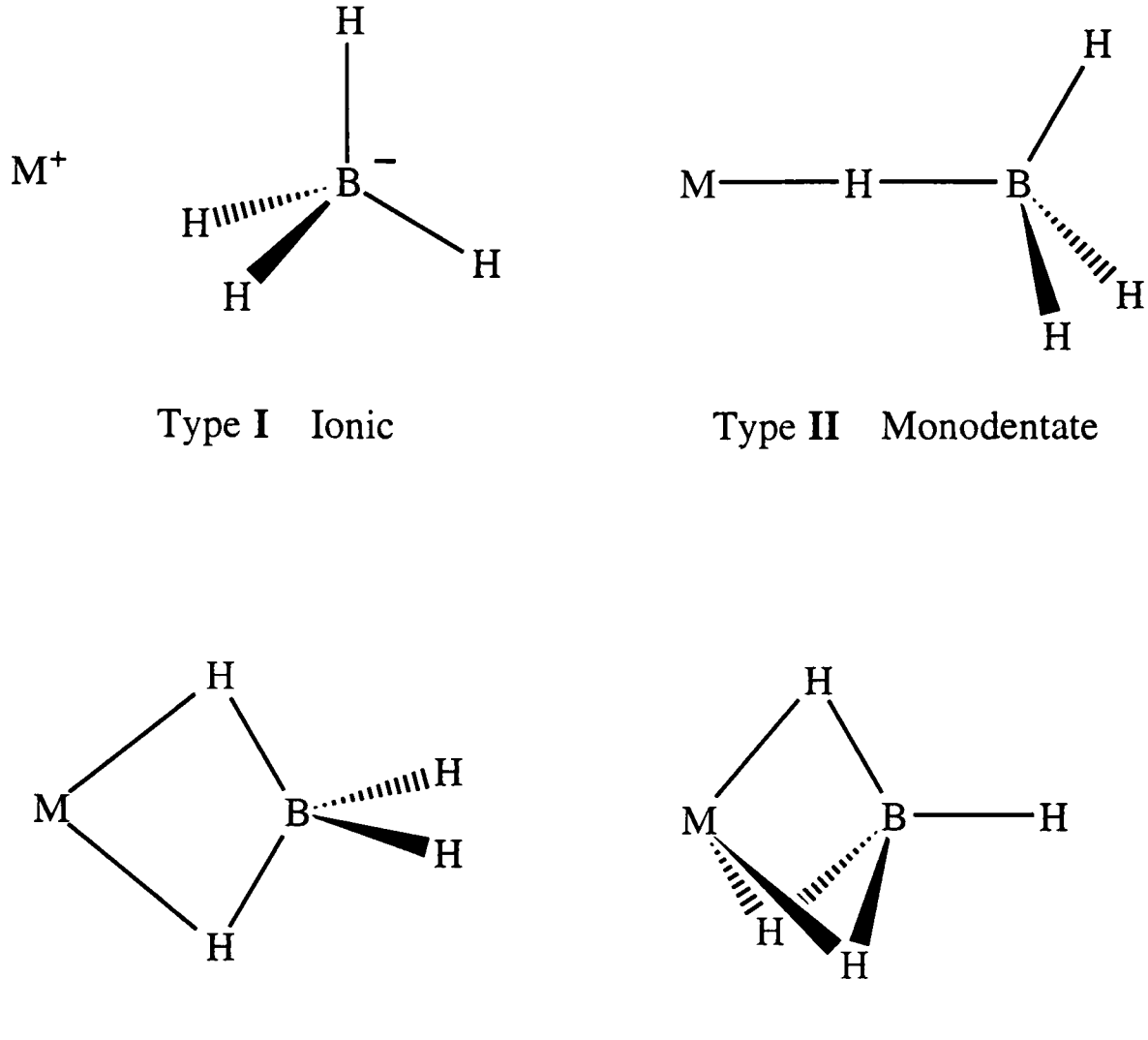

Type **I** Ionic

Type **II** Monodentate

Type **III** Bidentate

Type **IV** Tridentate

Figure 1.1 Modes of coordination of the tetrahydroborate group.

ligand is bidentate.[24]

Much more in evidence than monodentate BH_4 groups are bidentate and tridentate groups (types **III** and **IV**), with the bidentate unit being the more commonly encountered; tridentate ligation is found chiefly in association with the early transition metals, the lanthanides and the actinides.

Furthermore, the mode of coordination of the tetrahydroborate group to a given metal centre is not necessarily constant. This has two important consequences.

(i) The mode of binding of the BH_4 group may vary between different phases of the same compound. Thus, for example both $[Be(BH_4)_2]$[36,37] and $[U(BH_4)_4]$[38,39] have been shown to adopt monomeric structures in the vapour containing terminal B–H linkages, but are known to form polymeric structures in the solid phase in which the hitherto uncoordinated hydrogen atoms of some of the BH_4 groups interact with adjacent metal centres forming intermolecular bridges and increasing the coordination number of

these centres.

(ii) The differences in energy between various modes of coordination of the tetrahydroborate group are small {*e.g.* 9.1 kJ mol^{-1} between bidentate and tridentate ligation of a single BH_4 group in $[Al(BH_4)_3]$[40]}. Consequently, there has been much interest in the dynamic properties of tetrahydroborate ligands, particularly in relation to their NMR spectra and the temperature dependence of these spectra. For most tetrahydroborates, it has been found that all the hydrogen atoms in the BH_4 group are magnetically equivalent regardless of the mode of coordination.[6,41] Only in the case of $[Cp_2V(BH_4)]$[42] and complexes of the type $[MH_2(BH_4)L_2]$ (M = Ir or Rh; L = bulky tertiary phosphine)[43] has the motion interconverting terminal and bridging hydrogens been slowed sufficiently to enable distinct signals corresponding to the two sites to be observed at low temperatures.

The mode of coordination of the BH_4 group has been shown to depend on both steric and electronic factors.[44,45] In cases where electronic factors take precedence, monodentate, bidentate or tridentate coordination is favoured when the vacant symmetry-matched orbitals of appropriate energy on the metal number one, two or three, respectively. Where steric effects predominate, as for example in the case of the partially ionic tetrahydroborates of the lanthanide elements, tridentate ligation may well give way to bidentate ligation in order to reduce the degree of steric congestion at the metal centre.[46]

A summary of the structural features of a number of tetrahydroborate derivatives can be found in Table 1.1.

1.2.3 Chemical Properties of Tetrahydroborates

The chemistry of metal tetrahydroborate derivatives is dominated by three factors.

(i) *The hydridic nature of the hydrogen atoms*, hydrogen being more electronegative than boron or any metal.[47] Consequently, tetrahydroborates find

Table 1.1 Structural details of selected tetrahydroborate derivatives.

Compound	Phase	Structural method[a]	Nature of BH_4 group; other features	Ref.
KBH_4	solid	neutron	Ionic; K···B distance 3.36 Å; f.c.c. lattice	48
$(dmpe)_2V(BH_4)_2$	solid	X-ray	Monodentate; V–H–B angle of 140(3)°	34
$(triphos)CuBH_4$	solid	X-ray	Monodentate; Cu–H–B angle of 121(3)°	33
$(Ph_2PMe)_3CuBH_4$	solid	X-ray	Monodentate; Cu–H–B angle of 170°	32
$Al(BH_4)_3$	vapour	electron	Bidentate; planar AlB_3 unit; D_3 or D_{3h} symmetry	49
Me_2AlBH_4	vapour	electron	Bidentate; C_{2v} symmetry; *tetra*-coordinated aluminium	50
H_2GaBH_4	vapour	electron	Bidentate; C_{2v} symmetry; *tetra*-coordinated gallium	51
	solid	X-ray	Bidentate; contains $Ga(\mu\text{-}H)B(H)_2(\mu\text{-}H)Ga$ units linked to give an infinite chain	52
$MeAl(BH_4)_2$	vapour	electron	Bidentate; *penta*-coordinated aluminium; planar $CAlB_2$ unit	53
$HGa(BH_4)_2$	vapour	electron	Bidentate; *penta*-coordinate gallium; C_{2v} symmetry	54
$(tmen)Zn(Cl)BH_4$	solid	X-ray	Bidentate; monomeric; *penta*-coordinated zinc	55
$Be(BH_4)_2$	solid	X-ray	Helical polymer containing alternate $[BeBH_4]^+$ and $[BH_4]^-$ ions	36
$U(BH_4)_4$	vapour	electron	Monomeric; tridentate	39
	solid	neutron	Polymeric; two tridentate; two bridging bidentate	38
$Zr(BH_4)_4$	vapour	electron	Monomeric; tridentate; overall T_d symmetry	56
	solid	X-ray	Molecular; tridentate; overall T_d symmetry	57
$Ti(BH_4)_3$	vapour	electron	Tridentate; planar TiB_3 unit; C_{3h} symmetry	58
$Ti(BH_4)_3(PMe_3)_2$	solid	X-ray	One tridentate; two distorted side-on BH_4 groups	31
$(Cp^*Ir)_2H_3BH_4$	solid	X-ray	Bidentate; contains $Ir(\mu\text{-}H)B(H)_2(\mu\text{-}H)Ir$ units	59
$[R_2(H)_2Ru_2BH_4]^{+b}$	solid	X-ray	Bidentate; contains distorted $Ru(\mu\text{-}H)_2B(\mu\text{-}H)_2Ru$ unit	60
$[(Ph_3P)_4Cu_2BH_4]^+$	solid	X-ray	Bidentate; contains $Cu(\mu\text{-}H)_2B(\mu\text{-}H)_2Cu$ unit	61

[a] Neutron = neutron diffraction; X-ray = X-ray diffraction; electron = electron diffraction.
[b] R = *tripod* = $MeC(CH_2PPh_2)_3$.

widespread use as hydride transfer reagents [see reaction (5)[62]] and react vigorously with protonic acids [*e.g.* reaction (6)[63]].

$$2Al(BH_4)_3 + 6Me_3SiCl \longrightarrow 2AlCl_3 + 6Me_3SiH + 3B_2H_6 \quad (5)$$

$$2Al(BH_4)_3 + 6HCl \longrightarrow 2AlCl_3 + 6H_2 + 3B_2H_6 \quad (6)$$

(ii) *The electron deficient nature of such compounds.* As a result, adduct-formation, in which the metal tetrahydroborate functions as a Lewis acid, is a common feature, as exemplified by the addition reactions (7)[64] and (8)[65,66] and the displacement reaction (9).[67,68]

$$Al(BH_4)_3 + Me_3N \longrightarrow Me_3N{\cdot}Al(BH_4)_3 \quad (7)$$

$$Al(BH_4)_3 + LiBH_4 \longrightarrow Li[Al(BH_4)_4] \quad (8)$$

$$HGa(BH_4)_2 + CO \longrightarrow H_2GaBH_4 + H_3B{\cdot}CO \quad (9)$$

(iii) *The polarizability of the tetrahydroborate ion* which is calculated to be similar to that of the bromide ion.[69] On this basis, it would be expected that BH_4^- is displaced relatively easily from the coordination sphere of the metal. This is illustrated by the following ligand replacement, exchange and metathesis reactions [reactions (10),[70-72] (11)[28,29] and (12),[73] respectively].

$$Al(BH_4)_3 + 6NH_3 \longrightarrow [Al(NH_3)_6]^{3+}[BH_4]^-_3 \quad (10)$$

$$Al(BH_4)_3 + Me_6Al_2 \longrightarrow 3Me_2AlBH_4 \quad (11)$$

$$2Al(BH_4)_3 + 6EtLi \longrightarrow 6LiBH_4 + Et_6Al_2 \quad (12)$$

1.2.4 Catalytic Activity of Tetrahydroborates

Considerable experimental evidence has been amassed for the action of metal tetrahydroborates as effective catalysts in the polymerization, oligomerization,

isomerization and hydrogenation reactions of olefins.[74-78] Examples of both heterogeneous and homogeneous catalysis have been investigated. In the case of the oligomerization of 1,3-butadiene by $[Ni(H)(BH_4)(PR_3)_2]$, the initial step of the reaction mechanism is thought to involve elimination of $[H_3B{\cdot}PR_3]$, thereby facilitating complexation of the butadiene molecule.[79] Subsequent reductive elimination of dihydrogen frees a coordination site on the metal for a second molecule of butadiene. The rôle of the tetrahydroborate ligand in other catalytic processes is less clear, although the following possibilities have been suggested:[6]

(i) reduction of the metal to a lower oxidation state;

(ii) providing a source of hydrogen (forming, in effect, a metal hydride);

(iii) providing a means (by altering its denticity) through which the coordination sphere of the metal can be varied; and

(iv) functioning as a ligand which activates others in the coordination sphere of the metal.

1.2.5 Tetrahydroborates of Zinc and Cadmium

In their paper describing zinc dihydride, Schlesinger *et al.* noted that diborane is absorbed by a suspension of zinc dihydride in diethyl ether, resulting in the formation of a clear solution.[80] Removal of the ether left a solid residue which was shown by elemental analysis to have the composition $Zn(BH_4)_2$. Further studies by Wiberg and Henle showed that the reaction of two equivalents of lithium or potassium tetrahydroborate with zinc dichloride [reaction (13)] also generates $[Zn(BH_4)_2]$.[81] Furthermore, the reaction of zinc

$$ZnCl_2 + 2MBH_4 \longrightarrow Zn(BH_4)_2 + 2MCl \quad (M = Li \text{ or } Na) \qquad (13)$$

dichloride with a single equivalent of lithium tetrahydroborate was found to yield a solid which decomposed at *ca.* 120°C; analysis suggested that this was chlorozinc tetrahydroborate.[81] Subsequent reports by Russian workers implied that the complex tetra-

hydroborate $Na[Zn(BH_4)_3]\cdot OEt_2$ decomposes at 80°C to yield $[Zn(BH_4)_2]$,[82] although this reaction temperature exceeds the one reported earlier as the upper limit of stability of the *bis*(tetrahydroborate) (50°C).[83]

Research by Nöth and co-workers established that several anionic zinc tetrahydroborates can be synthesized *via* the reaction of zinc dichloride or zinc *bis*(tetrahydroborate) with appropriate quantities of $[LiBH_4]$ or $[NaBH_4]$ in ether or THF.[84] These include $[LiZn(BH_4)_3]$, $[NaZn(BH_4)_3]$ and $[Li_2Zn(BH_4)_2]$, reaction (14) representing a typical synthesis. The sodium compound can also be prepared by the

$$ZnCl_2 + 3LiBH_4 \longrightarrow LiZn(BH_4)_3 + 2LiCl \qquad (14)$$

reaction of diborane with $[NaZn(OMe)_3]$ or $[Na_2Zn(OMe)_4]$.[84] The infrared spectra of these compounds show features consistent with bidentate ligation of the BH_4 groups. Somewhat different products were obtained from the analogous reactions with potassium or barium tetrahydroborates [reactions (15) and (16)[84]].

$$3Zn(BH_4)_2 + 2KBH_4 \longrightarrow K_2Zn_3(BH_4)_8 \qquad (15)$$

$$3Zn(BH_4)_2 + Ba(BH_4)_2 \longrightarrow BaZn_3(BH_4)_8 \qquad (16)$$

Raston and co-workers have recently reported the synthesis of the complex $[(tmen)Zn(Cl)BH_4]$ *via* the reaction of $[(tmen)ZnCl_2]$ with $[LiBH_4]$.[55] The structure of the molecular unit determined by X-ray diffraction of a single crystal again reveals bidentate ligation of the BH_4 group.

Ridley reported in 1965[85] that diborane reacts with an excess of dimethylzinc in a sealed glass vessel to yield a volatile white solid which decomposes upon melting at *ca.* 50°C. Elemental analysis of the compound established that it was methylzinc tetrahydroborate, $[MeZnBH_4]$, formed *via* reaction (17). The compound was observed to

$$B_2H_6 + 2Me_2Zn \longrightarrow MeZnBH_4 + Me_3B + ZnH_2 \qquad (17)$$

become grey after 1-2 days *in vacuo* at room temperature and to react violently with water. Furthermore, it was shown to react with one equivalent of trimethylamine, yielding the complex [$MeZnBH_4 \cdot NMe_3$] which disproportionated according to reaction (18) upon

$$2MeZnBH_4 \cdot NMe_3 \longrightarrow Me_2Zn \cdot NMe_3 + Me_3N \cdot Zn(BH_4)_2 \qquad (18)$$

warming to room temperature.[85] The structure of solid methylzinc tetrahydroborate was investigated by Nibler and Cook who measured the infrared and Raman spectra of thin films of normal and deuteriated isotopomers.[86] The spectra were found to be consistent with a structure based around an "ionic polymer" incorporating alternate $MeZn^+$ and BH_4^- ions, and similar to that of solid beryllium *bis*(tetrahydroborate).[36]

Cadmium *bis*(tetrahydroborate) has been synthesized *via* a number of routes, including the reaction of cadmium dichloride with two equivalents of lithium tetrahydroborate and the reaction of cadmium methoxide with diborane or [$H_3B \cdot THF$] in THF.[87,88] The compound is thermally frail, decomposing into its elements at temperatures as low as -15°C. The presence of a septet in the ^{112}Cd NMR spectrum of a solution of [$Cd(BH_4)_2$] in THF was thought to indicate that each tetrahydroborate group is bonded to the cadmium centre through three bridging hydrogen atoms, although doubts have subsequently been expressed concerning the reliability of these results.[88]

Nöth and co-workers have also synthesized adducts of the type [$L \cdot Cd(BH_4)_2$] (where L = ammonia or pyridine) and [$LiCd(BH_4)_3$], the latter being prepared by the reaction between [$Cd(BH_4)_2$] and [$LiBH_4$] in diglyme solution.[88,89]

1.2.6 Tetrahydroborates of Aluminium, Gallium and Indium

In contrast to the tetrahydroborates of the Group 12 elements, the analogous compounds of aluminium and gallium are much more clearly defined in structural terms. Aluminium *tris*(tetrahydroborate), first synthesized from trimethylaluminium and diborane,[90] but now more commonly prepared from aluminium trichloride and [$LiBH_4$] at

90-100°C,[91] is a colourless, volatile liquid which decomposes slowly *in vacuo* at room temperature and explodes upon exposure to air. Spectroscopic studies indicate bidentate coordination of the BH_4 groups,[92,93] although analysis of the electron-diffraction pattern of the vapour has left open to question the precise molecular geometry.[49]

Thermal decomposition of $[Al(BH_4)_3]$ at 70°C eliminates diborane yielding a hydride derivative thought to be hydridoaluminium *bis*(tetrahydroborate), $[HAl(BH_4)_2]$.[94] This compound also formed by the reaction of $[Al(BH_4)_3]$ with [CO] [reaction (19)], is

$$Al(BH_4)_3 + CO \longrightarrow 1/n[HAl(BH_4)_2]_n + H_3B{\cdot}CO \qquad (19)$$

a viscous, involatile liquid incorporating oligomeric species linked, it appears, through bridging Al–H–Al units.[95,96]

The methylaluminium tetrahydroborates, $[Me_2AlBH_4]$ and $[MeAl(BH_4)_2]$ have been prepared by exchange between aluminium *tris*(tetrahydroborate) and trimethyl-aluminium in the appropriate proportions, according to reaction (20).[28,29] Both are

$$(6\text{-}2n)Al(BH_4)_3 + nMe_6Al_2 \longrightarrow 6Me_nAl(BH_4)_{3-n} \qquad (20)$$

colourless, volatile liquids and are monomeric in the gas phase. Structures have been determined for the gaseous molecules by electron diffraction; the BH_4 groups are found to exhibit bidentate ligation, the coordination numbers of the aluminium centre being four and five, respectively.[50,53] The vibrational spectra of both compounds hint at considerable structural change accompanying the transition from the vapour to the solid phase; solid $[Me_2AlBH_4]$ is thought to have a semi-ionic structure akin to that of $[Be(BH_4)_2]$.[36]

In contrast to the analogous reaction with aluminium trichloride, interaction of gallium trichloride with three equivalents of $[LiBH_4]$ yields not the expected gallium *tris*(tetrahydroborate), but hydridogallium *bis*(tetrahydroborate), $[HGa(BH_4)_2]$.[28,67,68] Unlike $[HAl(BH_4)_2]$, this is a thermally fragile, volatile material which has been shown by its mass and infrared spectra and electron-diffraction pattern to exist as a monomer in the

vapour phase, with the molecule incorporating *penta*-coordinated gallium and bidentate BH_4 groups to achieve overall C_{2v} symmetry.[54] NMR studies indicate the presence in solution of a second species, probably an oligomer of the type $[HGa(BH_4)_2]_n$.[67,68]

The compounds $[Me_2GaBH_4]$,[28,97] $[MeGa(BH_4)_2]$[98] and $[H_2GaBH_4]$[51] have all been synthesized recently from the corresponding chloride and $LiBH_4$, according to reactions (21)-(23), although Me_2GaBH_4 was originally synthesized from trimethyl-

$$1/2[Me_2GaCl]_2 + LiBH_4 \longrightarrow Me_2GaBH_4 + LiCl \quad (21)$$

$$1/2[MeGaCl_2]_2 + 2LiBH_4 \longrightarrow MeGa(BH_4)_2 + 2LiCl \quad (22)$$

$$1/2[H_2GaCl]_2 + LiBH_4 \longrightarrow H_2GaBH_4 + LiCl \quad (23)$$

gallium and diborane [reaction (24)].[30] All are volatile, thermally fragile materials; the

$$Me_3Ga + B_2H_6 \longrightarrow Me_2GaBH_4 + 1/2[MeBH_2]_2 \quad (24)$$

electron-diffraction patterns of $[Me_2GaBH_4]$[50] and $[H_2GaBH_4]$[51] in the vapour phase have each been shown to be consistent with a monomeric species possessing a diborane-like structure, $R_2Ga(\mu\text{-}H)_2BH_2$ (R = H or Me), and conforming to C_{2v} symmetry. Very recent work has shown that the structure of solid $[H_2GaBH_4]$ is based around a polymeric chain of alternate GaH_2^+ and BH_4^- ions.[52] Each BH_4 unit is linked *via* a single bridging hydrogen atom to two adjacent GaH_2 groups and thereby retains two *terminal* B–H bonds.

Reports of indium tetrahydroborates are largely confined to the preparation of the unstable adduct $[In(BH_4)_3{\cdot}THF]$ by the reaction of trimethylindium with diborane in THF solution, and to ill-characterized products derived from the reaction of indium trichloride with $[LiBH_4]$.[99] The reaction between trimethylindium and diborane under solvent-free conditions at ambient temperatures gives a white crystalline solid, $[Me_2InBH_4]$ which has been characterized by elemental analysis and by its vibrational and NMR spectra.[100] As

$$Me_3In + B_2H_6 \longrightarrow Me_2InBH_4 + 1/2[MeBH_2]_2 \quad (25)$$

with the analogous gallium compound,[97] the infrared spectrum of the matrix-isolated molecule is consistent with the structure $Me_2In(\mu\text{-}H)_2BH_2$, although the vibrational spectra of the solid indicate significant charge separation in the sense, $[Me_2In]^+[BH_4]^-$, consistent with the low vapour pressure of the compound.[100]

1.3 Octahydrotriborate Derivatives

Several comprehensive reviews detailing the chemistry and structures of compounds containing the octahydrotriborate group already exist,[3,4,101] and only a brief discussion of the chemistry relevant to the current investigations will be presented here. In addition, apposite spectroscopic properties of octahydrotriborate derivatives are discussed in Sections 2.2.1 and 2.2.2.

1.3.1 Occurrence and Synthesis of Octahydrotriborate Derivatives

Compounds containing the octahydrotriborate ion, $B_3H_8^-$, have been investigated not only because of their potential relevance as precursors in the synthesis of metallaborane and metallacarborane clusters,[3] but also in view of the comparisons they afford with the corresponding tetrahydroborate derivatives. In contrast to the tendency of some tetrahydroborates to polymerize in the solid state, octahydrotriborate derivatives generally persist as molecular species in the condensed phases and are therefore usually relatively volatile. Hence, for example, solid $[Be(B_3H_8)_2]$ contains discrete molecules of C_2 symmetry,[102] whereas $[Be(BH_4)_2]$ consists of helical polymers in the solid state.[36]

The first triborane species to be synthesized and characterized was $[NaB_3H_8]$, formed by the direct reaction of diborane with sodium amalgam in the presence of ether [reaction (26)].[1,103] A more recent synthesis of $[NaB_3H_8]$ involves the oxidation of

$$2Na/Hg + 2B_2H_6 \longrightarrow NaB_3H_8 + NaBH_4 + 2Hg \qquad (26)$$

[$NaBH_4$] with iodine, as set out in reaction (27).[104] The first step of this reaction is

$$3NaBH_4 + I_2 \longrightarrow NaB_3H_8 + 2H_2 + 2NaI \qquad (27)$$

thought to involve oxidation of BH_4^- to [B_2H_6], with $B_3H_8^-$ being generated by the subsequent reaction of [B_2H_6] with a second BH_4^- ion.[4] Indeed, [NaB_3H_8] can also be prepared on a large scale by the reaction of [$NaBH_4$] with [B_2H_6].[105-107]

Octahydrotriborates of the pre-transition metals are, like the corresponding tetrahydroborate derivatives, white, thermally stable salts containing more-or-less discrete $B_3H_8^-$ anions. Octahydrotriborates have also been synthesized for many of the transition and post-transition metals, typically *via* metathesis reactions involving the corresponding metal halide complex and the $B_3H_8^-$ anion, usually in the form of the caesium, thallium(I) or a tetraalkylammonium salt. The synthesis of dimethylaluminium octahydrotriborate [reaction (28)] is typical.[108] As with the corresponding tetrahydroborate derivatives,

$$Me_2AlCl + [^nBu_4N][B_3H_8] \longrightarrow Me_2AlB_3H_8 + [^nBu_4N]Cl \qquad (28)$$

simultaneous reduction of the metal centre may occur; for example, the reaction of [Cp_2TiCl_2] with CsB_3H_8, yields the titanium(III) derivative, [$Cp_2Ti(B_3H_8)$].[109]

The only other synthetic route to an octahydrotriborate derivative to be reported is exemplified by the reaction of aluminium *tris*(tetrahydroborate) with tetraborane(10); this is described as yielding [$Al(BH_4)_2(B_3H_8)$], together with diborane and hydrogen.[110]

1.3.2 Structures of Octahydrotriborate Derivatives

A summary of the structural features of a number of octahydrotriborate derivatives can be found in Table 1.2.

The structure of the $B_3H_8^-$ anion was determined by an X-ray diffraction study of the crystalline solid [$(H_3N)_2BH_2$][B_3H_8].[111] The structure, reproduced in Figure 1.2, conforms to the ~~2103~~ 2013 structure predicted from theoretical calculations,[112] the bridging

Table 1.2 Structural details of selected compounds containing the octahydrotriborate group.

Compound	Phase	Structural method[a]	Mode of coordination of the B_3H_8 group	Ref.
$[(H_3N)_2BH_2][B_3H_8]$	solid	X-ray	Ionic; orthorhombic; anion shown in Figure 1.2	111
$Be(B_3H_8)_2$	solid	X-ray	Bidentate; molecular; C_2 symmetry; *tetra*-coordinated beryllium	102
$Me_2AlB_3H_8$	vapour	electron	Bidentate; monomeric; overall C_s symmetry	113
$Me_2GaB_3H_8$	vapour	electron	Bidentate; monomeric; overall C_s symmetry	113
$H_2GaB_3H_8$	vapour	electron	Bidentate; monomeric; overall C_s symmetry	114
B_4H_{10}	vapour	electron, microwave	Effectively bidentate B_3H_8; molecular; *arachno* structure of C_{2v} symmetry	115
	solid	X-ray	Effectively bidentate B_3H_8; molecular	116
$(Ph_3P)_2CuB_3H_8$	solid	X-ray	Bidentate; molecular; *tetra*-coordinated copper	117
$[Me_4N][(OC)_4CrB_3H_8]$	solid	X-ray	Discrete $[Me_4N]^+$ and $[(OC)_4CrB_3H_8]^-$ ions; bidentate B_3H_8; approx. octahedral chromium environment	118
$(OC)_3MnB_3H_8$	solid	X-ray	Tridentate; molecular; overall C_s symmetry; approx. octahedral manganese environment (Figure 1.3)	119
$(OC)_6Mn_2(\mu\text{-}Br)B_3H_8$	solid	X-ray	*Bis*(bidentate); molecular; B_3H_8 ligand bridges two metal centres in "side-on" fashion; approx. octahedral manganese environment (Figure 1.3)	120

[a] X-ray = X-ray diffraction of a single crystal; electron = electron diffraction of the vapour; microwave = microwave spectroscopy of the gaseous molecule.

hydrogen atoms lying significantly closer to the two basal boron atoms than to the apical boron atom.

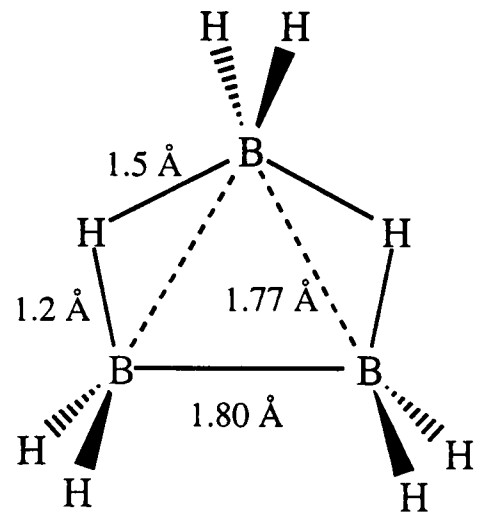

Figure 1.2 The structure of the $B_3H_8^-$ anion as determined by an X-ray diffraction study of crystalline $[(H_3N)_2BH_2][B_3H_8]$.

For the more covalently bound octahydrotriborate derivatives, three different modes of coordination have been established. The vast majority of structurally characterized compounds incorporate bidentate ligation of the B_3H_8 group, in which one of the hydrogen atoms attached to each of the two basal borons is involved in bonding to the metal centre. The resulting *arachno* four-vertex metallaborane is related to tetraborane(10) by replacement of one of the apical BH_2 units by the metal fragment.

Two further modes of coordination have been ascertained for the manganese compounds $[(OC)_3Mn(B_3H_8)]$[119] and $[(OC)_6Mn_2(\mu\text{-}Br)(B_3H_8)]$.[120] The molecular structures of these are illustrated in Figure 1.3. In the former compound involvement in bonding to the metal of one of the hydrogen atoms attached to the apical boron results in the only known example of a tridentate B_3H_8 group. This compound may be regarded as a *nido* four-vertex metallaborane species. In $[(OC)_6Mn_2(\mu\text{-}Br)(B_3H_8)]$ all four hydrogen atoms attached to the basal borons are involved in bonding, enabling the B_3H_8 ligand to bridge two manganese centres in a unique fashion.

No examples of monodentate coordination of the octahydrotriborate ligand have yet been reported.

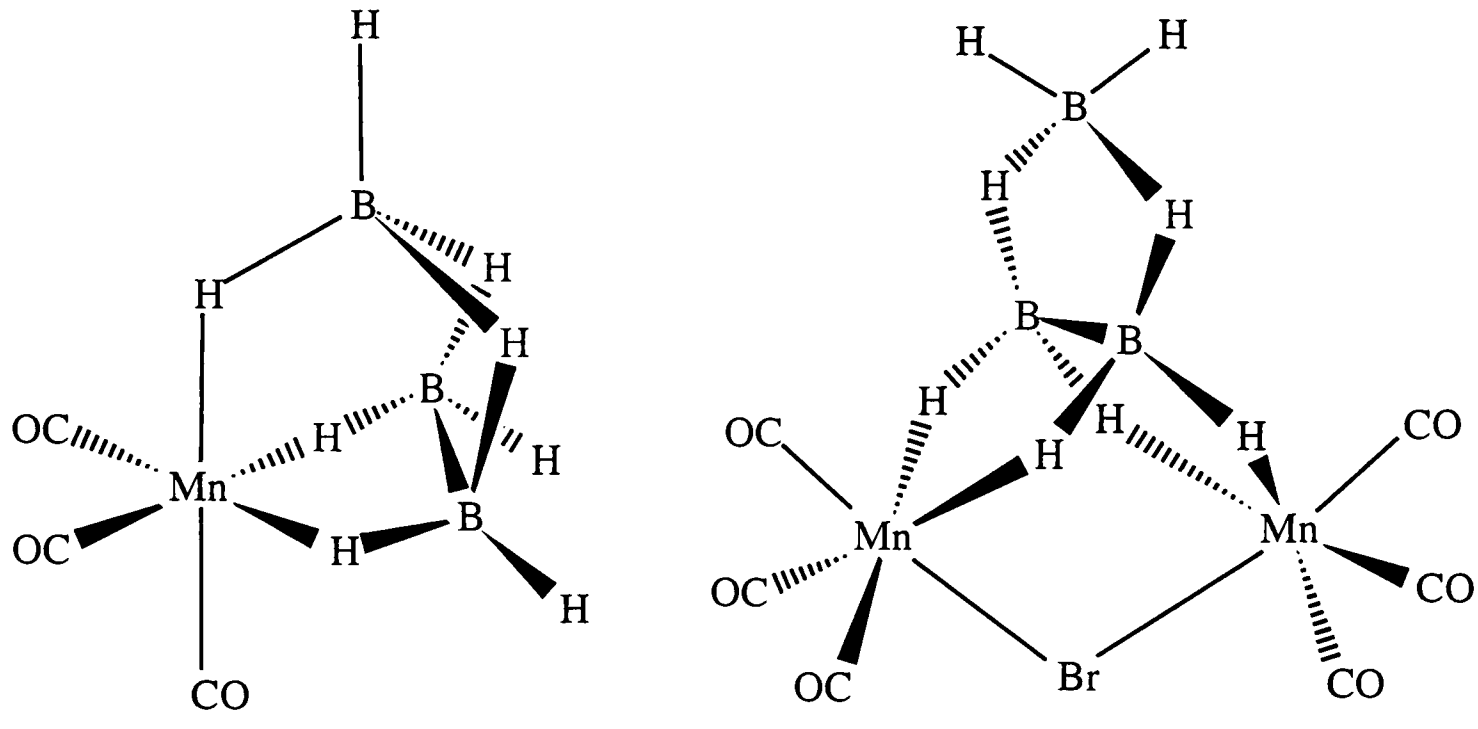

Figure 1.3 The molecular structures of $[(OC)_3Mn(B_3H_8)]$ and $[(OC)_6Mn_2(\mu\text{-}Br)(B_3H_8)]$.

1.4 Larger Metallaborane Derivatives

The chemistry and structure of metallaboranes have excited much interest since initial work carried out during the 1960's and have been the subject of several comprehensive review articles.[2,3,7] It is appropriate therefore to present here only a brief outline of some metallaborane chemistry relevant to the current investigations. In addition to probing general questions concerning the systematic synthesis and catalytic activity of clusters, much of the interest in larger metallaborane derivatives stems from investigating how far the patterns of electronic structure and bonding exhibited by boron hydrides can be enlarged to incorporate other atoms within the cluster.

Most of the research into the reactions of alkylmetal reagents with boron hydrides has centred to date on decaborane(14), $B_{10}H_{14}$, being initiated by Greenwood and co-workers in the 1960's and 1970's.[5] One exception to this is the reported synthesis of the thermally fragile compounds $[MeMB_6H_9]$ (M = Zn or Cd) *via* the reaction of hexaborane(10) with the appropriate dimethylmetal reagent [reaction (29)].[121] Little by

$$Me_2M + B_6H_{10} \longrightarrow MeMB_6H_9 + MeH \quad (M = Zn \text{ or } Cd) \qquad (29)$$

way of characterization of these compounds has been reported.

The earliest investigations concerning the reactions of decaborane(14) with aluminium and gallium reagents attempted to parallel the cluster expansion reactions which occur between decaborane(14) and tetrahydroborate or borane adducts under appropriate conditions.[122] Thus, the reaction between decaborane(14) and trimethylamine-alane [reaction (30)] yields the $[H_2AlB_{10}H_{12}]^-$ anion, which can be viewed either as a $B_{10}H_{14}^-$

$$Me_3N{\cdot}AlH_3 + B_{10}H_{14} \xrightarrow{Et_2O} [HNMe_3]^+[H_2AlB_{10}H_{12}]{\cdot}2OEt_2 + H_2 \quad (30)$$

species in which one of the boron atoms has been replaced by an aluminium or as an AlH_2^+ unit coordinated to a $B_{10}H_{12}^{2-}$ ligand.[123] This strategy was subsequently extended to the alkyl derivatives of magnesium, zinc, cadmium and mercury to give a variety of $B_{10}H_{12}^{2-}$ derivatives.[124-128] The compounds $[Ph_3PMe]_2[Zn(B_{10}H_{12})_2]$ and $[(Et_2O)_2Cd(B_{10}H_{12})]$ were synthesized according to reactions (31) and (32) and their structures determined by X-ray diffraction of single crystals.[129,130] The zinc compound

$$Et_2Cd + B_{10}H_{14} \xrightarrow{Et_2O} (Et_2O)_2Cd(B_{10}H_{12}) + 2EtH \quad (31)$$

$$\left.\begin{aligned} Me_2Zn + B_{10}H_{14} &\xrightarrow{Et_2O} (Et_2O)_2Zn(B_{10}H_{12}) + 2MeH \\ 2(Et_2O)_2Zn(B_{10}H_{12}) &\xrightarrow{H_2O} [Zn(B_{10}H_{12})_2]^{2-} + Zn^{2+} + 4Et_2O \\ [Zn(B_{10}H_{12})_2]^{2-} + 2[Ph_3PMe]^+ &\xrightarrow{H_2O} [Ph_3PMe]_2[Zn(B_{10}H_{12})_2] \end{aligned}\right\} \quad (32)$$

contains the $[Zn(B_{10}H_{12})_2]^{2-}$ anion in which the two $B_{10}H_{12}^{2-}$ groups each act as *tetra*-hapto ligands, thereby incorporating the metal fully within the polyhedral cluster.[129] The cadmium compound is, in fact, a dimer featuring a pair of cadmium centres which are bridged by two $B_{10}H_{12}^{2-}$ ions each acting as *bis*(*di*-hapto) ligands. In effect, each cadmium atom has replaced one of the bridging hydrogens in $[B_{10}H_{14}]$ to give an exopolyhedral three-centre, two-electron B–Cd–B bond.[130]

Both trimethylthallium and trimethylindium react with decaborane(14) in diethyl ether.[131,132] In the case of the thallium compound, there are two competing reactions [reactions (33) and (34)]. While the first simply yields the dimethylthallium salt of the

$$Me_3Tl + B_{10}H_{14} \longrightarrow [Me_2Tl][B_{10}H_{13}] + MeH \quad (33)$$

$$2Me_3Tl + B_{10}H_{14} \longrightarrow [Me_2Tl][Me_2TlB_{10}H_{12}] + 2MeH \quad (34)$$

$[B_{10}H_{13}]^-$ ion, the second yields the $[Me_2TlB_{10}H_{12}]^-$ anion, in which the $[B_{10}H_{12}]^{2-}$ ligand is linked to the dimethylthallium unit in a *tetra*-hapto fashion.[132] The thallium atom is perceived as being linked to each of two edges of the B_{10} polyhedron *via* B–Tl–B three-centre, two-electron bonds. The corresponding reactions with trimethylindium [equations (35) and (36)] are believed to yield similar metallaborane products, although no structural details have as yet been forthcoming.[131]

$$Me_3In + B_{10}H_{14} \longrightarrow [MeInB_{10}H_{12}] + 2MeH \quad (35)$$

$$2Me_3In + B_{10}H_{14} \longrightarrow [Me_2In][Me_2InB_{10}H_{12}] + 2MeH \quad (36)$$

1.5 Aims of the Present Research

The research described in this thesis had as its basis six major objectives.

(i) In view of the unusual polymeric structure of solid beryllium *bis*(tetrahydroborate) and the similar structure implied for solid methylzinc tetrahydroborate by spectroscopic measurements, it was planned to investigate further the nature of the solid zinc compound, primarily by recourse to X-ray diffraction, provided that suitable single crystals could be grown. Given that methylzinc tetrahydroborate is appreciably volatile, albeit thermally frail, it was planned also to investigate the nature of the species present in the vapour.

(ii) In view of the interesting chemical properties displayed by many other metal tetrahydroborates and the dearth of information concerning the reactivity of [$MeZnBH_4$], it was planned to investigate more fully the chemistry of methylzinc tetrahydroborate. The analogous cadmium compound [$MeCdBH_4$] might also be investigated with profit, if it were thermally robust enough to survive at or near ambient temperatures.

(iii) Given that both dimethylaluminium tetrahydroborate and methylaluminium *bis*(tetrahydroborate) are thought to have structures in the solid phase that are markedly different from the gaseous molecules, it was hoped to grow single crystals of both these compounds by slow cooling of the liquid and to investigate the solids by X-ray diffraction. It was anticipated that the successful realization of this aim would provide informative comparisons not only with the structures of the gaseous molecules, but also with that of solid methylzinc tetrahydroborate. In addition, there was the possibility that similar techniques might yield the structure of solid aluminium *tris*(tetrahydroborate), again with a view to comparisons with the gaseous molecule (the structure of which has already been determined by electron diffraction) and to establishing structural trends for compounds in the series $Me_nAl(BH_4)_{3-n}$ (n = 0-3).

(iv) In view of the known reactivity of dimethylzinc with respect to boron hydrides such as [B_2H_6], [B_6H_{10}] and [$B_{10}H_{14}$] *via* both proton abstraction and displacement of a BH_2 unit, it was planned to investigate its reaction with other boranes, principally [B_4H_{10}] and [B_5H_9].

(v) If the reaction of dimethylzinc with either [B_4H_{10}] or [B_5H_9] had a positive outcome it was proposed to investigate the reactions of these boron hydrides with other methylmetal and metal hydride derivatives. For example, the reactions of tetraborane(10) with trimethylindium and trimethylamine-alane were of potential interest as synthetic routes to the compounds [$Me_2InB_3H_8$] and [$H_2AlB_3H_8$], respectively.

(vi) The interaction of dimethylindium chloride with salts containing the octahydrotriborate anion was also to be investigated as a possible route to $[Me_2InB_3H_8]$, given that the analogous reactions with dimethylaluminium and dimethylgallium chlorides are known to yield the corresponding B_3H_8 derivatives. The synthesis and structural characterization of the indium compound would be of note in charting a rare example of an indium hydride derivative; hence, too, it might be possible to discern significant trends in structure and bonding for the series of compounds $Me_2MB_3H_8$ (M = B, Al, Ga and In).

References for Chapter 1

1. A. Stock, *Hydrides of Boron and Silicon*, Cornell University Press, 1933.
2. C.E. Housecroft, *Chem. Soc. Rev.*, 1995, **24**, 215.
3. J.D. Kennedy, *Prog. Inorg. Chem.*, 1985, **32**, 519.
4. D.F. Gaines and S.J. Hildebrandt, in *Metal Interactions with Boron Clusters*, ed. R.N. Grimes, Plenum, New York, 1982, p. 119.
5. N.N. Greenwood, *Pure Appl. Chem.*, 1977, **49**, 791.
6. T.J. Marks and J.R. Kolb, *Chem. Rev.*, 1977, **77**, 263.
7. N.N. Greenwood and I.M. Ward, *Chem. Soc. Rev.*, 1974, **3**, 231.
8. W.H. Eberhardt, B.L. Crawford, Jr., and W.N. Lipscomb, *J. Chem. Phys.*, 1954, **22**, 989.
9. W.N. Lipscomb, *Boron Hydrides*, W.A. Benjamin Inc., New York, 1963.
10. R.N. Grimes, in *Comprehensive Organometallic Chemistry*, eds. G. Wilkinson, F.G.A. Stone and E. Abel, Pergamon, Oxford, 1981, Vol. 1, p. 459.
11. M.E. O'Neill and K. Wade, in *Comprehensive Organometallic Chemistry*, eds. G. Wilkinson, F.G.A. Stone and E. Abel, Pergamon, Oxford, 1981, Vol. 1, p. 1.
12. K.F. Purcell and J.C. Kotz, *Inorganic Chemistry*, W.B. Saunders, Philadelphia, 1977, p. 980.
13. C.E. Housecroft and T.P. Fehlner, *Adv. Organomet. Chem.*, 1982, **21**, 59.
14. K. Wade, in *Transition Metal Clusters*, ed. B.F. Johnson, Wiley, New York, 1980, p. 193.
15. R.W. Rudolph, *Acc. Chem. Res.*, 1976, **9**, 446.
16. K. Wade, *Adv. Inorg. Chem. Radiochem.*, 1976, **18**, 1.
17. R.E. Williams, *Adv. Inorg. Chem. Radiochem.*, 1976, **18**, 67.
18. R. Mason and D.M.P. Mingos, *M.T.P. Int. Rev. Sci., Phys. Chem. Ser. 2*, 1975, **11**, 121.
19. D.M.P. Mingos, *Nature: Phys. Sci.*, 1972, **236**, 99.
20. R.W. Rudolph and W.R. Pretzer, *Inorg. Chem.*, 1972, **11**, 1974.

21. K. Wade, *J. Chem. Soc., Chem. Commun.*, 1971, 792.

22. T.J. Marks and L.A. Shimp, *J. Am. Chem. Soc.*, 1972, **94**, 1542.

23. B.D. James and M.G.H. Wallbridge, *Prog. Inorg. Chem.*, 1970, **11**, 99.

24. See, for example, S.J. Lippard and K.M. Melmed, *Inorg. Chem.*, 1967, **6**, 2223.

25. N. Davies, B.D. James and M.G.H. Wallbridge, *J. Chem. Soc., A,* 1969, 2601.

26. H. Nöth and R. Hartwimmer, *Chem. Ber.*, 1960, **93**, 2238.

27. W.E. Reid, J.M. Bish and A. Brenner, *J. Electrochem. Soc.*, 1957, **104**, 21.

28. P.D.P. Thomas, D.Phil. Thesis, University of Oxford, 1977.

29. P.R. Oddy and M.G.H. Wallbridge, *J. Chem. Soc., Dalton Trans.*, 1976, 869.

30. H.I. Schlesinger, H.C. Brown and G.W. Schaeffer, *J. Am. Chem. Soc.*, 1943, **65**, 1786; C.R. Pulham, unpublished results.

31. J.A. Jensen and G.S. Girolami, *J. Chem. Soc., Chem. Commun.*, 1986, 1160; J.A. Jensen, S.R. Wilson and G.S. Girolami, *J. Am. Chem. Soc.*, 1988, **110**, 4978.

32. J.C. Bommer and K.C. Morse, *J. Chem. Soc., Chem. Commun.*, 1977, 137; C. Kutal, P. Grutsch, J.L. Atwood and R.D. Rogers, *Inorg. Chem.*, 1978, **17**, 3558.

33. C.A. Ghilardi, S. Midollini and A. Orlandini, *Inorg. Chem.*, 1982, **21**, 4096.

34. J.A. Jensen and G.S. Girolami, *Inorg. Chem.*, 1989, **28**, 2107.

35. Y. Matsui and R.C. Taylor, *J. Am. Chem. Soc.*, 1968, **90**, 1363.

36. D.S. Marynick and W.N. Lipscomb, *J. Am. Chem. Soc.*, 1971, **93**, 2322; D.S. Marynick and W.N. Lipscomb, *Inorg. Chem.*, 1972, **11**, 820.

37. K. Brendhaugen, A. Haaland and D.P. Novak, *Acta Chem. Scand.*, 1975, **29A**, 801; G. Gundersen, L. Hedberg and K. Hedberg, *J. Chem. Phys.*, 1973, **59**, 3777.

38. E.R Bernstein, T.A. Keiderling, S.J. Lippard and J.J. Mayerle, *J. Am. Chem. Soc.*, 1972, **94**, 2552.

39. E.R. Bernstein, W.C. Hamilton, T.A. Keiderling, S.J. LaPlaca, S.J. Lippard and J.J. Mayerle, *Inorg. Chem.*, 1972, **11**, 3009.

40. I. Demachy and F. Volatron, *Inorg. Chem.*, 1994, **33**, 3965.

41. H. Beall and C.H. Bushweller, *Chem. Rev.*, 1973, **73**, 465.

42. T.J. Marks and W.J. Kennelly, *J. Am. Chem. Soc.*, 1975, **97**, 1439.

43. H.D. Empsall, E. Mentzner and B.L. Shaw, *J. Chem. Soc., Chem. Commun.*, 1975, 861.

44. M. Mancini, P.Bougeard, R.C. Burns, M. Mlekuz, B.G. Sayer, J.I.A. Thompson and M.J. McGlinchey, *Inorg. Chem.*, 1984, **23**, 1072.

45. A.P. Hitchcock, N. Hao, N.H. Werstick, M.J. McGlinchey and T. Ziegler, *Inorg. Chem.*, 1982, **21**, 793.

46. T.J. Marks and G.W. Grynkewich, *Inorg. Chem.*, 1976, **15**, 1302.

47. See, for example, J.E. Huheey, E.A. Keiter and R.L. Keiter, *Inorganic Chemistry: Principles of Structure and Reactivity*, 4th edn., Harper Collins, 1993.

48. E.R. Peterson, *Diss. Abstr.*, 1965, **25**, 5588.

49. A. Almenningen, G. Gundersen and A. Haaland, *Acta Chem. Scand.*, 1968, **22**, 328.

50. M.T. Barlow, A.J. Downs, D.W.H. Rankin and P.D.P. Thomas, *J. Chem. Soc., Dalton Trans.*, 1979, 1793.

51. C.R. Pulham, D.Phil. Thesis, University of Oxford, 1991; C.R. Pulham, P.T. Brain, A.J. Downs, D.W.H. Rankin and H.E. Robertson, *J. Chem. Soc., Chem. Commun.*, 1990, 177.

52. P.F. Souter, A.J. Downs and S. Parsons, unpublished results; P.F. Souter, D.Phil. Thesis, University of Oxford, 1995.

53. M.T. Barlow, C.J. Dain, A.J. Downs, P.D.P. Thomas and D.W.H. Rankin, *J. Chem. Soc., Dalton Trans.*, 1980, 1374.

54. A.J. Downs, T.M. Greene, L.A. Harman, P.F. Souter, P.T. Brain, C.R. Pulham, D.W.H. Rankin, H.E. Robertson, M. Hofmann and P.v.R. Schleyer, *Inorg. Chem.*, 1995, **34**, 1799.

55. G.A. Koutsantonis, F.C. Iee and C.L. Raston, *J. Chem. Soc., Chem. Commun.*, 1994, 1975.

56. V. Plato and K. Hedberg, *Inorg. Chem.*, 1971, **10**, 590.

57. P.H. Bird and M.R. Churchill, *J. Chem. Soc., Chem. Commun.*, 1967, 403.

58. C.J. Dain, A.J. Downs and D.W.H. Rankin, *Angew. Chem., Int. Ed. Engl.*, 1982, **21**, 534; C.J. Dain, A.J. Downs, M.J. Goode, D.G. Evans, K.T. Nicholls, D.W.H. Rankin and H.E. Robertson, *J. Chem. Soc., Dalton Trans.*, 1991, 967.

59. T.M. Gilbert, F.J. Hollander and R.G. Bergman, *J. Am. Chem. Soc.*, 1985, **107**, 3508.

60. L.F. Rhodes, L.M. Venanzi, D. Sorato and A. Albinati, *Inorg. Chem.*, 1986, **25**, 3335.

61. B.E. Green, C.H.L. Kennard, G. Smith, B.D. James, P.C. Healy and A.H. White, *Inorg. Chim. Acta*, 1984, **81**, 147.

62. E.R.H. Walker, *Chem. Soc. Rev.*, 1976, **5**, 23.

63. H.I. Schlesinger, R.T. Sanderson and A.B. Burg, *J. Am. Chem. Soc.*, 1940, **62**, 3421.

64. P.H. Bird and M.G.H. Wallbridge, *J. Chem. Soc.*, 1965, 3923.

65. H. Nöth and M. Ehemann, *J. Chem. Soc., Chem. Commun.*, 1967, 685.

66. D. Dou, J. Liu, J.A. Krause Bauer, G.T. Jordan, IV, and S.G. Shore, *Inorg. Chem.*, 1994, **33**, 5443.

67. A.J. Downs, L.A. Harman, P.D.P. Thomas and C.R. Pulham, *Polyhedron*, 1995, **14**, 935.

68. L.A. Harman, Part II Thesis, University of Oxford, 1990.

69. W.H. Stockmayer, D.W. Rice and C.C. Stephenson, *J. Am. Chem. Soc.*, 1955, **77**, 1980.

70. P.H. Bird and M.G.H. Wallbridge, *J. Chem. Soc., A*, 1967, 664.

71. J.C. Fauroux and S.J. Teichner, *Bull. Soc. Chim. Fr.*, 1967, **10**, 4053.

72. J. Pleseck, S. Hermanek and V. Gregor, Czech. Pat. 116107 (Nov. 15, 1965).

73. H.I. Schlesinger and H.C. Brown, *J. Am. Chem. Soc.*, 1940, **62**, 3429.

74. A.L.J. Raum and D.A. Fraser, British Pat. 801401 (Sept. 10, 1958).

75. D. Apotheker, A.L. Barney and N. Brodway, U.S. Pat. 3597367 (Aug. 3, 1971).

76. C.N. Zellner and A. Buerger, German Pat. 1070148 (Dec. 3, 1959).

77. S.B. Mirviss, H.W. Dougherty and R.W. Looney, U.S. Pat. 3310547 (Mar. 21, 1967).

78. J.Y. Beach and S.H. Bauer, *J. Am. Chem Soc.*, 1940, **62**, 3440.

79. M.L.H. Green and H. Munakata, *J. Chem. Soc., A*, 1974, 269.

80. G. Barbaras, C. Dillard, A.E. Finholt, T. Wartik, K.E. Wilzbach and H.I. Schlesinger, *J. Am. Chem. Soc.*, 1951, **73**, 4585.

81. E. Wiberg and W. Henle, *Z. Naturforsch.*, 1952, **7b**, 579.

82. N.N. Maltseva, N.S. Kedrova and V.I. Mikheeva, *Zh. Neorg. Khim.*, 1973, **18**, 1989.

83. V.I. Mikheeva, N.N. Maltseva and L.S. Alekseeva, *Zh. Neorg. Khim.*, 1968, **13**, 1303.

84. H. Nöth, E. Wiberg and L.P. Winter, *Z. Anorg. Allg. Chem.*, 1971, **386**, 73.

85. D. Ridley, Ph.D. Thesis, University of Durham, 1965.

86. J.W. Nibler and T.H. Cook, *J. Chem. Phys.*, 1973, **58**, 1596.

87. E. Wiberg and W. Henle, *Z. Naturforsch.*, 1952, **7b**, 582.

88. H. Nöth and M. Thomann, *Z. Naturforsch.*, 1990, **45b**, 1482.

89. H. Nöth and L.P. Winter, *Z. Anorg. Allg. Chem.*, 1975, **389**, 225.

90. H.I. Schlesinger, R.T. Sanderson and A.B. Burg, *J. Am. Chem. Soc.*, 1939, **61**, 536.

91. H.I. Schlesinger, H.C. Brown and E.K. Hyde, *J. Am. Chem. Soc.*, 1953, **75**, 209.

92. D.A. Coe and J.W. Nibler, *Spectrochim. Acta*, 1972, **29A**, 1789.

93. A.R. Emery and R.C. Taylor, *Spectrochim. Acta*, 1960, **16**, 1455.

94. R.A. Ogg and J.D. Ray, *Discuss. Faraday Soc.*, 1955, **19**, 239.

95. L.A. Jones, D.Phil. Thesis, University of Oxford, 1993.

96. A.J. Downs and L.A. Jones, *Polyhedron*, 1994, **13**, 2401.

97. A.J. Downs and P.D.P. Thomas, *J. Chem. Soc., Dalton Trans.*, 1978, 809.

98. C.R. Pulham, unpublished results.

99. See, for example, A.J. Downs (ed.), *Chemistry of Aluminium, Gallium, Indium and Thallium*, Blackie, Glasgow, 1993.

100. C.R. Pulham and A.J. Downs, unpublished results.

101. K.B. Gilbert, S.K. Bocock and S.G. Shore, in *Comprehensive Organometallic Chemistry*, eds. G. Wilkinson, F.G.A. Stone and E. Abel, Pergamon, Oxford, 1982, Vol. 6, p. 879.

102. J.C. Calabrese, D.F. Gaines, S.J. Hildebrandt and J.H. Morris, *J. Am. Chem. Soc.*, 1976, **98**, 5489.

103. W.V. Hough, L.J. Edwards and A.D. McElroy, *J. Am. Chem. Soc.*, 1956, **78**, 689.

104. G.E. Ryschkewitsch and K.C. Nainan, *Inorg. Synth.*, 1974, **15**, 111.

105. D.F. Gaines, R. Schaeffer and F. Tebbe, *Inorg. Chem.*, 1963, **2**, 526.

106. W.J. Dewkett, M. Grace and H. Beall, *Inorg. Synth.*, 1974, **15**, 115.

107. W.J. Dewkett, M. Grace and H. Beall, *J. Inorg. Nucl. Chem.*, 1971, **33**, 1279.

108. J.J. Borlin and D.F. Gaines, *J. Am. Chem. Soc.*, 1972, **94**, 1367.

109. F. Klanberg, E.L. Muetterties and L.J. Guggenberger, *Inorg. Chem.*, 1968, **7**, 2272.

110. P.R. Oddy, D.L. Shaw and M.G.H. Wallbridge, reported at the Third International Meeting on Boron Chemistry, Munich, July 1976.

111. C.R. Peters and C.E. Nordman, *J. Am. Chem. Soc.*, 1960, **82**, 5758.

112. M.L. McKee and W.N. Lipscomb, *Inorg. Chem.*, 1982, **21**, 2846.

113. C.J. Dain, A.J. Downs and D.W.H. Rankin, *J. Chem. Soc., Dalton Trans.*, 1981, 2465.

114. C.R. Pulham, A.J. Downs, D.W.H. Rankin and H.E. Robertson, *J. Chem. Soc., Dalton Trans.*, 1992, 1509.

115. C.J. Dain, A.J. Downs, G.S. Laurenson and D.W.H. Rankin, *J. Chem. Soc., Dalton Trans.*, 1981, 472.

116. C.E. Nordman and W.N. Lipscomb, *J. Am Chem. Soc.*, 1953, **75**, 4116; C.E. Nordman and W.N. Lipscomb, *J. Chem. Phys.*, 1953, **21**, 1856; G.S. Pawley, *Acta Crystallogr.*, 1966, **20**, 631.

117. S.J. Lippard and K.M. Melmed, *Inorg. Chem.*, 1969, **12**, 2755.

118. L.J. Guggenberger, *Inorg. Chem.*, 1970, **9**, 367.

119. S.J. Hildebrandt, D.F. Gaines and J.C. Calabrese, *Inorg. Chem.*, 1978, **17**, 790.

120. M.W. Chen, D.F. Gaines and L.G. Hoard, *Inorg. Chem.*, 1980, **19**, 2989.

121. D. Denton and S.G. Shore, Abstracts of the 162nd meeting of the A.C.S., 1971, INORG, 4.

122. N.N. Greenwood and J.A. McGinnety, *J. Chem. Soc., Chem. Commun.*, 1965, 331.

123. N.N. Greenwood and J.A. McGinnety, *J. Chem. Soc., A*, 1966, 1090.

124. N.N. Greenwood and N.F. Travers, *Inorg. Nucl. Chem. Lett.*, 1966, **2**, 169.

125. N.N. Greenwood and N.F. Travers, *J. Chem. Soc., A*, 1967, 880.

126. N.N. Greenwood and N.F. Travers, *J. Chem. Soc., Chem. Commun.*, 1967, 216.

127. N.N. Greenwood and N.F. Travers, *J. Chem. Soc., A*, 1968, 15.

128. N.N. Greenwood and N.F. Travers, *J. Chem. Soc., A*, 1971, 3257.

129. N.N. Greenwood, J.A. McGinnety and J.D. Owen, *J. Chem. Soc., A*, 1971, 809.

130. N.N. Greenwood, J.A. McGinnety and J.D. Owen, *J. Chem. Soc., A*, 1972, 989.

131. N.N. Greenwood, B.S. Thomas and D.W. Waite, *J. Chem. Soc., Dalton Trans.*, 1975, 299.

132. N.N. Greenwood and J.A. Howard, *J. Chem. Soc., Dalton Trans.*, 1976, 177.

Chapter Two
Experimental Techniques

2.1 The Manipulation of Air-Sensitive Compounds

The extreme sensitivity to air and moisture of many of the compounds handled during the course of this research precluded the use of conventional "bench-top" methods in their preparation and manipulation. Consequently a variety of high vacuum and inert atmosphere techniques was used on a routine basis. Several comprehensive reviews of such methods already exist[1-3] and so only a brief description of the methods of immediate relevance is warranted here.

2.1.1 High Vacuum Techniques

Vacuum line techniques are ideally suited to the handling of small quantities of volatile, air-sensitive compounds. The vacuum line used for much of the research described in this thesis (Figure 2.1) provided, in effect, a closed reaction system, with excellent exclusion of air, quantitative retention of all reaction products and a means for the transfer, analysis and quantitative measurement of volatile materials.

The line was constructed from Pyrex glass and comprised both greased and greaseless sections. The former incorporated ground-glass, high-vacuum stopcocks lubricated with "Apiezon-L" grease. However, the tendency of hydroborate derivatives to be absorbed by, or to react with, hydrocarbon-based grease necessitated the use of the greaseless section of the line equipped with a combination of Young's greaseless valves and unions which utilized Teflon O-rings to provide vacuum seals, ground-glass joints being lubricated with "Voltalef-90" fluorocarbon grease. The highly reactive nature of some compounds precluded the use even of Young's taps, since the residual moisture and other impurities retained by the Teflon surfaces resulted in decomposition. Under

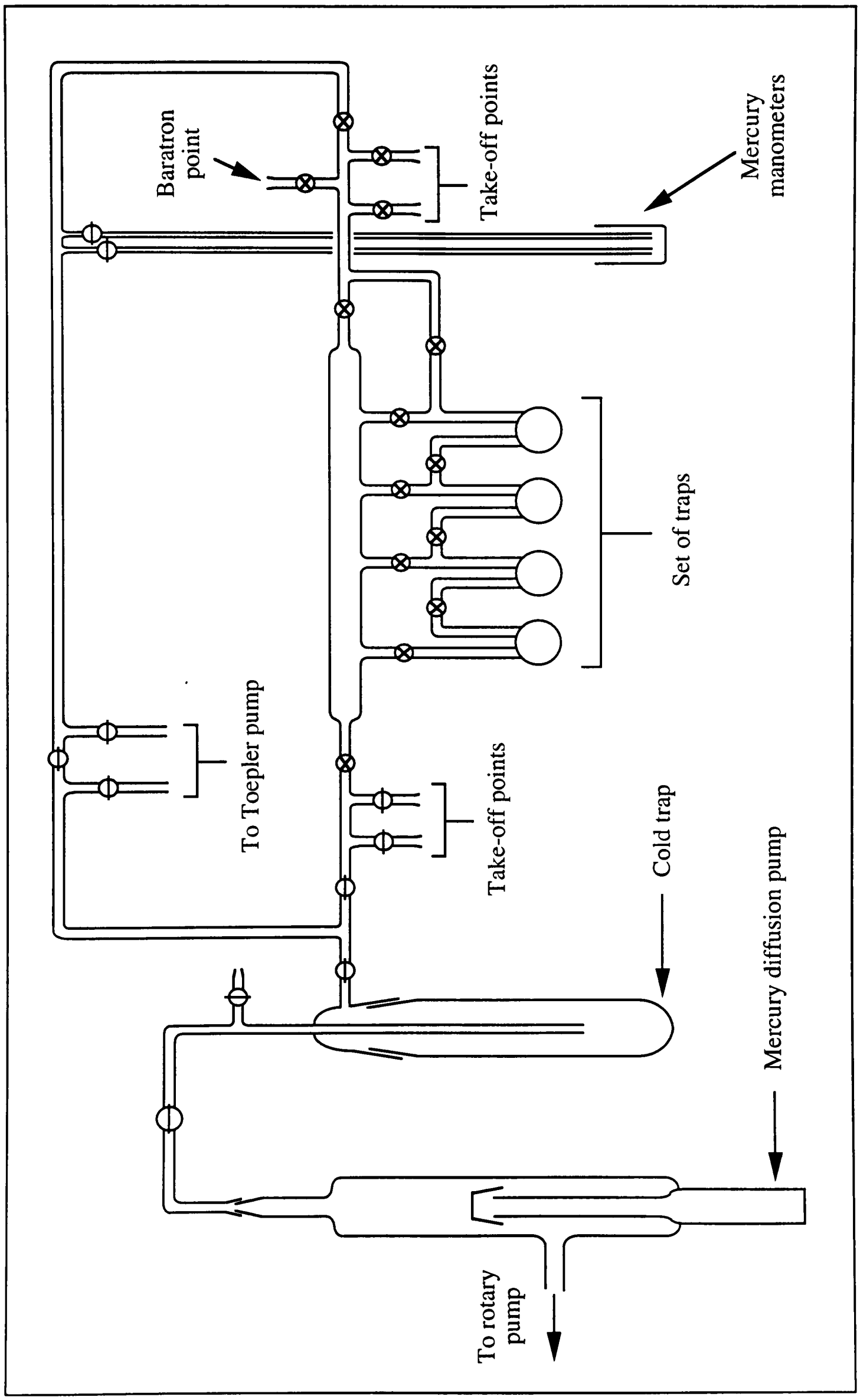

Figure 2.1 The vacuum line used in the course of this investigation.

such circumstances, purpose-built, all-glass vessels incorporating appropriate break-seals and constrictions were utilized. A typical sequence of vacuum transfer operations using all-glass apparatus is illustrated in Figure 2.2. Such apparatus was invariably pre-conditioned by heating under vacuum with a hand-torch ("flaming out") to remove residual moisture and other volatile material adsorbed on the inner surfaces of the glass.

Evacuation of the line was achieved by a mercury diffusion pump backed by an oil-sealed, single-stage rotary pump. A demountable cold-trap protected the mercury and pump oil from volatile contaminants and at the same time prevented back diffusion of mercury into the line. The combination of rotary and diffusion pumps enabled evacuation to a pressure of 10^{-4} - 10^{-5} Torr. This pressure was monitored qualitatively by the use of a Tesla coil which produced a high-voltage, high-frequency discharge at pressures between 1 and 10^{-3} Torr, and quantitatively by the use of a Baratron (capacitance) pressure-gauge (for measurements in the range 0.01-120 Torr). The quantitative handling of non-condensable gases (chiefly methane, hydrogen and carbon monoxide) was performed with the aid of a Toepler pump. This utilized a mercury "piston" to confine such gases to a known volume in which the resulting pressure was then measured.

Volatile materials were transferred on the vacuum line by vaporization and subsequent condensation at -196°C. Fractionation of compounds with significantly different volatilities was achieved by passing the vapours through a series of traps held at successively lower temperatures. Substances could be separated using this method typically only if the temperatures at which each gave rise to a given vapour pressure differed by more than 20°C. The temperature of each trap was controlled by the use of an appropriate low-temperature slush bath composed of a suitable solvent in solid-liquid equilibrium.

2.1.2 Inert Atmosphere Techniques

Compounds which were somewhat less sensitive to attack by air or moisture

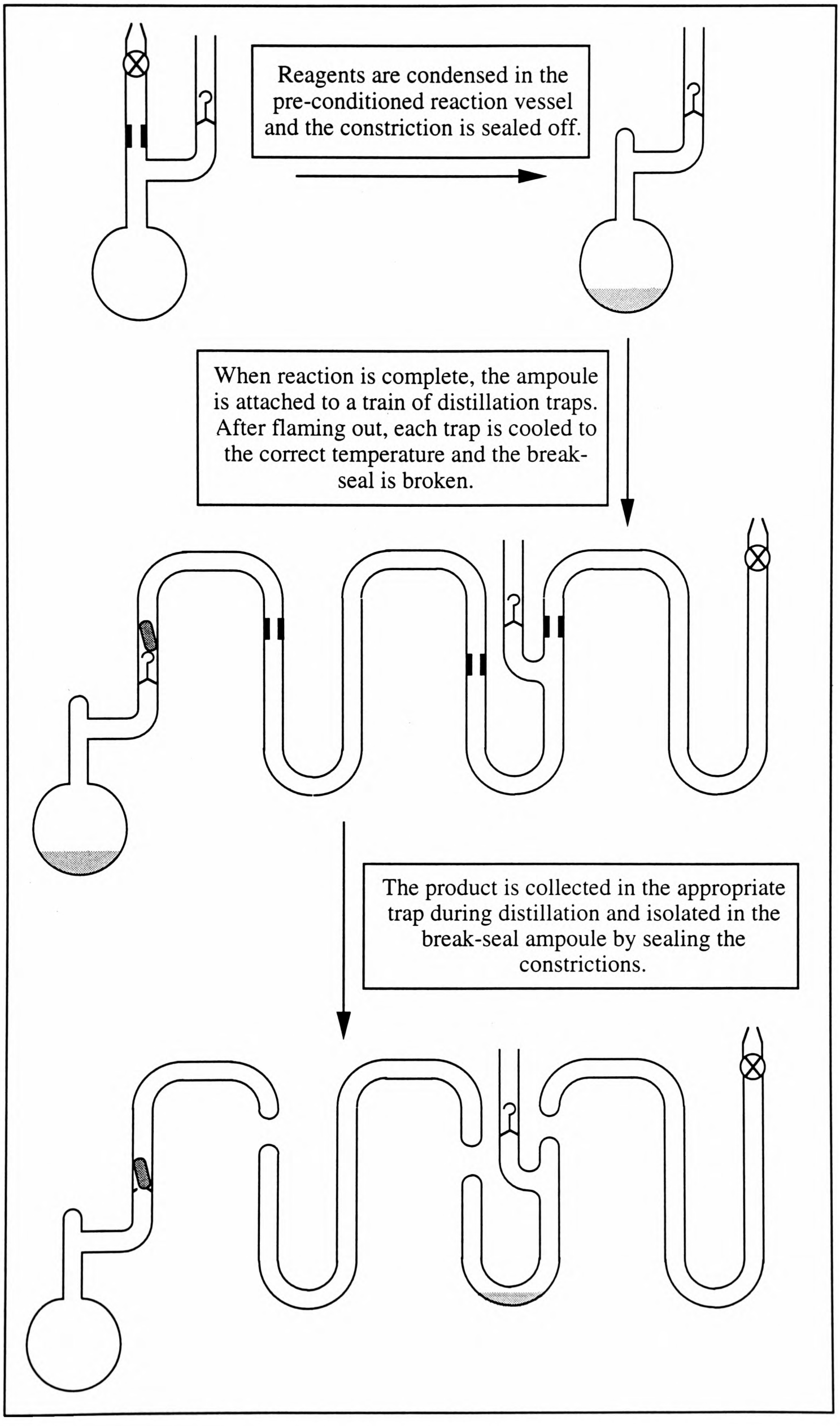

Figure 2.2 Distillation using all-glass apparatus.

were manipulated using either (i) techniques involving bench-top operations with special glassware (so-called Schlenk techniques) or (ii) glove-box methods, in which operations were performed in a closed chamber under an inert atmosphere.

Schlenk techniques, involving the use of glassware which had been pre-conditioned by repeated alternate evacuation and purging with dry nitrogen, were required for handling solutions of compounds which were susceptible to hydrolysis or oxidation (such as lithium tetrahydroborate in ether). The inert gas used, nitrogen, was dried by passage through a column of molecular sieve.

Operations involving air-sensitive solids such as trimethylindium were performed under a dry nitrogen atmosphere in a sealed container. As most of the compounds in question were highly air sensitive, a "Vacuum Atmospheres" dry-box was used. This was equipped with neoprene gloves, an evacuable side-port and a source of nitrogen catalytically purged of moisture and oxygen by passage through columns containing an oxygen scavenger (Cu/MnO) and molecular sieve. Nitrogen, admitted to the box directly from the laboratory supply, was allowed to circulate through these columns typically for 30 min prior to the commencement of operations. Such provisions ensured that the oxygen and moisture contents of the atmosphere were normally only a few ppm.

2.1.3 Single Crystal Loading

Two of the compounds investigated during the course of this research, $[MeZnBH_4]$ and $[(MeZn)_2B_3H_7]_2$ proved so sensitive to attack by oxygen and moisture that crystalline samples decomposed rapidly even in a rigorously purged glove-box atmosphere. Accordingly, loading single crystals of these compounds suitable for X-ray diffraction necessitated the design of new apparatus, in which capillaries were fused directly onto the reaction vessel. The apparatus used, illustrated in Figure 2.3, incorporated a 1-litre bulb to which a cold finger was attached *via* a large "Rotaflo" tap. Pyrex capillary side-arms, each *ca.* 0.3 mm in diameter and containing a small quantity

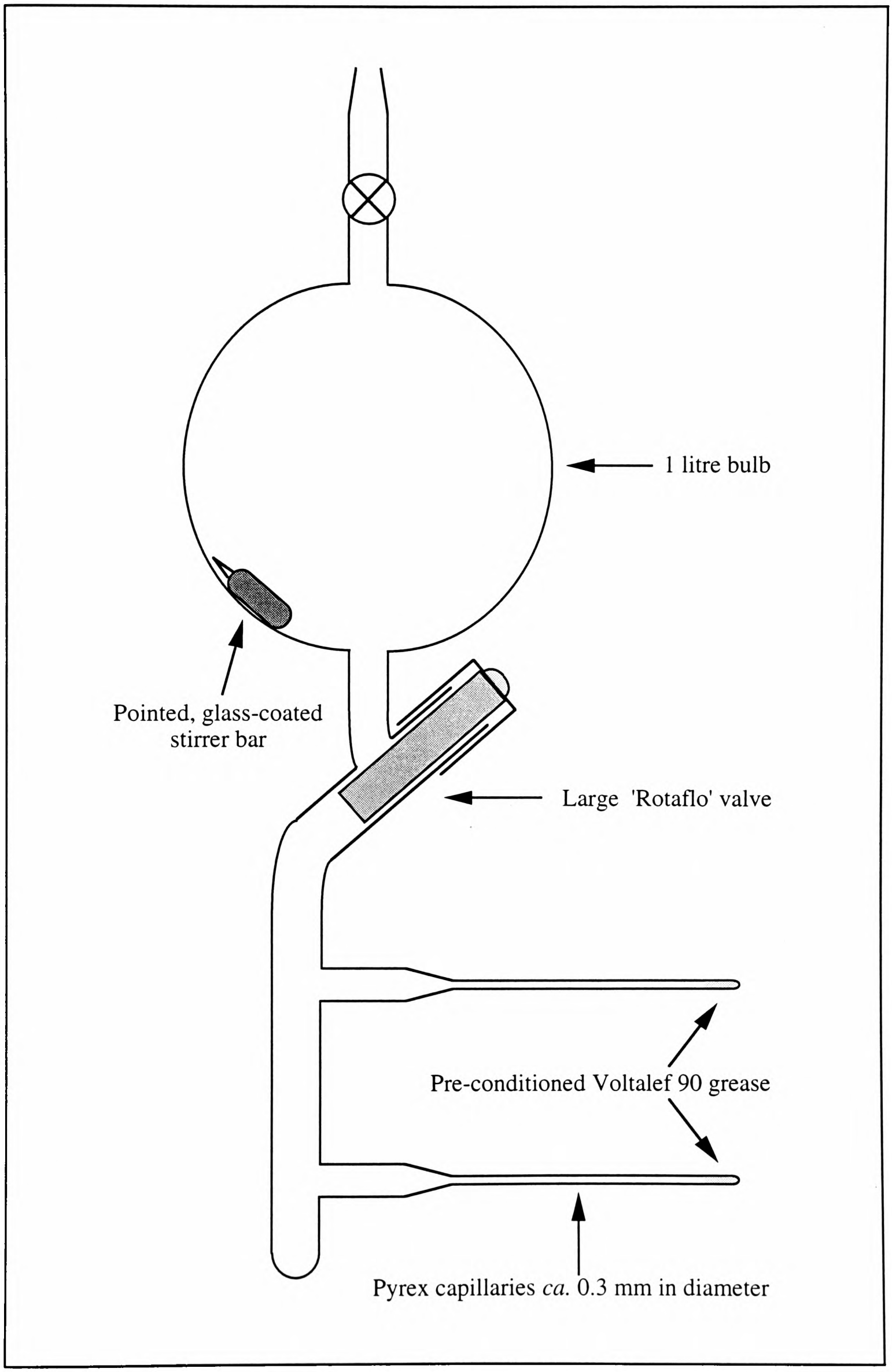

Figure 2.3 Apparatus for loading single crystals grown from the vapour phase.

of Voltalef-90 grease, were fused to the cold finger. The entire apparatus was first pre-conditioned by exposure to dimethylzinc vapour (at a pressure of *ca.* 20 Torr) for 24 h. Crystals suitable for X-ray diffraction were grown from the vapour by admitting the appropriate reagents to the main part of the bulb only, and then manipulated by the use of a pointed glass-coated stirrer bar until held firmly in place in one of the capillary side-arms.

2.2 Methods Available for the Characterization of Metal Hydroborate Derivatives

This section outlines some of the principal techniques available for the characterization of metal hydroborate derivatives, in particular those relevant to the structural investigation of compounds containing BH_4, B_3H_7 or B_3H_8 groups.

2.2.1 Vibrational Spectroscopy

(a) Tetrahydroborate (BH_4) derivatives

As discussed previously, the mode of attachment of the tetrahydroborate ligand to a metal centre is an important structural feature of the complex, and for relatively simple, mononuclear species it is often possible to elucidate the mode of ligation by examining the vibrational (infrared and Raman) spectra of such molecules in the solid, liquid and vapour phases. Table 2.1 sets out the normal modes and infrared activities for an isolated MBH_4 unit subject to various modes of ligation.[4] The regions of the spectrum associated with the stretching motions of terminal and bridging B–H bonds (2300-2600 cm^{-1} and 1650-2200 cm^{-1}, respectively) are particularly diagnostic of the mode of coordination of the BH_4 group.[4] The positions of the bands associated with these two types of stretching motion are particularly revealing because (i) they are relatively unperturbed by mixing with lower-frequency modes of the same irreducible representations, (ii) they are not coupled significantly to other BH_4 groups within the

Structure (point group)	Approximate freq./cm^{-1}	Type of internal coordinate change	Symmetry type	Comments
Monodentate	2300-2450	B–H_t stretching	a_1, e	Strong, possibly a doublet
(C_{3v})	*ca.* 2000	B–H_b stretching	a_1	Strong
	ca. 1700-2000	M–H_b stretching	a_1	May be very broad
	1000-1150	BH_3 deformation	a_1, e	Strong band, possibly with weaker one at slightly higher frequency
Bidentate	2400-2600	B–H_t stretching	a_1, b_1	Strong doublet, 50-80 cm^{-1} splitting
(C_{2v})	1650-2150	B–H_b stretching	a_1, b_2	Strong band, possible shoulder
	1300-1500	Bridge stretching	a_1	Strong broad
	1100-1200	BH_2 deformation	b_2	Strong
Tridentate	2450-2600	B–H_t stretching	a_1	Strong singlet
(C_{3v})	2100-2200	B–H_b stretching	a_1, e	Doublet, 50-80 cm^{-1} splitting
	1150-1250	Bridge deformation	e	Strong
Ionic	2200-2300	B–H_t stretching	t_2	Strong, broad
(T_d)	1050-1150	BH_2 deformation	t_2	Strong, broad

Table 2.1 Normal modes and infrared activities predicted for various ligation geometries of an isolated MBH_4 unit (from reference 4).

same molecule (owing to the large number of intervening bonds), and (iii) they involve relatively little motion of the heavier boron atom and so splitting of bands due to the existence of the two naturally occurring boron isotopes is not normally observed. Bands due to the stretching of MH_nB units are generally broad and uninformative as a result of coupling to the M–B stretching vibration at lower frequency. Similarly, vibrational features associated with MH_nB deformation and H_tBH_b deformation modes yield little information, principally because of interaction with skeletal modes of the same symmetry. It is unfortunate also that the low scattering cross-section and vulnerability to laser damage of many tetrahydroborate derivatives limits the information available from Raman spectroscopy.

In cases where a tetrahydroborate group bridges more than one metal centre, the vibrational spectra can be somewhat more complicated, and, in contrast to the wealth of information pertaining to the vibrational spectra of mononuclear species, the dearth of data precludes any systematic analysis even of binuclear species $M(BH_4)M$. This said, the vibrational spectra of several tetrahydroborates containing metal centres bridged by $(\mu\text{–H})_2B(\mu\text{–H})_2$ groups have been examined.[5-8] These show typically a single infrared band in the B–H stretching region at *ca.* 2250 cm^{-1}, with a further low-frequency absorption at *ca.* 1300 cm^{-1} attributed to the antisymmetric BH_2 deformation. Such spectra are consistent either with the formulation $M^+ BH_4^- M^+$ or with the *bis*(bidentate) moiety $M(\mu\text{-H})_2B(\mu\text{-H})_2M$ in which distortion of the central BH_4 unit from idealized T_d symmetry is small.

(b) Octahydrotriborate (B_3H_8) derivatives

Vibrational spectroscopy has also been used, although to a lesser extent, in differentiating between the various modes of ligation of the B_3H_8 ligand. Essentially ionic derivatives (*e.g.* CsB_3H_8[9]) show no vibrational features in the region of the spectrum associated with M–H stretching vibrations of the bridging M–H–B unit (1300-1500 cm^{-1}), in contrast to covalently bound $M(\mu\text{-H})_2B_3H_6$ (**I**) and $M(\mu\text{-H})_3B_3H_5$ (**II**) species.[10,11] Bidentate ligation, $[M(\mu\text{-H})_2B_3H_6]$, is typically marked by a doublet

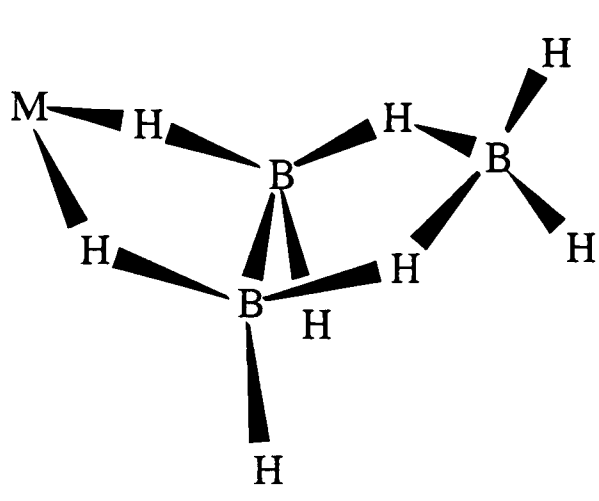

I

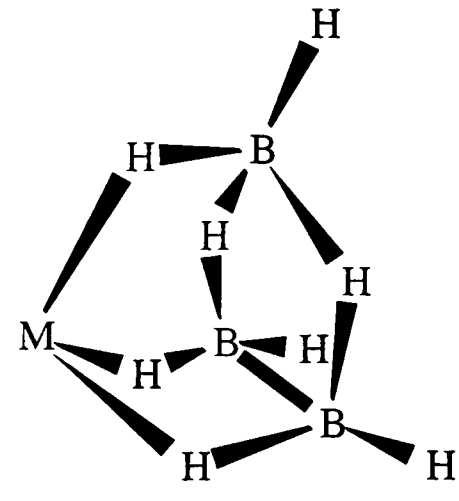

II

in the B–H_t region of the spectrum associated with the symmetric and antisymmetric stretching vibrations of the apical BH_2 unit. This feature is absent from the spectrum of the one authenticated tridentate derivative, $[(OC)_3Mn(\mu\text{-}H)_3B_3H_5]$.[11] The infrared spectrum of solid $[Mn(CO)_6(\mu\text{-}Br)(B_3H_8)]$,[12] which contains a *bis*(bidentate) B_3H_8, group is very similar to that of the mononuclear complex $[Mn(CO)_4(B_3H_8)]$.[10]

2.2.2 NMR Spectroscopy

NMR properties of some typical BH_4, B_3H_8 and metallaborane derivatives are listed in Table 2.2.

(a) Tetrahydroborate derivatives

^1H and ^{11}B NMR measurements have proved to be much less useful than vibrational studies in probing the coordination geometry of covalently bound tetrahydroborate groups. The anticipated difference in chemical shifts and boron-hydrogen spin-spin coupling constants for bridging and terminal hydrogens has been observed only for a very limited number of molecules.[17,18] Most tetrahydroborate derivatives display a proton resonance consisting of a 1:1:1:1 quartet and an ^{11}B resonance consisting of a 1:4:6:4:1 quintet, indicating magnetic equivalence of all four protons of the BH_4 unit irrespective of the mode of ligation to the metal centre. The origin of this equivalence is thought to lie in a fast intramolecular process

Compound[a]	Temp.	Structure	^{11}B spectrum	^{1}H spectrum	$J(^{11}B-^{1}H)$	Comments
Tetrahydroborates						
$Zr(BH_4)_4$[13]	25°C	Tridentate	Quintet, δ_B -8.5	Quartet	90.0 Hz	$^{91}Zr[^{11}B]$ spectrum shows 17 lines, $J(^{91}Zr-^{1}H)$ = 28 Hz, implying 16 equivalent H's
Me_2AlBH_4[14]	25°C	Bidentate	Quintet, δ_B -28.2	Quartet, δ_H 0.67	86.3 Hz	Unlike $Al(BH_4)_3$, no coupling to ^{27}Al
$(MePh_2P)_3CuBH_4$[15]	25°C	Monodentate	*b*	Broad singlet, δ_H 0.9	*b*	Fluxional, all H's equivalent
$NaBH_4$[16]	25°C	Ionic	Quintet, δ_B -42.9	Quartet	82 Hz	Fluxional, all H's equivalent
B_2H_6[17]	*b*	Bidentate	Triplet of triplets, δ_B 17.5	Two signals, δ_H 0.53 (quartet), -3.95 (septet of quintets)	135 Hz[c] 46.1 Hz[d] 7.0 Hz[e]	Distinct bridging and terminal H's observed for vapour, although more fluxional in ether solution
$(^tBu_2MeP)_2IrH_2(BH_4)$[18a]	25°C	Bidentate	Broad singlet, δ_B -13.1	Two broad singlets, δ_H 6.8, -6.5	*b*	Non-fluxional, IrH_2B at higher field than BH_2

[a] All data refer to solution-phase measurements, except in the case of B_2H_6, for which the parameters refer to the vapour phase. [b] Not reported. [c] $J(^{11}B-^{1}H_t)$, t = terminal. [d] $J(^{11}B-^{1}H_b)$, b = bridging. [e] $J(^{1}H_t-^{1}H_b)$.

Table 2.2(a) NMR properties of some typical tetrahydroborate complexes.

Compound	Temp.	Structure	^{11}B spectrum	^{1}H spectrum	$J(^{11}B-^{1}H)$	Comments
Octahydrotriborates						
NaB_3H_8[19]	20°C	Ionic	Nonet, δ_B -29.8	Decet, δ_H 0.3, rapid exchange even at -127°C	33 Hz	Fluxional, all borons and hydrogens equivalent
$Me_2GaB_3H_8$[20]	35°C -23°C	Bidentate	Nonet, δ_B -32.2 2 signals, δ_B -12.9 B(2); -41.9 B(1,3)	Broad, unresolved Broad, indication of more than one signal	34 Hz *a*	Methyl groups become inequivalent at -70°C
$(OC)_4MnB_3H_8$[10]	0°C	Bidentate	2 signals, δ_B 1.5 B(2); -42.2 B(1,3)	5 signals (1:1:2:2:2), δ_H 3.03, 2.74, 1.03, -0.80, -12.05	133 Hz[b] 58-65 Hz[c]	Distinct signals for 5 proton and 2 boron environments imply static structure
$(OC)_3MnB_3H_8$[11]	0°C	Tridentate	Broad singlet, all borons equivalent	2 signals, δ_H -0.1, -11.5 (5:3)	*d*	3 Mn–H–B bridging H's equivalent, 5 non-bridging H's also equivalent
$(OC)_6Mn_2(\mu\text{-}Br)B_3H_8$[12]	0°C	*Bis*(bidentate)	2 signals, δ_B 10.4 B(2); -38.3 B(1,3)	3 signals (2:2:4), δ_H 3.3, 0.7,-8.3	*d*	Static structure, distinct signals due to Mn–H–B, B–H–B and B–H protons

[a] Not reported, but $Me_2AlB_3H_8$ gives a value of 125 Hz for coupling of B(2) to terminal H's (see reference 18). [b] $J(^{11}B-^{1}H_t)$ for basal borons, B(1,3). [c] $J(^{11}B-^{1}H_b)$ for basal borons, B(1,3). [d] Not reported.

Table 2.2(b) NMR properties of some typical octahydrotriborate complexes in solution.

Compound	Structure	^{11}B Spectrum	$J(^{11}B-^{1}H)$	Comments
Metallaboranes				
B_5H_9[21]	1 apical, 4 basal boron atoms	2 signals (1:4), δ_B -12.5, multiplet (B_{basal}); -51.8, doublet (B_{apical})	166 Hz[a] 38 Hz[b]	Each basal boron coupled strongly to single terminal H, more weakly to two bridging H's. $^{11}B[^{1}H]$ reveals coupling to B_{apical}
$(OC)_3FeB_4H_8$[22]	Formally derived from B_5H_9 by replacement of apical BH by $Fe(CO)_3$	1 signal, δ_B 4.69, broad doublet	162 Hz	Only coupling to terminal H's resolved.
$(OC)_6Fe_2B_3H_7$[23]	Apical and one basal BH units formally replaced by $Fe(CO)_3$	2 signals (2:1), δ_B 4.2 (doublet), 12.4 (quartet)	*c*	Two of the three borons related by mirror plane and hence only two signals
$(OC)_9Ru_3B_2H_6$[24]	Apical and two basal BH units formally replaced by $Ru(CO)_3$	1 signal, δ_B 17.0	*c*	^{1}H spectrum shows signals due to Ru–H–M and B–H–B protons, so the boron atoms must be adjacent

[a] Coupling to terminal protons. [b] Coupling to bridging protons. [c] Not reported.

Table 2.2(c) NMR properties of selected metallaboranes in solution.

interconverting bridging and terminal hydrogens, possibly *via* an intermediate incorporating a different number of bridging hydrogens, although quantum mechanical tunnelling has also been invoked as a possible explanation.[4]

Lowering the temperature of the sample, in order to slow down the rate of bridge/terminal hydrogen exchange, results in collapse of the multiplet structure and eventual "washing out" of the B–H coupling. This phenomenon, known as "correlation time decoupling," is due to rapid spin-lattice relaxation of ^{11}B (and ^{10}B) nuclei, principally through interaction of the nuclear quadrupole moment with the rapidly rotating electric field gradient. In general the spin-lattice relaxation time, T_1, is related to the temperature (T) and macroscopic viscosity (η) of the sample through $T_1 \alpha T/\eta$. Cooling the sample usually causes its viscosity to increase, and hence T_1 to decrease, resulting in more rapid interconversion between ^{11}B (and ^{10}B) spin states; this leads ultimately, to decoupling of ^{11}B and ^{1}H nuclei.

(b) Octahydrotriborate derivatives

Metal octahydrotriborate derivatives show a range of fluxional behaviour in solution. Essentially uncomplexed $B_3H_8^-$ salts (*e.g.* NaB_3H_8[19]) typically show ^{11}B and ^{1}H resonances consistent with magnetic equivalence of all the boron and hydrogen atoms even at low temperatures. This has been attributed to a fast intramolecular rearrangement, possibly involving pseudorotation.[25] Covalently bound octahydrotriborate derivatives tend to be less fluxional; some, such as $Me_2GaB_3H_8$,[20] display two resonances in the ^{11}B NMR spectrum [with relative intensities 2:1] consistent with distinct "apical" and "hinge" environments, although in several cases these resonances converge at higher temperatures.[26] Coupling patterns of the ^{11}B resonances, though often apparently simple, are invariably determined by second order effects. ^{1}H spectra of covalently bound B_3H_8 derivatives are often broad and uninformative as a result of coupling to quadrupolar ^{11}B and ^{10}B nuclei and in some cases, intramolecular exchange processes. Broad-band or selective ^{11}B decoupling is often used in order to help interpret such spectra.

(c) Metallaboranes

^{1}H and ^{11}B NMR measurements have played important rôles in the characterization of cluster compounds containing both metal and boron atoms. Several of the important generalizations derived from such studies are discussed here.

Boron atoms occupying apical position in clusters tend to give rise to ^{11}B chemical shifts at lower frequency than do basal boron atoms (*e.g.* δ_B -51.8 and δ_B -12.5, respectively, for the apical and basal boron atoms in B_5H_9). Successive replacement of boron atoms by metal atoms within a cluster [for example, in the series B_5H_9, $(OC)_3Fe(B_4H_8)$, $(OC)_6Fe_2(B_3H_7)$ and $(OC)_9Ru_3(B_2H_6)$] usually causes the signals due to the remaining boron nuclei to move to higher frequency.[27]

The chemical shifts of protons within a cluster are generally indicative of their nature, *viz.* B–H (terminal), B–H–B (bridging), M–H–B (bridging), M–H–M (bridging) or M–H (terminal).[28] Furthermore, examination of ^{11}B-^{1}H coupling constants allows differentiation between signals due to terminal and bridging hydrogen atoms, [$J(^{11}B$-$^{1}H)$ typically being > 100 Hz for terminal protons but < 60 Hz for bridging protons].

2.2.3 Diffraction Studies

In order to understand more fully aspects of bonding and chemical reactivity of metal tetrahydroborate complexes, it is first necessary to have a firm structural foundation on which to base arguments. To this end, numerous studies involving X-ray, neutron or electron diffraction have been carried out.[4]

(a) X-ray Diffraction

In most areas of chemistry today, the proposal of a novel or unexpected structure gains much weight if based upon the results of X-ray diffraction of a single crystal. However, in the case of tetrahydroborate derivatives, even if crystals of suitable quality can be grown, the usefulness of this technique is limited, principally by the difficulties inherent in locating hydrogen atoms.

Since X-ray scattering is proportional to the square of the atomic number, it is very difficult accurately to locate hydrogen atoms in the vicinity of metal atoms of much higher atomic number. In addition, the vibrational amplitudes of hydrogen atoms at room temperature are often large, rendering X-ray scattering more diffuse. Even when hydrogen atoms can be located with a degree of certainty, the apparent B–H bond lengths are systematically short. This effect is due to involvement of the single hydrogen 1s electron in bonding, causing the electron density no longer to be symmetrical about the nucleus.

Disorder in crystals is a phenomenon known to occur when there are multiple minima in a potential energy surface (*e.g.* in C_5H_5 complexes[29]), with consequent reduction in the precision of the structural results. Given the known fluxionality of BH_4 derivatives in solution,[30] disordering such as may be derived by rotation around the C_3 axis of a $HB(\mu\text{-}H)_3M$ unit is perfectly plausible.

The problems of disorder and large vibrational amplitudes can often be alleviated by cooling the crystal; this has been successfully achieved in the case of $[Al(BH_4)_3{\cdot}NMe_3]$,[31] for example, although the more accurate location of hydrogen atoms may call for neutron diffraction studies.

(b) Neutron Diffraction

Neutron scattering amplitudes reflect the nuclear properties of atoms, and since the amplitude for hydrogen and, better still, deuterium are sufficiently large, precise location of hydrogen atoms is made possible by using this technique. Nuclear scattering also eliminates the systematic shortening of bonds to hydrogen inherent in the X-ray diffraction experiment. However, the large size (0.5-5 mm) of single crystals required for such studies, together with the high cost and low intensity of the neutron beam, restricts the widespread use of this method.

(c) Gas-phase Electron Diffraction

For information about a molecule free from the distortions imposed by crystal

packing forces, electron diffraction is an extremely useful technique. Electron scattering arises from the electrostatic potentials of atoms and, as with X-ray diffraction, the intensity of scattering by an atom depends upon the atomic number. The existence of nuclear and electronic components to the scattering, however, eliminates the phenomenon of anomalously short bonds to hydrogen. The technique is limited, however, to those compounds which give rise to a sufficient flux of molecules in the vapour phase without decomposition. The presence in the vapour of impurities is another potential problem, particularly if the impurity molecule has interatomic spacings similar to the molecule under investigation.

The amount of information contained in a single electron-diffraction plate is very small in comparison with what can be achieved by collection of several thousand reflections during the X-ray diffraction of a single crystal. Consequently electron diffraction is suitable only for quite small, symmetrical molecules, and, even then, determination of all structural parameters may not be possible because of problems of correlation caused by overlapping of peaks in the radial-distribution curve. In addition, it may not be possible to differentiate between two quite distinct structural models on the basis of electron-diffraction results, as appears to be the case with the compound beryllium *bis*(tetrahydroborate).[32]

2.3 Physical Measurements

2.3.1 Infrared Spectroscopy

Infrared spectra in the range 400-4000 cm^{-1} were normally recorded on a Mattson "Polaris" or Mattson "Galaxy" FT-IR spectrometer operating at a maximum resolution of 0.5 cm^{-1}. Measurements in the range 200-400 cm^{-1} were made with a Perkin-Elmer Model 580B dispersive instrument.

Compounds with sufficient stability and vapour pressure at room temperature were sampled in the gas phase by allowing the vapour to expand into a Pyrex-bodied cell

with a path length of *ca.* 10 cm fitted with caesium iodide windows. Measurements involving compounds of limited thermal stability or low volatility were carried out at low temperature with the aid of a "cold cell" (Figure 2.4). The sample vapour was admitted *via* an inlet nozzle and condensed as a thin, polycrystalline film on a caesium iodide window held perpendicular to the molecular beam and cooled to -196°C using a liquid nitrogen reservoir. Good thermal contact between the window and the reservoir was achieved *via* a copper block and indium gaskets. After deposition of the sample, the window could be rotated by means of a ground-glass joint lubricated with silicone grease to realign it parallel to the outer caesium iodide windows, thereby enabling the spectrum of the condensate to be measured. The sample could be annealed as required by pouring away the liquid nitrogen and, if necessary, replacing it with another refrigerant. It was also possible to investigate reactions using the cold cell by co-condensing the reagents on the central window at -196°C, and allowing the condensate to warm slowly; the course of the reaction could then be monitored by reference to the infrared spectrum of the deposit. Solid samples were investigated in the form of discs formed by compressing a powdered sample with a ten-fold excess of dry, powdered KBr in the glove box. The KBr was pre-conditioned by heating under continuous pumping.

2.3.2 Infrared Spectroscopy of Matrix-Isolated Species

One of the principal uses of matrix isolation is to permit spectroscopic measurements to be made on species whose volatility or stability is too low to allow direct investigation of the vapour phase.[33] Typically the method involves trapping a molecule in a weakly interacting solid host at low temperatures. This technique proved particularly useful in obtaining infrared measurements for compounds which could not be studied satisfactorily in the vapour phase, although the bands are typically shifted from the "true" gas-phase frequencies by interaction with the host lattice. Furthermore, infrared absorptions are often split by so-called "matrix site effects" resulting from the occupation by guest molecules of a number of different sites within the solid host. On

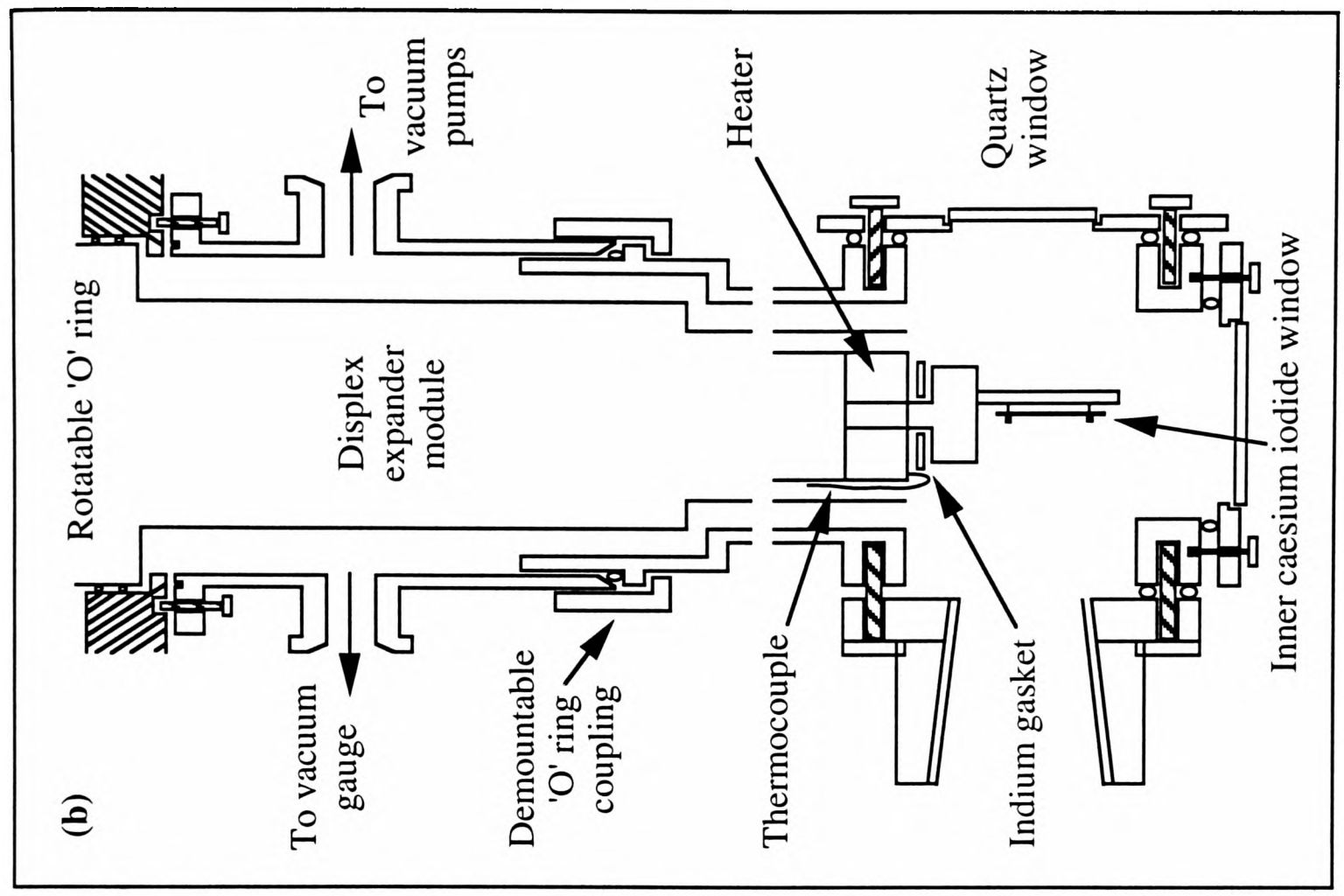

Figure 2.4 Schematic diagrams (a) of the 'cold' cell and (b) of the matrix shroud used in these investigations.

the other hand, matrix-isolated species usually give extremely sharp infrared absorptions since the matrix cage has the effect of quenching the rotational motion of the captive molecule.

The apparatus used in these studies, depicted in Figure 2.4, provided for condensation of samples on a caesium iodide window enclosed within an evacuated shroud and cooled to *ca.* 20 K by an Air Products CS202 "Displex" unit (in effect a two-stage closed-cycle helium refrigerator). The temperature of the window could be varied by the use of a resistive heater and monitored by a thermocouple, each of these being attached to the cold stage of the refrigerator.

Samples were deposited using the so-called "slow spray-on" method over a period of 1-4 h with a 500-fold excess of matrix gas (nitrogen or argon). The rate of depositon of the material to be isolated was controlled by immersing the ampoule containing the sample in an appropriate low-temperature bath, thereby regulating its vapour pressure.

2.3.3 FT-Raman Spectroscopy

FT-Raman spectra of solid samples sealed within evacuated, thin-walled 5 mm Pyrex tubes were recorded on a Perkin Elmer NIR FT-Raman 1700X instrument, being excited by a CW Nd-YAG laser (Spectron Ltd.) operating at a wavelength of 1064 nm. The spectrometer was located in the Chemistry Department at the University of Southampton. Barium sulphate was used as a standard with which to align the laser prior to insertion of the sample into a similar holder. In order to counter the thermal fragility of some of the compounds as well as their tendency to decompose under the action of the laser beam, cooling of the sample, typically to -196°C, could be achieved using a specially designed cold cell. This enabled the sample to be held in an atmosphere of helium which served as a heat exchanger between the sample and the refrigerant of choice.

2.3.4 NMR Spectroscopy

NMR spectra were recorded on Bruker FT Model AM 300 and Varian UNITY-plus 500 spectrometers operating ,respectively, at 300.13 and 499.87 MHz for ^{1}H and 96.25 and 160.37 MHz for ^{11}B measurements. Both spectrometers incorporated facilities for low-temperature and double-resonance experiments. Solution samples were made by co-condensation of the dry deuteriated solvent with the sample in a pre-conditioned 5 mm Pyrex glass NMR tube, or by condensation of the solvent in a pre-conditioned Pyrex glass U-tube containing the sample, followed by tipping of the resultant solution into an NMR tube attached *via* a side-arm, prior to sealing off.

2.3.5 Mass Spectroscopy

Mass spectra were recorded on two different instruments.

(i) Some measurements were made with an AEI MS 302 mass spectrometer updated with a data-handling system from Mass Spectrometry Services Ltd and equipped with an evacuable all-glass inlet system. This is a low-resolution instrument, with ionization effected by electron impact (8 kV accelerating voltage).

(ii) Studies of methylzinc tetrahydroborate vapour also made use of a Hiden HAL/3F residual gas analyser located in the Department of Chemistry at the University of Edinburgh.

2.3.6 Chemical analysis

Microanalysis of air- and moisture-sensitive compounds was performed by the Analytische Laboratorien Gmbh, Gummersbach, Germany. Analysis of air-stable solids and solutions was performed by the Microanalytical Department of the Inorganic Chemistry Laboratory at Oxford.

2.3.7 X-ray Crystallography

Many of the deductions about physical and chemical properties made during the course of this research depended principally on the the results of X-ray crystallographic studies. In cases of wholly new or unexpected structural types, the deduction even of gross structural features on the basis of spectroscopic measurements proved to be difficult. Even in cases where such measurements yielded appreciable information, differentiation, for example between $M^+BH_4^-M^+$ and $M(\mu\text{–}H)_2B(\mu\text{–}H)_2M$ formulations (for $[MeZnBH_4]$ and $[Me_2AlBH_4]$) could be made ultimately only by recourse to the results of X-ray diffraction experiments.

2.3.7.1 Crystal growth

The quality of crystals used in X-ray diffraction studies is of paramount importance, especially in the case of metal tetrahydroborate derivatives where location of hydrogen atoms plays a vital part in determining the mode of coordination.

(a) Growth of Crystals from the Vapour Phase

Two of the compounds investigated, $[MeZnBH_4]$ and $[(MeZn)_2B_3H_7]_2$, were prepared by the reaction in the gas phase between $[Me_2Zn]$ and the appropriate borane ($[B_2H_6]$ and $[B_4H_{10}]$, respectively). The apparatus used for producing and manipulating crystals of these compounds suitable for X-ray diffraction has been described previously (Section 2.1.3), and specific details relating to the procedure used for each compound are described in the appropriate chapter.

(b) Growth of Crystals from the Liquid Phase[34]

Several of the compounds studied were liquid at ambient temperatures, and the growth of single crystals was brought about by using careful cooling with the sample already mounted on the diffractometer itself. Typically, the compound in question was

condensed in a Pyrex glass capillary of 0.2-0.7 mm in diameter to a depth of *ca.* 2 cm. The capillary was then sealed under vacuum to a length of not greater than 3 cm and secured with Araldite glue in a stainless steel pip which was then fixed to a goniometer head and mounted in the cold stream of an Oxford Cryosystems low-temperature device attached to a Stoë Stadi-4 four circle diffractometer.[35] The apparatus is shown schematically in Figure 2.5(a), and the procedure for crystal growth outlined in Figure 2.5(b). For compounds which have more than one solid phase, growth of crystals *via* this method gives access only to the high-temperature form. In order to obtain a single crystal of the phase stable at lower temperatures, the entire sample can be frozen to a temperature below the transition temperature and a crystal then grown by zone-refining techniques.[36] In practice, this involved moving a thin, heated copper wire along a section of the stationary sample, creating a mobile liquid zone, behind which a single crystal could grow. The quality of crystals grown using this technique was found to be inferior to that of crystals grown by the simpler slow cooling method.

Crystals grown using either technique were photographed to ascertain their quality. Measurements on a crystal grown *via* the slow cooling method were then typically made with the crystal at 20 K below the melting point to obtain a provisional data set, prior to final cooling to 150 K to secure a better data set. This procedure ensured that even if crystallinity was lost on cooling to 150 K (as a result of a phase change, for example), the results collected at the higher temperature were still available.

(c) Data Collection and Processing

Where possible (within the constraints of phase transition temperatures), X-ray data were collected with the crystals at 150 K. As already outlined (Section 2.2.3) this improves the quality of the data collected and thus offers the best chance of locating hydrogen atoms.

All structure solutions and refinements were carried out by Drs. S. Parsons and S. Blake in the Chemistry Department at the University of Edinburgh.

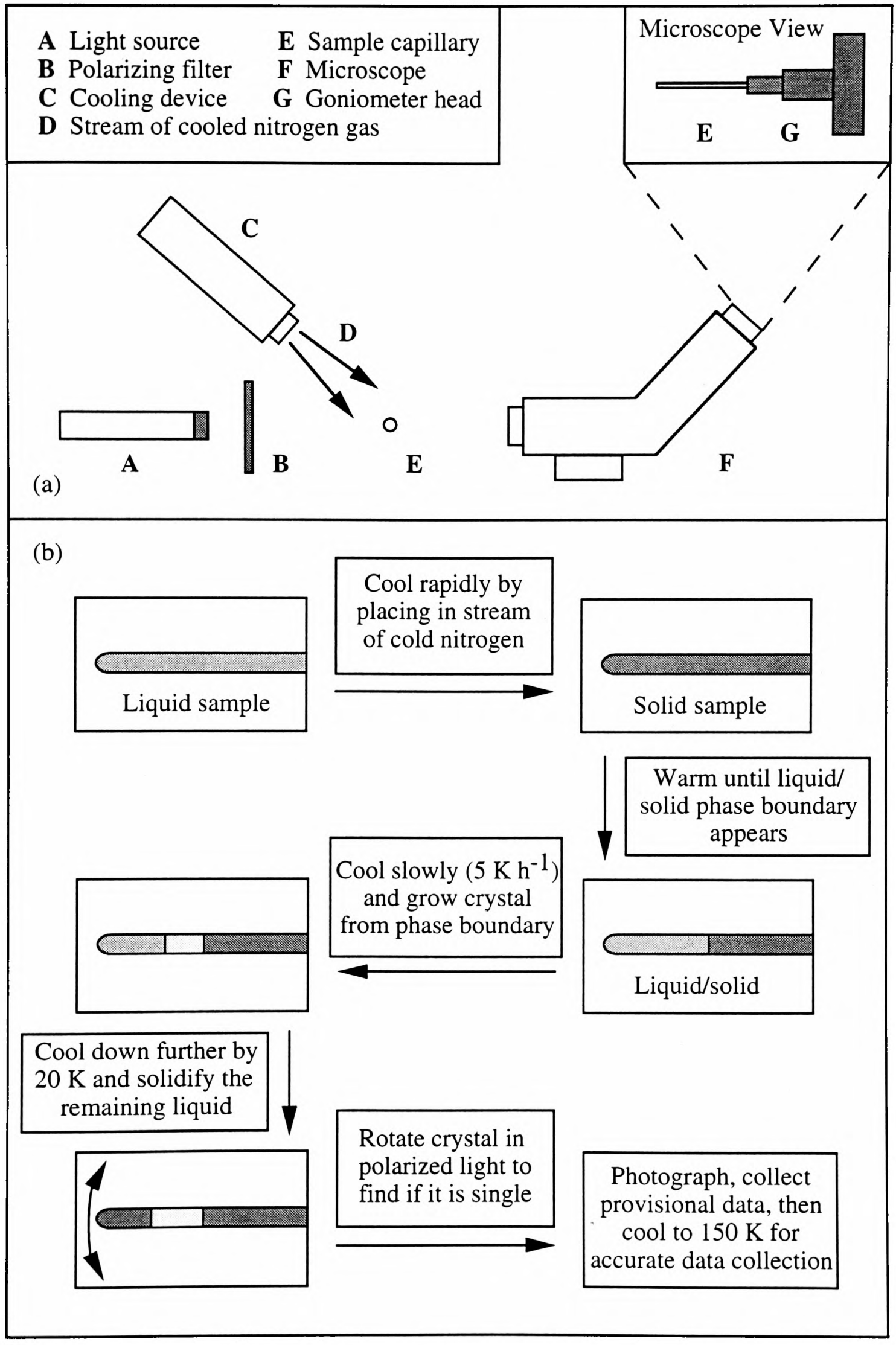

Figure 2.5 (a) Schematic diagram of the low-temperature crystal-growing apparatus. (b) Key steps in crystal growth by controlled cooling of a liquid sample.

2.3.8 Theoretical Calculations

All calculations were carried out by M. Hofmann of Professor P. von Ragué Schleyer's research group at the University of Erlangen-Nürnberg. Computations made use of the GAUSSIAN 92 package of programs[37] and standard procedures.[38] The basis sets used were the fully optimized contracted Gaussian basis sets reported by Ahlrichs *et al.*[39] The split valence (sv) basis set was augmented by polarization functions on the heavy atoms only (resulting in svp) with the following exponents:

B 0.6 (one set of d orbitals)

C 0.8 (one set of d orbitals)

Zn 0.123 (one set of p orbitals)

For the larger triple zeta (tz) basis set polarization functions were also included on the hydrogen atoms, the exponents in this case being:

B 0.401 (one set of d orbitals)

C 0.626 (one set of d orbitals)

Zn 0.055 (two sets of p orbitals)

H 0.750 (one set of p orbitals)

Geometries were optimized at the SCF level of theory; analytical frequency calculations were carried out at the HF/svp level making use of the harmonic approximation to obtain vibrational frequencies and to determine the nature of the stationary points.

2.4 Preparation and Purification of Essential Reagents and Solvents

Many of the compounds synthesized during the course of this research had as precursors, compounds which were not themselves readily available. Such starting materials had, therefore, to be prepared from commercially available laboratory chemicals. In addition, it was often necessary to purify *these* reagents prior to use; solvents, too, were invariably subjected to rigorous drying and purification procedures.

Table 2.3 records the sources and steps taken for purification of commerically available precursors, and Table 2.4 the methods of purification used for those starting materials which were either unavailable commercially or prohibitively expensive.

Table 2.3 Sources of chemicals.

Compound	Source	Quoted purity	Procedure
Reagents			
Zinc powder	Aldrich	>95 %	Heated to 210°C for 5 h under continuous pumping
Copper powder	Aldrich	99.5 %	
Methyl iodide	Aldrich	99.5 %	Distillation from flamed-out molecular sieves
Red phosphorus	Aldrich	99 %	Washed with water then dried in a desiccator
$NaBH_4$	B.D.H.	98 %	Used as supplied
$LiBH_4$	Aldrich	95 %	Recrystallization from dry diethyl ether
Sulphuric acid	B.D.H	97-99 %	Outgassed by continuous pumping
Nitric acid	B.D.H.	*a*	Outgassed by repeated freeze-pump-thaw cycles
Ammonia	B.O.C.	99 %	Condensed on sodium, then trap-to-trap distillation *in vacuo*
Carbon monoxide	B.O.C.	99.9995 %	Used as supplied
Dimethyl sulphide	Aldrich	>99.5 %	Heated under reflux over sodium, then fractional distillation in a dry nitrogen atmosphere
Triphenylphosphine	*b*	*a*	Recrystallization from a mixture of diethyl ether and THF
Hydrogen chloride	Air Products	99.6 %	Used as supplied
Iodine	Aldrich	99.999 %	Used as supplied
$[^nBu_4N]I$	Aldrich	98 %	Used as supplied
Trimethylaluminium	Aldrich	97 %	Trap-to-trap distillation *in vacuo*
Aluminium trichloride	Aldrich	99.99 %	Used as supplied
Dimethylmercury	Aldrich	95 %	Trap-to-trap distillation *in vacuo*

a Information not available. *b* Courtesy of Mr. T. James, Inorganic Chemistry Laboratory, Oxford.

Table 2.3 (cont.) Sources of chemicals.

Compound	Source	Quoted purity	Procedure
Indium powder	Aldrich	99.999 %	Heated to 120°C for 6 h under continuous pumping
Boron tribromide	Aldrich	99.9 %	Condensed on mercury then trap-to-trap distillation *in vacuo*
Deuteriated reagents			
$[^2H_4]$Methanol	Aldrich	99.8 atom %	Distillation from flamed-out molecular sieves
Solvents			
Diethyl ether	Fisons	99.5 %	Heated under reflux over CaH_2, followed by distillation
Dichloromethane	Fisons	99 %	Heated under reflux over P_2O_5, followed by distillation
Diglyme	Aldrich	>99 %	Heated under reflux over sodium, followed by distillation
Methanol	B.D.H.	99 %	Distillation from flamed-out molecular sieves
Toluene	Prolabo	99 %	Heated under reflux over sodium, followed by distillation
Deuteriated solvents			
$[^2H_8]$Toluene	Aldrich	>99 atom %	Distillation from flamed-out molecular sieves
$[^2H_8]$Tetrahydrofuran	Aldrich	>99 atom %	
$[^2H_2]$Dichloromethane	Aldrich	>99.6 atom %	
Matrix gases			
Argon	B.O.C.	99.9995 %	Used as supplied
Nitrogen	B.O.C.	99.994 %	Used as supplied

Compound	Synthesis	Purification	Assessment of purity	References	
				Prep.	Purity
CD_3I	$6CD_3OD + 2P + 3I_2 \longrightarrow 6CD_3I + 2DP(O)(OD)_2$ Crystalline iodine added slowly to cooled mixture of [$^2H_4$]methanol and red phosphorus. Product was distilled and collected under water. Traces of I_2 removed with sodium thiosulphate.	Final purification brought about by trap-to-trap distillation *in vacuo* and drying on flamed-out molecular sieves	IR spectrum of the vapour	40	41
$(CH_3)_2Zn$/ $(CD_3)_2Zn$	$2Zn + 2CH_3I \xrightarrow{\text{Copper}} (CH_3)_2Zn + ZnI_2$ Methyl iodide condensed on a mixture of baked-out copper and zinc powders in a thick-walled ampoule. Ampoule sealed and heated to 150°C for 36 h.	Trap-to-trap distillation *in vacuo*	IR spectrum of the vapour. ^1H NMR spectrum of solution	42	43, 44
$(CH_3)_3In$	$3(CH_3)_2Hg + 2In \longrightarrow 2(CH_3)_3In + 3Hg$ Condensation of dimethyl mercury on an excess of dried indium powder in a high-pressure Pyrex glass tube. Tube sealed off and heated to 150°C for 48 h.	Repeated sublimation *in vacuo*	IR spectrum of the solid. ^1H NMR spectrum of solution	45	46, 47
B_2H_6	$2H_2SO_4 + 2NaBH_4 \longrightarrow 2NaHSO_4 + H_2 + B_2H_6$ Slow addition of $NaBH_4$ to constantly-stirred out-gassed H_2SO_4. Removal of volatile products under continuous pumping.	Trap-to-trap distillation *in vacuo*	IR spectrum of the vapour. Vapour pressure at -111°C	48	49, 50

Table 2.4 Preparation and Purification of Starting Materials.

Compound	Synthesis	Purification	Assessment of purity	References	
				Prep.	Purity
B_2D_6	$GaCl_3 + 3LiBD_4 \longrightarrow DGa(BD_4)_2 + 3LiCl + 1/2B_2D_6$ By-product from the preparation of $DGa(BD_4)_2$ Sample provided by courtesy of Mr. P.F. Souter.	Trap-to-trap distillation *in vacuo*	IR spectrum of the vapour	51	49
$[^nBu_4N][B_3H_8]$	$3NaBH_4 + I_2 \xrightarrow{\text{Diglyme}} NaB_3H_8 + 2H_2 + 2NaI$ $NaB_3H_8 + [^nBu_4N]I \xrightarrow{\text{Water}} [^nBu_4N][B_3H_8] + NaI$ Slow addition of iodine solution to a vigorously stirred slurry of $NaBH_4$ in diglyme at 100°C. Cautious addition of the resultant solution to an aqueous solution of $[^nBu_4N]I$.	Washing with water to remove excess of $[^nBu_4N]I$, pumped to dryness, ground up and pumped on again. Recrystallization from a mixture of dry Et_2O/CH_2Cl_2 under nitrogen.	IR spectrum of the solid	52	52
B_4H_{10}	$[^nBu_4N][B_3H_8] + BBr_3 \longrightarrow 1/2B_4H_{10} + 1/n[BH_2]_n + [^nBu_4N][HBBr_3]$ Continuous stirring of finely-divided $[^nBu_4N][B_3H_8]$ with freshly distilled BBr_3 *in vacuo* at 0°C for 2-3 h.	Trap-to-trap distillation *in vacuo*	IR spectrum of the vapour	53	54
$Al(BH_4)_3$	$AlCl_3 + 3LiBH_4 \longrightarrow Al(BH_4)_3 + 3LiCl$ Excess (4 equiv.) of $LiBH_4$ stirred with $AlCl_3$ (no solvent). Reaction mixture heated to 80°C and volatile product removed under continuous pumping.	Trap-to-trap distillation *in vacuo*	IR spectrum of the vapour	55	56

Table 2.4 (cont.) Preparation and Purification of Starting Materials.

References for Chapter 2

1. D.F. Shriver and M.A. Drezdzon, *The Manipulation of Air-Sensitive Compounds*, 2nd edn., Wiley-Interscience, 1986.
2. R.T. Sanderson, *Vacuum Manipulation of Volatile Compounds,* Chapman and Hall, 1940.
3. R.E. Dodd and P.L. Robinson, *Experimental Inorganic Chemistry*, Elsevier, 1954.
4. T.J. Marks and J.R. Kolb, *Chem. Rev.*, 1977, **77**, 273.
5. J.W. Nibler, D.F. Shriver and T.H. Cook, *J. Chem. Phys.*, 1971, **54**, 5257.
6. T.J. Marks and G.W. Grynkewich, *Inorg. Chem.*, 1976, **15**, 1302.
7. B.E. Green, C.H.L. Kennard, G. Smith, B.D. James, P.C. Healy and A.H. White, *Inorg. Chim. Acta*, 1984, **81**, 147.
8. F. Cariati and L. Naldini, *J. Inorg. Nucl. Chem.*, 1966, **28**, 2243.
9. J. Tomkinson, C.J. Ludman and T.C. Waddington, *Spectrochim. Acta*, 1979, **35A**, 117.
10. D.F. Gaines and S.J. Hildebrandt, *Inorg. Chem.*, 1978, **17**, 794.
11. D.F. Gaines and S.J. Hildebrandt, *J. Am. Chem. Soc.*, 1974, **96**, 5574.
12. M.W. Chen, D.F. Gaines and L.G. Hoard, *Inorg. Chem.*, 1980, **19**, 2989.
13. T.J. Marks and L.A. Shimp, *J. Am. Chem. Soc.*, 1972, **94**, 1542.
14. P.R. Oddy and M.G.H. Wallbridge, *J. Chem. Soc., Dalton Trans.*, 1976, 869.
15. J.C. Bommer and K.W. Morse, *J. Chem. Soc., Chem. Commun.*, 1977, 137.
16. T.P. Onak, H. Landesman, R.E. Williams and I. Shapiro, *J. Phys. Chem.*, 1959, **63**, 1533.
17. G.R. Eaton and W.N. Lipscomb, *NMR Studies of Boron Hydrides and Related Compounds*, Benjamin, 1969; D.F. Gaines, R. Schaeffer and F. Tebbe, *J. Phys. Chem.*, 1963, **67**, 1937; D.F. Gaines, *Inorg. Chem.*, 1963, **2**, 523.

18. (a) H.D. Empsall, E. Mentzer and B.L. Shaw, *J. Chem. Soc., Chem. Commun.*, 1975, 861; (b) J.B. Letts, T.J. Mazanec and D.W. Meek, *J. Am. Chem. Soc.*, 1982, **104**, 3898.

19. R.E. Williams, *J. Inorg. Nucl. Chem.*, 1961, **20**, 265.

20. J.J. Borlin and D.F. Gaines, *J. Am. Chem. Soc.*, 1972, **94**, 1367.

21. J.D. Odom, P.D. Ellis and H.C. Walsh, *J. Am. Chem. Soc.*, 1971, **93**, 3529.

22. N.N. Greenwood, C.G. Savory, R.N. Grimes, L.G. Sneddon, A. Davison and S.S. Wreford, *J. Chem. Soc., Chem. Commun.*, 1974, 718.

23. E.L. Andersen, K.J. Haller and T.P. Fehlner, *J. Am. Chem. Soc.*, 1979, **101**, 4390.

24. C.R. Eady, B.F.G. Johnson and J. Lewis, *J. Chem. Soc., Dalton Trans.*, 1977, 477.

25. W.N. Lipscomb, *Adv. Inorg. Chem. Radiochem.*, 1959, **1**, 132.

26. See, for example, D.F. Gaines and S.J. Hildebrandt, in *Metal Interactions with Boron Clusters*, ed. R.N. Grimes, Plenum Press, 1982, p. 119.

27. N.P. Rath and T.P. Fehlner, *J. Am. Chem. Soc.*, 1988, **110**, 5345.

28. See, for example, C.E. Housecoft, *Boranes and Metallaboranes: Structure, Bonding and Reactivity*, 2nd edn., Ellis Horwood, 1994.

29. R.A. Schunn, C.J. Fritchie and C.J. Prewitt, *Inorg. Chem.*, 1966, **5**, 892.

30. H. Beall and C.H. Bushweller, *Chem. Rev.*, 1973, **73**, 465.

31. N.A. Bailey, P.H. Bird and M.G.H. Wallbridge, *J. Chem. Soc., Chem. Commun.*, 1965, 438; N.A. Bailey, P.H. Bird and M.G.H. Wallbridge, *J. Chem. Soc., Chem. Commun.*, 1966, 286.

32. G. Silibiger and S.H. Bauer, *J. Am. Chem. Soc.*, 1946, **68**, 312; S.H. Bauer, *J. Am. Chem. Soc.*, 1950, **72**, 622; A. Almenningen, G. Gundersen and A. Haaland, *J. Chem. Soc., Chem. Commun.*, 1967, 557; A. Almenningen, G. Gundersen and A. Haaland, *Acta Chem. Scand.*, 1968, **22**, 859; G. Gundersen, L. Hedberg and K. Hedberg, *J. Chem. Phys.*, 1973, **59**, 377; K. Brendhaugen, A. Haaland and D.P. Novak, *Acta Chem. Scand.*, 1975, **29A**, 801.

33. See, for example, A.J. Downs and S.C. Peake in *Molecular Spectroscopy,* Chemical Society Specialist Periodical Reports, Vol. 1, 1973, Chapter 9; M.J. Almond and A.J. Downs, *Adv. Spectrosc.*, 1989, **17**, 1.

34. See, for example, R. Rudman, *Low Temperature X-Ray Diffraction. Apparatus and Techniques*, Plenum Press, New York, 1976.

35. J. Cosier and A.M. Glazer, *J. Appl. Crystallogr.*, 1986, **19**, 105.

36. W.D. Lawson and S. Nielsen, *Preparation of Single Crystals*, Butterworths, 1958.

37. M.J. Frisch, G.W. Trucks, M. Head-Gordon, P.M.W. Gill, M.W. Wong, F.B. Foresman, H.B. Schlegal, K. Raghavachari, M.A. Robb, E.S. Replogle, R. Gomberts, J.L. Andres, J.S. Binkley, C. Gonzalez, R. Martin, D.J. Fox, D.J. DeFreer, J. Baker, J.J.P. Stewart and J.A. Pople, Gaussian Inc., Pittsburgh, 1992.

38. J. Foreman and A.E. Frisch, *Exploring Chemistry with Electronic Structure Methods: A Guide to Using Gaussian*, Gaussian Inc., Pittsburgh, 1993; W.J. Hehre, L. Radom, P.v.R. Schleyer and J.A. Pople, *Ab Initio Molecular Orbital Theory*, Wiley, New York, 1986.

39. A. Schaefer, H. Horn and R. Ahlrichs, *J. Chem. Phys.*, 1992, **97**, 2571.

40. I.B. Douglass, *Int. J. Sulfur Chem.*, 1973, **8**, 441.

41. A.D. Dickson, I.M. Mills and B. Crawford, Jr., *J. Chem. Phys.*, 1957, **27**, 445.

42. N.K. Hota and C.J. Willis, *J. Organomet. Chem.*, 1967, **9**, 169.

43. A.M. Coats, D.C. McKean, H.G.M. Edwards and V. Fawcett, *J. Mol. Struct.*, 1994, **320**, 159.

44. J.F. Hanlan and J.D. McCowan, *Can. J. Chem.*, 1972, **50**, 747.

45. P. Krommes and J. Lorberth, *Inorg. Nucl. Chem. Lett.*, 1973, **9**, 587.

46. J.R. Hall, L.A. Woodward and E.A.V. Ebsworth, *Spectrochim. Acta*, 1964, **20**, 249.

47. N. Muller and A.L. Otermat, *Inorg. Chem.*, 1963, **2**, 1075.

48. H. Schroeder, T.L. Heyling and J.R. Reuer, *Inorg. Chem.*, 1963, **2**, 1092.

49. K. Nakamoto, *Infrared and Raman Spectra of Inorganic and Coordination Compounds,* 4th edn., Wiley, 1986.

50. D.R. Lide (ed.), *Handbook of Chemistry and Physics,* 75th edn., C.R.C. Press, Boca Raton, FL, 1994-1995.

51. A.J. Downs, L.A. Harman, P.D.P. Thomas and C.R. Pulham, *Polyhedron*, 1995, **14**, 935; P.D.P. Thomas, D.Phil. Thesis, University of Oxford, 1977.

52. G.E. Ryschkewitsch and K.C. Nainan, *Inorg. Synth.*, 1974, **15**, 111.

53. M.A. Toft, J.B. Leach, F.L. Himpsl and S.G. Shore, *Inorg. Chem.*, 1982, **21**, 1952.

54. A.J. Dahl and R.C. Taylor, *Inorg. Chem.*, 1971, **10**, 2508.

55. H.I. Schlesinger, H.C. Brown and E.K. Hyde, *J. Am. Chem. Soc.*, 1953, **75**, 209.

56. D.A. Coe and J.W. Nibler, *Spectrochim. Acta*, 1973, **29A**, 1789.

Chapter Three
The Structure and Physical and Chemical Properties of Methylzinc Tetrahydroborate

3.1 Synthesis, Physical Properties and Structure of the Solid

3.1.1 Previous Investigations of Group 12 Metal Tetrahydroborates

Of the Group 12 metal tetrahydroborates, $[Zn(BH_4)_2]$ and $[Cd(BH_4)_2]$ have both been synthesized from $[LiBH_4]$ and the corresponding metal dichloride,[1-3] or by the reaction of $[H_3B{\cdot}THF]$ with the appropriate dimethyl derivative.[3] Furthermore, adducts containing the anions $[M(BH_4)_3]^-$ (M = Zn and Cd) and $[M(BH_4)_4]^{2-}$ (M = Zn) have also been prepared,[3,4] reaction (1) being typical of the synthetic routes employed. Little

$$Cd(BH_4)_2 + LiBH_4 \longrightarrow Li[Cd(BH_4)_3] \qquad (1)$$

is known about the structures of any of these compounds in the solid phase. Similarly, at the outset of the present research, the volatile, white solid methylzinc tetrahydroborate had received relatively little attention since an initial report of its synthesis by Ridley in 1965.[5] Elemental analysis of the compound, estimation of reacting proportions and examination of the infrared spectra of the volatile products led Ridley to postulate that its synthesis can be accomplished *via* reaction (2):

$$2ZnMe_2 + B_2H_6 \longrightarrow BMe_3 + MeZnBH_4 + ZnH_2 \qquad (2)$$

Nibler and Cook investigated the structure of solid methylzinc tetrahydroborate by examination of the infrared and Raman spectra of thin films of normal and deuteriated forms deposited on a caesium iodide window at 12 K.[6] On the basis of

spectra containing no strong absorptions in the regions characteristic of the stretching modes of either terminal or bridging B–H bonds of a covalently bound BH_4 group,[7] it was postulated that the solid is an ionic polymer involving more-or-less discrete $MeZn^+$ and BH_4^- ions, with a structure not unlike that of $[Be(BH_4)_2]$.[8,9]

In view of the dearth of structural data existing for the Group 12 tetrahydroborates in the solid phase, and the necessarily speculative nature of results based purely on spectroscopic information, it was decided to investigate the structure of solid methylzinc tetrahydroborate by X-ray diffraction. In the light of these results it proved necessary also to re-evaluate the infrared spectra of the solid. In addition, a new synthetic route to methylzinc tetrahydroborate was investigated.

3.1.2 Synthesis of Methylzinc Tetrahydroborate

(a) From dimethylzinc and diborane. A method based on, but somewhat revised from that employed by Ridley was used.[5] Typically, a 1-litre bulb guarded by a Young's tap was conditioned by exposure to dimethylzinc vapour at *ca.* 20 Torr pressure for 3 h, this serving to scavenge any residual moisture retained by the Teflon and glass surfaces. Such pre-conditioning was found to increase significantly the yields of methylzinc tetrahydroborate, and to reduce the amounts of non-condensable gas and grey metallic deposits produced. After re-evacuation, diborane (typically 23 mg, 0.83 mmol) and a six-fold excess of dimethylzinc were allowed to react at room temperature over a period of 16 h. In accordance with Ridley's observations,[5] clusters of long, acicular crystals were observed to form. After 16 h the bulb was attached to a train of three traps leading to the main vacuum line. These were cooled to -23, -95, and -196°C. Initially the contents of the bulb were fractionated *in vacuo* in a closed system, the excess of dimethylzinc collecting as a white solid in the -95°C trap, and a mixture of unchanged diborane and a slightly less volatile species collecting in the -196°C trap. This procedure ensured that little $[MeZnBH_4]$ was entrained through the -23°C trap by the more volatile components. Subsequently, $[MeZnBH_4]$ was distilled out of the reaction vessel under

continuous pumping and collected in the -23°C trap as a white polycrystalline solid. Measurements of the infrared spectrum of the contents of the -196°C trap showed that the principal component was $[Me_3B]$[10] (together with some unchanged $[B_2H_6]$).

Attempts to use reaction times significantly shorter than 16 h resulted in relatively poor conversion and the recovery of large quantities of unchanged diborane, whereas much longer reaction times resulted in sizeable amounts of grey decomposition product.

(b) From methylzinc chloride and lithium tetrahydroborate. Typically, methylzinc chloride was prepared *in situ* by the reaction of dimethylzinc (150 mg, 1.59 mmol) with hydrogen chloride (44 mg, 1.2 mmol) at -23°C. After the mixture had been left at room temperature for 2 h to ensure complete reaction, the amount of methane (1.15 mmol) was determined by the use of a Toepler pump, and a quantity of dimethylzinc (0.4 mmol) was also recovered. To the methylzinc chloride so formed were added 100 mg (4.5 mmol) of $[LiBH_4]$, and the solid mixture was stirred for 10 h at room temperature while volatile products were removed and trapped at -196°C under continous pumping. Fractionation of the volatile material gave methylzinc tetrahydroborate in overall yields of 10-15% based on equations (3) and (4) and the

$$ZnMe_2 + HCl \longrightarrow MeZnCl + MeH \quad (3)$$

$$MeZnCl + LiBH_4 \longrightarrow MeZnBH_4 + LiCl \quad (4)$$

amount of dimethylzinc consumed. Small quantities of dimethylzinc were also obtained as a side-product of the final step, possibly through the disproportionation reaction (5).

$$2MeZnCl \longrightarrow ZnMe_2 + ZnCl_2 \quad (5)$$

This, together with the inherently inefficient nature of the reaction, involving as it does the mixing of two solids, may well be responsible for the low yields of $[MeZnBH_4]$.

In conclusion, the synthesis based on the reaction reported by Ridley[5] was found to afford the most convenient route to methylzinc tetrahydroborate, inasmuch as it facilitated growth from the vapour of crystals suitable for X-ray diffraction. Yields, based on reaction (2) and the amount of diborane taken, were typically 40%. This synthetic route is far from ideal, however, being awkward to perform on a scale sufficient to give significant amounts (150 mg or more) of the tetrahydroborate, and involving the manipulation of relatively large quantities of gaseous reagents. Consequently, attempts were made to prepare [$MeZnBH_4$] from the corresponding chloride and [$LiBH_4$], following a commonly used route to tetrahydroborate derivatives exemplified by reaction (6).[11] In fact, this route proved to be inferior, not only in its

$$1/2[H_2GaCl]_2 + LiBH_4 \longrightarrow H_2Ga(\mu\text{-}H)_2BH_2 + LiCl \qquad (6)$$

yields but also in its ability to deliver good crystalline samples of methylzinc tetrahydroborate.

(c) Growth of crystals suitable for X-ray diffraction. Crystals suitable for X-ray diffraction were grown from the vapour using the synthetic route of Ridley.[5] Owing to the tendency of the crystals to decompose, even in the most rigorously dried glove box atmosphere and to sublime, the specially constructed apparatus shown in Figure 2.3 was used to load crystals into Pyrex glass capillaries. After pre-conditioning the entire apparatus, especially the Voltalef 90 grease used ultimately to hold the crystals, the reaction between [Me_2Zn] and [B_2H_6] was carried out in the main bulb only. This prevented the deposition of grey decomposition product on the surface of the grease during the 16 h reaction time. Repetition of the experiment with different vapour pressures of the two reagents revealed that the best crystals could be grown by using 120 Torr of [Me_2Zn] and 20 Torr of [B_2H_6]. Significantly lower vapour pressures resulted in much slower crystal growth and consequently more decomposition on the walls of the reaction vessel, whereas much higher pressures deposited only very small crystals of

poor quality unsuitable for X-ray diffraction. Once suitable crystals had been grown, these were manipulated by the use of the pointed glass-coated stirrer bar and knocked through the "Rotaflo" tap into the cold finger. This operation had to be carried out without prior evacuation of the bulb, since removal of the small proportion of [$MeZnBH_4$] in the vapour phase caused the crystals to sublime. Once in the cold finger, crystals were selected by eye and transferred to the capillaries by careful tapping of the glass vessel. This achieved, the "Rotaflo" tap was shut, the volatile contents of the cold finger were frozen down at -196°C, and the capillaries were quickly sealed using a hand-held torch before the crystals were able to sublime away. Initial attempts to secure the crystals in place without grease were made by forcing them down a tapered capillary until wedged firmly. However, this proved inappropriate for low temperature measurements since contraction of the crystals on cooling caused them to move. Pre-conditioned Voltalef 90 grease was found to be the least reactive with respect to the crystals, and to hold them securely even for data collection at 150 K. Selection of crystals using this method proved to be difficult, and five or six would have to be loaded, typically, in order to produce one suitable for X-ray diffraction measurements.

3.1.3 X-ray Diffraction of Methylzinc Tetrahydroborate Crystals at Low Temperature

Several acicular crystals *ca.* 1 mm in length were loaded in hand-drawn Pyrex capillaries approximately 0.3 mm in internal diameter using the method described in Section 3.1.2. Initial investigation of several crystals by oscillation photography showed that these typically became amorphous over a period of 72 h in keeping with the known thermal instability of the compound (*vide infra*). Consequently, following transferral of the crystal to a diffractometer, data collection was carried out at 150 K.

(a) Crystal data. CH_7BZn, M = 95.25, trigonal, $R3c$, $a = b = 15.831(10)$, $c = 8.36(2)$ Å, $U = 1814(4)$ Å^3, $\lambda = 0.71073$ Å, $Z = 18$, $D_c = 1.569$ g cm^{-3}, $F(000) = 864$,

colourless acicular crystals, 1.00 x 0.10 x 0.05 mm, μ(Mo-Kα) = 5.84 mm^{-1}.

(b) Data Collection. Data were collected on a Stoë Stadi-4 four circle diffractometer with graphite monochromated Mo-Kα X-radiation; ω-2θ mode, ω half width (1.32 + 0.35 tan θ)°. Of the 1693 reflections measured (θ_{max} = 22.5°; $-9 \leq h \leq 16$, $-16 \leq k \leq 8$, $-8 \leq l \leq 8$), 502 were unique. An absorption correction was performed with ψ-scan data (T_{min} = 0.731, T_{max} = 0.938); R = 0.085. Variation of three intensity standards, measured every 60 min of X-ray exposure time, was never greater than 1.5%.

(c) Structure solution and refinement. This was carried out by Drs. S. Parsons and S. Blake of the University of Edinburgh. Following data reduction and the application of an absorption correction, direct methods (SHELXS-86[12]) yielded the position of the zinc atom, and the carbon and boron atoms were located in subsequent difference syntheses. The hydrogen atoms were located in difference maps (SHELXL-93[13]): those on the carbon were refined using a riding model; those on the boron were refined with restraints such that all B–H and all Zn–H bond lengths were set to be equal, as were equivalent HBH angles. All hydrogen atoms were assigned isotropic thermal parameters equal to 1.2 times the equivalent thermal parameters of the atom to which they were joined (*i.e.* the carbon or boron). Refinement (against F^2) converged to a conventional R value of 7.2% [based on F and 462 data with $F > 4\sigma(F)$] and wR_2 = 17.9% (based on F^2 and all 502 data) with anisotropic thermal parameters on all non-hydrogen atoms (41 parameters). The final ΔF synthesis maximum and minimum were +0.66 and -0.63 $eÅ^{-3}$, respectively, and the Flack absolute structure parameter refined to 0.2(2). A fuller account of the data collection, structure solution and refinement parameters can be found in Appendix 1.

(d) Discussion. The structure of [$MeZnBH_4$] is illustrated in Figures 3.1 and 3.2, while the view along the axis of the helix is represented in Figure 3.3. Relevant bond distances and angles can be found in Table 3.1. The structural results show that the

3.1

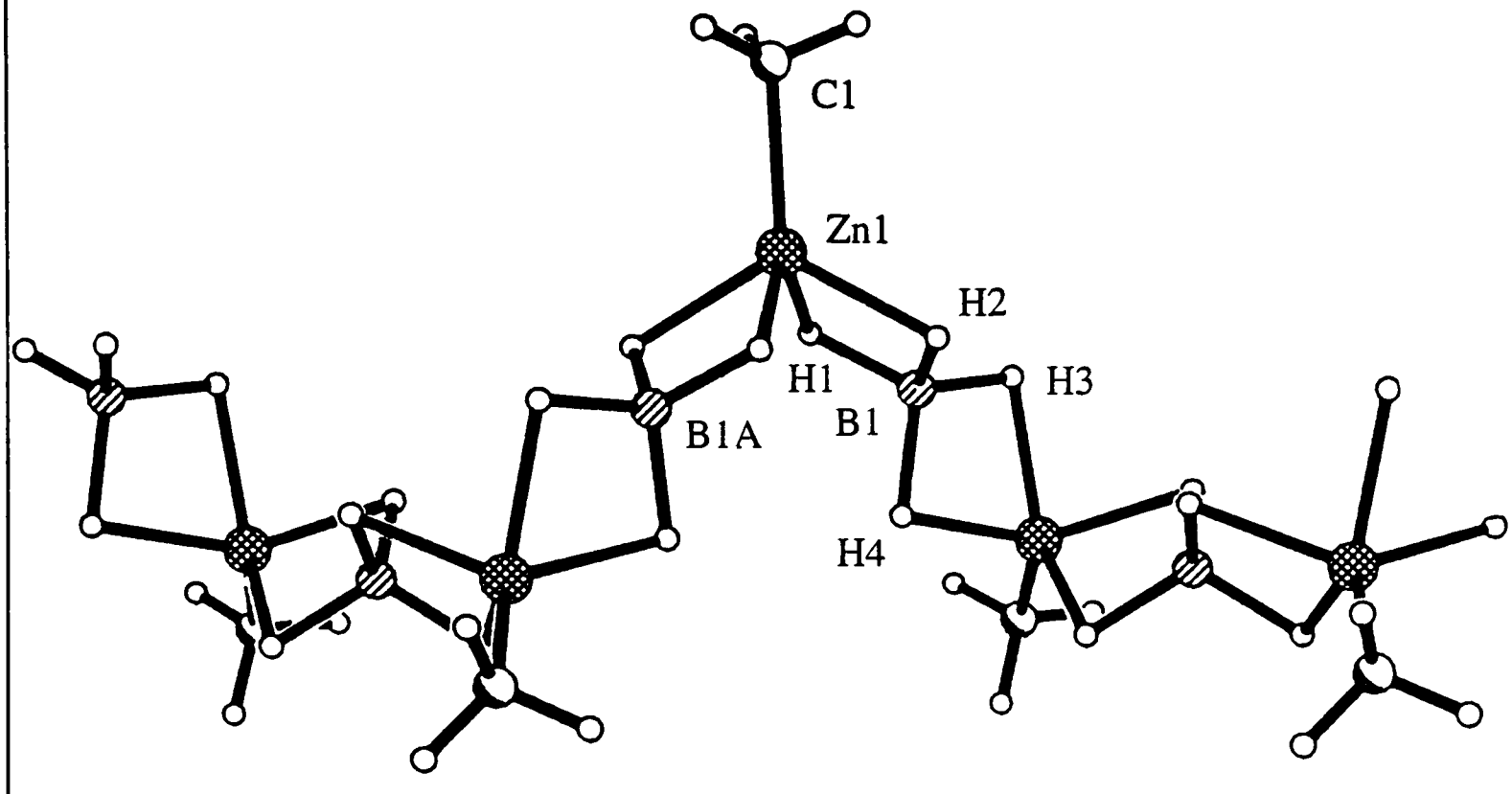

3.2

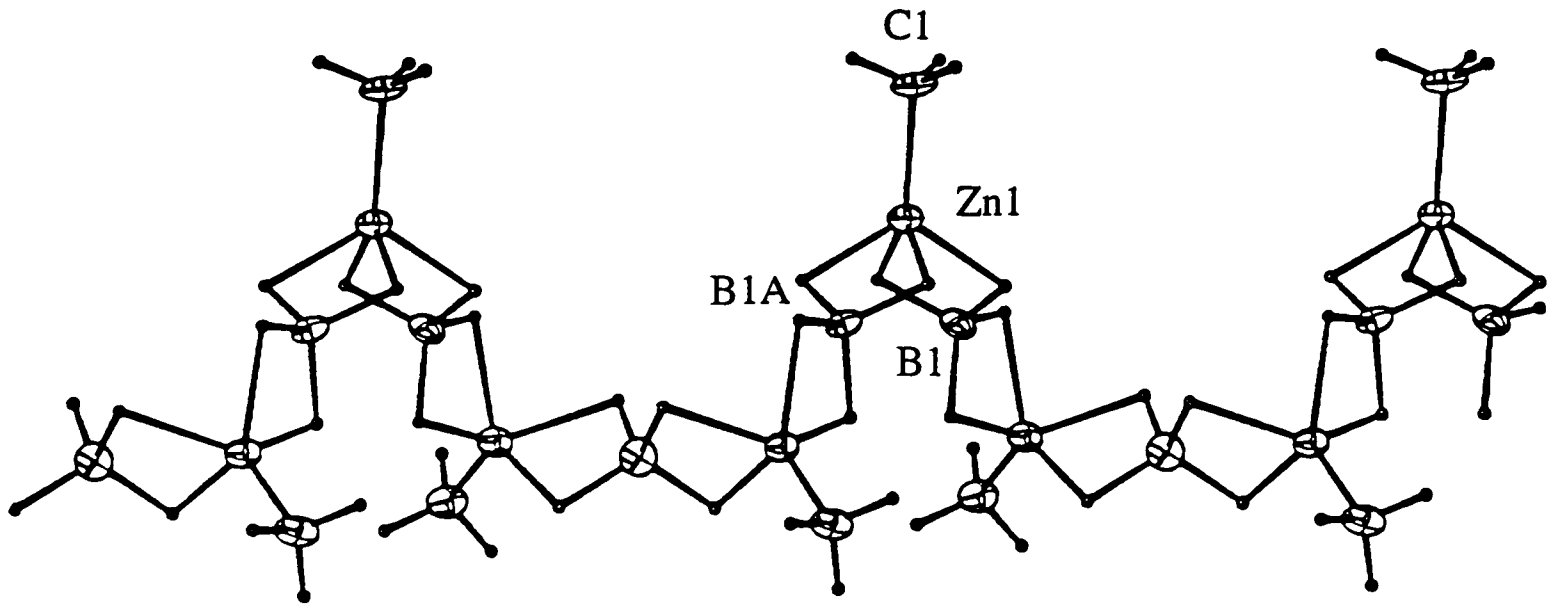

Figures 3.1 and 3.2 The helical polymeric structure of solid methylzinc tetrahydroborate at 150 K as determined by X-ray diffraction.

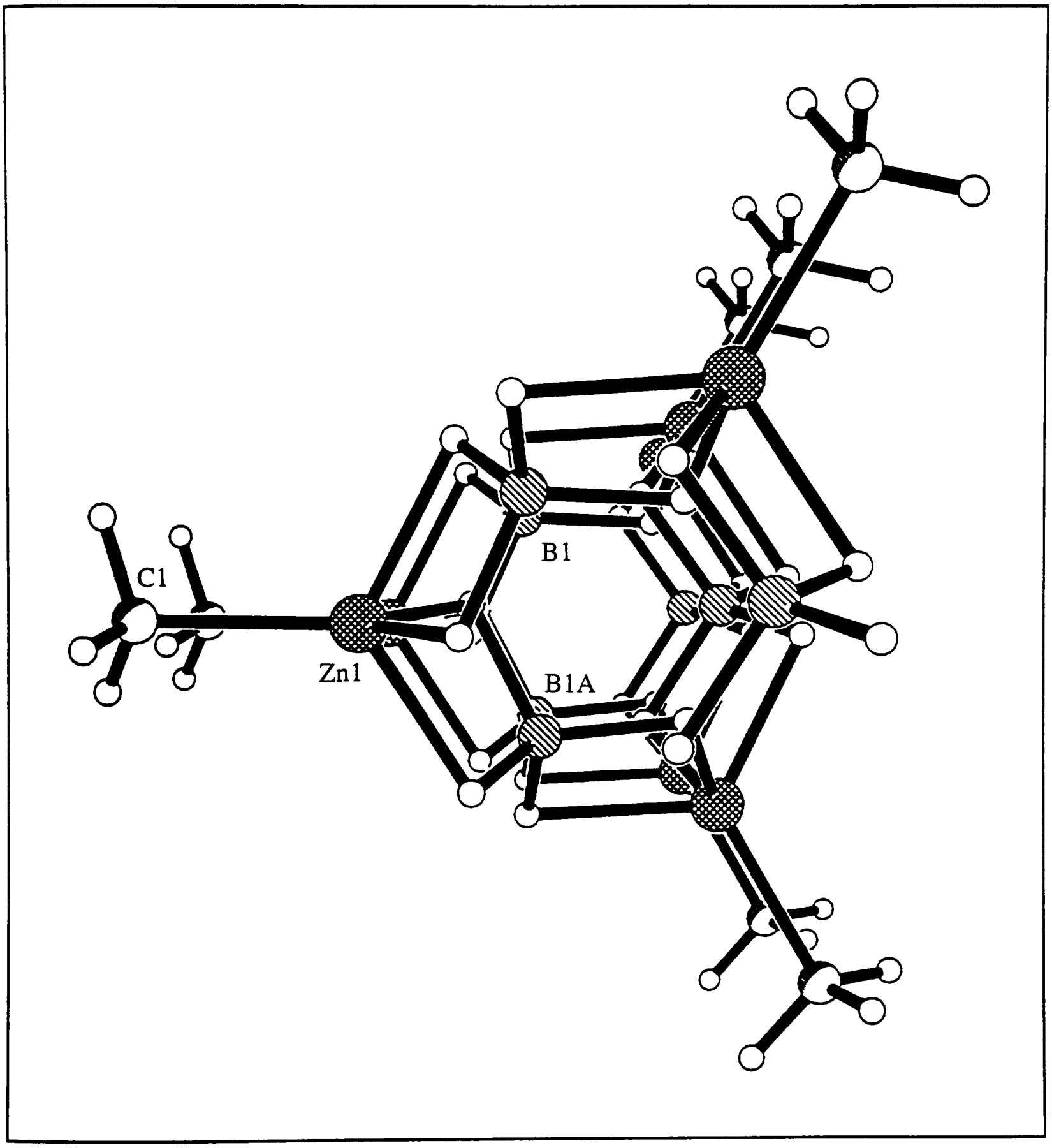

Figure 3.3 The structure of solid methylzinc tetrahydroborate at 150 K as viewed along the axis of the helix.

Table 3.1 Bond distances (Å) and angles (°) for crystalline [$MeZnBH_4$] at 150 K.[a]

Zn1—C1	1.94(2)	Zn1—H2	1.81(5)
Zn1—B1	2.30(2)	B1—H1	1.33(4)
Zn1—B1'	2.32(2)	B1—H2	1.33(4)
B1—Zn1"	2.32(2)	B1—H3	1.32(4)
Zn1—H1	1.82(5)	B1—H4	1.36(5)
C1—Zn1—B1	129.8(7)	Zn1—B1—H2	52(2)
C1—Zn1—B1'	131.5(7)	Zn1"—B1—H2	125(3)
B1—Zn1—B1'	98.6(7)	H1—B1—H2	103(3)
C1—Zn1—H1	117(3)	Zn1—B1—H3	137(3)
B1—Zn1—H1	35.2(14)	Zn1"—B1—H3	51(2)
B1'—Zn1—H1	101(4)	H1—B1—H3	115(4)
C1—Zn1—H2	122(4)	H2—B1—H3	114(4)
B1—Zn1—H2	35.3(14)	Zn1—B1—H4	121(2)
B1'—Zn1—H2	98(4)	Zn1"—B1—H4	51(2)
H1—Zn1—H2	70(2)	H1—B1—H4	111(4)
Zn1—B1—Zn1"	171.9(3)	H2—B1—H4	112(4)
Zn1—B1—H1	52(2)	H3—B1—H4	102(3)
Zn1"—B1—H1	132(2)		

[a] Symmetry operations: single prime: $-y + 4/3, x - y - 1/3, z - 1/3$;
double prime: $-x + y + 5/3, -x + 4/3, z + 1/3$.

solid consists of helical polymers in which successive methylzinc units are bridged by BH_4 ligands exhibiting bidentate ligation with respect to both adjacent metal atoms. The methyl groups are orientated such that the Zn–C bond is approximately perpendicular to the axis of the helix, each successive Zn–C vector being displaced by 120° from the previous one, so that the polymeric structure spirals along a 3_1 axis.

In many ways, the structure resembles that of solid beryllium *bis*(tetrahydroborate), which has been shown to consist of $Be(\mu\text{-}H)_2BH_2$ units bridged by BH_4 ligands.[8,9] In the beryllium compound, the interaction of the metal with six hydrogen atoms leads to approximately trigonal prismatic coordination of the metal centre. In the case of methylzinc tetrahydroborate, however, the zinc atom is clearly only *penta*-coordinated, the ligands adopting a distorted square pyramidal geometry about the metal atom, which is situated *ca.* 0.8 Å above the best plane through the four adjacent hydrogen atoms furnished by the BH_4 ligands.

Further comparison with the structure of solid beryllium *bis*(tetrahydroborate) shows that, whereas polymeric chains of the beryllium compound are disposed around a 4_1 axis, those in solid methylzinc tetrahydroborate spiral along a 3_1 axis. Since, in each case, the MBM angle within the chain is close to 180° {171.9 (3)° in $[MeZnBH_4]$, 175.4(7)° in $[Be(BH_4)_2]$}, this difference reflects the contrasting coordination geometries at the metal centres and, in particular, the BMB angles within the helical chain. The BMB angle is 98.6(7)° in methylzinc tetrahydroborate, compared with 111.7° in beryllium *bis*(tetrahydroborate), a difference which may in part depend upon the greater separation of the zinc and boron atoms. This facilitates closure of the BMB angle while keeping the B···B non-bonded distance, and hence electrostatic repulsion between adjacent BH_4 ligands, approximately constant {adjacent B···B distances are 3.49 Å in $[MeZnBH_4]$ and 3.29 Å in $[Be(BH_4)_2]$[8,9]}.

The structures of both $[MeZnBH_4]$ and $[Be(BH_4)_2]$ exhibit some degree of charge separation, $RM^{\delta+}BH_4^{\delta-}$ (M = Be, R = BH_4; M = Zn, R = Me), but the compounds are volatile, giving rise to more covalently bound species in the vapour phase.[14,15] On the basis of infrared measurements and of comparisons with the spectra

of ionic tetrahydroborates, Nibler and Cook[6] suggested that solid methylzinc tetrahydroborate was based around a linear ZnBZn framework and, consequently, around a BH_4^- ion effectively possessing D_{2d} symmetry. In fact, the crystal structure shows a ZnBZn angle of 171.9° and, although it does suggest loss of all symmetry elements from the BH_4^- ion {as is indeed also the case for $[Be(BH_4)_2]$[8,9]}, the observed distortion from D_{2d} symmetry is small. Nibler and Cook further asserted that the BH_4^- ion is less strongly coupled to the metal in $[MeZnBH_4]$ than in $[Be(BH_4)_2]$.[6] Comparison of the two crystal structures and examination of the structures of $[(Ph_3P)_4Cu_2(BH_4)]^+$ [16] and $[U(BH_4)_4]$[17] [which feature metal centres bridged by *bis*(bidentate) BH_4 groups] reveal some evidence to the contrary. Some relevant structural data are listed in Table 3.2.

Firstly, the B–H bonds within the helical chain are significantly longer in $[MeZnBH_4]$ than in $[Be(BH_4)_2]$ {typically 1.33(4) Å, compared with 1.10(4) Å in $[Be(BH_4)_2]$[8,9]}, indicating that the interaction of the metal centre with the bridging hydrogens is in fact somewhat stronger in the zinc compound. The B–H bond lengths in $[MeZnBH_4]$ are comparable with those found in $[(Ph_3P)_2Cu_2(BH_4)]^+$ [16] and in the $U(\mu\text{-}H)_2B(\mu\text{-}H)_2U$ bridging units in $[U(BH_4)_4]$.[17] Enhanced interaction with the metal might also be expected to cause greater distortion of the HBH angles from the tetrahedral value, manifesting the existence of two distinct bidentate BH_2 units. In fact, although these angles do show greater distortion in $[MeZnBH_4]$ than in $[Be(BH_4)_2]$[8,9] {and similar to that found in $[(Ph_3P)_4Cu_2(BH_4)]^+$ [16] and the bridging BH_4 units in $[U(BH_4)_4]$[17]}, the difference between the values is exceeded by the relatively large uncertainties in the measurements.

Metal to boron distances have often been used as an indication of the type of bonding between a BH_4 group and a metal centre, [7,18] especially in cases where bridging hydrogens are difficult to locate. Comparison of M···B distances and effective ionic radii for $[MeZnBH_4]$, $[(Ph_3P)_4Cu_2(BH_4)]^+$ and $[Be(BH_4)_2]$[19] reveals that the difference in bond length for the zinc and copper compounds can be accounted for almost entirely by the difference in effective ionic radii of the metal. The Be···B bond length is, however, somewhat longer than would be expected on this basis, implying that interaction

Parameter	$[MeZnBH_4]$	$[(Ph_3P)_2Cu_2(BH_4)]^+$	$[U(BH_4)_4]^a$	$[Be(BH_4)_2]^a$
HBH angle (within bidentate unit)	103(3),102(3)	108	106, 102	109
HBH angle (between bidentate units)	111(4), 112(4)	116	110-116	111
M···B distance	2.30(2), 2.32(2)	2.23, 2.20	2.86	2.001, 1.999
B–H distances	1.32(4)-1.36(5)	1.31	1.18-1.33	1.08-1.17
M–H distances	1.81(5)-1.82(5)	1.81-1.86	2.33-2.38	1.59-1.65
Effective ionic radius[b]	0.82	0.74	1.03	0.41
Reference	This work	16	17	8, 9

[a] Data given for the bridging BH_4 units only. [b] Taken from reference 19.

Table 3.2 Selected bond lengths (Å) and angles (°) for compounds featuring BH_4 groups bridging two metal centres.

between metal and tetrahydroborate fragments is weaker in $[Be(BH_4)_2]$ than in $[MeZnBH_4]$ and $[(Ph_3P)_4Cu_2(BH_4)]^+$.

If one considers a continuous spectrum of bonding between extreme ionic $[M^+ BH_4^- M^+]$ and covalent $[M(\mu\text{-}H)_2B(\mu\text{-}H)_2M]$ limits, it seems likely that the bonding in $[MeZnBH_4]$ {and in $[(Ph_3P)_4Cu_2BH_4]^+$} tends more towards the latter, bridging formulation than does that in $[Be(BH_4)_2]$. Further weight is added to this argument by comparison of the dimensions of the $Zn(\mu\text{-}H)_2B$ unit with those recently reported for the compound $[(tmen)Zn(Cl)BH_4]$, in which the zinc atom is also *penta*-coordinated.[20] In particular, the Zn···B distances {2.30 Å and 2.32 Å in $[MeZnBH_4]$; 2.29 Å for $[(tmen)Zn(Cl)BH_4]$}, Zn–H_b distances {1.81 and 1.82 Å; 1.98 and 1.96 Å} and HZnH angles {70° and 62°} are very similar. On the basis of the structural parameters and the measured infrared spectrum, Raston and co-workers proposed that the bonding of the BH_4 group to the zinc atom in $[(tmen)Zn(Cl)BH_4]$ is best described in terms of bidentate ligation through two Zn–H–B linkages. The similarities in the geometry of the $Zn(\mu\text{-}H)_2B$ moieties of these two compounds therefore supports a formulation of solid methylzinc tetrahydroborate in terms of $[Zn(\mu\text{-}H)_2B(\mu\text{-}H)_2Zn]$ rather than as $[Zn^+ BH_4^- Zn^+]$ units.

Finally, comparison of the terminal Zn–H bond in $[HZnN(Me)CH_2CH_2NMe_2]_2$ with the Zn–H_b bond length in $[MeZnBH_4]$ shows an increase from 1.61 to 1.81 Å.[21] Such an increase is entirely consistent with that expected on going from a terminal M–H to a bridging M–H–B unit {*e.g.* r(Ga–H_t) = 1.58 Å, r(Ga–H_b) = 1.82 Å in $[H_2GaBH_4]$;[11] r(Al–H_t) = 1.56 Å in $[H_3Al{\cdot}NMe_2CH_2Ph]$,[22] r(Al–H_b) = 1.67 - 1.75 Å in $[Al(BH_4)_3]$[23]}.

Polymeric structures incorporating bridging ligands are relatively common in zinc chemistry (*e.g.* $[ZnH_2]$[24]), but *penta*-coordinated centres are encountered less often. Most examples of either square pyramidal or trigonal bipyramidal coordination, including the newly reported $[(tmen)Zn(Cl)BH_4]$,[20] are complexes involving polydentate ligands with O, S, Se or N donor atoms.[25] Among authenticated simple hydride derivatives of zinc, though, methylzinc tetrahydroborate is certainly a rare example of

this mode of coordination, another instance being the very recently reported $[(MeZn)_2B_3H_7]_2$ (*vide infra*).[26] The X-ray crystal structure of this compound contains two methylzinc units bridged not by BH_4 groups but by two novel B_3H_7ZnMe ligands to give a centrosymmetric dimeric cluster.[26] The geometry of the Zn(1) centre in $[(MeZn)_2B_3H_7]_2$ resembles closely that in $[MeZnBH_4]$, both featuring *penta*-coordinated zinc with Me and H ligands adopting a distorted square pyramidal geometry about the metal centre. In each case, the methylzinc unit is linked to the borane ligand *via* Zn–H–B bonds and this is reflected in the similar Zn···B distances {2.30 and 2.32 Å in $[MeZnBH_4]$; 2.41 and 2.45 Å in $[(MeZn)_2B_3H_7]_2$[26]}. Presumably the fact that $[MeZnBH_4]$ is polymeric but $[(MeZn)_2B_3H_7]_2$ is a dimer reflects the different constraints imposed by the two ligands in order for the zinc centres to achieve maximum coordination. Each BH_4 ligand must bond in bidentate fashion to each adjacent zinc atom to achieve *penta*-coordination, implying an approximately linear Zn···B···Zn skeleton and hence a polymeric structure. In $[(MeZn)_2B_3H_7]_2$ *penta*-coordination is achieved by using all four hydrogens of the basal $H_2B–BH_2$ unit of the B_3H_7ZnMe ligand, a situation which allows folding of the skeleton and a dimeric structure.

3.1.4 Physical Properties of Methylzinc Tetrahydroborate

In agreement with the findings of Ridley[5] and Nibler and Cook,[6] methylzinc tetrahydroborate is a thermally fragile material decomposing *in vacuo* in all-glass apparatus at room temperature, typically over a period of several days. Continuous pumping at room temperature causes gradual disproportionation to $[Me_2Zn]$ and $[Zn(BH_4)_2]$, such that transferral of methylzinc tetrahydroborate, even in all-glass apparatus, always results in a small amount of residual $[Zn(BH_4)_2]$. The vapour pressure of $[MeZnBH_4]$ is *ca.* 0.5 Torr at room temperature, the thermal instability of the material ruling out further measurements at significantly higher temperatures. The thermal decomposition of methylzinc tetrahydroborate is examined at greater length in Section 3.3.1.

(a) ^{1}H and ^{11}B NMR spectra. The ^{1}H and ^{11}B NMR spectra of methylzinc tetrahydroborate in [$^{2}H_8$]toluene solution at various temperatures are illustrated in Figures 3.4 and 3.5 respectively. The ^{1}H spectrum of the solution at room temperature shows a sharp singlet centred at δ_H -0.36 and a relatively broad 1:1:1:1 quartet centred at δ_H 0.82. The relative intensities of the signals (3:4) confirm that they are due to the methyl and tetrahydroborate protons, respectively. The quartet is the expected coupling pattern for a BH_4 group (^{11}B, $I = 3/2$) in which there is rapid interchange of bridging and terminal hydrogen atoms.[7] The coupling constant $J(^{11}B-^{1}H)$ (83.2 Hz) and the chemical shift of the BH_4 resonance correspond closely to those found for related compounds, *e.g.* [Me_2GaBH_4][27] and [$Al(BH_4)_3$].[28,29] The chemical shift of the methyl protons is also characteristic of a methyl group bound to zinc.[30] Cooling the sample caused the methyl resonance to remain unchanged but the BH_4 quartet progressively to collapse, giving a single, broad signal centred at δ_H 0.85 at -40°C. This behaviour is characteristic of the protons of a molecular tetrahydroborate group;[7,31] the collapse of the multiplet structure of the BH_4 resonance can be rationalized in terms of correlation-time decoupling.[7] As is the case with most other molecular tetrahydroborates,[7] the ^{1}H NMR spectrum showed no sign of distinct resonances due to terminal and bridging BH_4 protons, even at -80°C.

The ^{11}B NMR spectrum of methylzinc tetrahydroborate in [$^{2}H_8$]toluene solution at room temperature shows a 1:4:6:4:1 quintet centred at δ_B -39, a chemical shift in close agreement with that expected on the basis of the spectra of related compounds.[32] Collapse of the multiplet structure was observed to occur on cooling, for the reasons given above. ^{11}B NMR spectra were measured at temperatures as low as -95°C to see whether there was evidence of any other signals, such as might be associated with the presence of different oligomers, $[MeZnBH_4]_n$ {as is known to be case for $[HGa(BH_4)_2]$[33]}. No such signals were observed.

(b) Infrared spectrum of solid methylzinc tetrahydroborate. Nibler and Cook measured the infrared and Raman spectra of [CH_3ZnBH_4] and [CD_3ZnBH_4] and interpreted their results in terms of a structure containing more-or-less discrete $[MeZn]^+$

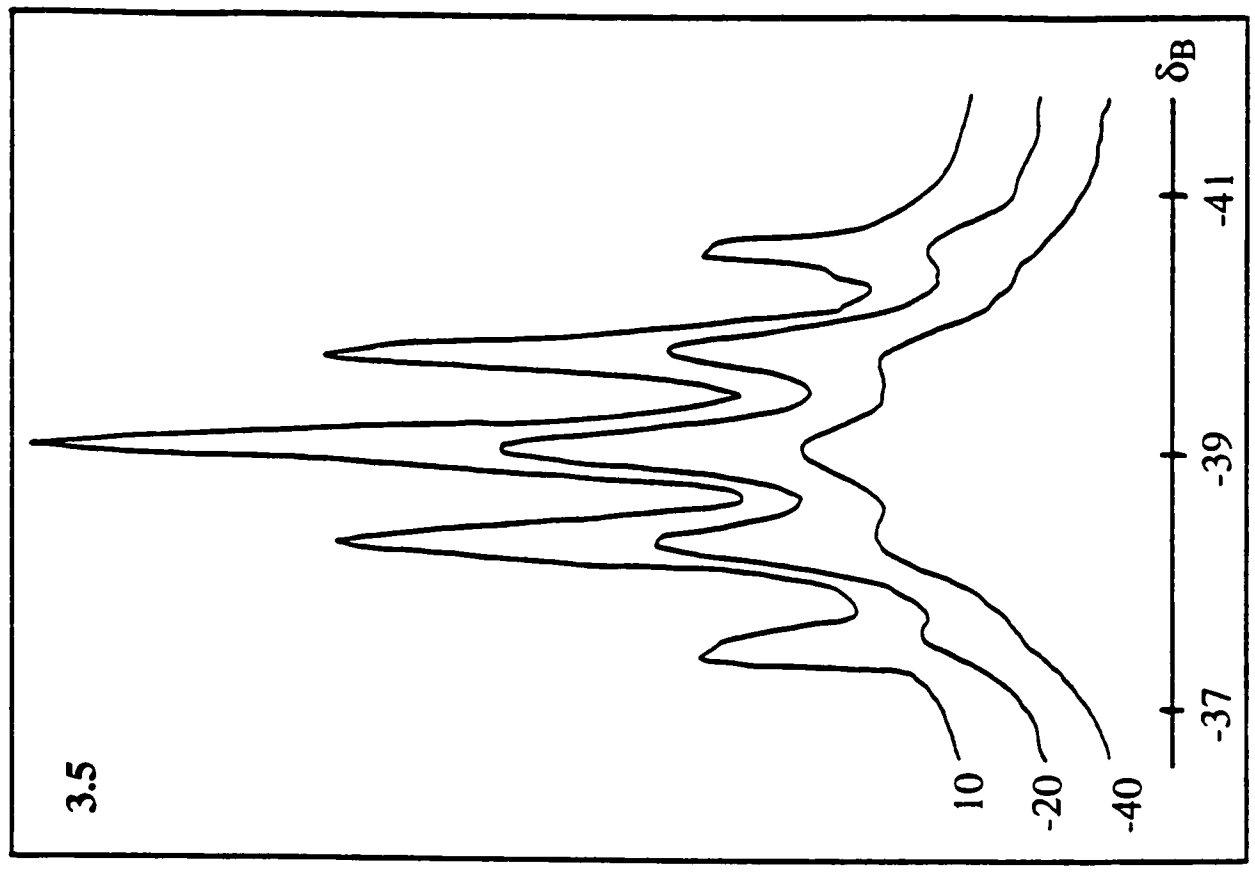

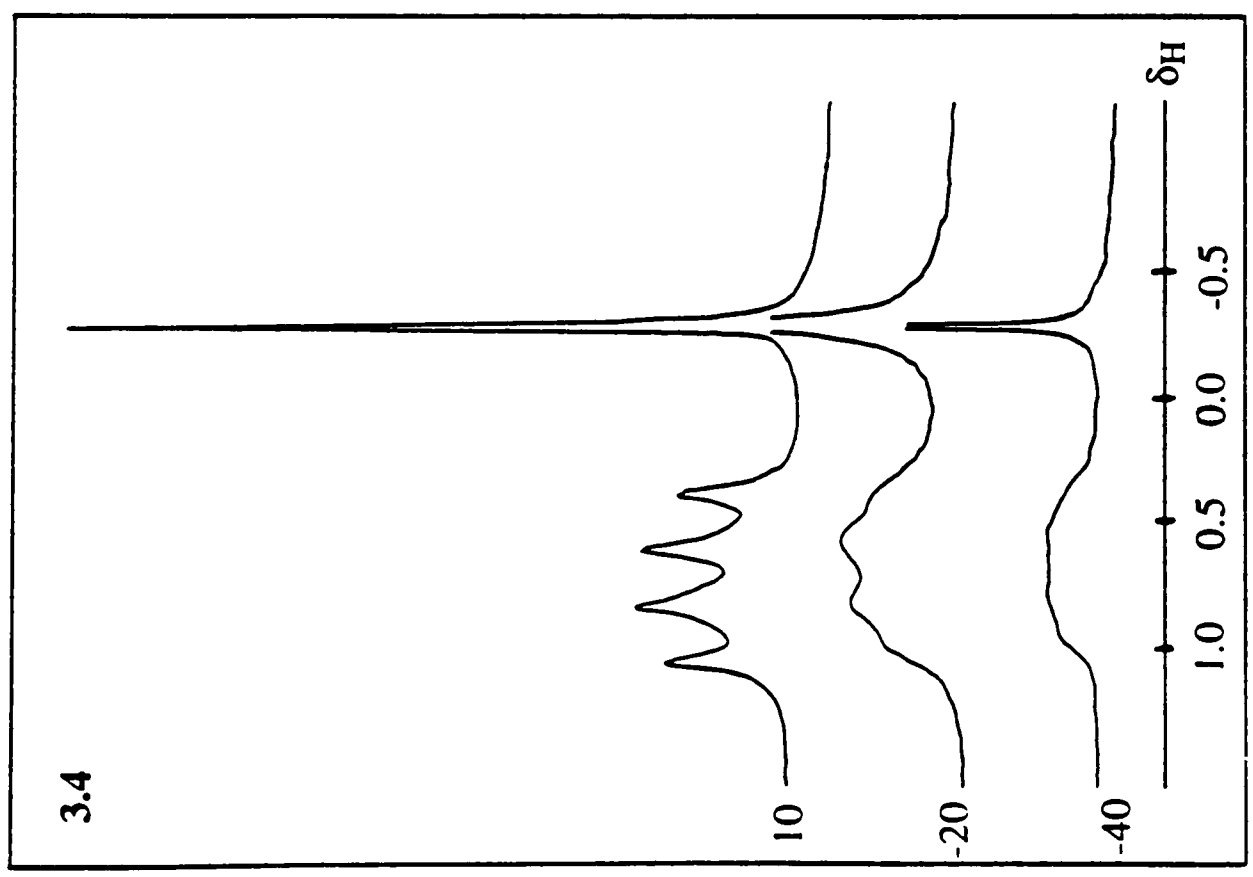

Figures 3.4 and 3.5 The ^1H and ^{11}B NMR spectra of [MeZnBH$_4$] in [$^2H_8$]toluene solution at -40, -20 and +10°C.

and $[BH_4]^-$ ions with C_{3v} and D_{2d} symmetries, respectively.[6] They were unable to determine the extent of distortion of the $[BH_4]^-$ ion from D_{2d} symmetry using least squares valence force constant calculations, however, because of problems of correlation between the force constants and distortion parameters. In the light of the X-ray crystal structure (*vide supra*), which shows Zn–H, Zn···B and B–H distances and BH_2 angles more in keeping with a structure comprising $[Zn(\mu\text{-}H)_2B(\mu\text{-}H)_2Zn]$ units than of discrete $[MeZn]^+$ and $[BH_4]^-$ ions, the infrared spectra of annealed solid samples of $[CH_3ZnBH_4]$, $[CD_3ZnBH_4]$ and $[CH_3ZnBD_4]$ at -196°C have been measured in an attempt to shed further light on the bonding situation in solid $[MeZnBH_4]$. Typical spectra are illustrated in Figures 3.6, 3.7 and 3.8.

Table 3.3 lists the infrared-active fundamentals expected for a $[BH_4]^-$ ion of D_{2d} symmetry and the extra vibrational modes expected for a $[Zn(\mu\text{-}H)_2B(\mu\text{-}H)_2Zn]$ fragment of the same symmetry. Coordination of the BH_4 ligand to both adjacent zinc atoms in *bis*(bidentate) fashion would be expected to give rise to three new infrared-active vibrational modes. The Zn–B–Zn skeletal bending motions would be expected to give rise to bands in the region 200-300 cm^{-1},[33,34] that is, beyond the range of the present measurements. The antisymmetric Zn–B stretching fundamental can, however, reasonably be ascribed to the medium-strong band found at 443 cm^{-1} (412 cm^{-1} in $[CH_3ZnBD_4]$, 414 cm^{-1} in $[CD_3ZnBH_4]$), by analogy with similar assignments made to the corresponding modes of $[H_2GaBH_4]$ (468 cm^{-1}),[35] $[Me_2GaBH_4]$ (445 cm^{-1})[36] and $[Me_2AlBH_4]$ (465 cm^{-1}).[36] Furthermore, the vibrational mode approximating to a $Zn–H_b$ stretching vibration (where 'b' denotes a bridging atom) can be assigned to a weak feature at 1383 cm^{-1} (1028 cm^{-1} in $[CH_3ZnBD_4]$), analogous bands being found at 1400 cm^{-1} in the infrared spectra of both $[H_2GaBH_4]$[35] and $[Me_2GaBH_4]$.[36] Bands associated with M–H–B stretching modes are often found to be weak and broad, the broadening apparently depending on factors similar to those in operation for hydrogen-bonded systems.[7,37,38]

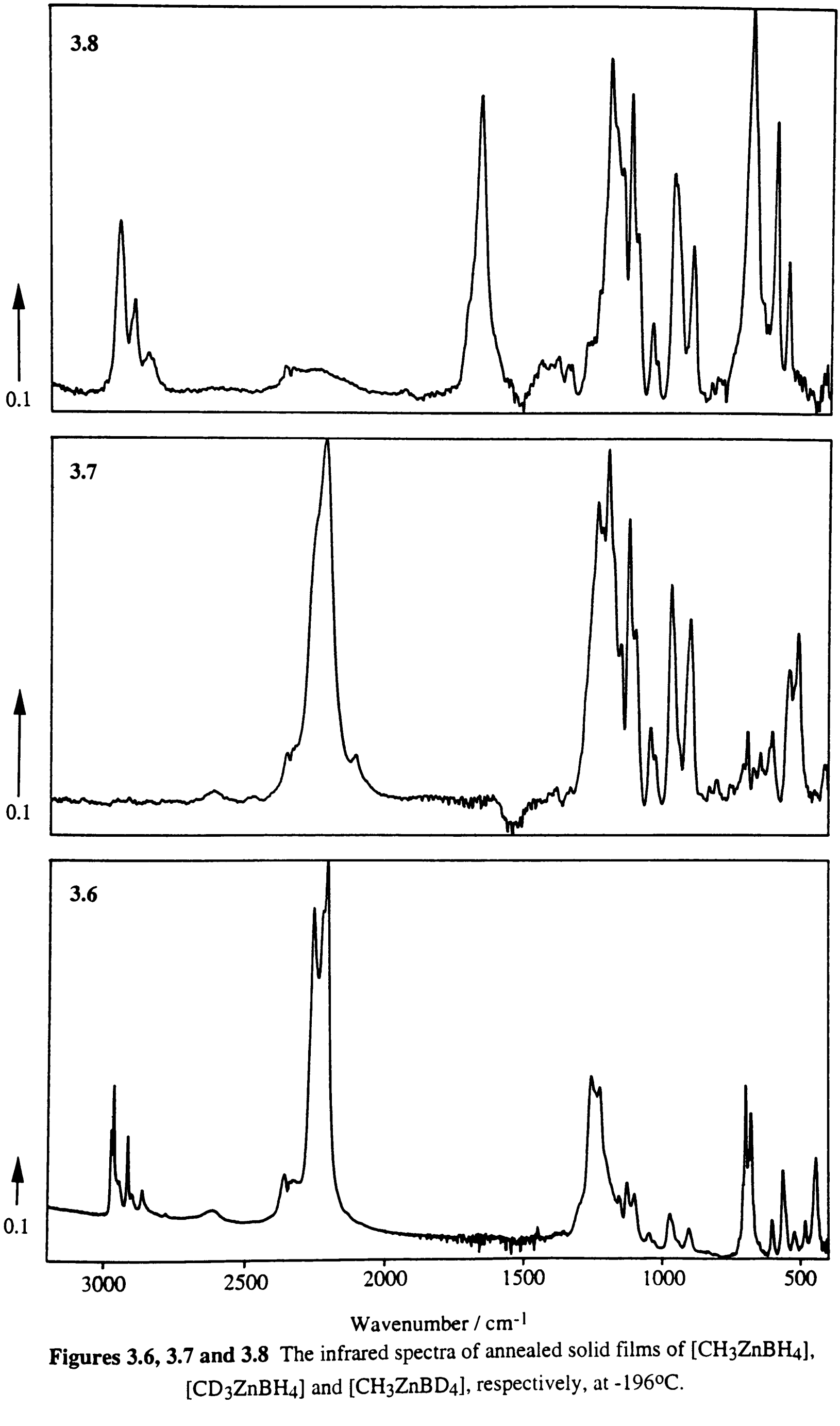

Figures 3.6, 3.7 and 3.8 The infrared spectra of annealed solid films of $[CH_3ZnBH_4]$, $[CD_3ZnBH_4]$ and $[CH_3ZnBD_4]$, respectively, at -196°C.

Table 3.3 (a) Infrared-active modes of vibration expected for an isolated $[BH_4]^-$ ion of D_{2d} symmetry. (b) Extra modes expected for a covalently bound $Zn(\mu\text{-}H)_2B(\mu\text{-}H)_2Zn$ fragment.

Symmetry type	Symmetry coordinate	Approx. description	
(a)			
b_2	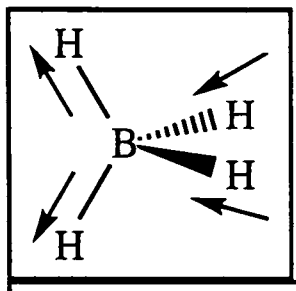	ν_a(B–H)	Bond stretching
e	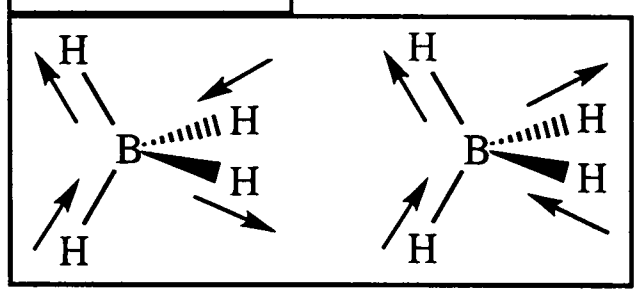	ν_a(B–H)	
b_2	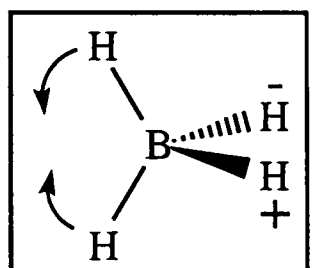	$\delta_a(BH_2)$	Angle bending
e	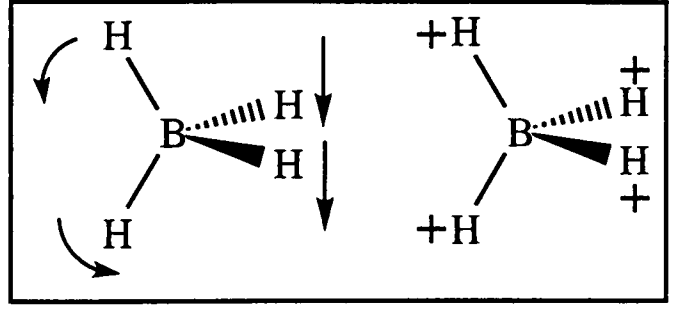	$\delta_a(BH_2)$	
(b)			
b_2	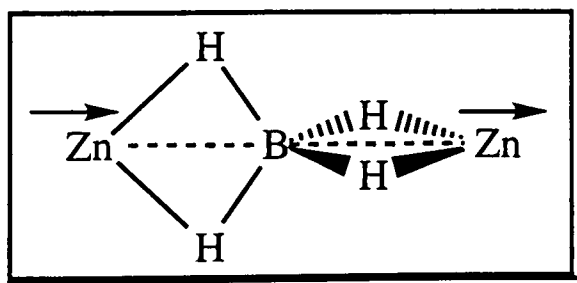	ν_a(Zn–B)	Bond stretching
e	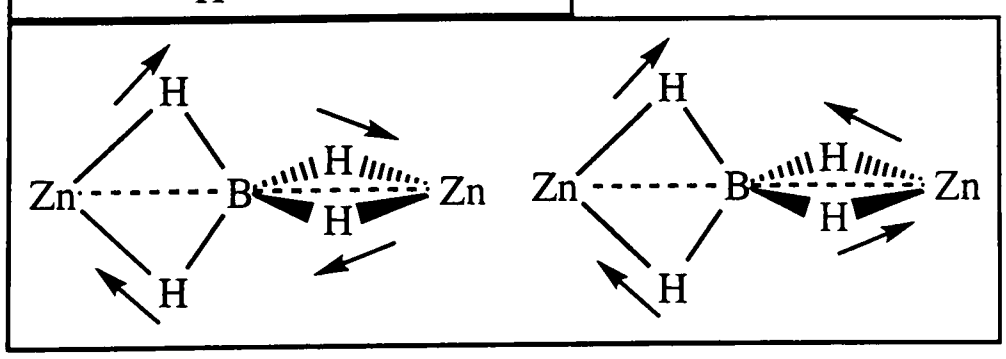	ν_a(Zn–H_b)	
e	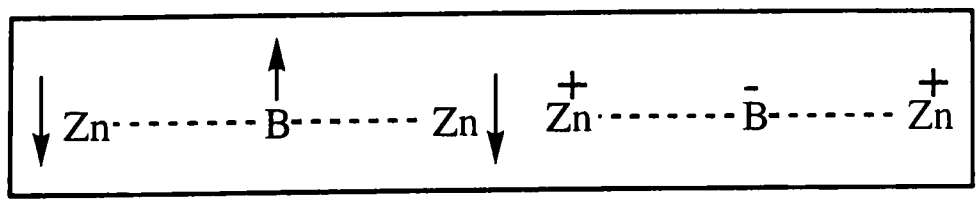	Skeletal bends	Angle bending

The existence of bands in the infrared spectra of [CH_3ZnBH_4], [CH_3ZnBD_4] and [CD_3ZnBH_4], attributable to Zn–B and Zn–H_b stretching motions lends weight to the conclusions drawn from the X-ray crystal structure that solid [$MeZnBH_4$] is best formulated in terms of a helix of repeating [$Zn(\mu\text{-}H)_2B(\mu\text{-}H)_2Zn$] units, and the remaining bands in the spectra have been assigned on the basis of this model, with the results listed in Table 3.4. The bands attributable to the methylzinc unit have been assigned on the basis of a CH_3Zn fragment of C_{3v} symmetry, along the lines adopted by Nibler and Cook.[6]

That there is *some* degree of charge separation is reflected, however, in the position of bands attributed to the B–H_b stretching modes, which at 2256 and 2224/2209 cm^{-1} for the b_2 and e modes, respectively, have frequencies somewhat higher than usual for bidentate BH_4 ligation (< 2180 cm^{-1}) and tending towards the values expected for a more ionic formulation.[7] {Raston and co-workers did report a value of 2207 cm^{-1} for one of the B–H_b stretching modes in [(*tmen*)Zn(Cl)BH_4] in which the BH_4 group is bound to zinc in a bidentate fashion[20]}. The distortion of the [$Zn(\mu\text{-}H)_2B(\mu\text{-}H)_2Zn$] and [$CH_3Zn$] fragments from ideal D_{2d} and C_{3v} symmetries shown in the crystal structure is reflected in splitting of bands associated with modes of e symmetry. Only in the case of the weak $\delta_a(CH_3)$ and $\nu(Zn\text{–}H_b)$ features is this splitting not observed. Splittings between components are typically in the order of 10-20 cm^{-1} reflecting the small magnitude of the distortions. Reduction in the symmetry of the [$Zn(\mu\text{-}H)_2B(\mu\text{-}H)_2Zn$] unit (from D_{2d} to C_s) is brought about by bending of the Zn···B···Zn framework.

3.2 Investigation of Methylzinc Tetrahydroborate in the Vapour Phase

Although the structure of solid methylzinc tetrahydroborate had been investigated by Nibler and Cook,[6] the nature of the vapour species had received virtually no attention prior to this investigation. Vibrational spectroscopy has been used in a large number of cases to determine the mode of ligation of a BH_4 group to a metal centre (see Section 2.2.1), and the infrared spectrum of gaseous [$MeZnBH_4$] was to provide a

Table 3.4 The infrared spectra of $[CH_3ZnBH_4]$, $[CH_3ZnBD_4]$ and $[CD_3ZnBH_4]$ in the range 400-4000 cm^{-1}: wavenumbers of absorptions displayed by solid films at -196°C.

Assignment [a]	Symmetry type	Infrared absorption ν/cm^{-1} [b] CH_3ZnBH_4	CH_3ZnBD_4	CD_3ZnBH_4	ν_H/ν_D
$\nu_a(C-H)$	*e*	2972 s	2965 s	*c*	-
		2963 s	2956 s	*c*	-
$\nu_s(C-H)$	a_1	2910 m	2910 m	2110 mw	1.379
$\nu_a(B-H_b)$	b_2	2256 s, sh	1691 m	2253 s	1.334
$\nu_a(B-H_b)$	*e*	2224 vs	1664 s	2216 s, br	1.337
		2209 vs	1661 s		1.330
$\delta_a(CH_3)$	*e*	1443 vw	1447 vw	1045 vw	1.381
$\nu_a(Zn-H_b)$	*e*	1383 vw, br	1028 w	1385 w, br	1.345
$\delta_a(BH_2)$	*e*	1256 s	970 s	1238 s	1.295
		1226 s	962 s	1199 s	1.274
$\delta_s(CH_3)$	a_1	1180 w	1155 m	972 m	1.214
$\delta_a(BH_2)$	b_2	1128 w	833 vw	1124 w	1.354
$\rho(CH_3)$	*e*	700 s	699 s	524 m	1.336
		679 s	681 s	511 m, sh	
$\nu(Zn-C)$	a_1	557 m	556 m	543 mw	1.026
$\nu(Zn-B)$	b_2	443 m	412 w	414 mw	1.075

[a] The assignments relate to a structure based around a $[Zn(\mu\text{-}H)_2B(\mu\text{-}H)_2Zn]$ moiety approximating to D_{2d} symmetry and an orthogonal CH_3Zn unit approximating to C_{3v} symmetry. [b] Intensity abbreviations are listed in the notes. [c] Obscured by more intense feature.

primary means of investigating its structure. Furthermore, the structures of several volatile metal tetrahydroborates have been determined by electron-diffraction studies of the vapours {*e.g.* $[Me_2GaBH_4]$,[39] $[Me_2AlBH_4]$,[39] $[HGa(BH_4)_2]$,[40] $[Ti(BH_4)_3]$,[41] $[Al(BH_4)_3]$,[42] and $Zr(BH_4)_4$[43]} some structural parameters frequently being constrained by the results of *ab initio* calculations or vibrational studies.

In the case of methylzinc tetrahydroborate, however, attempts to measure the infrared spectrum of the vapour were thwarted by its prohibitively low vapour pressure at room temperature and its tendency to decompose on the caesium iodide windows and halocarbon wax of the infrared cell. Consequently, it was planned to sample the vapour by matrix isolation in order to obtain infrared measurements, albeit giving frequencies slightly perturbed with the respect to the expected gas-phase values as a result of matrix site effects.[44] Furthermore, infrared frequencies calculated for minimum energy structures on the basis of Density Functional Theory were to be used as an aid to the interpretation of the measured spectra. Comparison of observed and calculated frequencies should also give some indication of the likely accuracy of the calculated structural parameters.

Mass spectrometry was to be used to investigate the possibility that oligomeric species $[MeZnBH_4]_n$ exist in the vapour. The low vapour pressure of $[MeZnBH_4]$ and its tendency to decompose on warming mean that it has proved impossible so far to produce a molecular flux of the vapour sufficient for electron-diffraction measurements.

3.2.1 Mass Spectrometry

Initial experiments were carried out using the apparatus in the Inorganic Chemistry Laboratory at Oxford. The sample was attached to the evacuable, all-glass inlet system of the apparatus *via* a ground-glass joint lubricated with Voltalef 90 grease. The manifold was conditioned by exposure to a sample of the vapour for *ca.* 10 min, prior to re-evacuation and admission of fresh vapour to the chamber of the mass spectrometer. The vapour was sampled over the solid at -23°C and at room temperature

in order to investigate the possibility that different oligomers, $[MeZnBH_4]_n$, are present in the vapour.

Peaks corresponding to the molecular ion $CH_3ZnBH_4^+$ were observed, the intensity pattern of the peaks at m/z = 98, 96 and 94 matching the natural abundances of the zinc isotopes ^{68}Zn, ^{66}Zn and ^{64}Zn.[45] This characteristic intensity pattern is also observed for the peaks assigned to CH_3Zn^+ and Zn^+. On the other hand, the mass spectrum at neither temperature gave any suggestion of a species containing more than one zinc atom ($m/z > 128$). Hence there was no sign of any oligomer of $[MeZnBH_4]$, irrespective of whether the vapour came from a sample at -23°C, or one at room temperature.

These results can be explained in two ways: either methylzinc tetrahydroborate exists in the vapour phase exclusively as the monomer, $[MeZnBH_4]$, or any oligomeric species are relatively loosely bound and readily fragmented under the conditions of electron impact used in this experiment. The second possibility is known to be arise with $[Me_2GaH]_n$, which has been shown by infrared spectroscopy to exist as a mixture of dimeric (n = 2) and higher oligomeric species in the vapour, but which fails to give a peak in the mass spectrum corresponding to any species other than the dimer.[46,47] The mass spectrum of $[Me_2GaH]_n$ was also measured on the Oxford instrument.

Further investigation was therefore carried out using a Hiden HAL/3F residual gas analyser at the University of Edinburgh.

Spectra were recorded by sampling the vapour from methylzinc tetrahydroborate at -30 and at 0°C. Typical spectra are illustrated in Figure 3.9. Mass peaks corresponding to the molecular ion of the dimer $[MeZnBH_4]_2^+$ and to other fragments containing two zinc atoms were observed in the spectrum of the vapour above the solid at 0°C, although not above that at -30°C. In addition, was some indication of any peak corresponding to a species with three zinc atoms (at m/z = 283). The intensities of peaks due to the dimer were observed to increase relative to those of the monomer as the temperature of the solid increased, implying that the vapour above solid $[MeZnBH_4]$ becomes richer in the higher oligomer as the temperature of the solid is raised.

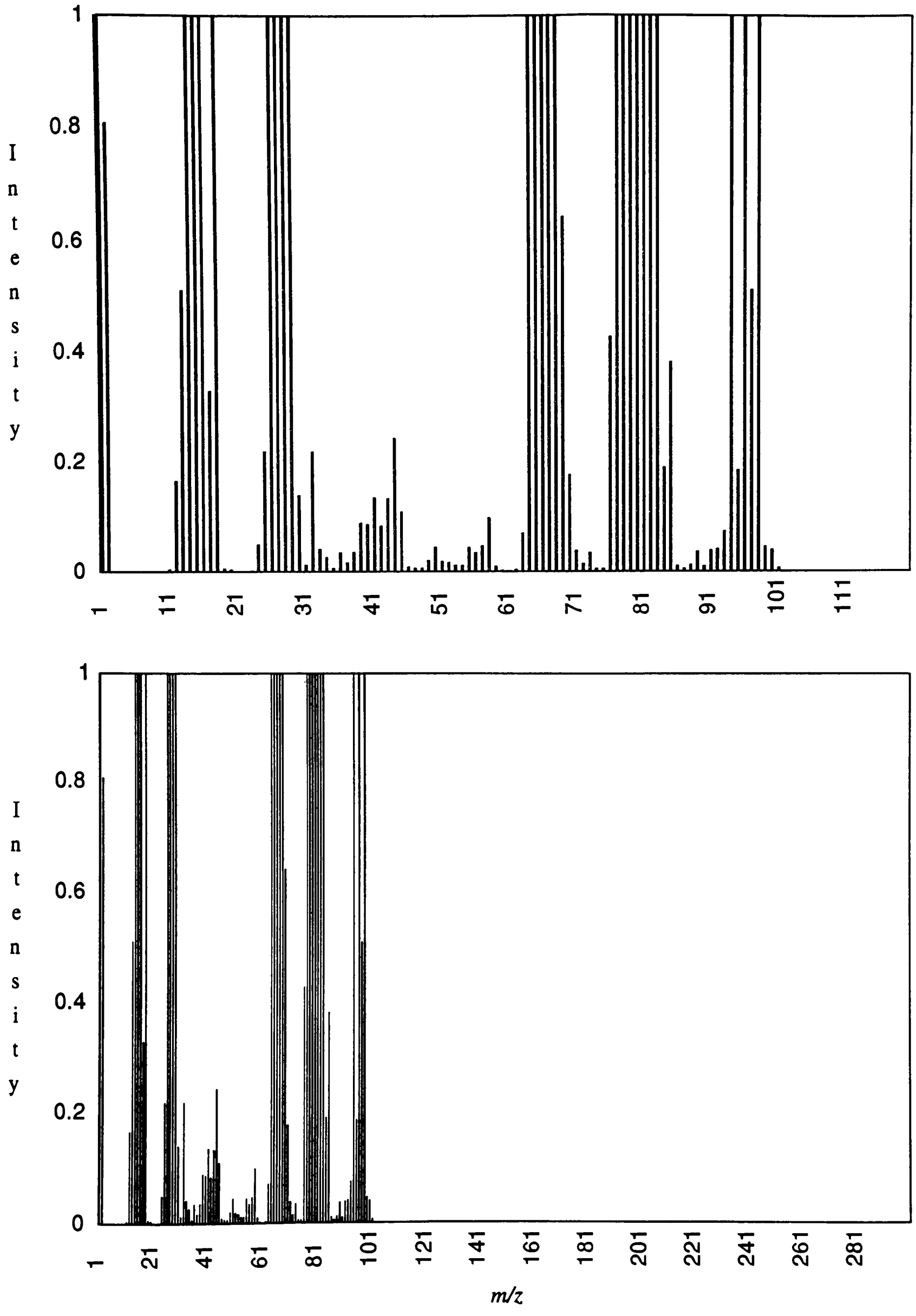

Figure 3.9 (a) The mass spectrum of methylzinc tetrahydroborate vapour sampled above the solid at -30°C.

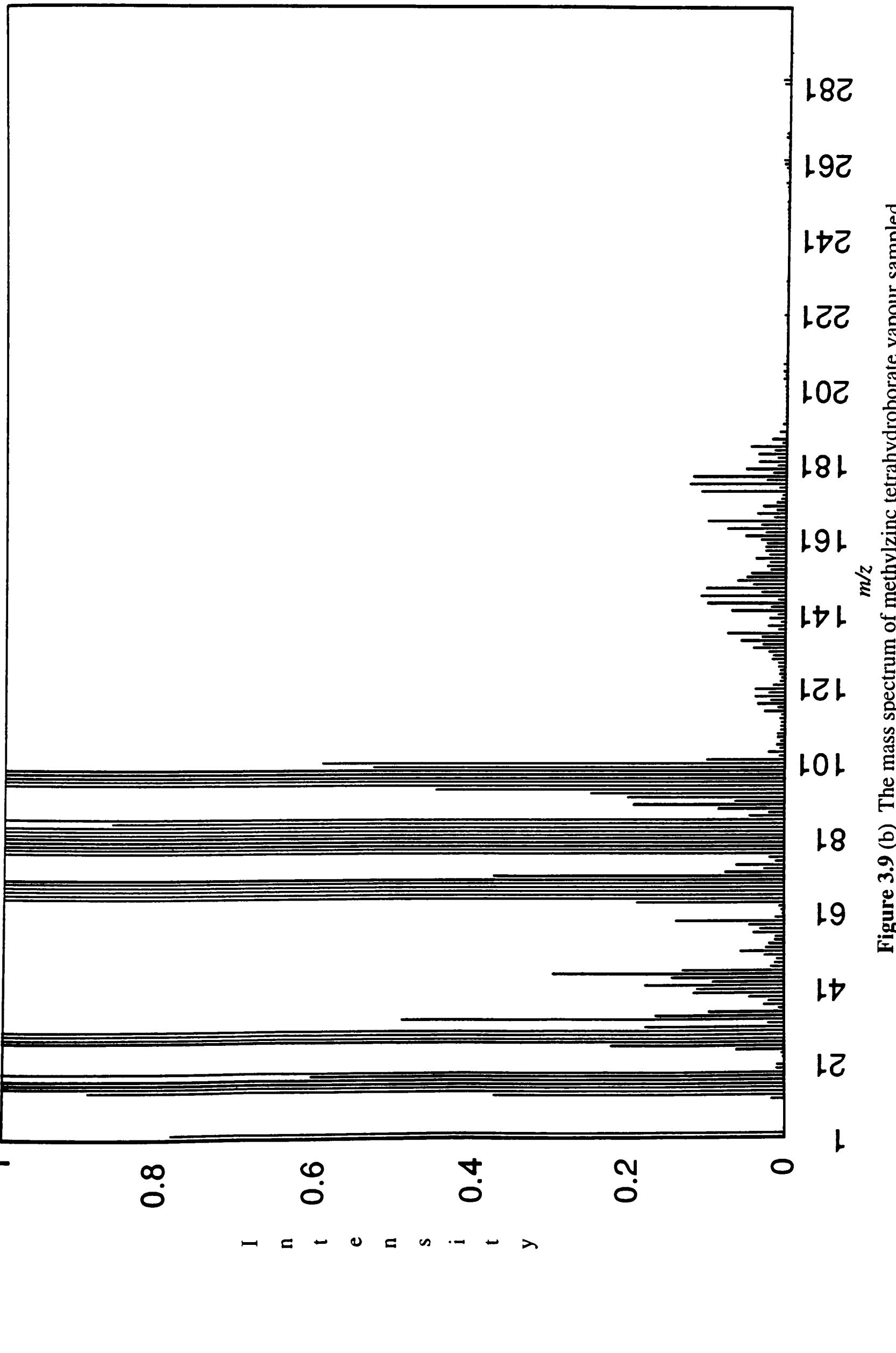

Figure 3.9 (b) The mass spectrum of methylzinc tetrahydroborate vapour sampled above the solid at 0°C.

The existence of more than one species in the vapour above a polymeric solid is not entirely unexpected, and could derive from fragmentation of polymer chains into units containing more than one zinc atom. Indeed, it has been postulated by Hedberg *et al.* that the range of different results obtained from the electron-diffraction studies of gaseous beryllium *bis*(tetrahydroborate) may be due to the existence of two or more different species coexisting in equilibrium in the vapour and derived from fragmentation of the polymeric solid.[48]

It is intriguing that the proportion of $[MeZnBH_4]_2$ in the vapour should increase as the temperature of the solid is raised. An analogous situation is reported by Borlin and Gaines to occur with $[Me_2AlB_3H_8]$ and $[Me_2GaB_3H_8]$.[49] Mass spectral studies at "normal operating temperatures" were complicated by the existence of oligomeric species $[Me_2MB_3H_8]_n$ (M = Al or Ga; $n > 1$), the extent of oligomerization being reduced by cooling of the sample reservoir. One possible explanation for these results is that raising the temperature increases the vapour pressure above the solid and results in more frequent intermolecular collisions in the gas phase. If the dimeric species $[MeZnBH_4]_2$ is formed *via* collisions between $[MeZnBH_4]$ monomers in the vapour, then doubling the pressure may be expected to increase roughly fourfold the proportion of dimer present. This is known to be the case with $[MeBeBH_4]$ and the methyl-bridged dimer $[MeBeBH_4]_2$.[50] Increasing the pressure of $[MeBeBH_4]$ inside a specially constructed infrared cell caused the absorptions due to the dimer to increase in intensity, relative to those of the monomer. Only at appreciably higher temperatures (in a regime made inaccessible to methylzinc tetrahydroborate by virtue of its thermal instability) is the monomer likely to prevail over the dimer.

3.2.2 Matrix Isolation of Methylzinc Tetrahydroborate

(a) Measurement of the spectra. In a typical experiment, a sample of methylzinc tetrahydroborate was attached to the matrix-isolation assembly *via* an all-glass nozzle, and the glassware thoroughly conditioned by "flaming out" under continous

evacuation. Initial experiments were carried out with the sample maintained at -23°C for 90 min and co-condensation of the vapour with the matrix gas introduced at *ca.* 3.2 mmol h^{-1}. The condensate formed at 14 K gave sharply defined infrared absorptions suggesting that the vapour molecules were well isolated. Either dinitrogen or argon was used as the matrix gas in order to investigate the rôle of matrix site effects. The spectra of $[CH_3ZnBD_4]$ and $[CD_3ZnBH_4]$ were recorded in an analogous manner. Typical spectra are depicted in Figures 3.10-3.12, and Table 3.5 lists the wavenumbers as well as provisional assignments to fundamentals each described in terms of the principal component of the molecular motion.

Two features are evident from a survey of the spectra measured using the two matrix gases.

(i) The spectrum of methylzinc tetrahydroborate isolated in an argon matrix shows both a larger number of bands (for example, in the region of the spectrum associated with the deformation modes of the BH_4 group[7]) and substantial broadening of some bands. This reflects the more weakly interacting nature of argon as a matrix gas and the availability to guest molecules of a number of matrix sites. Depending on the different degrees of perturbation imposed by these matrix sites and the resolution of the spectrometer, the population of different sites leads either to multiplet structure or to band broadening for a given vibrational transition.[44] All the results listed are for matrices prepared with dinitrogen as the matrix gas.

(ii) The spectra of the matrix-isolated vapours from $[CH_3ZnBH_4]$, $[CD_3ZnBH_4]$ and $[CH_3ZnBD_4]$ each contain more bands than expected for a single species. For example, a monomeric $[MeZnBH_4]$ molecule incorporating a bidentate BH_4 group is expected to give a strong doublet in the region characteristic of $B–H_t$ stretching modes.[7] It is found, however, that the spectrum of the vapour from $[CH_3ZnBH_4]$ exhibits four bands - two strong bands and two somewhat weaker satellites appearing to high frequency of each of the stronger bands. Furthermore, two bands are observed in the region of the spectrum associated with the stretching of Zn–C bonds,[51] *viz.* at 604 and 585 cm^{-1}, where only one would be expected. In each case, the splitting between the bands (20-35 cm^{-1}) is too

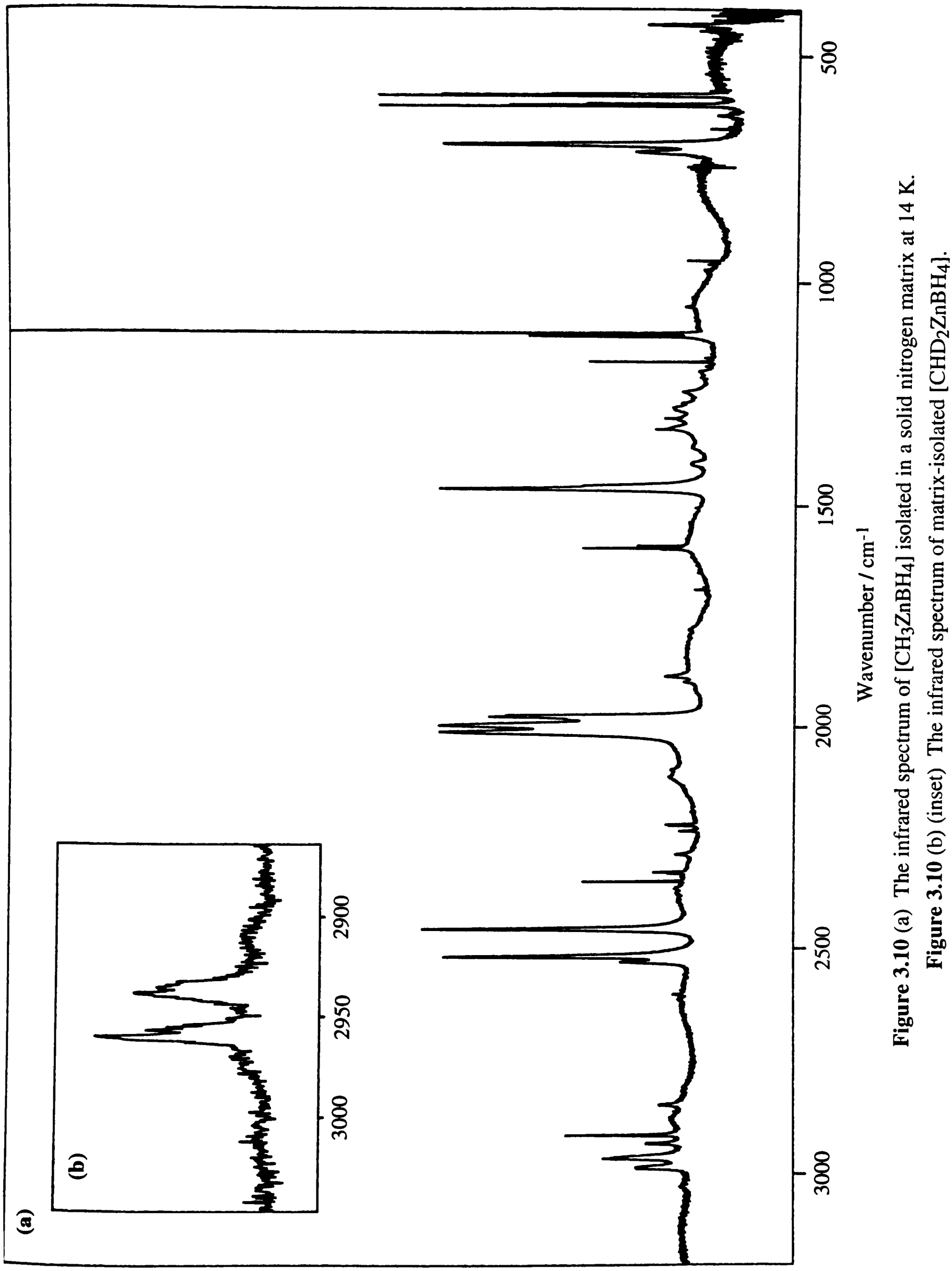

Figure 3.10 (a) The infrared spectrum of $[CH_3ZnBH_4]$ isolated in a solid nitrogen matrix at 14 K.

Figure 3.10 (b) (inset) The infrared spectrum of matrix-isolated $[CHD_2ZnBH_4]$.

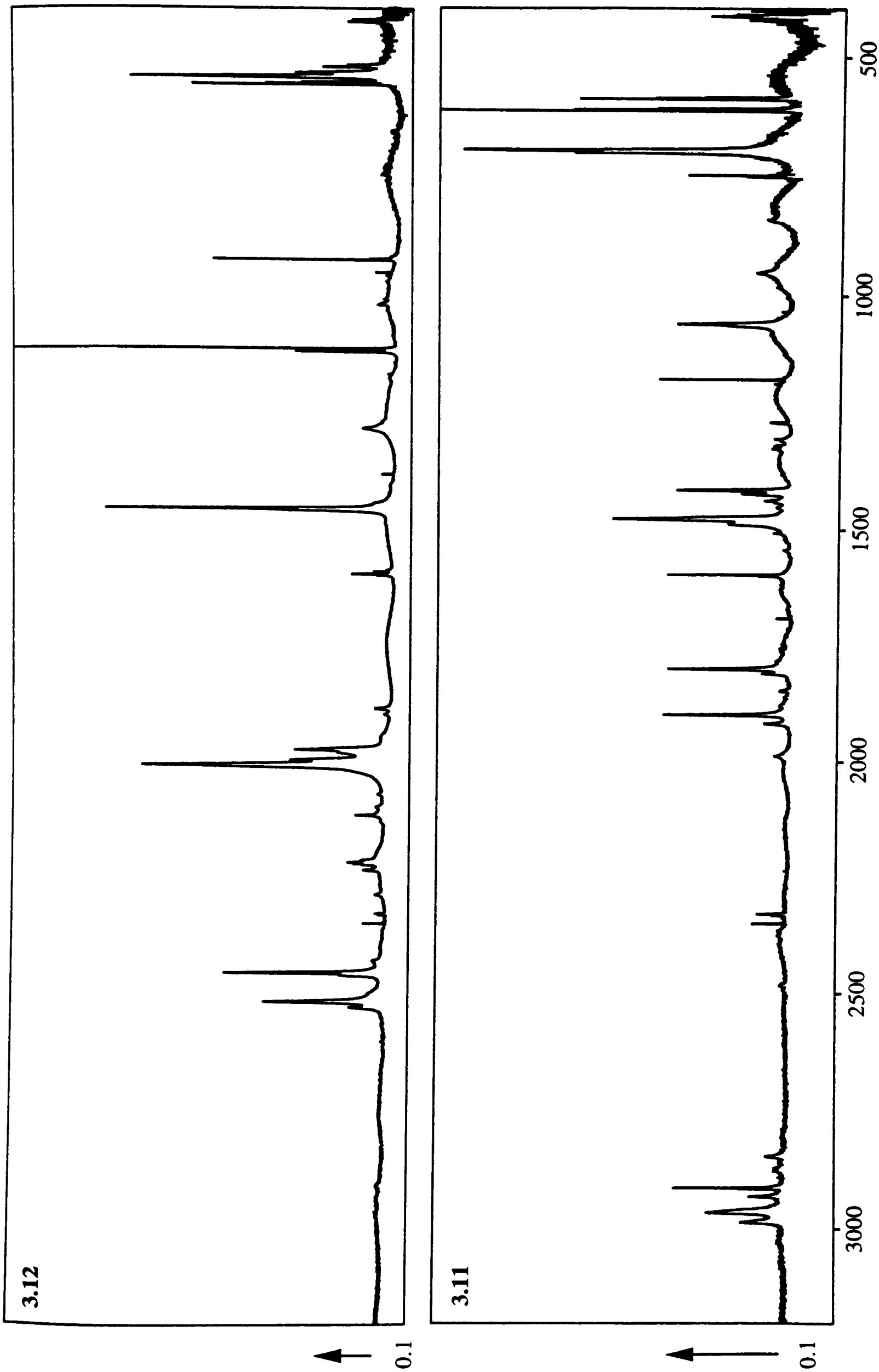

Figures 3.11 and 3.12 The infrared spectra of $[CH_3ZnBD_4]$ and $[CD_3ZnBH_4]$, respectively, isolated in solid nitrogen matrices at 14 K.

Table 3.5 Infrared spectra of matrix-isolated [CH_3ZnBH_4], [CH_3ZnBD_4] and [CD_3ZnBH_4] in the range 400-4000 cm^{-1}: wavenumbers (cm^{-1}) of absorptions displayed by the condensate at 14 K.

Provisional assignment	Infrared absorption, ν/cm^{-1} *a, b*					
	CH_3ZnBH_4		CH_3ZnBD_4		CD_3ZnBH_4	
ν_a(C–H)	2987	m	2987	w	2223	w, sh
	2965	m	2962	m	2221	w
	2953	mw, sh			2217	w
ν_s(C–H)	2932	m	2931	w	2117	w
	2915	m	2914	w	2098	w, br
2 x $\delta_a(CH_3)$	2847	w	2847	w, br		
1463 + 1122	2602	vw			2603	vw
ν_a(B–H_t)	2530	m	1918	w	2529	w
	2516	s	1899	s	2516	s
ν_s(B–H_t)	2461	m, sh	1810	w	2460	m, sh
	2454	s	1800	s	2454	s
CO_2	2348	mw	2348	w	2348	vw
	2330	w	2330	vw	2329	vw
	2327	w	2327	vw	2327	vw
?	2287	w			2287	vw
2 x BH_2 twist or 2 x $\delta(BH_2)$	2235	vw	1690	vw		
	2222	vw				
	2220	vw				
953 + 1121	2097	vw, br			2099	vw
ν_a(B–H_b)	2011	s	1488	m, sh	2008	vs
	1997	s	1477	vs	1998	m, sh
ν_s(B–H_b)	1983	m	1423	m	1981	m, sh
	1977	s	1415	s	1976	m
2 x $\rho(BH_2)$	1898	vw			1899	w
	1887	w			1887	vw

Table 3.5 (cont.) Infrared spectra of matrix-isolated $[CH_3ZnBH_4]$, $[CH_3ZnBD_4]$ and $[CD_3ZnBH_4]$ in the range 400-4000 cm^{-1}: wavenumbers (cm^{-1}) of absorptions displayed by the condensate at 14 K.

Provisional assignment	Infrared absorption, ν/cm^{-1} [a, b]					
	CH_3ZnBH_4		CH_3ZnBD_4		CD_3ZnBH_4	
$\nu_a(Zn–H_b)$	1463	s	1065	m	1460	s, sh
	1457	m, sh	1061	s, sh	1458	vs
$\delta_a(CH_3)$	1408	w, br			1019	w
					1017	vw
696 + 633	1330	w, br	1325	vw		
			1319	vw		
696 + 604	1306	w, br	1305	vw		
$\nu_s(Zn–H_b)$	1285	w, br	961	w	1285	w
?			1270	vw		
$\delta_s(CH_3)$	1179	m	1189	w	927	s
	1177	m, sh	1179	s	925	w
BH_2 twist	1122	m	750	w	1123	m
	1121	m, sh			1122	m, sh
$\delta(BH_2)$	1116	vs	844	m, br	1117	s, sh
	1115	vs, sh			1115	vs
$\rho(BH_2)$	953	w	747	m	953	w
BH_2 wag	713	m				
$\rho(CH_3)$	696	s	701	s, sh	545	vs
	633	mw	696	vs	540	s, sh
			630	w	536	m
$\nu(Zn–C)$	604	s	602	vs	561	s
	585	vs	586	s	524	m
$\nu(Zn–B)$	446	m, br	418	m, br	429	w, br

[a] Intensity abbreviations are listed in the notes. [b] All data refer to molecules isolated in solid nitrogen.

large to be attributed readily to matrix site effects (which typically produce splittings in the order of 5-10 cm^{-1}).[44] Such findings are entirely in keeping with the results of the mass spectrometry experiments, which pointed to a monomer/dimer equilibrium in the vapour phase.

Further evidence that there are two species present in the vapour being sampled comes from examination of the infrared spectrum of the matrix-isolated vapour [CHD_2ZnBH_4] illustrated in Figure 3.10 (b). The technique of partial deuteriation has been used by McKean *et al.* to probe the geometries of methyl groups.[52] In contrast to CH_3, CHD_2 groups give rise to a single, "isolated" C–H stretching frequency, little perturbed by interaction with other vibrational modes. A single absorption associated with this C–H stretching mode is therefore consistent with a single C–H environment. The existence of two bands (at 2941 and 2960 cm^{-1}) in the spectrum of the matrix-isolated vapour from [CHD_2ZnBH_4] is therefore consistent with the two distinct methyl environments expected for a two-component vapour phase system. Given that mass spectrometry experiments implied that the relative proportions of the two components vary with the temperature of the solid sample, it was decided to perform further matrix-isolation experiments in which the vapour was analyzed at different sample temperatures. It was hoped that changes in band intensity as a function of temperature would allow particular absorptions to be assigned to the different components of the vapour.

(b) Variation of sample temperature. The apparatus used was identical to that described previously, the sample of methylzinc tetrahydroborate being maintained at -30 or -5°C by the use of an appropriate low-temperature bath. In each case, [$MeZnBH_4$] was co-condensed with dinitrogen, this being introduced at a greater rate (*ca.* 5 mmol h^{-1}) in the case of the -5°C experiment in order to compensate for the increased vapour pressure of [$MeZnBH_4$] and ensure that the sample was well isolated. Representative spectra under the two sets of conditions are illustrated in Figure 3.13, together with the spectrum recorded previously for the vapour above the sample held at

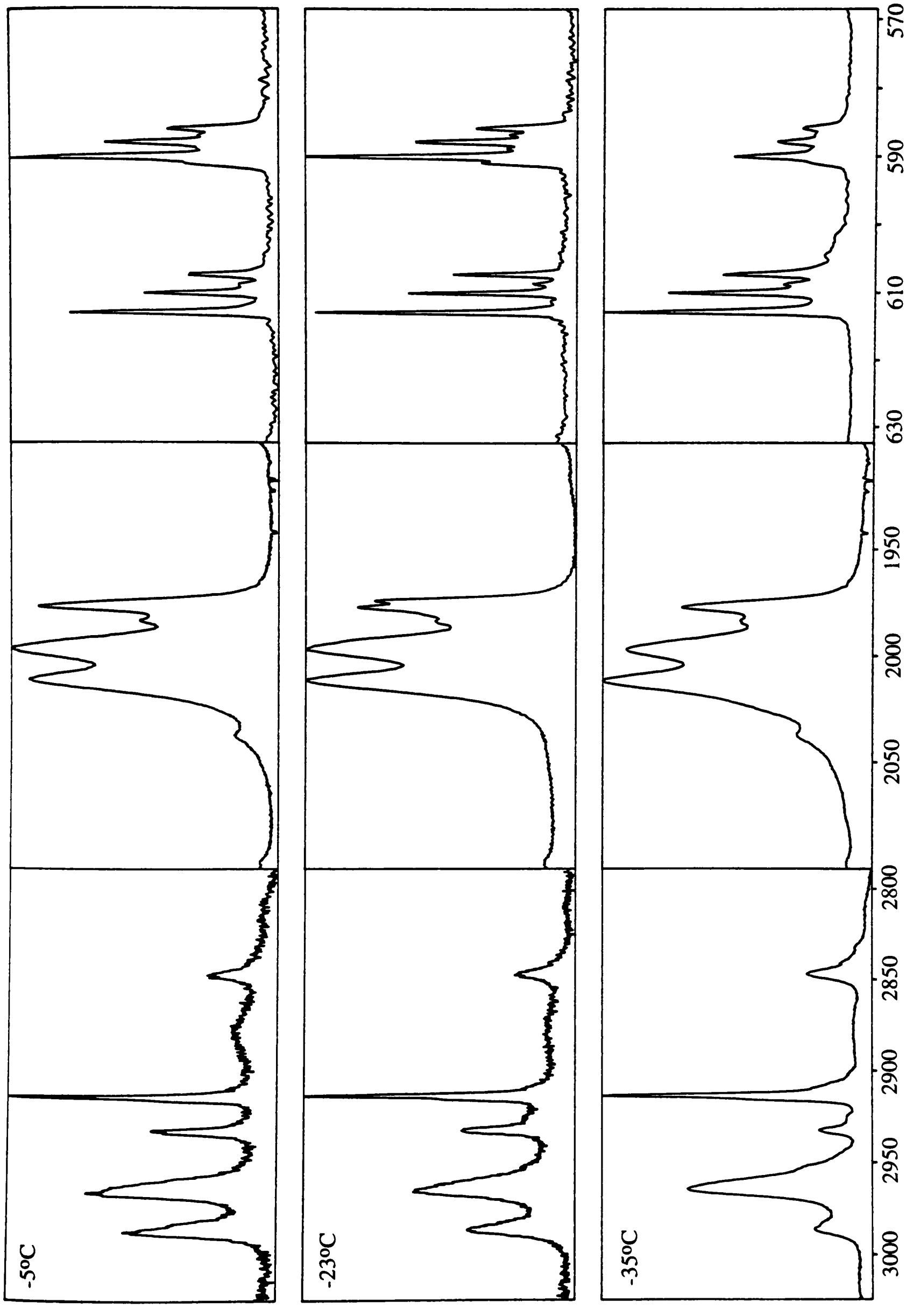

Figure 3.13 Infrared spectrum of matrix-isolated methylzinc tetrahydroborate: responses of band intensity to changes in sample temperature.

-23°C. Responses of band intensity to changes of sample temperature allowed provisional assignment of infrared bands to one of two species **A** and **B**. Further evidence for these assignments, and for the existence of a vapour-phase equilibrium between two species featuring different states of aggregation of $[MeZnBH_4]$, was obtained by examining the responses of band intensity to annealing of the matrix. Warming the matrix to *ca.* 35 K allows formerly isolated $[MeZnBH_4]_n$ molecules to interact by boiling away some of the intervening matrix gas. Consequently, bands due to higher oligomers would be expected to grow on annealing. Indeed, repeated annealing causes the appearance of bands attributable to solid methylzinc tetrahydroborate, the polymeric chain structure representing the limit of the aggregation process. In particular, there appear strong, broad bands at *ca.* 2200 and 560 cm^{-1} characteristic of the $\nu_a(B–H_b)$ and $\nu_a(Zn–C)$ motions of solid $[MeZnBH_4]$. Assignments of bands to the species **A** and **B** on the basis of experiments involving changes of spray-on temperature and annealing are listed in Table 3.6.

(c) Discussion of Matrix Isolation Results. The complexity of the infrared spectra measured in the initial experiments suggested the presence of more than one guest species. Subsequent experiments allowed the assignment of the observed absorptions to either of two species **A** and **B**. The nature of the bands assigned to each of these species is now discussed in detail.

Species A

Bands due to species **A** are found to decrease in intensity as the sample temperature is raised (and also on annealing) in a fashion analogous to the bands attributable to monomeric $[MeZnBH_4]$ in the mass spectrum (*vide supra*). The absorptions due to species **A** have been analysed in terms of the group vibrations appropriate to the molecule $[MeZn(\mu\text{-}H)_2BH_2]$ featuring bidentate ligation of the BH_4 group and conforming to C_s symmetry, to arrive at the assignments listed in Table 3.7.

Assignment	A			B		
	CH_3ZnBH_4	CH_3ZnBD_4	CD_3ZnBH_4	CH_3ZnBH_4	CH_3ZnBD_4	CD_3ZnBH_4
ν_a(C–H)	2965 2953	2962	2223 2221	2987	2987	2213
ν_s(C–H)	2915	2914	2117	2932	2931	2098
ν_a(B–H_t)	2516	1899	2516	2530	1918	2529
ν_s(B–H_t)	2454	1800	2454	2461	1810	2460
ν_a(B–H_b)	2011	1477	2008	1997	1448	1998
ν_s(B–H_b)	1983	1415	1981	1977	1423	1976
ν_a(Zn–H_b)	1463	1061	1458	1457	1065	1460
δ_a(CH_3)	1408	-	1023 1017	-	-	-
ν_s(Zn–H_b)	1285	961	1285	1306 ?	-	-
δ_s(CH_3)	1179	1179	927	1177	1189	925
BH_2 twisting	1121	750	1123	1122	-	1123
δ(BH_2)	1116	844	1116	1115	-	1115
ρ(BH_2)	953	747	953	-	-	-
BH_2 wagging	713	-	-	-	-	-
ρ(CH_3)	696 633	696 630	545 536	694	701	540
ν(Zn–C)	604	602	561	585	586	524
ν(Zn–B)	446	418	429			

Table 3.6 Assignment of the infrared bands of matrix-isolated methylzinc tetrahydroborate to species **A** and **B** on the basis of responses of band intensity to changes of sample temperature and to annealing of the matrix to *ca.* 35 K.

Table 3.7 Proposed assignment of the fundamentals of monomeric methylzinc tetrahydroborate

Symmetry type and number		Approximate description	Infrared absorption ν/cm^{-1} CH_3ZnBH_4	CH_3ZnBD_4	CD_3ZnBH_4	ν_H/ν_D
a'	ν_1	ν_a(C–H)	2965	2962	2223	1.334
	ν_2	ν_s(C–H)	2915	2914	2117	1.377
	ν_3	ν_a(B–H_t)	2516	1899	2516	1.325
	ν_4	ν_s(B–H_t)	2454	1800	2454	1.363
	ν_5	ν_s(B–H_b)	1983	1415	1981	1.401
	ν_6	$\delta_a(CH_3)$	1408	*a*	1017	1.384
	ν_7	ν_s(Zn–H_b)	1285	961	1285	1.337
	ν_8	$\delta_s(CH_3)$	1179	1179	927	1.272
	ν_9	$\delta(BH_2)$	1116	844	844	1.322
	ν_{10}	$\rho(BH_2)$	953	747	953	1.276
	ν_{11}	$\rho(CH_3)$	696	696	545	1.277
	ν_{12}	ν(Zn–C)	604	602	561	1.077
	ν_{13}	ν(Zn–B)	448	418	429	1.072, 1.044
	ν_{14}	CZnB in-plane bending	-	-	-	-
	ν_{15}	Ring torsion	-	-	-	-
a"	ν_{16}	ν_a(C–H)	2953	2962	2221	1.330
	ν_{17}	ν_a(B–H_b)	2011	1477	2008	1.362
	ν_{18}	ν_a(Zn–H_b)	1463	1061	1458	1.379
	ν_{19}	$\delta_a(CH_3)$	1408	*a*	1017	1.384
	ν_{20}	BH_2 twisting	1121	*ca.* 850	1123	-
	ν_{21}	BH_2 wagging	713	*a*	-	-
	ν_{22}	$\rho(CH_3)$	633	630	536	1.181
	ν_{23}	CZnB out-of-plane bending	-	-	-	-
	ν_{24}	CH_3 torsion	-	-	-	-

[a] Probably obscured by more intense features.

Such a molecule has 24 normal modes spanning the representations 15a' + 9a", all of which are active in infrared absorption. The low symmetry of the molecule, combined with similarities in energy of some of the modes, particularly those at low frequency, means that there will inevitably be some mixing of the normal coordinates. The description of the normal modes as written does appear to be self-consistent, although it is difficult to say, in the absence of a detailed normal coordinate analysis, how closely they relate to the true picture. These normal modes are consistent with the results calculated from Density Functional Theory (for a harmonic force field) inasmuch as they specify the *principal* component of each motion in most cases. The only significant exceptions arise in the cases of the low-frequency torsional and skeletal bending modes and the BH_2 wagging and CH_3 rocking modes which are appreciably mixed.

The assignments proposed are based on one or more of the following criteria: (i) analogy with the vibrational assignments favoured for other molecules containing methylzinc {*e.g.* $[Me_2Zn]$[51] and [MeZnX] (X = Cl, Br or I)[53]} or bidentate BH_4 groups {*e.g.* $[Me_2GaBH_4]$,[27] $[Me_2AlBH_4]$,[36] $[H_2GaBH_4]$[35] and $[Al(BH_4)_3]$[54]}; (ii) the effect of selective deuteriation at the CH_3 and BH_4 groups on the frequency of a given spectroscopic feature; (iii) reference to the infrared spectrum of solid methylzinc tetrahydroborate; (iv) the appearance of distinct features arising from different naturally occurring isotopes (notably ^{68}Zn, ^{66}Zn and ^{64}Zn); and (v) comparison with the frequencies calculated using Density Functional Theory (see Section 3.2.3).

The infrared spectrum of **A** is most plausibly interpreted in terms of a molecular model of C_s symmetry involving three-fold coordination of the zinc centre and a *bis*(hydrogen-bridged) $Zn(\mu\text{-}H)_2B$ moiety. Not only are the spectral features characteristic of the MeZn group readily apparent,[51,53] but the pattern of absorptions normally associated with a doubly bridged tetrahydroborate group is also strongly in evidence.[7] These features are now discussed in more detail.

(i) The CH_3Zn unit. Infrared absorptions at 2965 (2223) and 2915 (2117) cm^{-1} are assigned to the ν_a(C–H) and ν_s(C–H) modes, respectively, by analogy with the

corresponding bands in [$(CH_3)_2Zn$] [2965.8 (2216.6) and 2913.4 (2117.6) cm^{-1}][51] and in solid [CH_3ZnBH_4] [2972 and 2910 cm^{-1}]. Imposition of overall C_s molecular symmetry upon the CH_3Zn group would be expected to remove the degeneracy of the two ν_a(C–H) modes (of *e* symmetry in C_{3v}), giving rise to two distinct bands [ν_1(a') and ν_{16}(a")]. A shoulder to the low-wavenumber side (2953 cm^{-1}) of the band at 2965 cm^{-1} has been tentatively assigned to the second of these modes. A splitting of *ca.* 5 cm^{-1} is predicted by Density Functional Theory.

A weak feature at 1408 (1017) cm^{-1} and a much stronger one at 1179 (927) cm^{-1} are assigned to the antisymmetric and symmetric deformation modes of the CH_3 group, the corresponding bands being observed at 1445 and 1186.3 (922.9) cm^{-1} for [$(CH_3)_2Zn$][51] and at 1443 (1045) and 1180 (972) cm^{-1} for solid [CH_3ZnBH_4]. Again, splitting of $\delta_a(CH_3)$ into two components ν_6(a') and ν_{19} (a") in C_s symmetry is expected, although the weak and somewhat broad nature of the features renders any such splitting unresolvable (Density Functional Theory calculates a splitting of only 2 cm^{-1}). Methyl rocking modes, $\rho(CH_3)$, are predicted at 712.2 and 646.4 cm^{-1} from DFT calculations (with relative intensities of *ca.* 4:1). These are assigned to bands at 696 (545) and 633 (536) cm^{-1}, the observed intensity of the latter being much smaller than that of the former. The analogous rocking mode in dimethylzinc appears at 704 (553.5) cm^{-1}.[51]

Furthermore, the position of the Zn–C stretching fundamental, *viz.* 604 (561) cm^{-1} is similar to that found in gaseous dimethylzinc [617.5 (565) cm^{-1}].[51] Further support for this assignment is provided by the isotopic splitting observed at higher resolution; the band is resolved into a triplet with components having relative intensities of *ca.* 2:3:5 in order of increasing wavenumber. Such a pattern is consistent with the assignment of components to $\nu(^{68}Zn–C)$, $\nu(^{66}Zn–C)$ and $\nu(^{64}Zn–C)$, respectively (the natural abundances of ^{68}Zn, ^{66}Zn and ^{64}Zn are 18.6, 27.8 and 48.9%, respectively[45]).

(ii) The $Zn(\mu\text{-}H)_2BH_2$ unit. The two bands at 2516 (1899) and 2454 (1800) cm^{-1} are characteristic of the $\nu_a(B–H_t)$ and $\nu_s(B–H_t)$ vibrations of a molecule containing a bidentate tetrahydroborate group {*cf.* [$Al(BH_4)_3$],[54] [Me_2AlBH_4],[36] [Me_2GaBH_4],[27]

$[H_2GaBH_4]$[35] and $[HGa(BH_4)_2]$[33]}. In addition to the B–H_b stretching fundamentals at 2011 (1477) and 1983 (1415) cm^{-1} which are similarly characteristic of a bidentate BH_4 group,[27,33,35,36,54] two further bands at 1463 (1061) and 1285 (961) cm^{-1} are plausibly assigned to the antisymmetric and symmetric Zn–H_b stretching motions of the Zn(μ-H)$_2$B group. In the absence of reported infrared frequencies for structurally authenticated compounds containing the Zn(μ-H)$_2$B moiety, comparisons with the analogous Ga–H_b stretching modes in $[H_2GaBH_4]$ [1435 (1060) and 1320 (980) cm^{-1} [35]] and $[HGa(BH_4)_2]$ [1450 (1028) and 1312 (987) cm^{-1} [33]] and with *harmonic* frequencies calculated on the basis of Density Functional Theory (1437.4 and 1299.8 cm^{-1}) corroborate these assignments.

Assignments of the deformation, rocking, wagging and twisting modes of the (μ-H)$_2$BH$_2$ unit were achieved principally by analogy with the corresponding frequencies for $[Me_2GaBH_4]$[27] and $[H_2GaBH_4]$,[35] and by reference to the frequencies calculated by Density Functional Theory. [Observed (calculated) values in cm^{-1}: δ(BH$_2$) 1116 (1136.5); ρ(BH$_2$) 953 (971.1); BH$_2$ twisting 1121 (1179.4); BH$_2$ wagging 713 (741.0)]. Finally, the assignment of the Zn–B stretching mode to a band at 448 cm^{-1} is consistent with values expected for this sort of motion in analogous M(μ-H)$_2$B units {*cf.* 445 cm^{-1} for $[Me_2GaBH_4]$ and 468 cm^{-1} for $[H_2GaBH_4]$}. It is interesting to note how close this value is to the frequency of the feature assigned to the antisymmetric Zn–B stretching mode of the Zn(μ-H)$_2$B(μ-H)$_2$Zn unit in solid methylzinc tetrahydroborate.

Species B

The relatively small number of bands distinguishable for species **B** in the infrared spectra means that any conclusions concerning its likely structure are necessarily tentative. Many of the bands appear at frequencies similar to those of features attributable to monomeric $[MeZnBH_4]$, and the assignments have been made with the aid of similar criteria.

There are several possibilities regarding the nature of species **B**, and examination of the infrared bands allows some conclusions to be drawn. That **B** is a monomeric species, for example [$MeZn(\mu\text{-}H)BH_3$] or [$MeZn(\mu\text{-}H)_3BH$] incorporating different modes of ligation of the BH_4 group (as was suggested by Gaines for [$Be(BH_4)_2$][55]) seems unlikely. Infrared features attributable to **B** are inconsistent with either monodentate or tridentate ligation, showing neither the characteristic features due to the stretching vibrations of terminal B–H bonds of the former (2300-2450 cm^{-1} [7]) nor those due to the stretching vibrations of bridging B–H bonds of the latter (2000-2100 cm^{-1} [7]).

Indeed, the similarities between the positions of bands attributable to **A** and **B** (typically differing by no more than 30 cm^{-1}), together with the results of the mass spectrometry experiments suggests that **B** is in fact the dimer [$MeZnBH_4]_2$ retaining bidentate coordination of the BH_4 group. Such an equilibrium is thought to exist in the gas phase for [$MeBeBH_4$] (monomer/dimer)[50,56] and also finds precedents in the cases of dimethyalane (dimer/trimer or dimer/tetramer equilibria in the vapour and in the solution[57]) and [H_2GaBH_4] (monomer/oligmer equilibrium in toluene solution[35]).

Dimeric methylberyllium tetrahydroborate is thought to have a methyl-bridged

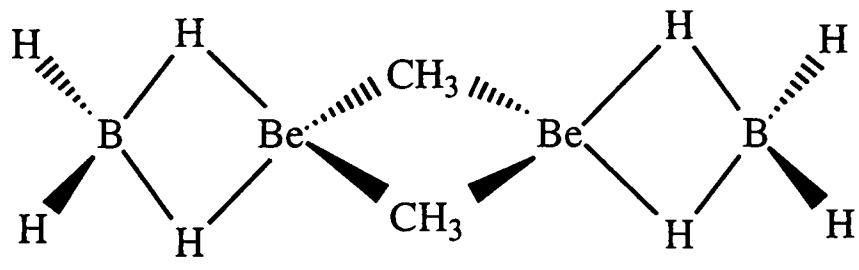

I

structure, **I**, akin to that of gaseous [Me_2Be].[58] An analogous structure for [$MeZnBH_4]_2$ seems unlikely given that dimethylzinc, unlike its beryllium counterpart, shows no tendency to engage in methyl-bridged oligomerization. In addition, dimethylberyllium and the methylberyllium tetrahydroborate dimer give rise to strong infrared bands at 798 and 754 cm^{-1}, respectively, attributable to the perpendicular rocking mode of the bridging methyl group [50,56] (the rocking motion of the terminal methyl group in monomeric [$MeBeBH_4$] comes at 627 cm^{-1} [56]). No such band is observed among the absorptions attributable to species **B**. Indeed, the methyl rocking mode for **B** is shifted

only slightly from that of **A** *i.e.* monomeric [$MeZnBH_4$]. Another possible structure for [$MeZnBH_4$]$_2$ is $MeZn(\mu\text{-}H)_2B(\mu\text{-}H)_2Zn(Me)(\mu\text{-}H)_2BH_2$, **II,** incorporating non-equivalent BH_4 groups, and arising from breakage of the polymeric chain present in the

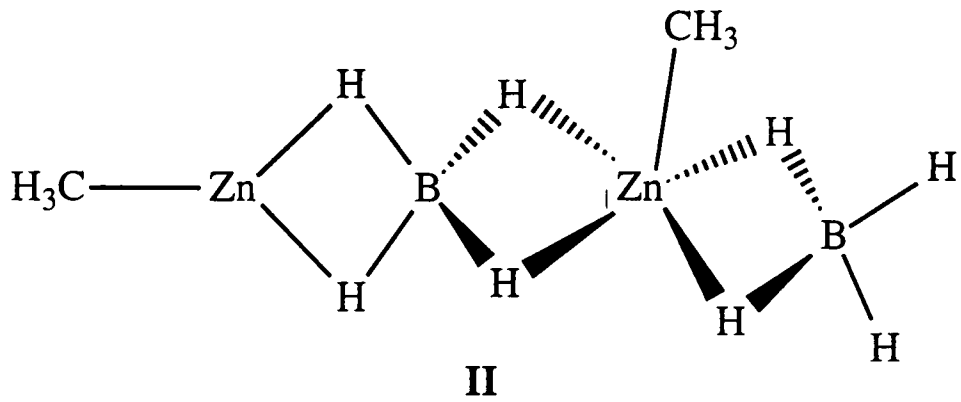

II

solid state into binuclear fragments. Such a species would in all probability give rise to a pattern of absorptions due to the stretching motions of the B–H_b bonds different from that observed for **B**. Thus, one might reasonably expect the $Zn(\mu\text{-}H)_2B(\mu\text{-}H)_2Zn$ unit to give rise to features similar to those seen for the corresponding unit in the solid (2256, 2224 and 2209 cm^{-1}).

A third possibility incorporates a pair of μ_2,η^2-BH_4 groups bridging the two zinc centres to give a cyclic dimer, **III**. Such a structure is not without precedent, the

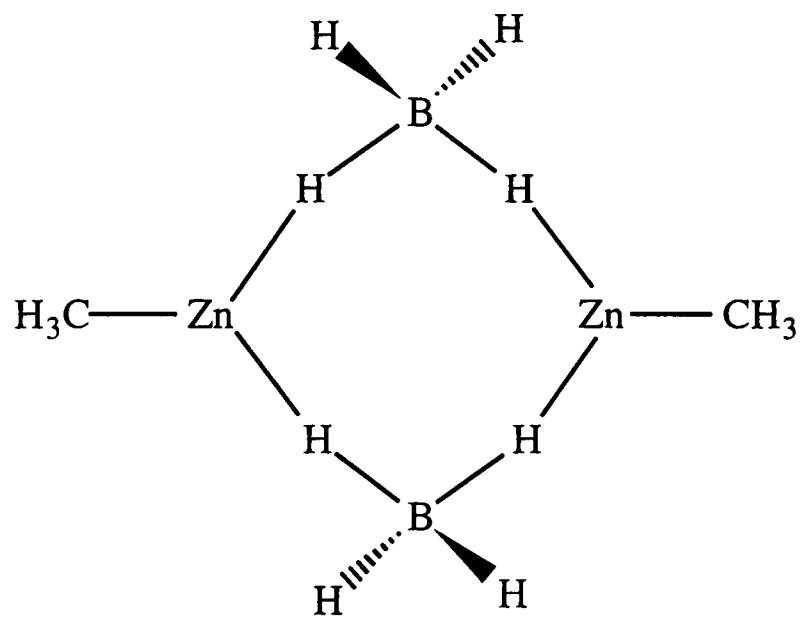

III

$M(\mu\text{-}H)B(H)_2(\mu\text{-}H)M$ moiety also occurring in the compound $(Cp^*Ir)_2H_3(BH_4)$.[59] An analogous dimeric structure incorporating an eight-membered ring has also been proposed for [$Cp^*Cr(BH_4)$]$_2$ in solution.[60] This type of structure would be expected to give a pattern of bands in the infrared spectrum similar to that of monomeric

[$MeZnBH_4$]. By forcing the BH_4 ligands to bridge two metal centres, the Zn···B distance would necessarily increase, reducing considerably the interaction between the zinc and boron atoms and therefore lowering the frequency of any Zn–B stretching vibration. That no such feature is observed, even at frequencies as low as 250 cm^{-1}, is therefore consistent with such a structure, although it provides no positive evidence and can be explained equally plausibly in terms of the broad nature typical of absorptions arising from this sort of motion.[61] The Zn–C stretching frequency is located at 590 cm^{-1} for species **B**, intermediate between the frequency for monomeric [$MeZn(\mu\text{-}H)_2BH_2$] (604 cm^{-1}) and that for the solid (557 cm^{-1}), a finding consistent with an intermediate state of aggregation.

Although no firm conclusions can be drawn concerning the nature of species **B**, the observed increases in intensity of its infrared bands on annealing and on increasing the sample temperature, taken together with the results of the mass spectrometry experiments, provide persuasive evidence that it is the dimer $[MeZnBH_4]_2$. Of the possible structures considered, the infrared bands are best interpreted in terms of a cyclic dimer of the type [$MeZn(\mu_2,\eta^2\text{-}BH_4)_2ZnMe$].

3.2.3 Calculated Structures and Frequencies of $[MeZnBH_4]$ and $[MeZnBH_4]_2$

In order to assist in assigning the infrared bands for $[MeZnBH_4]$ and $[MeZnBH_4]_2$, Density Functional Theory (DFT) calculations were carried out by Professor Schleyer's research group at the University of Erlangen-Nürnberg. Harmonic force fields and geometry optimizations were calculated for each model, yielding atomic coordinates, cartesian force constants and harmonic vibrational frequencies.

In the event of obtaining reasonable electron-diffraction patterns for the vapour of methylzinc tetrahydroborate, amplitudes of vibration and perpendicular amplitude corrections calculated from the DFT results (and scaled if necessary) were to be used in constraining the structure refinement. Even in the absence of electron-diffraction measurements, it was hoped that satisfactory agreement between observed and

calculated infrared frequencies (with due allowance for anharmonicity) would allow useful conclusions to be reached concerning the geometries of the molecules $[MeZnBH_4]$ and $[MeZnBH_4]_2$. Details of the calculations can be found in Section 2.3.8.

3.2.3.1 Discussion of Results

(a) [MeZnBH$_4$]. Tables of atomic coordinates, harmonic frequencies, infrared intensities and cartesian force constants, together with details of the distance matrix are listed in Appendix 2. Perspective and plan views and relevant bond lengths and angles of the final geometry optimization of $[MeZnBH_4]$ are shown in Figure 3.14 and Table 3.8, respectively. In addition, Table 3.9 compares the observed and calculated (harmonic) frequencies for $[MeZnBH_4]$. In order to allow for the effects of anharmonicity, the relationship

$$\nu_i = \omega_i (1 - x_i)$$

was employed, where ν_i = the anharmonic frequency, ω_i = the harmonic frequency and x_i = an anharmonicity constant. The values of x_i used are those suggested by Duncan *et al.* in their study of $[B_2H_6]$,[62] and which have subsequently been used to compared observed and calculated frequencies for $[H_2Ga(\mu\text{-}Cl)_2GaH_2]$,[63] $[HGa(BH_4)_2]$[40] and $[Si_2H_6]$[64] Hence,

x_i = 0.035 for C–H and B–H_t stretching modes

= 0.030 for B–H_b and Zn–H_b stretching modes

= 0.020 for angle deformation modes

= 0.010 for Zn–C and Zn–B stretching modes.

Frequencies derived from theoretical methods are typically 10% higher than those measured by experiment.[65] For $[MeZnBH_4]$, the root-mean-square difference between observed and calculated values is 68.6 cm^{-1} (3.21%), although, when due allowance is made for the anharmonic nature of the experimental frequencies, this value is reduced to 27.2 cm^{-1} (2.01%). The level of agreement is therefore pleasingly close, the discrepancy

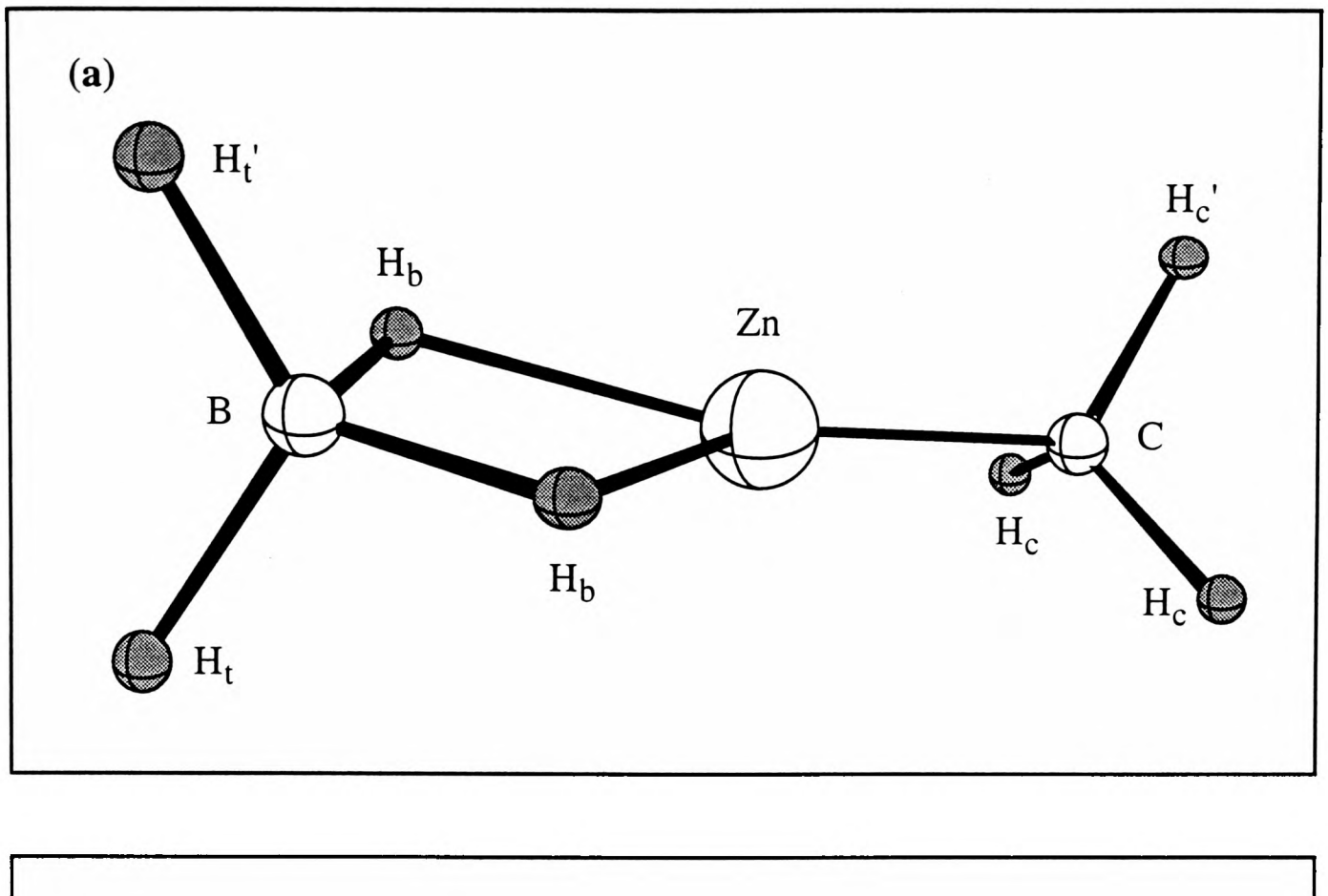

Figure 3.14 (a) Perspective view and (b) plan views of the final geometry optimization of [$MeZnBH_4$] using Density Functional Theory.

Table 3.8 Bond lengths (Å) and angles (°) for the final geometry optimization of monomeric [$MeZnBH_4$] using Density Functional Theory.[a,b]

$B–H_t$	1.1971	Zn–C	1.9448
$B–H_t'$	1.1960	$C–H_c$	1.0917
$B–H_b$	1.2739	$C–H_c'$	1.0923
$Zn–H_b$	1.7830	Zn···B	2.1483
$H_t–B–H_t'$	119.06	$Zn–H_b–B$	87.64
$H_b–B–H_b$	111.77	$C–Zn–H_b$	143.71
$H_b–B–H_t$	105.87	$Zn–C–H_c$	110.84
$H_b–B–H_t'$	107.18	$Zn–C–H_c'$	110.32
$H_b–Zn–H_b$	72.53	$H_c–C–H_c$	108.39
B···Zn–C	178.97	$H_c–C–H_c'$	108.18

[a] Abbreviations used: t = terminal, b = bridging, c = bonded to carbon. [b] Prime denotes an atom lying within the plane defined by the $B(H_t)_2$ unit.

Table 3.9 Comparison of observed and calculated frequencies for monomeric [$MeZnBH_4$].

Approximate description		Wavenumbers / cm^{-1}			
		$\nu_{i,\,obs}$[a]	$\omega_{i,\,obs}$[a]	$\omega_{i,\,calc}$[a]	$\Delta\omega_i$[b]
a' block					
ν_a(C–H)	ν_1	2965	3073	3109.8	37
ν_s(C–H)	ν_2	2915	3021	3032.7	12
ν_a(B–H_t)	ν_3	2516	2607	2610.8	4
ν_s(B–H_t)	ν_4	2454	2543	2535.6	-7
ν_s(B–H_b)	ν_5	1983	2044	2074.8	31
$\delta_a(CH_3)$	ν_6	1408	1437	1455.7	19
ν_s(Zn–H_b)	ν_7	1285	1325	1299.8	-25
$\delta_s(CH_3)$	ν_8	1179	1203	1229.2	26
$\delta(BH_2)$	ν_9	1116	1139	1136.6	-2
$\rho(BH_2)$	ν_{10}	953	972	971.1	-1
$\rho(CH_3)$	ν_{11}	696	710	712.2	2
ν(Zn–C)	ν_{12}	604	610	579.6	-30
ν(Zn–B)	ν_{13}	448	453	444.8	-8
CZnB in-plane bending	ν_{14}	-	-	247.0	-
Ring torsion	ν_{15}	-	-	70.0	-
a'' block					
ν_a(C–H)	ν_{16}	2953	3060	3114.2	54
ν_a(B–H_b)	ν_{17}	2011	2073	2073.7	1
ν_a(Zn–H_b)	ν_{18}	1463	1508	1437.3	71
$\delta_a(CH_3)$	ν_{19}	1408	1437	1453.7	17
BH_2 twisting	ν_{20}	1121	1144	1179.4	35
BH_2 wagging	ν_{21}	713	728	741.0	13
$\rho(CH_3)$	ν_{22}	633	646	646.4	0
CZnB out-of-plane bending	ν_{23}	-	-	121.2	-
CH_3 torsion	ν_{24}	-	-	96.1	-

[a] Abbreviations: obs = observed; calc = calculated. [b] $\Delta\omega_i = \omega_{i,\,calc} - \omega_{i,\,obs}$.

being similar in magnitude to that observed between experimental and DFT calculated values for [$HGa(BH_4)_2$] (25.1 cm^{-1}).[40] Furthermore, the ordering of vibrational modes is in good agreement [the only discrepancy involving the $\delta_a(CH_3)$ and $\nu_a(Zn–H_b)$ modes of a" symmetry] and so lends weight to the assignments proposed. The discrepancies are mostly well within the range set by the approximations inherent in the theoretical methods, although there are some places where the experimentally determined values are less well defined, reflecting the inherently weak or broad nature of the absorption in question.

The greatest difference between experimental and theoretical values occurs for the Zn–C and $Zn–H_b$ stretching modes. In each case, the calculated values are *ca.* 4.8% *less* than the experimental frequencies, possibly reflecting a slight underestimation in the strength of interaction between the methylzinc and BH_4 centres. In general though, the level of agreement between calculated and experimental frequencies is good, a finding tending to validate the bond lengths and angles determined using DFT.

The calculated structure conforms to C_s symmetry, the plane of symmetry passing through H_t, B, Zn, C and one of the methyl H atoms. The final geometry optimization was found to be only 4 kJ mol^{-1} lower in energy than a structure featuring tridentate ligation of the BH_4 group. The corresponding energy difference for [$Al(BH_4)_3$] [between $Al(\eta^2\text{-}BH_4)_2(\eta^3\text{-}BH_4)$ and $Al(\eta^2\text{-}BH_4)_3$] was found to be 9.1 kJ mol^{-1}, whereas the geometry with monodentate ligation [$Al(\eta^2\text{-}BH_4)_2(\eta^1\text{-}BH_4)$] was found to be *ca.* 58 kJ mol^{-1} higher in energy.[66] These findings lend further weight to the presumption that bidentate/tridentate equilibration is the likely cause of the fluxionality displayed by many tetrahydroborate derivatives in solution.[7,29] Distortions (i) of the B–Zn–C framework from linearity and (ii) of the $B(H_b)_2Zn$ framework from planarity, are slight, and almost certainly reflect the fixed methyl orientation and differing interactions between H_b and H_c and H_b and H_c' (H_c denoting a hydrogen atom bound to carbon). It is expected that rapid rotation about the Zn–C bond will average these differences to zero and that a linear B–Zn–C framework will be found in the gaseous molecule.

Several of the calculated structural parameters call for further comment.

(i) At 2.148 Å, the Zn–B bond length is comparable in magnitude to the sum of the covalent radii of zinc and boron (2.15 Å),[19] and very similar to the corresponding bond length determined for [Me_2GaBH_4] by electron diffraction (2.14 Å) (the covalent radii for Ga and Zn being 1.26 and 1.31 Å, respectively).[39] The calculated Zn–B bond length is, on the other hand, significantly shorter than that found in the solid (2.30-2.32 Å), although the difference (0.17 Å) is less than that between the Be–B distances found in gaseous [$Be(BH_4)_2$] and within the polymeric chain of solid [$Be(BH_4)_2$] (0.24 Å).[8,9,48] It is likely that this difference originates in the more tightly bound nature of zinc and BH_4 centres in *solid* $MeZnBH_4$ (*vide supra*), rather than in any anomalous bonding in the monomer.

(ii) The calculated Zn–H_b distances (1.783 Å) are very similar to the M–H_b distances determined by electron diffraction for [Me_2GaBH_4] (1.79 Å),[39] [Me_2AlBH_4] (1.77 Å)[39] and [$Al(BH_4)_3$] (1.80 Å)[42] (the covalent radii for Ga, Al and Zn being 1.26, 1.26 and 1.31 Å, respectively). It is interesting to note that the calculated Zn–H_b bond length for *monomeric* [$MeZnBH_4$] is within one standard deviation of that found in the solid phase [1.82 (5) Å]. This finding supports the view that there is significant Zn–H interaction in the solid, and consequently the formulation of the solid in terms of [$Zn(\mu\text{-}H)_2B(\mu\text{-}H)_2Zn$] units. In addition, there is no significant difference between the H_b–Zn–H_b angles for the calculated structure and for the solid (72.5 and 70(2)°, respectively)

(iii) The Zn–C bond length is unremarkable, being similar to that determined by electron diffraction for [$ZnMe_2$] [1.930(2) Å].[67]

(iv) The calculated dimensions of the BH_4 ligand are also as expected for linkage to a metal atom *via* two bridging hydrogens. The B–H_t and B–H_b bond lengths and the $B(H_t)_2$ and $B(H_b)_2$ angles are very similar to those found for [Me_2GaBH_4],[39] [Me_2AlBH_4][39] and [$Al(BH_4)_3$].[42]

In conclusion, the pleasing agreement between observed and calculated frequencies, together with the similarities in structural parameters with those obtained

experimentally for other molecules containing the MeZn and $M(\mu\text{-}H)_2BH_2$ units, suggests that the final geometry optimization represents a reasonable approximation to the actual structure of monomeric [$MeZnBH_4$].

(b) [$MeZnBH_4$]$_2$ Of the possible structures considered for the dimer [$MeZnBH_4$]$_2$, a cyclic species incorporating BH_4 ligands bridging two zinc centres appeared best to fit the observed infrared spectrum. In order to test this as a potential structure, *ab initio* methods were used to optimize the geometry for such a species and to calculate harmonic vibrational frequencies. It was hoped that comparison of observed and calculated frequencies would then provide a means of assessing the plausibility of such a model.

Perspective and plan views of the final geometry optimization at the HF/tzp level are shown in Figure 3.15 and relevant bond lengths and angles are listed in Table 3.10. The minimum energy structure is based on a puckered $Zn(\mu\text{-}H)B(H)_2(\mu\text{-}H)Zn(\mu\text{-}H)B(H)_2(\mu\text{-}H)Zn$ ring, and conforms to C_{2v} symmetry, the dihedral angle (that is, the angle between the two ZnB_2 planes) being 148.4°. A full list of harmonic frequencies, force constants and infrared intensities together with details of the atomic coordinates are to be found in Appendix 3.

In general, the coupling between the normal modes of vibration of individual CH_3 groups and between distinct BH_4 units is extremely small. For example, the separation between ν_{53} and ν_{54} {corresponding to antisymmetric and symmetric combinations of ν_a(C–H) (ν_{16} for monomeric [$MeZnBH_4$])} is calculated to be less than 0.1 cm^{-1}. Likewise, the splitting between ν_{47} and ν_{48} (2684.3 and 2685.5 cm^{-1}), corresponding to symmetric and antisymmetric combinations of $\nu_a(B\text{–}H_t)$ {ν_3 for monomeric [$MeZnBH_4$]} is very small.

It is difficult to compare calculated frequencies for the monomer and dimer because of the markedly different levels of theory used in the two sets of calculations. However, the conclusion that coupling between different CH_3 groups and between different BH_4 groups in the dimer is barely significant is consistent with the small

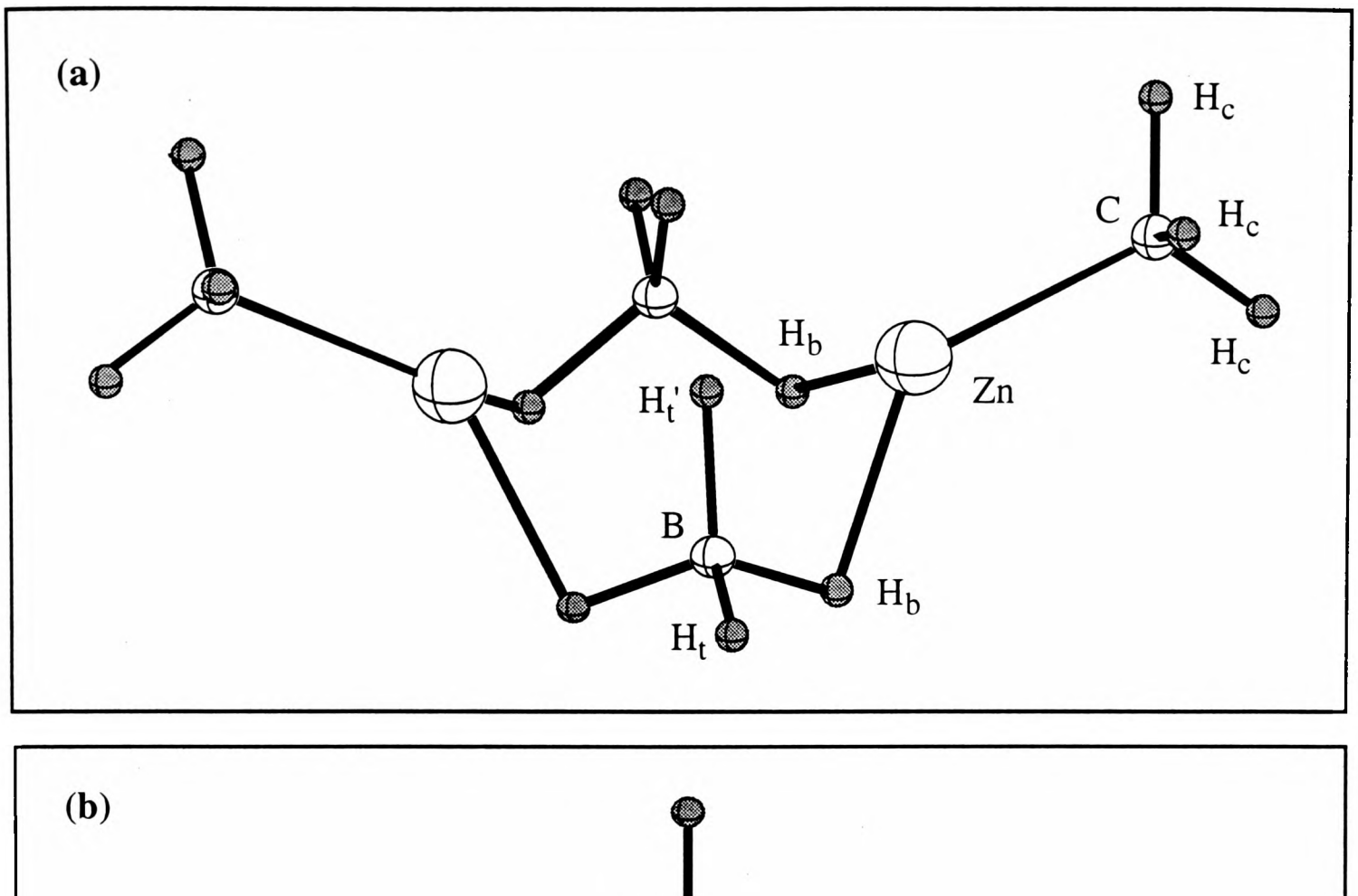

Figure 3.15 (a) Perspective and (b) plan views of the final geometry optimization of the cyclic dimer $[MeZnBH_4]_2$ at the HF/tzp level.

Table 3.10 Bond lengths (Å) and angles (°) for the final geometry optimization of the cyclic dimer $[MeZnBH_4]_2$ at the HF/tzp level.[a]

$B–H_t$	1.1906	$C–H_c$	1.0860
$B–H_t'$	1.2421	Zn···B	2.4667
$B–H_b$	1.2456	Zn···Zn	3.4122
$Zn–H_b$	1.8931	B···B	3.4301
Zn–C	1.9949		
$H_t–B–H_t'$	109.28	$H_b–Zn–C$	128.55
$H_b–B–H_b$	104.16	$Zn–C–H_c$	110.90
$H_b–B–H_t$	110.66	$H_c–C–H_c$	107.72
$H_b–B–H_t'$	110.01	B–Zn–B	88.90
$H_b–Zn–H_b$	88.91	Zn–B–Zn	87.52
B–Zn–C	134.53	Dihedral angle	148.44
$Zn–H_b–B$	101.61		

[a] Abbreviations used: t = terminal, b = bridging, c = bonded to carbon.

frequency shifts separating the observed features ascribed to the various internal modes of the CH_3 and BH_4 groups in the monomer and dimer.

The *pattern* of bands predicted by the *ab initio* calculations for $[MeZnBH_4]_2$ and the relative ordering of the vibrational modes are both in good agreement with experiment, but the root-mean-square deviation between the observed (harmonized) and calculated values is less satisfactory (114 cm^{-1}, 7.4%). Although one might reasonably expect the agreement to be poorer for the dimer than for the monomer (27.2 cm^{-1}, 2.01%), in keeping with the the much lower level of theory which has to be used with the larger molecule, this cannot be the sole reason for such a discrepancy. Frequencies calculated for $[HGa(BH_4)_2]$ by Density Functional Theory differed from observed values by 25.1 cm^{-1} (RMS deviation), this figure increasing to 39.9 cm^{-1} for lower level *ab initio* methods.[40] Clearly, the much larger discrepancy for $[MeZnBH_4]_2$ must call into question the validity of the theoretical model and, in the absence of reliable electron-diffraction results, it is difficult to reach any definite conclusions about the structure of the dimer.

It is interesting to note that the ordering of calculated frequencies for the Zn–C stretching fundamental of monomer and dimer (579.6 and 557.5 cm^{-1}, respectively) agrees with that found experimentally (604 and 585 cm^{-1}). Indeed, the predicted splitting (22.1 cm^{-1}) is remarkably similar to the measured value (19 cm^{-1}). The value of the ratio ν/ν' (where ν refers to the monomer and ν' to the dimer) found experimentally (1.032) and that derived from the calculated frequencies (1.039) are similar to the ratio expected simply by considering the methyl group as a point mass oscillating harmonically against a much heavier zinc-containing fragment (this gives ν/ν' = 1.045). Furthermore, the position of ν(Zn–C) shows a steady decrease as the state of aggregation increases (604, 585 and 557 cm^{-1} for the monomer, dimer and solid, respectively). This probably reflects greater electron deficiency in the MeZn unit in the solid, as compared with monomeric $[MeZnBH_4]$, the properties of the dimer implying an intermediate state of aggregation.

3.3 Chemical Properties of Methylzinc Tetrahydroborate

Some of the chemical properties of methylzinc tetrahydroborate have been investigated, with the results summarized in Figure 3.16. This survey has taken in not only the decomposition of the compound at or near ambient temperatures, but also its behaviour with respect to each of four selected Lewis bases (NH_3, SMe_2, PPh_3 and CO). The reaction pathways thus revealed will now be treated in turn.

3.3.1 Thermal decomposition

As mentioned by Nibler and Cook,[6] continuous pumping at room temperature causes methylzinc tetrahydroborate gradually to disproportionate with the formation of volatile dimethylzinc and involatile zinc *bis*(tetrahydroborate), as in equation (7).

$$2MeZnBH_4 \longrightarrow Me_2Zn + Zn(BH_4)_2 \qquad (7)$$

Heating the compound in a sealed ampoule to temperatures approaching 100°C causes the solid to turn grey, with the evolution of dimethyldiborane and hydrogen. Under these conditions, the decomposition proceeds according to equation (8).

$$2MeZnBH_4 \longrightarrow [MeBH_2]_2 + 2H_2 + 2Zn \qquad (8)$$

The H_2 given off {typically, 0.69 mmol from a sample of $[MeZnBH_4]$ originally weighing 70 mg (0.73 mmol)} was estimated with the aid of a Toepler pump. $[MeBH_2]_2$ was measured tensimetrically (0.33 mmol) and its purity ascertained by comparing its infrared spectrum with that of an authentic sample.[68] The amount of zinc (0.72 mmol) was measured by dissolving the remaining solid residue in dilute nitric acid and determining the concentration of Zn^{2+} by atomic absorption spectrometry.

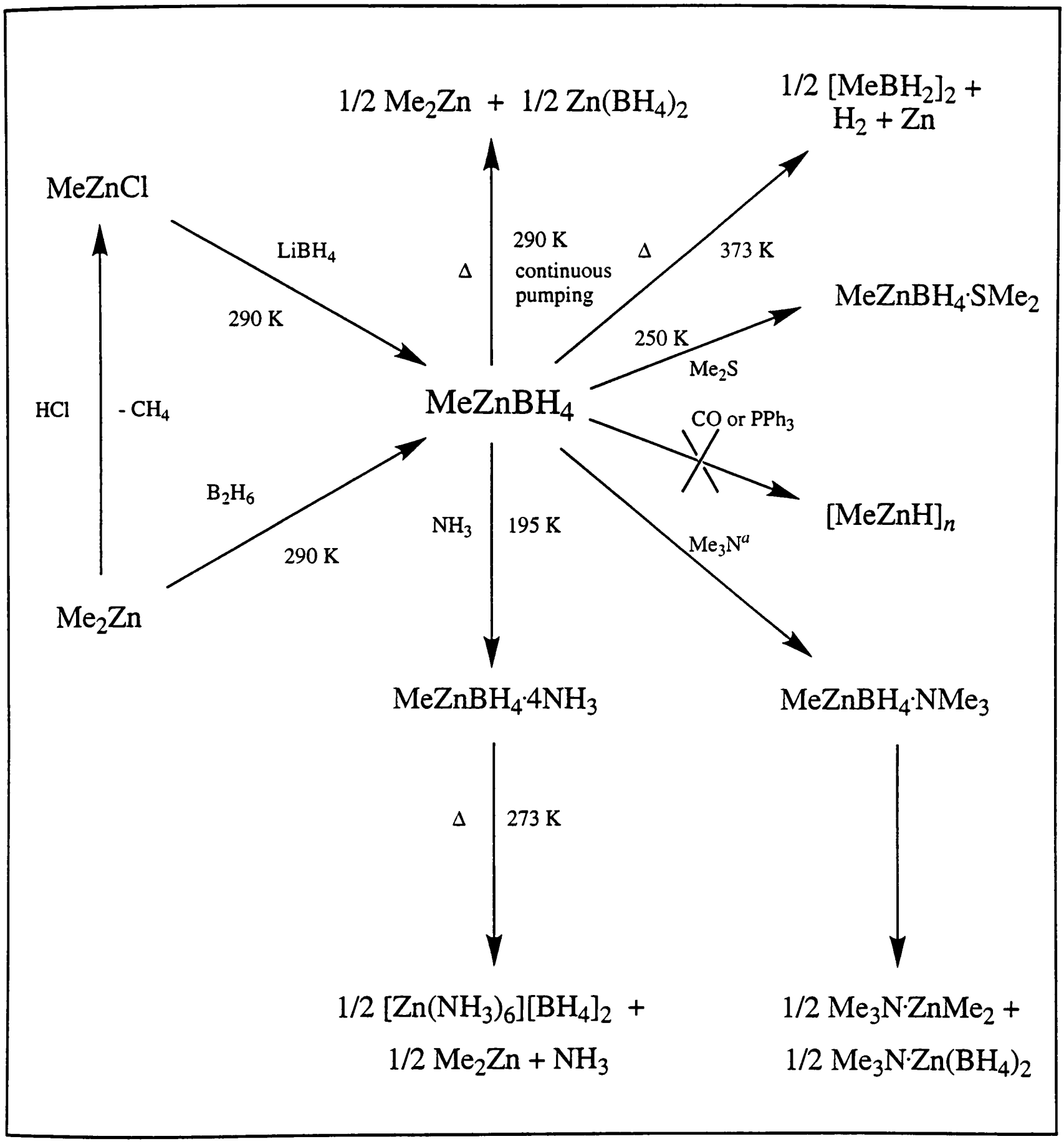

[a] See reference 5.

Figure 3.16 Chemical properties of methylzinc tetrahydroborate.

Care had to be taken rigorously to exclude moisture from the reaction vessel, since this typically resulted in the evolution of methane and diborane. Furthermore, raising the temperature in excess of *ca.* 250°C invariably resulted in the retention of boron in the solid residue and the evolution of methane. This may be due to decomposition of $[MeBH_2]_2$ occurring on the zinc surface, for example *via* reaction (9).

$$[MeBH_2]_2 \longrightarrow 2MeH + H_2 + 2B \qquad (9)$$

3.3.2 Reaction with Ammonia

The reaction of methylzinc tetrahydroborate with ammonia was of interest for two principal reasons: (a) as a route to a more thermally robust species which might provide a reliable method of analysis; and (b) for the comparison it affords with the reaction with trimethylamine reported by Ridley to proceed as follows:[5]

$$\left.\begin{aligned} MeZnBH_4 + NMe_3 &\longrightarrow MeZnBH_4{\cdot}NMe_3 \\ 2MeZnBH_4{\cdot}NMe_3 &\longrightarrow Me_3N{\cdot}ZnMe_2 + Me_3N{\cdot}Zn(BH_4)_2 \end{aligned}\right\} \quad (10)$$

In a typical experiment, 18 mg (1.05 mmol) of ammonia were co-condensed with 19 mg (0.2 mmol) of methylzinc tetrahydroborate and the reaction mixture was maintained at -78°C for *ca.* 24 h. The excess of ammonia recovered at -78°C (0.275 mmol) implied the formation at this temperature of an adduct with the composition $MeZnBH_4{\cdot}4NH_3$. The reaction vessel was then allowed to warm slowly to room temperature under continuous pumping. Warming to 0°C led to the evolution of 0.114 mmol of dimethylzinc and a further 0.22 mmol of ammonia. There remained an involatile, white solid, the infrared spectrum of which showed bands at the following wavenumbers (in cm^{-1}; s = strong, m = medium, w = weak, sh = shoulder, br = broad): 3350 s,br, 3267 m,sh, 3252 m, 3205 m,sh, 2287 s,sh, 2237 s, 2171 s,sh, 1739 w, 1606 m, 1263 m,sh, 1246 s, 1222 s, 1125 m, 1067 m, 706 s, 667 m, 606 w,sh. Found: H, 12.75;

B, 11.00; N, 41.39; Zn, 32.25; calc. for $Zn(NH_3)_6(BH_4)_2$: H, 13.29; B, 10.96; N, 42.61; Zn, 33.15%.

The infrared spectrum of the adduct initially formed at low temperatures was investigated by co-condensing the reagents on a CsI window at -196°C, warming the window to -50°C, and pumping away any unchanged ammonia. The spectrum showed bands at the following wavenumbers (in cm^{-1}): 3362 m, 3311 s, 3240 m, 3205 mw, 3165 mw, 2924 m, 2868 w, 2332 m, 2245 s, 2177 m, 1610 m, 1263 m,sh, 1244 s, 1217 m, 1178 m, 1125 m, 1101 s, 715 m, 657 m, 549 mw.

Methylzinc tetrahydroborate reacts with ammonia at -78°C to give an adduct [$MeZnBH_4 \cdot 4NH_3$] which decomposes on warming to 0°C. That the infrared spectrum of this adduct contains bands associated with the $MeZn^+$ unit,[6] with the BH_4^- anion (absorbing at 2332, 2245, 1244 and 1101 cm^{-1}),[7] and with coordinated ammonia[69,70] suggests the formulation $[MeZn(NH_3)_4]^+[BH_4]^-$. Other molecular tetrahydroborates, such as $[Al(BH_4)_3]$,[71,72] $[H_2GaBH_4]$,[35] $[Me_2GaBH_4]$[36] and even $[B_2H_6]$ itself,[73] are known to react with an excess of ammonia in a similar fashion to yield products in which the BH_4^- ion has been displaced from the coordination sphere of the metal.

The thermal decomposition of [$MeZnBH_4 \cdot 4NH_3$] at 0°C proceeds with the evolution of one mol of ammonia and half a mol of dimethylzinc, leaving an involatile, white solid with the composition $ZnN_6B_2H_{26}$ on the evidence of elemental analysis. Comparison of the infrared spectrum of the solid residue with those of ammines of the type $[Zn(NH_3)_6]X_2$ (X = Cl, Br or I)[69,74,75] and of ionic tetrahydroborates[7] implies the presence of more-or-less discrete $[Zn(NH_3)_6]^{2+}$ and BH_4^- ions.

The reaction with ammonia is therefore probably best written as in equation (11),

$$\left.\begin{aligned} MeZnBH_4 + 4NH_3 &\longrightarrow [MeZn(NH_3)_4]^+[BH_4]^- \\ 2[MeZn(NH_3)_4]^+[BH_4]^- &\longrightarrow ZnMe_2 + 2NH_3 + \\ &\quad [Zn(NH_3)_6]^{2+}[BH_4]^-_2 \end{aligned}\right\} \quad (11)$$

and mirrors both the thermal decomposition at room temperature and the reaction with trimethylamine,[5] in that it effectively brings about disproportionation into dimethylzinc and zinc *bis*(tetrahydroborate). The reaction also provides a reliable method of analyzing methylzinc tetrahydroborate, other methods being thwarted by the thermal fragility of the parent compound. Chemical analysis of the more robust $[Zn(NH_3)_6][BH_4]_2$, together with tensimetric measurements of the amount of dimethylzinc evolved and the net amount of ammonia taken up, yielded the following results. Found: H, 6.64; B, 11.01; Zn, 69.03; C, 13.2; calc. for CH_3ZnBH_4: H, 7.41; B, 11.35; Zn, 68.63; C, 12.61%. The indirect nature of the analysis, incorporating several stages and various measurements, and the presence of a small quantity of occluded dimethylzinc in the $[Zn(NH_3)_6][BH_4]_2$ probably account for the small discrepancies between the measured and calculated values.

3.3.3 Studies with Triphenylphosphine and CO

Both $[PPh_3]$ and [CO] are reported to react with metal tetrahydroborate derivatives to yield the corresponding metal hydride and the adduct $L{\cdot}BH_3$ ($L = PPh_3$ or CO),[33,76] *e.g.*

$$HGa(BH_4)_2 + CO \longrightarrow H_2GaBH_4 + OC{\cdot}BH_3 \qquad (12)$$

$$Be(BH_4)_2 + 2PPh_3 \longrightarrow BeH_2 + 2Ph_3P{\cdot}BH_3 \qquad (13)$$

Accordingly, the reactions of $[PPh_3]$ and [CO] with $[MeZnBH_4]$ were investigated as potential routes to $[MeZnH]_n$ *via* reaction (14):

$$MeZnBH_4 + L \longrightarrow 1/n[MeZnH]_n + L{\cdot}BH_3 \qquad (14)$$

$L = PPh_3$ or CO

In a typical experiment, a [$^2H_8$]toluene solution containing 0.5 mmol of [$MeZnBH_4$] and a 5-10 fold excess of either [PPh_3] or [CO] was allowed to warm from -80°C to room temperature in 10°C steps, the progress of any reaction being monitored by measuring the ^{11}B and ^1H NMR spectra. In the case of the [CO] experiments, no evidence of any resonance attributable to [$OC{\cdot}BH_3$][32] was observed, even with samples maintained at 0°C for more than a week. Very weak resonances attributable to [$Ph_3P{\cdot}BH_3$][77] appeared at δ_B 37.1 and δ_H 1.70 for samples maintained at 0°C for several days, although the intensities of the signals relative to those due to unchanged [$MeZnBH_4$] implied a conversion of less than 1%.

Attempts to induce reactions at significantly higher temperatures were frustrated by the thermal fragility of [$MeZnBH_4$] itself.

3.3.4 Reaction with Dimethyl Sulphide

Adducts of the type [$MeZnBH_4{\cdot}nL$], where L = a nitrogen-donor base (NH_3 or NMe_3), tend to decompose below ambient temperatures.[5] In view of the tendency of zinc to form stable complexes with ligand containing second row elements such as sulphur,[78] it was decided to examine the reaction of [$MeZnBH_4$] with dimethyl sulphide in the hope of isolating a more tractable product.

In a typical experiment, 62 mg (1.0 mmol) of dimethyl sulphide were co-condensed with 20 mg (0.21 mmol) of methylzinc tetrahydroborate and the reaction mixture was warmed slowly to -23°C. The methylzinc tetrahydroborate was observed to dissolve smoothly and, after a further 2 h at this temperature to ensure complete reaction, the excess of dimethyl sulphide was removed under continuous pumping. There remained in the reaction vessel a colourless viscous liquid which proved sufficiently volatile to be transferred under continuous pumping at room temperature. (The liquid had a vapour pressure of *ca.* 1 Torr under these conditions, as judged by its distillation properties.) The amount of dimethyl sulphide recovered (0.81 mmol) implied the formation of the 1:1 adduct [$MeZnBH_4{\cdot}SMe_2$].

Further characterization was achieved by measuring (i) the infrared spectrum of the solid formed by condensation on a caesium iodide window held at 77 K and (ii) the infrared spectrum of the matrix-isolated species formed by co-condensation of the vapour with an excess of dinitrogen at 14 K, and (iii) the ^{1}H and ^{11}B NMR spectra of solutions in [$^{2}H_8$]toluene at -20°C. Typical spectra are illustrated in Figures 3.17 (cold cell), 3.18 (matrix) 3.19 and 3.20 (^{1}H and ^{11}B NMR). Provisional assignments of the features present in the infrared spectra of the solid and of the matrix-isolated vapour are listed in Tables 3.11 and 3.12, respectively.

The ^{1}H NMR spectrum of a solution of the adduct in [$^{2}H_8$]toluene shows singlets at δ_H 1.50 and -0.39 and a quartet centred at δ_H 0.9. These are assigned to the $(CH_3)_2S$, CH_3Zn and BH_4 protons respectively. Integration of the signals proved difficult because of overlapping of the $(CH_3)_2S$ singlet and one component of the BH_4 quartet. The ^{11}B spectrum shows a single resonance - a quintet centred at δ_B -47.8 [$J(^{11}B\text{-}^{1}H)$ = 86.0 Hz]. The measured ^{1}H chemical shift of "free" dimethyl sulphide (approximately 1 mol dm^{-3}) in [$^{2}H_8$]toluene solution at room temperature is 1.73 ppm, and the fact that the observed signals for [$MeZnBH_4 \cdot SMe_2$] are shifted from those expected for "free" [SMe_2] and [$MeZnBH_4$] implies that the complex remains more-or-less intact in solution.

The infrared spectrum of an annealed solid film of [$MeZnBH_4 \cdot SMe_2$] exhibits several features of note. Clearly in evidence are bands associated with coordinated SMe_2.[79,80] The bands are shifted typically by 10-20 cm^{-1} from those expected for "free" [SMe_2] in the vapour phase {*e.g.* ν(S–C) appears at 665 cm^{-1} in [$MeZnBH_4 \cdot SMe_2$] but at 684 cm^{-1} in [SMe_2]}.[80] Shifts are typically in the same direction and comparable in magnitude to those found in *trans*-[$PtCl_2(SMe_2)_2$] and *trans*-[$PdCl_2(SMe_2)_2$].[79] In stark contrast to the infrared spectrum of solid [$MeZnBH_4$], absorptions attributable to the stretching fundamentals of both terminal and bridging B–H bonds are found in the spectrum of solid [$MeZnBH_4 \cdot SMe_2$]. Furthermore, features attributable to the twisting, deformation and wagging motions of a $B(H_t)_2$ unit are found at 1153, 1114 and 741 cm^{-1}, respectively. It seems likely, therefore, that [$MeZnBH_4 \cdot SMe_2$] exhibits a molecular structure, **IV,** in the solid phase, contrasting with the polymeric nature of the

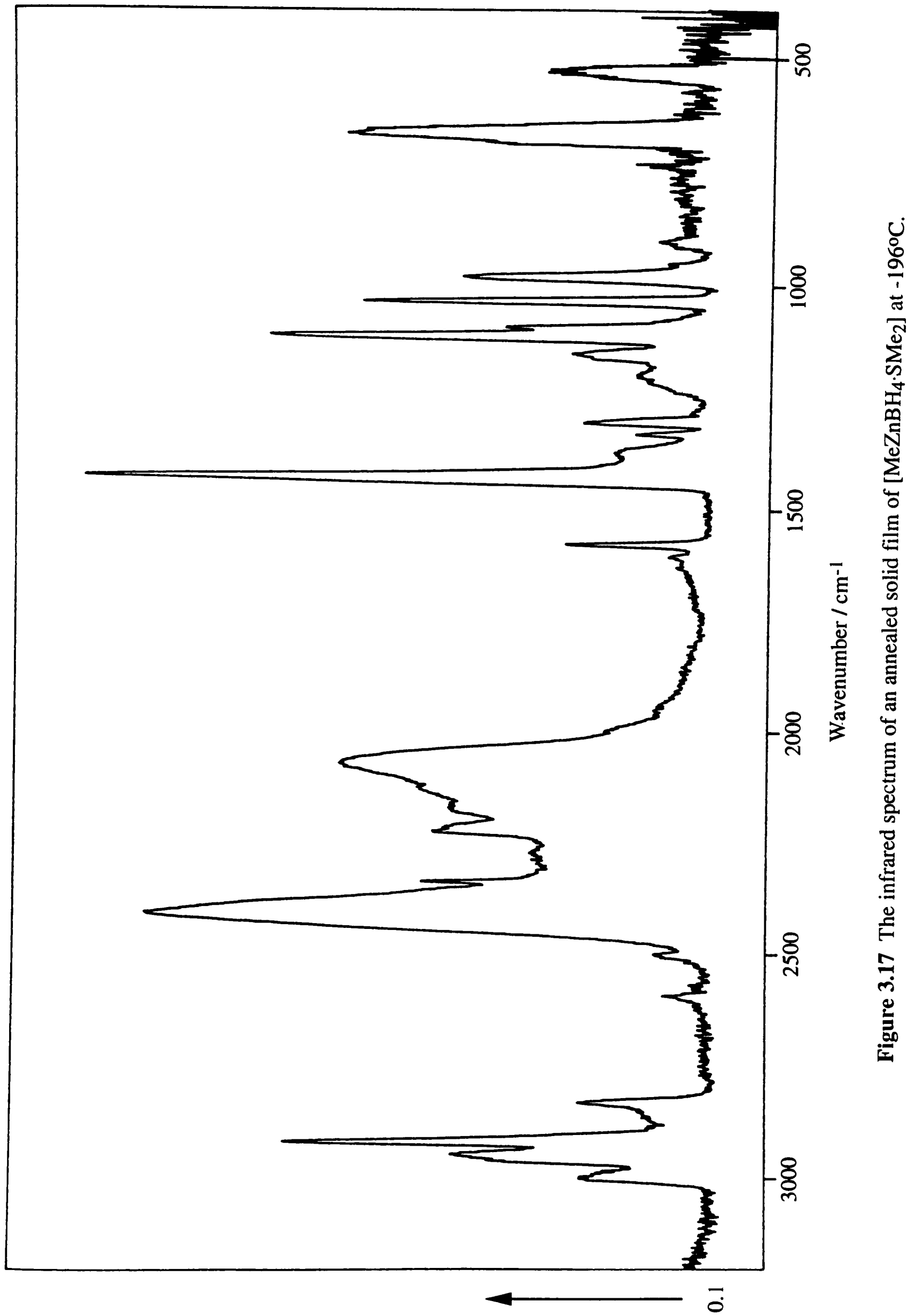

Figure 3.17 The infrared spectrum of an annealed solid film of $[MeZnBH_4{\cdot}SMe_2]$ at -196°C.

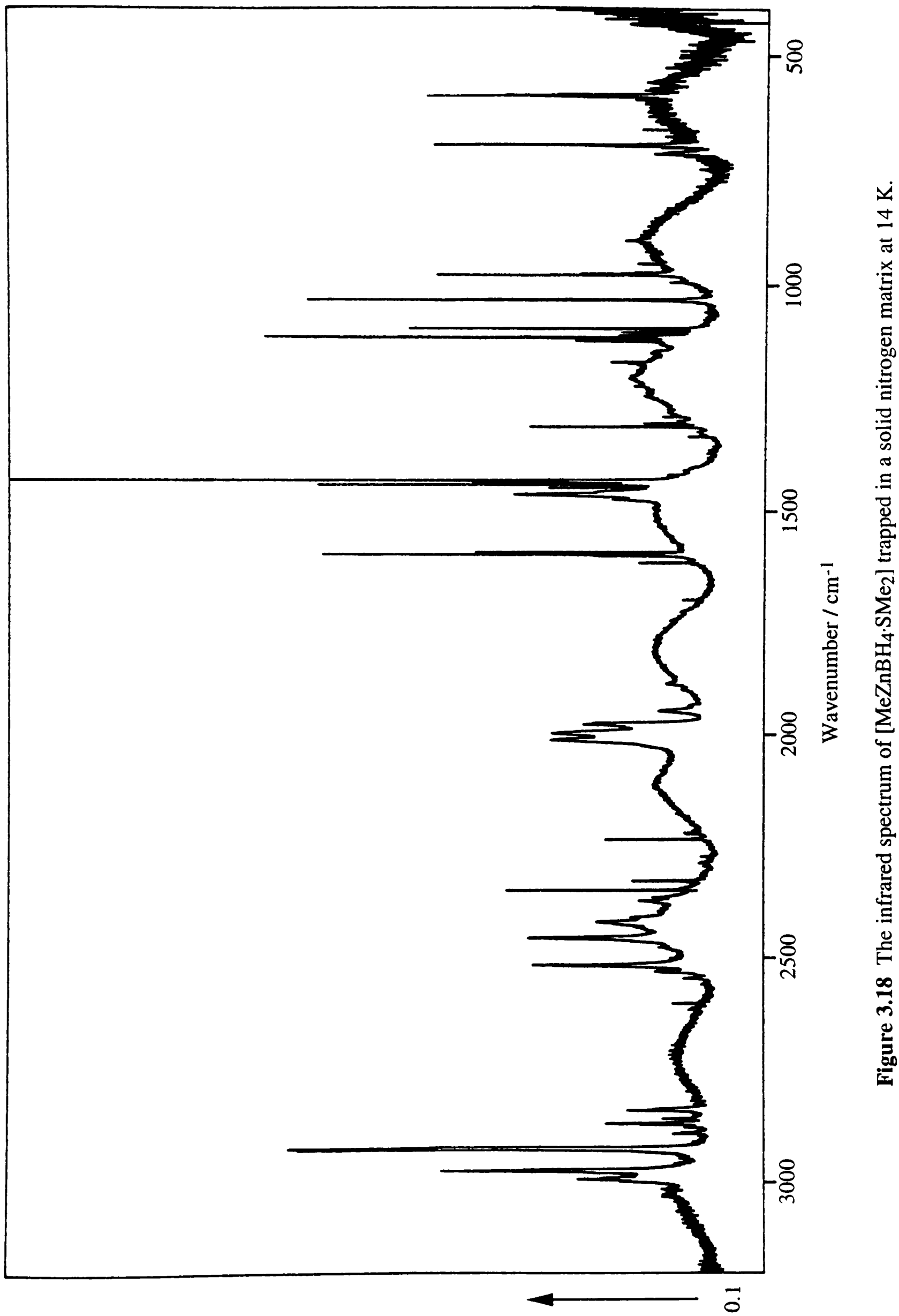

Figure 3.18 The infrared spectrum of [$MeZnBH_4{\cdot}SMe_2$] trapped in a solid nitrogen matrix at 14 K.

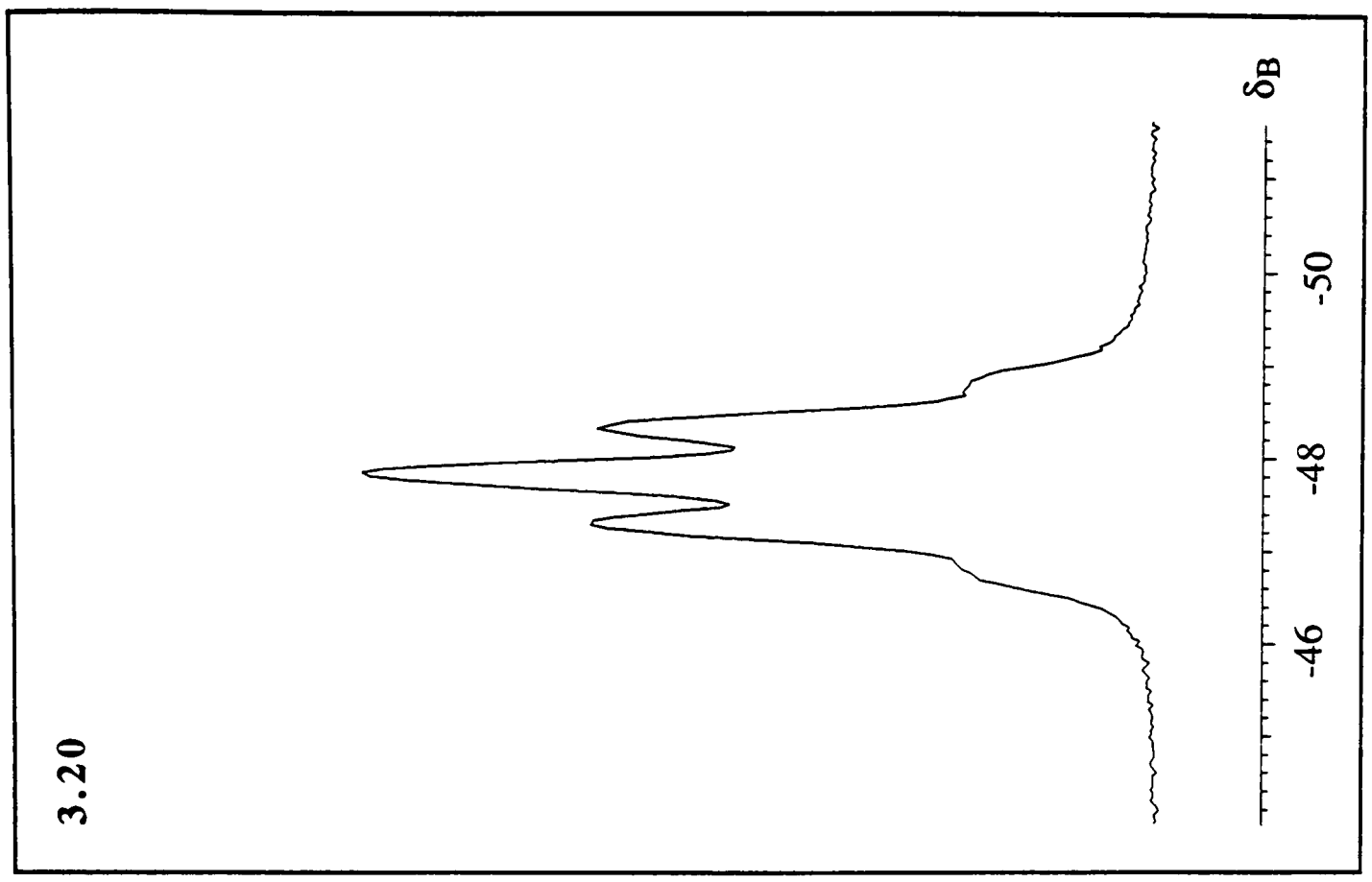

Figures 3.19 and 3.20 The ^{1}H and ^{11}B NMR spectra of $[MeZnBH_4{\cdot}SMe_2]$ in $[^2H_8]$toluene solution at -10°C.

Table 3.11 The infrared spectrum of [$MeZnBH_4 \cdot SMe_2$] in the range 400-4000 cm^{-1}: wavenumbers of absorptions displayed by a solid film at 77 K.

Wavenumber / cm^{-1} [a]		Assignment [b]	
2999	w	ν_a(C–H)	Me_2S, $MeZnBH_4$
2947	m		
2917	s	ν_s(C–H)	Me_2S, $MeZnBH_4$
2832	w	2 x 1428	Me_2S
2596	vw	2 x 1307	
2502	vw	1307 + 1204	
2408	vs, br	ν_a(B–H_t)	$MeZnBH_4$
2336	m, sh	ν_s(B–H_t)	$MeZnBH_4$
2225	m, sh	ν_a(B–H_b)	$MeZnBH_4$
2173	m, sh		
2074	s, br	ν_a(B–H_b)	$MeZnBH_4$
1579	w	906 + 665	
1428	vs	$\delta_a(CH_3)$	Me_2S
1377	w	ν(Zn–H_b)	$MeZnBH_4$
1334	w		
1307	w	$\delta_s(CH_3)$	Me_2S
1204	w, br	$\delta_s(CH_3)$	$MeZnBH_4$
1153	w	BH_2 twist	$MeZnBH_4$
1114	s	$\delta(BH_2)$	$MeZnBH_4$
1095	m, sh		
1038	m	$\rho(CH_3)$ [c]	Me_2S
983	s	$\rho(CH_3)$ [d]	Me_2S
906	vw	$\rho(CH_3)$ [c]	Me_2S
741	w	BH_2 wag	$MeZnBH_4$
689	w	$\rho(CH_3)$	$MeZnBH_4$
665	s, br	ν(S–C)	Me_2S
532	m, br	ν(Zn–C)	$MeZnBH_4$

[a] Intensity abbreviations are listed in the notes. [b] Assignments made by analogy with similar compounds containing (i) a methylzinc unit,[6,51,53] (ii) a bidentate BH_4 group,[27,35,36,54] and (iii) dimethyl sulphide complexed to a metal centre.[79,80] [c] Rocking motion parallel to the CSC plane. [d] Rocking motion perpendicular to the CSC plane.

Table 3.12 Infrared spectrum of [$MeZnBH_4 \cdot SMe_2$] isolated in a solid nitrogen matrix at 14 K: wavenumbers (cm^{-1}) of absorptions in the range 400-4000 cm^{-1}.

Wavenumber / cm^{-1} [a]		Assignment [b]	
2993	w	ν_a(C–H)	Me_2S, $MeZnBH_4$
2976	s		
2928	vs	ν_s(C–H)	Me_2S, $MeZnBH_4$
2925	vs		
2869	w	2 x 1428	Me_2S
2840	w		
2517	m	ν_a(B–H_t)	$MeZnBH_4$
2455	m	ν_s(B–H_t)	$MeZnBH_4$
2419	w	1313 + 1095	
2349	w	ν(C–O)	CO_2
2238	w	2 x 1122	$MeZnBH_4$
2012	m, br	ν_a(B–H_b)	$MeZnBH_4$
1975	m, br	ν_s(B–H_b)	$MeZnBH_4$
1946	vw	2 x 978	
1600	w	ν(O–H)	H_2O
1465	ms, br	ν_a(Zn–H_b)	$MeZnBH_4$
1449	w	$\delta_a(CH_3)$	Me_2S
1442	s		
1437	m		
1432	vs		
1313	m	ν_s(Zn–H_b)	$MeZnBH_4$
1306	w	$\delta_s(CH_3)$	Me_2S
1122	w	BH_2 twisting	$MeZnBH_4$
1116	vs	$\delta(BH_2)$	$MeZnBH_4$
1095	m, sh		

Table 3.12 (cont.) Infrared spectrum of [$MeZnBH_4 \cdot SMe_2$] isolated in a solid nitrogen matrix at 14 K: wavenumbers (cm^{-1}) of absorptions in the range 400-4000 cm^{-1}.

Wavenumber / cm^{-1} [a]		Assignment [b]	
1033	vs	$\rho(CH_3)$ [c]	Me_2S
978	s	$\rho(CH_3)$ [d]	Me_2S
955	vw	$\rho(CH_3)$ [d]	Me_2S
907	vw	$\rho(CH_3)$ [c]	Me_2S
741	w	BH_2 wagging	$MeZnBH_4$
706	s	$\rho(CH_3)$	$MeZnBH_4$
694	m	ν(S–C)	Me_2S
590	s	ν(Zn–C) [e]	$MeZnBH_4$
588	ms		
586	m		

[a] Intensity abbreviations are listed in the notes. [b] Assignments made by analogy with similar compounds containing (i) a methylzinc unit,[6,51,53] (ii) a bidentate BH_4 group[27,35,36,54] and (iii) dimethyl sulphide complexed to a metal centre.[79,80] [c] Rocking motion parallel to the CSC plane. [d] Rocking motion perpendicular to the CSC plane. [e] Components assigned to $\nu(^{64}Zn–C)$, $\nu(^{66}Zn–C)$ and $\nu(^{68}Zn–C)$, respectively.

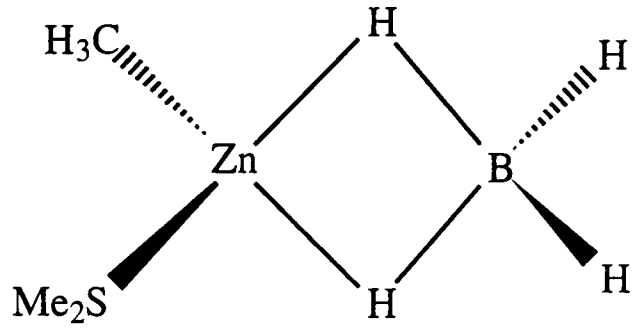

IV

parent compound.

The infrared spectrum of [$MeZnBH_4 \cdot SMe_2$] isolated in solid dinitrogen at 14 K shows a pattern of bands similar to that observed for the solid, although all of the bands are somewhat sharper. The positions of bands associated with the $MeZnBH_4$ fragment show only small shifts from those characteristic of the uncomplexed, monomeric molecule, the overall pattern remaining similar. In particular, the region of the spectrum associated with the stretching motions of B–H bonds resembles closely that of "free" monomeric [$MeZnBH_4$], and is therefore highly suggestive of bidentate ligation of the BH_4 group. It seems likely, therefore, that the molecular structure of [$MeZnBH_4 \cdot SMe_2$] in the vapour is also along the lines of **IV**.

Evidence for small structural changes accompanying the transition from solid [$MeZnBH_4 \cdot SMe_2$] to the vapour phase is provided by increasing differences between the frequencies associated with $B–H_t$ and $B–H_b$ stretching vibrations, and by a somewhat higher Zn–C stretching frequency for the matrix-isolated species. Such features are consistent with charge separation $[MeZn(SMe_2)]^+[BH_4]^-$ in the solid, although clearly to a much smaller extent than that found in the parent compound.

3.4 Conclusions and Suggestions for Further Research

Methylzinc tetrahydroborate, [$MeZnBH_4$], has been prepared by two routes and initially characterized by elemental analysis and its spectroscopic properties. The structure of the solid at 150 K has been determined by X-ray crystallography [trigonal, $R3c$, $a = b = 15.831(10)$, $c = 8.36(2)$ Å, $Z = 18$, $R = 0.072$] to reveal helical polymers in which MeZn and BH_4 units alternate, with the latter functioning as a bidentate ligand

with respect to both of the adjacent metal atoms. It thus resembles the structure of solid beryllium *bis*(tetrahydroborate), with the difference that the zinc is *penta*-coordinated, the Me and H ligands adopting a distorted square pyramidal geometry. Examination of structural parameters and of the infrared spectra of normal and deuteriated isotopomers suggest that the degree of interaction between the metal centre and the tetrahydroborate group is somewhat greater than in $[Be(BH_4)_2]$.

Investigation by mass spectrometry and matrix isolation shows that the vapour consists of an equilibrium mixture of monomeric and dimeric species. Density Functional Theory calculations yield a minimum energy structure for the monomer incorporating bidentate ligation of the BH_4 group and a *tri*-coordinate zinc centre. The calculated infrared frequencies for this species are in good agreement with those measured experimentally for the matrix-isolated monomer.

Chemical properties of methylzinc tetrahydroborate which have been investigated include its thermal decomposition and its reactions with ammonia, dimethyl sulphide, triphenylphosphine and carbon monoxide. Disproportionation into $[Me_2Zn]$ and $[Zn(BH_4)_2]$ appears to be a common feature of its chemistry, although it has been possible to isolate a more stable adduct $[MeZnBH_4{\cdot}SMe_2]$ from the reaction with dimethyl sulphide.

The unusual polymeric structure of methylzinc tetrahydroborate in the solid phase suggests that it would be interesting to investigate the structures of several other hydroborate derivatives for which the vibrational spectra show marked changes on condensation. Potential candidates include $[Me_2AlBH_4]$,[23,39] $[Me_2GaBH_4]$,[27,39] $[Me_2InBH_4]$,[81] $[MeAl(BH_4)_2]$,[34] $[MeGa(BH_4)_2]$,[81] $[Me_2AlB_3H_8]$[49] and $[Me_2GaB_3H_8]$.[49]

Very recent developments in the electron-diffraction apparatus located in the Chemistry Department of the University of Oslo involving modifications to the focusing lens for the electron beam (giving an order of magnitude increase in sensitivity) mean that it may now be possible to measure a scattering pattern for methylzinc tetrahydroborate vapour. Given that the vapour is made up of two components,

however, it would be necessary to perform the measurements at two different sample temperatures in order to vary the relative proportions of these components. Accordingly, the experiments would still represent a highly challenging problem.

References for Chapter 3

1. G.D. Barbaras, C. Dillard, A.E. Finholt, T. Wartik, K.E. Wilzbach and H.I. Schlesinger, *J. Am. Chem. Soc.*, 1951, **73**, 4585.
2. E. Wiberg and W. Henle, *Z. Naturforsch.*, 1952, **7b**, 579.
3. H. Nöth and M. Thomann, *Z. Naturforsch.*, 1990, **45b**, 1482.
4. H. Nöth, E. Wiberg and L.P. Winter, *Z. Anorg. Allg. Chem.*, 1971, **386**, 73.
5. D. Ridley, Ph.D. Thesis, University of Durham, 1965.
6. J.W. Nibler and T.H. Cook, *J. Chem. Phys.*, 1973, **58**, 1596.
7. See, for example, T.J. Marks and J.R. Kolb, *Chem. Rev.*, 1977, **77**, 263.
8. D.S. Marynick and W.N. Lipscomb, *J. Am. Chem. Soc.*, 1971, **93**, 2322.
9. D.S. Marynick and W.N. Lipscomb, *Inorg. Chem.*, 1972, **11**, 820.
10. W.J. Lehmann, C.O. Wilson, Jr., and I. Shapiro, *J. Chem. Phys.*, 1958, **28**, 777.
11. C.R. Pulham, P.T. Brain, A.J. Downs, D.W.H. Rankin and H.E. Robertson, *J. Chem. Soc., Chem Commun.*, 1990, 177.
12. G.M. Sheldrick, *Acta. Crystallogr.*, 1990, **46A**, 467.
13. SHELXL-93, G.M. Sheldrick, University of Göttingen, 1993.
14. T.J. Marks and L.A. Shimp, *J. Am. Chem. Soc.*, 1972, **94**, 1542.
15. J.W. Nibler, *J. Am. Chem. Soc.*, 1972, **94**, 3349.
16. B.E. Green, C.H.L. Kennard, G. Smith, B.D, James, P.C. Healy and A.H. White, *Inorg. Chim. Acta*, 1984, **81**, 147.
17. E.R. Bernstein, W.C. Hamilton, T.A. Keiderling, S.J. LaPlaca, S.J. Lippard and J.J. Mayerle, *Inorg. Chem.*, 1972, **11**, 3009.
18. N. Edelstein, *Inorg. Chem.*, 1981, **20**, 297.
19. J.E. Huheey, E.A. Keiter and R.L. Keiter, *Inorganic Chemistry: Principles of Structure and Reactivity*, 4th edn., Harper Collins, 1993.
20. G.A. Koutsantonis, F.C. Iee and C.L. Raston, *J. Chem. Soc., Chem. Commun.*, 1994, 1975.

21. N.A. Bell, P.T. Moseley, H.M.M. Shearer and C.B. Spencer, *J. Chem. Soc., Chem. Commun.*, 1980, 359.

22. J.L. Atwood, F.R. Bennett, F.M. Elms, C. Jones, C.L. Raston and K.D. Robinson, *J. Am. Chem. Soc.*, 1991, **113**, 8183.

23. Chapter 5, this thesis.

24. J.J. Watkins and E.C. Ashby, *Inorg. Chem.*, 1974, **13**, 2350.

25. T.P.E. Auf der Heyde and L.R. Nassimbeni, *Acta Crystallogr.*, 1984, **40B**, 582.

26. Chapter 4, this thesis; S. Aldridge, A.J. Blake, A.J. Downs and S. Parsons, *J. Chem. Soc., Chem. Commun.*, 1995, 1363.

27. A.J. Downs and P.D.P. Thomas, *J. Chem. Soc., Dalton Trans.*, 1978, 809.

28. P.R. Oddy and M.G.H. Wallbridge, *J. Chem. Soc., Dalton Trans.*, 1976, 869.

29. H. Beall and C.H. Bushweller, *Chem. Rev.*, 1973, **73**, 465 and refs. therein.

30. J.F. Hanlan and J.D. McCowan, *Can. J. Chem.*, 1972, **50**, 747.

31. G.R. Eaton and W.N. Lipscomb, *N.M.R. Studies of Boron Hydrides and Related Compounds*, Benjamin, New York, 1969.

32. H. Nöth and B. Wrackmeyer, *N.M.R., Basic Principles and Progress*, No. 14, Springer, Berlin, 1978.

33. A.J. Downs, L.A. Harman, P.D.P. Thomas and C.R. Pulham, *Polyhedron*, 1995, **14**, 935; L.A. Harman, Part II Thesis, University of Oxford, 1990.

34. M.T. Barlow, C.J. Dain, A.J. Downs, P.D.P. Thomas and D.W.H. Rankin, *J. Chem. Soc., Dalton Trans.*, 1980, 1374.

35. C.R. Pulham, D.Phil. Thesis, University of Oxford, 1991.

36. P.D.P. Thomas, D.Phil. Thesis, University of Oxford, 1977.

37. D.C. Harris and H.B. Gray, *J. Am. Chem. Soc.*, 1975, **97**, 3073.

38. M.D. Joesten and L.J. Schaad, *Hydrogen Bonding*, Marcel Dekker, New York, 1974; S.N. Vinogradov and R.H. Linnell, *Hydrogen Bonding*, Van Nostrand-Reinhold, New York, 1971; S.F. Fischer, G.L. Hofacker and M.A. Ratner, *J. Chem. Phys.*, 1970, **52**, 1934; J. Bournay and Y. Marechal, *ibid*, 1973, **59**, 5077.

39. M.T. Barlow, A.J. Downs, P.D.P. Thomas and D.W.H. Rankin, *J. Chem. Soc., Dalton Trans.*, 1979, 1793.

40. A.J. Downs, T.M. Greene, L.A. Harman, P.F. Souter, P.T. Brain, C.R. Pulham, D.W.H. Rankin, H.E. Robertson, M. Hofmann and P.v.R. Schleyer, *Inorg. Chem.*, 1995, **34**, 1799.

41. C.J. Dain, A.J. Downs and D.W.H. Rankin, *Angew. Chem., Int. Ed. Engl.*, 1982, **21**, 534; C.J. Dain, A.J. Downs, M.J. Goode, D.G. Evans, K.T. Nicholls, D.W.H. Rankin and H.E. Robertson, *J. Chem. Soc., Dalton Trans.*, 1991, 967.

42. A. Almenningen, G. Gundersen and A. Haaland, *Acta Chem. Scand.*, 1968, **22**, 328.

43. V. Plato and K. Hedberg, *Inorg. Chem.*, 1971, **10**, 590.

44. See, for example, A.J. Downs and S.C. Peake, in *Molecular Spectroscopy,* Chemical Society Specialist Periodical Reports, Vol. 1, 1973, Chapter 9; M.J. Almond and A.J. Downs, *Adv. Spectrosc.*, 1989, **17**, 1.

45. D.R. Lide (ed.), *Handbook of Chemistry and Physics,* 75th edn., C.R.C. Press, Boca Raton, FL, 1994-1995.

46. P.L. Baxter, D.Phil. Thesis, University of Oxford, 1984.

47. M.J. Goode, D.Phil. Thesis, University of Oxford, 1987.

48. G. Gundersen, K. Hedberg and L. Hedberg, *J. Chem. Phys.,* 1973, **59**, 3777.

49. J.J. Borlin and D.F. Gaines, *J. Am. Chem. Soc.*, 1972, **94**, 1367.

50. T.H. Cook and G.L Morgan, *J. Am. Chem. Soc.,* 1970, **92**, 6487.

51. A.M. Coats, D.C. McKean, H.G.M. Edwards and V. Fawcett, *J. Mol. Struct.*, 1994, **320**, 159.

52. D.C. McKean, G.P. McQuillan, A.R. Morrison and I. Torto, *J. Chem. Soc., Dalton Trans.*, 1985, 1207.

53. D.F. Evans and I. Wharf, *J. Chem. Soc., A*, 1968, 783.

54. D.A. Coe and J.W. Nibler, *Spectrochim. Acta*, 1973, **29A**, 1789.

55. D.F. Gaines, J.L. Walsh, J.H. Morris and D.F. Hillenbrand, *Inorg. Chem.*, 1978, **17**, 1516.

56. L.J. Allamandola and J.W. Nibler, *J. Am. Chem. Soc.*, 1976, **98**, 2096.

57. L.A. Jones, D.Phil. Thesis, University of Oxford, 1993.

58. R.A. Kovar and G.L. Morgan, *Inorg. Chem.*, 1969, **8**, 1099.

59. T.M. Gilbert, F.J. Hollander and R.G. Bergman, *J. Am. Chem. Soc.*, 1985, **107**, 3508.

60. J. Ho, K.J. Deck, Y. Nishihara, M. Shang and T.P. Fehlner, *J. Am. Chem. Soc.*, 1995, **117**, 10292.

61. See, for example, N.N. Greenwood and N.F. Travers, *J. Chem. Soc., A*, 1971, 3257.

62. J.L. Duncan, J. Harper and E. Hamilton, *J. Mol. Spectrosc.*, 1983, **102**, 416.

63. C.R. Pulham, A.J. Downs, M.J. Goode, T.M. Greene and I.M. Mills, *Spectrochim. Acta*, 1995, **51A**, 769.

64. D.C. McKean, *Spectrochim. Acta,* 1992, **48A**, 1335.

65. K. Lammertsma and J. Leszczynski, *J. Chem. Soc., Chem. Commun.*, 1989, 1005; B.J. Duke, T.P. Hamilton and H.F. Schaeffer III, *Inorg. Chem.*, 1991, **30**, 4225.

66. I. Demachy and F. Volatron, *Inorg. Chem.*, 1994, **33**, 3965.

67. A. Almenningen, T.U. Helgaker, A. Haaland and S. Samdal, *Acta Chem. Scand.*, 1982, **36A**, 159.

68. W.J. Lehmann, C.O. Wilson, Jr., and I. Shapiro, *J. Chem. Phys.*, 1960, **33**, 590.

69. K. Nakamoto, *Infrared and Raman Spectra of Inorganic and Coordination Compounds,* 4th edn., Wiley, 1986.

70. J. Fujita, K. Nakamoto and M. Kobayashi, *J. Am. Chem. Soc.*, 1956, **78**, 3295.

71. P.H. Bird and M.G.H. Wallbridge, *J. Chem. Soc., A,* 1967, 664.

72. K.N. Semenenko, S.P. Shilkin, O.V. Kravchenko and P.B. Polyakova, *Izv. Akad. Nauk. SSSR, Ser. Khim.*, 1974, 1455.

73. See, for example, K. Wade, *Electron Deficient Compounds*, Nelson, London, 1971, p. 174.

74. K.H. Schmidt and A Müller, *Coord. Chem. Rev.*, 1976, **19**, 41.

75. L. Sacconi, A. Sabatini and P. Gans, *Inorg. Chem.*, 1964, **3**, 1772.

76. L. Banford and G.E. Coates, *J. Chem. Soc.*, 1964, 5591.

77. M. Durand, C. Jouany, G. Fugie, L. Elegant and J.-F. Gal, *J. Chem. Soc., Dalton Trans.*, 1977, 57.

78. See, for example, R.H. Prince, in *Comprehensive Coordination Chemistry*, Vol. 5, eds. G. Wilkinson, R.D. Gillard and J.A. McCleverty, Pergamon, 1987, p. 925.

79. J.R. Allkins and P.J. Hendra, *Spectrochim. Acta*, 1968, **24A**, 1305.

80. J.R. Allkins and P.J. Hendra, *Spectrochim. Acta*, 1966, **22**, 2075.

81. C.R. Pulham and A.J. Downs, unpublished results.

Chapter Four

The Synthesis, Characterization and Structure of the Methylzinc Hydroborate $[(MeZn)_2B_3H_7]_2$

4.1 Introduction

4.1.1 Previous Work in this Area

Despite their synthetic potential, very few hydroborate complexes of zinc have been reported to date. In addition to $Zn(BH_4)_2$[1] and complexes containing the $[Zn(BH_4)_3]^-$ and $[Zn(BH_4)_4]^{2-}$ anions,[2] only $[MeZnB_6H_9]$,[3] $[(Et_2O)_2Zn(B_{10}H_{12})]$,[4] $[Ph_3PMe]_2[Zn(B_{10}H_{12})_2]$,[5] $[MeZnBH_4]$[6] and [(*tmen*)Zn(Cl)BH_4][7] have been characterized. Structural results have been obtained only for the last three compounds. Furthermore, $[Ph_3PMe]_2[Zn(B_{10}H_{12})_2]$[5] is the only compound known to contain a direct (*i.e.* non hydrogen-bridged) Zn–B bond.

Gaines *et al.* have claimed that a more volatile fraction obtained from the reaction between dimethylzinc and beryllium *bis*(octahydrotriborate), used to make methylberyllium octahydrotriborate, may be methylzinc octahydrotriborate, produced according to reaction (1). No characterization was reported.[8]

$$Me_2Zn + Be(B_3H_8)_2 \longrightarrow MeBeB_3H_8 + MeZnB_3H_8 \qquad (1)$$

One potential route to metal hydroborate complexes is the reaction of the appropriate methyl derivative with the parent borane. This is a commonly used route to metal tetrahydroborate derivatives, as exemplified by reactions (2) and (3),[9,10] and

$$Me_3In + B_2H_6 \longrightarrow Me_2InBH_4 + 1/2[MeBH_2]_2 \qquad (2)$$

$$2Me_2Zn + B_2H_6 \longrightarrow MeZnBH_4 + ZnH_2 + Me_3B \qquad (3)$$

effectively involves replacement of a BH_2 unit by a methylmetal fragment.

Methylmetal reagents are also known to react with boranes *via* proton abstraction yielding methane and the corresponding borane anion. For example, dimethylzinc reacts with hexaborane(10) according to reaction (4).[3] In the absence of definitive structural

$$Me_2Zn + B_6H_{10} \longrightarrow MeZnB_6H_9 + MeH \qquad (4)$$

results for $[MeZnB_6H_9]$, the extent of interaction between the metal fragment and anion remains uncertain. In addition, diethylcadmium and dimethyl-, diethyl- and diphenylzinc are known to abstract two protons from decaborane(14).[4,11] In the cadmium case, this reaction yields the crystalline derivative $[(Et_2O)_2Cd(B_{10}H_{12})]$ together with ethane, as shown in reaction (5). The ether adduct has been shown by X-ray diffraction to be

$$Et_2Cd + B_{10}H_{14} + 2Et_2O \longrightarrow [(Et_2O)_2Cd(B_{10}H_{12})] + 2EtH \qquad (5)$$

dimeric and to feature cadmium bonded to one edge of the $B_{10}H_{12}$ cluster *via* CdB_2 three-centre, two-electron bonds.[12]

A third type of reaction between boron hydrides and methylmetal reagents is methylation. Dimethylmercury, for example, reacts with tetraborane(10) producing 2-methyltetraborane(10) in yields of up to 68%. However, in this case, as with other methylmetal reagents, significant amounts of side-products (including methyldiboranes and trimethylborane) are produced, as a result of fragmentation of the parent borane.[13]

4.1.2 Aims of the Present Research

In view of the speculative nature of the reports concerning $[MeZnB_3H_8]$, it was decided to investigate potential synthetic routes to this compound, with a view to fuller spectroscopic and structural characterization. Initially it was hoped that reaction (6) might

$$MeZnCl + [^nBu_4N][B_3H_8] \longrightarrow MeZnB_3H_8 + [^nBu_4N]Cl \quad (6)$$

provide a viable synthetic route to the compound, this being analogous to one of the preparative routes to $[MeZnBH_4]$[6] and also to that used to prepare $[Me_2MB_3H_8]$ (M = Al or Ga).[14] In view of the propensity of Me_2Zn to replace a BH_2 unit in diborane [reaction (3)], an analogous reaction between dimethylzinc and tetraborane(10) [reaction (7)] was also to be investigated.

$$2Me_2Zn + B_4H_{10} \longrightarrow MeZnB_3H_8 + ZnH_2 + Me_3B \quad (7)$$

4.2 Synthesis of the Methylzinc Hydroborate $[(MeZn)_2B_3H_7]_2$

4.2.1 Studies with Methylzinc Chloride and Tetra-*n*-butylammonium Octahydrotriborate

Initial attempts to synthesize $[MeZnB_3H_8]$ from methylzinc chloride and $[^nBu_4N][B_3H_8]$ *via* reaction (6) met with little success. The apparatus used was identical to that described in Section 3.1.2 for the preparation of $[MeZnBH_4]$ from methylzinc chloride and lithium tetrahydroborate. As before, the methylzinc chloride was made *in situ* and finely divided $[^nBu_4N][B_3H_8]$ was added at -196°C. The solids were then mixed thoroughly whilst warming to room temperature. Any volatile products were to be condensed in a cold trap held at -196°C under continuous evacuation. Despite variations of reacting proportions and temperature, no volatile products were obtained in any of the experiments. During some experiments, traces of a viscous, involatile oil were observed in the reaction vessel. However, because of the extremely small yields of this oil and problems of separation from unchanged starting materials, this reaction was not pursued any further.

4.2.2 Reaction of Dimethylzinc with Tetraborane(10)

Attention was therefore turned to the reaction between dimethylzinc and tetraborane(10). In initial experiments, a 250 cm^3 bulb, equipped with a break-seal and a constriction, was conditioned by exposure to dimethylzinc vapour at *ca.* 20 Torr for 3-4 h, this serving to scavenge any residual moisture retained by the Teflon and glass surfaces. After re-evacuation, tetraborane(10) (*ca.* 26 mg, 0.5 mmol) and a six-fold excess of dimethylzinc were condensed in the reaction vessel. The constriction was sealed and the mixture allowed to warm to room temperature. After approximately 4 h, very thin acicular crystals of what was shown subsequently to be $[(MeZn)_2B_3H_7]_2$ (*vide infra*) were observed to start growing. Typically after 12 h reaction time, the crystals ceased to grow further; reaction times significantly greater than 12 h brought about deposition of considerable quantities of grey metallic solid on the walls of the reaction vessel. Invariably, formation of the crystalline product was accompanied by the deposition of a white powdery solid on the walls of the vessel. This too underwent thermal decomposition over a period of 12-24 h at room temperature.

Attachment of the reaction vessel to a train of traps allowed fractionation of volatile material. The crystalline product was not volatile at any temperatures below that at which it underwent decomposition. Isolation of the volatile products showed these to consist of unchanged dimethylzinc and tetraborane(10) together with a quantity of trimethylborane (identified by comparison of its infrared spectrum with that of an authentic sample[15]). In a typical experiment, 0.572 mmol of tetraborane(10), and 4.138 mmol of dimethylzinc were initially condensed in the bulb; the amounts of each recovered were 0.475 and 3.860 mmol, respectively. The amount of trimethylborane recovered was 0.091 mmol. These results are summarized in Table 4.1.

In every experiment there was also evolved a non-condensable gas, the identity of which was shown by its infrared spectrum to be methane.[16] The quantity produced was estimated with the aid of a Toepler pump, but the proportion of methane evolved

[compared to those of the trimethylborane produced and the dimethylzinc and tetraborane(10) consumed] was found to vary from experiment to experiment.

	B_4H_{10}	$ZnMe_2$	BMe_3
Amount added / mmol	0.572	4.138	-
Amount recovered / mmol	0.475	3.860	-
Amount used or evolved / mmol	0.097	0.278	0.091
Ratio	1	2.86	0.94

Table 4.1 Changes in the amounts of volatile species present during the reaction of dimethylzinc with tetraborane(10).

In addition, it was found that the proportions depended on the extent to which the bulb was initially pre-conditioned, increasing markedly if the reaction vessel was poorly conditioned. That methane is a product of the reaction between dimethylzinc and tetraborane(10), and not just of side reactions between methylzinc species and residual moisture, is shown by the significant amounts still produced even under the most rigorous conditioning regime employing all-glass apparatus. Under these circumstances, it was found that the ratio of methane to trimethylborane evolved typically lay between 0.95:1 and 1.15:1.

4.2.3 Growth of Single Crystals Suitable for X-ray Diffraction

In order to obtain single crystals suitable for X-ray diffraction, it was necessary to use the specially designed apparatus illustrated in Figure 2.3 used for $[MeZnBH_4]$. Rigorous pre-conditioning of all the glass surfaces and, in particular of the Voltalef 90 grease used to secure the crystals was invariably required. This was achieved by exposure to dimethylzinc vapour at a pressure of *ca.* 20 Torr for 12 h. Crystals most suitable for X-ray diffraction were then grown by admitting dimethylzinc and tetraborane(10) vapours

to the main part of the bulb to pressures of 140 and 45 Torr, respectively, and allowing them to react over a period of 12 h. Substantially higher vapour pressures resulted in the formation of poor quality crystals (as determined by oscillation photography), whereas much lower pressures resulted in slower rates of crystal growth and consequently in problems of thermal decomposition resulting from the longer reaction times required. After removal of all volatile material from the reaction vessel, crystals grown in this way were manipulated by the use of a pointed, glass-coated stirrer bar until held firmly in place in one of the capillary side-arms.

Initial attempts to isolate samples of the crystalline solid for other forms of characterization involved dissolving the crystals in a suitable solvent and filtration through a sintered glass frit, followed by removal of the solvent. Such procedures met with two problems:

(*i*) the difficulty of pre-conditioning the glass frit adequately led to problems of decomposition with deposition of grey metallic solid on the frit itself; and

(*ii*) the solubility of the crystalline solid in solvents such as dichloromethane was low, yet attempts to use more polar solvents, such as diethyl ether or THF, resulted in the recovery of a viscous oil.

Samples of the crystalline solid suitable for chemical analysis and NMR, infrared or Raman spectroscopy were therefore prepared using apparatus similar to that employed for crystal-loading, with appropriate modification of the cold finger.

4.2.4 Physical Properties of $[(MeZn)_2B_3H_7]_2$

$[(MeZn)_2B_3H_7]_2$ is extremely air- and moisture-sensitive and, in addition, is a thermally fragile material which decomposes *in vacuo* in all-glass apparatus over a period of *ca.* 48 h at room temperature. The compound is involatile at room temperature and attempts to vaporize it by warming merely result in decomposition of the sample. The thermal decomposition of $[(MeZn)_2B_3H_7]_2$ is dealt with at greater length in Section 4.3.2.

4.3 Elemental Analysis of $[(MeZn)_2B_3H_7]_2$

Reliable elemental analysis of $[(MeZn)_2B_3H_7]_2$ proved to be difficult to secure. Initial measurements were carried out using samples which had been prepared by filtration through a sintered glass frit, followed by removal of the solvent *in vacuo*. Decomposition of the sample by reaction with water or methanol produced a quantity of non-condensable gas (which could be assayed with the aid of a Toepler pump) and a solution containing boron [as $B(OMe)_3$ or $B(OH)_3$] and Zn^{2+}. The quantities of zinc and boron present were determined by atomic absorption methods in the Microanalytical Department of the Inorganic Chemistry Laboratory. Results proved to be unreliable and to vary unacceptably, typically showing Zn:B ratios incompatible with the empirical formulation $(CH_3Zn)_2B_3H_7$.

In order to obtain more reliable results, all subsequent analyses were carried out using crystalline samples, so as to eliminate the possibility that a mixture of products was being analyzed. One possible explanation for the unreliable results obtained from samples recovered from solution is that the reaction delivers a mixture of two or more products (in proportions varying from one experiment to the next), all components of which are soluble in the solvent used. Alternatively, the deviation of the Zn:B ratio from that expected may have resulted from the inherent resistance of B_3 clusters to fragmentation upon reaction with water (NaB_3H_8, for example, is perfectly stable in aqueous solution[17]).

The thermal instability of the crystalline compound precluded sending samples to Germany for analysis at ambient temperatures. Instead, storage and transportation at -78°C were necessary. However, despite handling under the most rigorous conditions, the results were still unsatisfactory; the material was reported to be extremely difficult to handle and appropriate reference substances were not available.

4.3.1 Reaction with Nitric Acid

Ultimately, the method which proved to give satisfactory analytical results involved

assaying the products of the reaction of crystalline samples with concentrated nitric acid. The reaction is extremely violent at room temperature and results in the evolution of non-condensable gas, the quantity of which was estimated using a Toepler pump. Dilution of the resulting yellow solution with distilled water allowed the concentrations of $B(OH)_3$ and Zn^{2+} to be determined by atomic absorption spectroscopy. The relative proportions of methane and hydrogen making up the non-condensable gas mixture were also estimated. Typically, this involved measurement of the infrared spectrum of a known pressure of the non-condensable gas and from it calculating the intensity of the band due to the antisymmetric C–H stretching fundamental of methane (ν_3 = 3017 cm^{-1}) over a fixed wavenumber range. An initial rough estimate of the partial pressure of methane in the infrared cell could then be obtained by comparison with the measured intensities for known pressures of methane in the same cell. More accurate determination was then achieved by repeatedly filling the cell with (known) pressures of methane until the exact integrated intensity of the initial sample was reproduced. In this way, the partial pressure of methane in a known total pressure of non-condensable gas (assumed to be only methane and hydrogen) could be determined. Typical results are set out in Table 4.2.

	Zinc	Boron	Non-condensable gas	
Quantity / mmol	0.101	0.144	0.422	
			0.095 (methane)	0.327 (hydrogen)

Table 4.2 Analysis of the products formed by the reaction of the methylzinc hydroborate with concentrated nitric acid.

If the methane evolved is taken to arise from the reaction of methyl groups bound to zinc, and the hydrogen gas from the reaction of hydrogen atoms bound to boron, then the elemental analysis set out in Table 4.3 can be drawn up. This is consistent with the formulation of the crystalline solid as $Zn_2B_3C_2H_{13}$, the reaction with concentrated nitric

acid therefore proceeding in accordance with equation (8).

$$(CH_3Zn)_2B_3H_7 \xrightarrow{\text{conc. } HNO_3} 2CH_4 + 7H_2 + 3B(OH)_3 + 2Zn^{2+} \quad (8)$$

	Zinc	Boron	Carbon	Hydrogen
Quantity / mmol	0.101	0.144	0.095	0.612
Ratio	2.13	3.03	2	12.86
Calculated ratio	2	3	2	13

Table 4.3 Observed and calculated elemental ratios for $[(MeZn)_2B_3H_7]$.

Establishing the crystalline product to be $[(CH_3Zn)_2B_3H_7]$ allied to the relative amounts of starting materials consumed and reaction products formed, implies that the reaction of dimethylzinc with tetraborane(10) is best described by equation (9). Yields

$$3Zn(CH_3)_2 + B_4H_{10} \longrightarrow [(CH_3Zn)_2B_3H_7] + B(CH_3)_3 + CH_4 + ZnH_2 \quad (9)$$

based upon this reaction and the amount of tetraborane(10) taken were typically in the range 10-15%.

The reaction of dimethylzinc with tetraborane(10) shows interesting parallels with the reaction with diborane [equation (11)]. In each case, key steps in the reaction could be thought of as replacement of a BH_2 group in the parent borane by a methylzinc fragment, followed by reaction of the $[MeBH_2]_2$ produced in the initial step with a further molecule of dimethylzinc, yielding trimethylborane and zinc dihydride.

$$\begin{aligned} ZnMe_2 + B_4H_{10} &\longrightarrow \text{"}MeZnB_3H_8\text{"} + 1/2[MeBH_2]_2 \\ 1/2[MeBH_2]_2 + ZnMe_2 &\longrightarrow BMe_3 + ZnH_2 \end{aligned} \quad (10)$$

$$ZnMe_2 + B_2H_6 \longrightarrow MeZnBH_4 + 1/2[MeBH_2]_2$$
$$1/2[MeBH_2]_2 + ZnMe_2 \longrightarrow BMe_3 + ZnH_2 \qquad (11)$$

In each case, dimethylzinc can be thought of as bringing about asymmetric cleavage of the parent borane in a manner analogous to the respective reactions with ammonia.[18,19]

$$B_2H_6 + 2NH_3 \longrightarrow H_2B(NH_3)_2^+ + BH_4^- \qquad (12)$$
$$B_4H_{10} + 2NH_3 \longrightarrow H_2B(NH_3)_2^+ + B_3H_8^- \qquad (13)$$

In the tetraborane(10) system the proposed intermediate "$MeZnB_3H_8$" would then be deprotonated by dimethylzinc to give $[(MeZn)_2B_3H_7]$ and methane.

$$MeZnB_3H_8 + ZnMe_2 \longrightarrow [(MeZn)_2B_3H_7] + MeH \qquad (14)$$

Alternatively, the initial step in the reaction could involve deprotonation of tetraborane(10) by dimethylzinc, this being analogous to the reaction of dimethylzinc with

$$ZnMe_2 + B_4H_{10} \longrightarrow "MeZnB_4H_9" + MeH \qquad (15)$$

hexaborane(10) [equation (4)][3] and to the reaction of tetraborane(10) with potassium hydride [equation(16)].[20] Under this scheme, reaction of a second molecule of dimethyl-

$$KH + B_4H_{10} \longrightarrow KB_4H_9 + H_2 \qquad (16)$$

zinc with the intermediate "$MeZnB_4H_9$" would proceed by replacement of a BH_2 group by a methylzinc fragment.

$$"MeZnB_4H_9" + ZnMe_2 \longrightarrow [(MeZn)_2B_3H_7] + 1/2[MeBH_2]_2 \qquad (17)$$

4.3.2 Thermal Decomposition of $[(MeZn)_2B_3H_7]_2$

At room temperature $[(MeZn)_2B_3H_7]$ decomposes *in vacuo* in all-glass apparatus over a period of *ca.* 48 h. In order to investigate the thermal decomposition further samples were sealed in break-seal ampoules and heated to 150°C for 12 h. Invariably this led to the deposition of a metallic grey solid on the glass surfaces of the ampoule.

Initial investigation revealed that the volatile products consisted of condensable and non-condensable fractions and that the remaining solid residue contained both zinc and boron. The infrared spectrum of the non-condensable fraction showed no absorptions in the region 4000-400 cm^{-1} and therefore implied that the gas was hydrogen. Examination of the infrared spectrum of the condensable fraction showed that it contained absorptions characteristic of a mixture of BMe_3[15] and $[MeBH_2]_2$.[21]

In order to corroborate the elemental analysis results outlined in Section 4.3.1, the thermal decomposition was repeated, to allow quantitative measurements of the products to be made. The quantity of hydrogen formed was measured using a Toepler pump; condensable gases were assayed tensimetrically. The residual solid was dissolved in nitric acid and analyzed for zinc and boron by atomic absorption spectroscopy. Typical results are set out in Table 4.4.

	Zinc	Boron	Hydrogen gas	Condensable gas
Amount / mmol	0.052	0.052	0.079	0.021

Table 4.4 Products of the thermal decomposition of $[(MeZn)_2B_3H_7]$.

The very similar volatilities of BMe_3 and $[MeBH_2]_2$ precluded their separation by fractionation on the vacuum line. Therefore, in order to estimate the relative amounts of each present in the condensable fraction, a sample giving a measured pressure in a known volume was allowed to react with methanol; after acidification, the resulting solution was

analyzed for boron by atomic absorption spectroscopy. Using the relative amouts of BMe_3 and $[MeBH_2]_2$ determined in this way, it was then possible to arrive at the elemental analysis set out in Table 4.5.

Element	State[a]	Amount / mmol		Ratio	Calculated ratio[b]
Zinc	as solid residue	0.052	0.052	2	2
Boron	as solid residue	0.052	0.080	3.08	3
	as BMe_3	0.014			
	as $[MeBH_2]_2$	0.014			
Carbon	as BMe_3	0.042	0.056	2.15	2
	as $[MeBH_2]_2$	0.014			
Hydrogen	as H_2	0.158	0.354	13.61	13
	as BMe_3	0.126			
	as $[MeBH_2]_2$	0.070			

[a] A sample of the condensable fraction was found tensimetrically to contain 0.12 mmol of molecules in the vapour phase; analysis by atomic absorption showed that the solution formed by decomposition of this sample contained 0.16 mmol of boron atoms. This implies a mixture of 67% BMe_3 and 33% $[MeBH_2]_2$. [b] Calculated ratio for $[(CH_3Zn)_2B_3H_7]$.

Table 4.5 Observed and calculated elemental ratios for $[(CH_3Zn)_2B_3H_7]$ on the basis of thermal decomposition.

Given these results it is likely that the thermal decomposition of $[(MeZn)_2B_3H_7]$ proceeds in accordance with equation (18). The formation of a mixture of methylboranes

$$[(MeZn)_2B_3H_7] \longrightarrow 2Zn + 2B + 3H_2 + 1/2[Me_2BH]_2$$
$$[Me_2BH]_2 \longrightarrow Me_3B + 1/2[MeBH_2]_2 \qquad (18)$$

by the disproportionation of the intermediate $[Me_2BH]_2$ has also been proposed as a key step in the thermal decomposition of $[Me_2GaBH_4]$.[22]

4.4 Crystal Structure of $[(MeZn)_2B_3H_7]_2$

Several acicular crystals 0.5-0.8 mm in length were loaded into hand-drawn Pyrex capillaries each *ca.* 0.3 mm in internal diameter using the method described in Section 4.2.3. Initial investigation of such crystals using oscillation photography showed that they typically became amorphous over a period of 36-48 h, in keeping with the thermal instability described in Section 4.3.2. Consequently, following transfer of the crystal to the diffractometer, data collection was carried out with the crystal at 150 K.

4.4.1 Crystal Data

$P2_1/c$

$C_2H_{13}B_3Zn_2$, M = 400.59, monoclinic, ~~$P2(1)/c$~~, a = 10.038(2), b = 7.814(2), c = 11.076(2) Å, β = 111.92(3)°, U = 806.0(3) Å^3 [from 2θ values of 60 reflections measured at ±ω (24° ≤ 2θ ≤ 34°), λ = 0.71073 Å] , Z = 2, D_c = 1.651 gcm^{-3}, T = 150 K, colourless needle, 0.65 x 0.15 x 0.11 mm.

4.4.2 Data Collection

Data were collected on a Stoe Stadi-4 four-circle diffractometer fitted with an Oxford Cryosystems low-temperature device,[23] and employing graphite-monochromated Mo-Kα radiation with ω-θ scans, ω-halfwidth (1.5 + 0.35tanθ)°. Of the 1735 reflections (θ_{max} = 24.95°, -11 ≤ h ≤ 10, -8 ≤ k ≤ 8, 0 ≤ l ≤ 11) so collected, 1077 were unique.

4.4.3 Structure Solution and Refinement

All structure solution and refinement procedures were carried out by Drs. S.

Parsons and S. Blake at the Department of Chemistry, Edinburgh University. Following data reduction and the application of an absorption correction, the structure was solved for all non-H atoms by direct methods (SIR-92[24]) and refined against F^2 with full-matrix least-squares (SHELXL-93[25]). The hydrogen atoms on the methyl groups were located in a difference synthesis which described the loci of the possible positions of these atoms, and subsequently refined using a riding model, with $U_{iso}(H) = 1.5U_{eq}(C)$. Four of the remaining hydrogen atoms [H(1), H(2), H(5) and H(13)] were located in a difference synthesis performed after several cycles of least squares weighted towards the high angle data; the remaining hydrogen positions were inferred from this map. These hydrogen atoms were then refined within variable-metric rigid groups with the restraint that chemically equivalent B–H and Zn–H distances were equal, and that $U_{iso}(H) = 1.2U_{eq}(B)$. The refinement converged to a conventional R value of 6.23% [based on F and 623 data with $F > 4\sigma(F)$] and wR_2 of 15.61% (based on F^2 and all 1069 data) for 70 refined parameters. The final difference synthesis maximum and minimum were 1.064 and -0.616 e $Å^{-3}$, respectively.

4.4.4 Discussion

The structure of $[(MeZn)_2B_3H_7]_2$ at 150 K is illustrated in Figure 4.1 and relevant bond lengths and angles are listed in Table 4.6. A fuller account of data collection, structure solution and refinement parameters including fractional atomic coordinates and anisotropic displacement parameters can be found in Appendix 4.

Although the nature of the heavy atom skeleton is well defined by X-ray diffraction, the positions of hydrogen atoms are less well determined. However, comparison with similar structures and examination of the infrared, Raman and NMR spectra of the compound (*vide infra*) provide strong evidence that the hydrogen locations are as indicated.

The crystal structure of $[(MeZn)_2B_3H_7]_2$ consists of discrete, centrosymmetric, dimeric $Me_4Zn_4B_6H_{14}$ clusters in which two novel B_3H_7ZnMe units are linked through

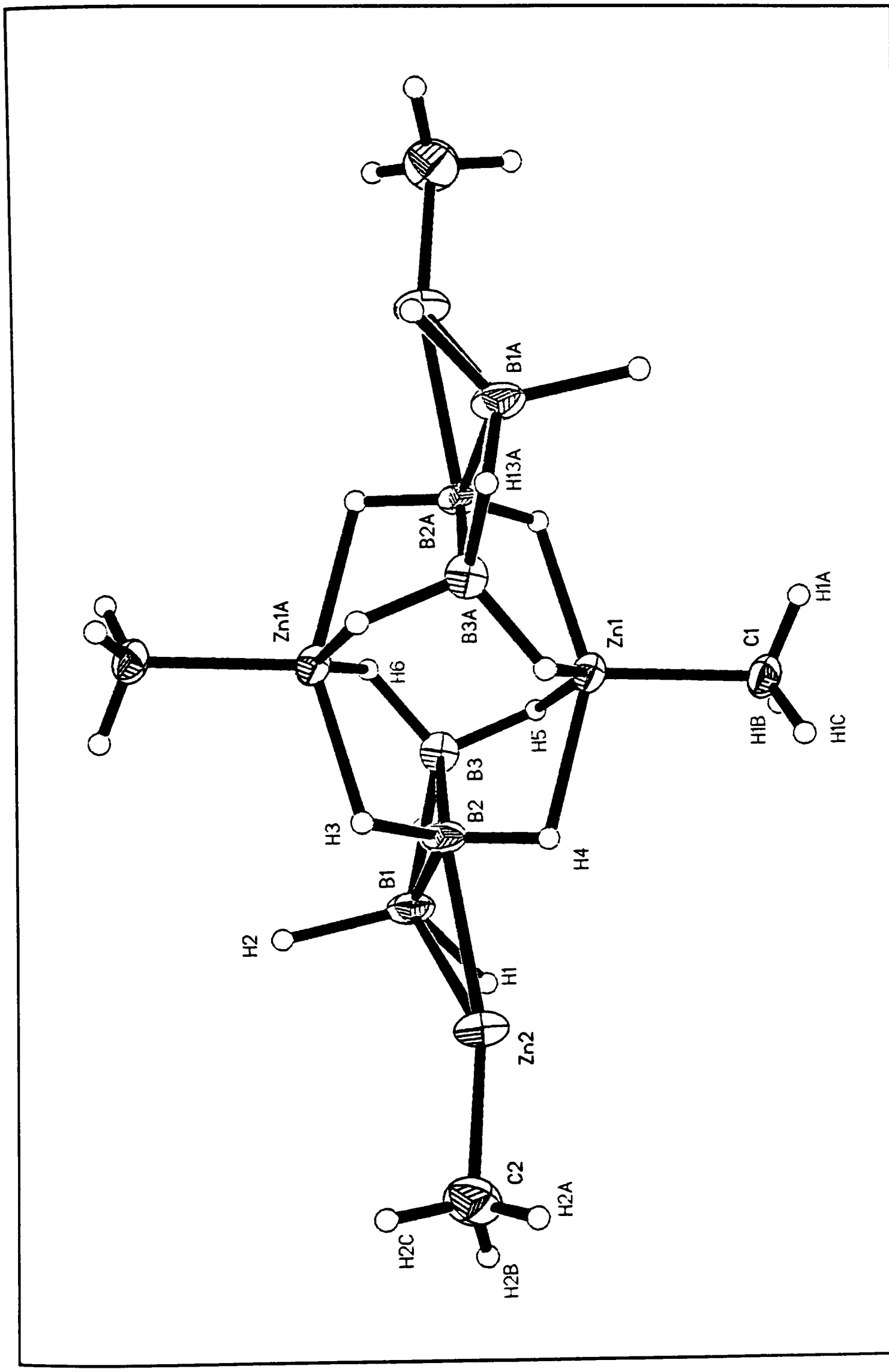

Figure 4.1 The molecular structure of $[(MeZn)_2B_3H_7]_2$ at 150 K.

Table 4.6 Selected bond lengths (Å) and angles (°) for $[(MeZn)_2B_3H_7]_2$.[a]

Zn(1)-C(1)	1.951(14)	Zn(2)-B(2)	2.15(2)
Zn(1)-B(2A)	2.41(2)	Zn(2)-B(1)	2.21(2)
Zn(1)-B(2)	2.41(2)	B(1)-B(2)	1.78(3)
Zn(1)-B(3)	2.45(2)	B(1)-B(3)	1.84(3)
Zn(1)-B(3A)	2.53(2)	B(2)-B(3)	1.76(2)
Zn(1)-Zn(1A)	3.014(3)	B(2)-Zn(1A)	2.41(2)
Zn(2)-C(2)	1.92(2)	B(3)-Zn(1A)	2.53(2)
C(1)-Zn(1)-B(2A)	127.9(6)	B(2)-B(1)-Zn(2)	64.0(9)
B(2A)-Zn(1)-B(2)	102.5(5)	B(3)-B(1)-Zn(2)	118.7(12)
C(1)-Zn(1)-B(3)	128.3(6)	B(3)-B(2)-B(1)	62.7(10)
B(2A)-Zn(1)-B(3)	90.0(6)	B(3)-B(2)-Zn(2)	126.2(11)
B(2)-Zn(1)-B(3)	42.5(6)	B(1)-B(2)-Zn(2)	67.9(9)
C(1)-Zn(1)-B(3A)	126.1(6)	B(3)-B(2)-Zn(1A)	72.8(8)
B(2A)-Zn(1)-B(3A)	41.7(6)	B(1)-B(2)-Zn(1A)	113.7(11)
B(2)-Zn(1)-B(3A)	88.3(6)	Zn(2)-B(2)-Zn(1A)	150.6(9)
B(3)-Zn(1)-B(3A)	105.6(5)	B(3)-B(2)-Zn(1)	70.2(8)
C(1)-Zn(1)-Zn(1A)	177.7(5)	B(1)-B(2)-Zn(1)	123.6(11)
B(2A)-Zn(1)-Zn(1A)	51.2(5)	Zn(2)-B(2)-Zn(1)	127.7(8)
B(2)-Zn(1)-Zn(1A)	51.3(4)	Zn(1A)-B(2)-Zn(1)	77.5(5)
B(3)-Zn(1)-Zn(1A)	53.9(4)	B(2)-B(3)-B(1)	59.1(10)
B(3A)-Zn(1)-Zn(1A)	51.7(4)	B(2)-B(3)-Zn(1)	67.3(8)
C(2)-Zn(2)-B(2)	154.5(7)	B(1)-B(3)-Zn(1)	118.3(10)
C(2)-Zn(2)-B(1)	143.8(8)	B(2)-B(3)-Zn(1A)	65.5(8)
B(2)-Zn(2)-B(1)	48.1(7)	B(1)-B(3)-Zn(1A)	106.4(10)
B(2)-B(1)-B(3)	58.3(10)	Zn(1)-B(3)-Zn(1A)	74.4(5)

[a] 'A' indicates the symmetry transformation *-x*, *-y*, *-z*+2.

hydride bridges about a central MeZn···ZnMe vector [3.014(3) Å] in an unusual example of a molecule containing two chemically distinct zinc environments.

Zn(1) is *penta*-coordinated, being bound to a terminal methyl group and four bridging hydrogen atoms (supplied by the B_3H_7ZnMe units) forming a distorted square pyramid. A similar arrangement of the methyl and hydrogen ligands occurs in the structure of crystalline $[MeZnBH_4]$,[6] in which BH_4 groups bridge successive methylzinc units with bidentate coordination at each metal centre. In each case the bonding between the borane ligand and the zinc centre involves bridging hydrogen atoms, and this is reflected in the similar Zn···B distances {2.41(2) and 2.45(2) Å in $[(MeZn)_2B_3H_7]_2$; 2.30(2) and 2.32(2) Å in $[MeZnBH_4]$[6]}. The dimeric nature of $[(MeZn)_2B_3H_7]_2$ contrasts with the polymeric skeleton of $[MeZnBH_4]$ and presumably reflects the fact that coordination of each B_3H_7ZnMe ligand occurs through all four hydrogens of the basal $H_2B–BH_2$ unit, a situation which permits folding of the heavy atom skeleton.

In effect, the MeZn(1) unit has replaced an apical BH_2 unit in tetraborane(10) and in this way its geometry resembles that of the Me_2M unit (M = Al or Ga) in $Me_2MB_3H_8$.[14] Presumably the dimeric nature of $[(MeZn)_2B_3H_7]_2$ (as opposed to the monomeric structures found for $Me_2MB_3H_8$[14]) is related to the increase in coordination number of Zn(1) from three to five which can be accomplished by sharing of two further terminal hydrogen atoms.

The 'side-on' bridging function of the B_3 units is reminiscent of the structure of $[Mn_2(CO)_6(\mu\text{-}Br)(B_3H_8)]$,[26] as illustrated in Figure 4.2. In each case, the B_3 ligand bridges two metal atoms using all four hydrogens of the basal $H_2B–BH_2$ unit. This is reflected by similarities in both the M···B {2.41(2) and 2.45(2) Å in $[(MeZn)_2B_3H_7]_2$; 2.30(2)-2.36(2) Å in $[Mn_2(CO)_6(\mu\text{-}Br)(B_3H_8)]$[26]} and basal B–B distances {1.76(2) Å in $[(MeZn)_2B_3H_7]_2$; 1.71(2) Å in $[Mn_2(CO)_6(\mu\text{-}Br)(B_3H_8)]$[26]}. In each case, the M···M distance is too long to permit any bonding interaction between the two metal centres.

The B_3H_7ZnMe unit can be conceived as being derived from the well-known B_3H_8 ligand by replacement of one bridging hydrogen by a methylzinc unit. Zn(2) is thus

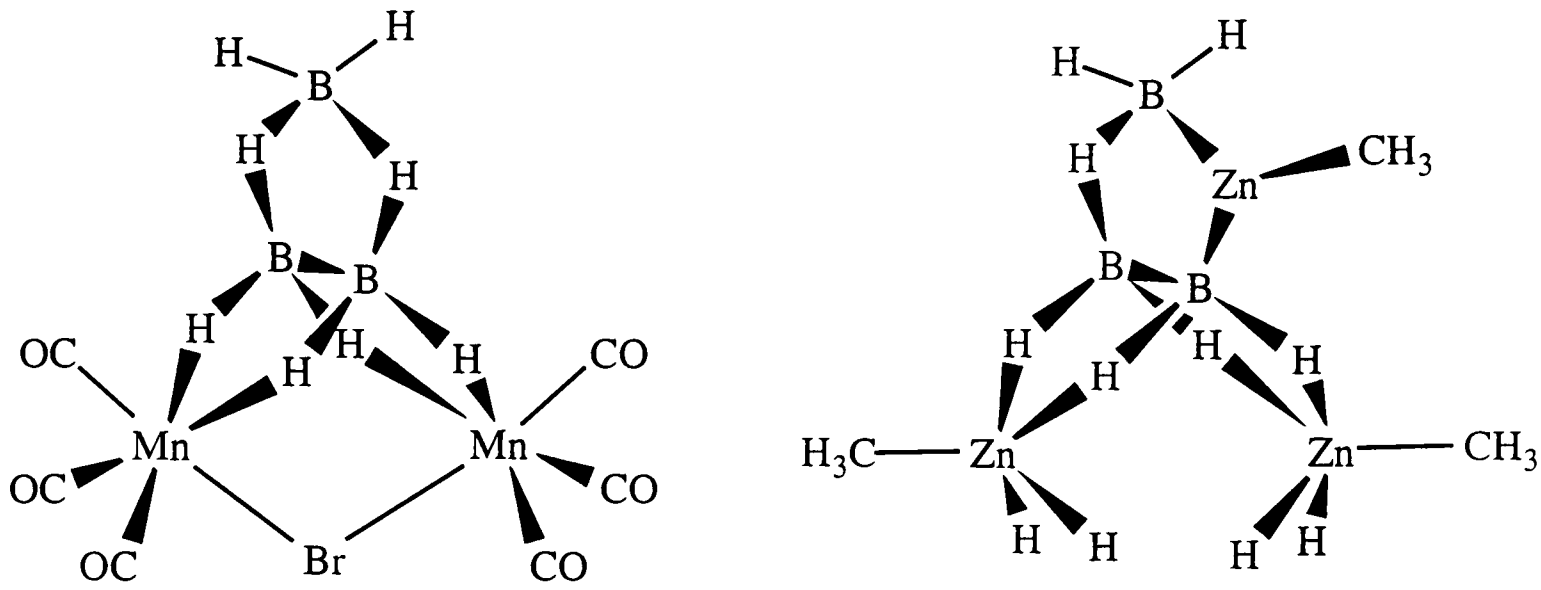

Figure 4.2 Comparison of bridging B_3 ligands in $[Mn_2(CO)_6(\mu\text{-}Br)(B_3H_8)]$[26] and $[(MeZn)_2B_3H_7]_2$.

tri-coordinated, being attached to a terminal methyl group and, in an especially remarkable feature, to two boron atoms [B(1) and B(2)] forming one edge of the B_3 unit. The Zn(2)–B(1,2) bond lengths [2.21(2) and 2.15(2) Å] are significantly shorter than the Zn(1)···B(2,3) distances [2.41(2) and 2.45(2) Å], but very similar to the distances observed in the cluster $[Zn(B_{10}H_{12})_2]^{2-}$ [2.197(10) and 2.209(10) Å],[5] in which the zinc is bound directly to four boron atoms. Consistently, the BZnB bond angle in $[(MeZn)_2B_3H_7]_2$ [48.1(7)°] is also similar to those in $[Zn(B_{10}H_{12})_2]^{2-}$ [42.7(4)°],[5] $[B_{10}H_{12}TlMe_2]^-$ [37.3(6)°],[27] and $[(Et_2O)_2Cd(B_{10}H_{12})]$ [37.6°],[12] as are the angles subtended at the boron atoms. In each of these cluster compounds, the metal atom is thought of as having formally replaced a bridging hydrogen atom, being bonded to a B_2 unit *via* a three-centre, two-electron bond. It seems likely, therefore, that the bonding in the B_3H_7ZnMe unit is best viewed in terms of replacement of one of the bridging hydrogens in a B_3H_8 group by a methylzinc unit which is bonded to B(1) and B(2) *via* a ZnB_2 three-centre, two-electron bond.

Interestingly, the Zn(2)–B(1,2) bond lengths [2.21(2) and 2.15(2) Å] are comparable with the sum of the covalent radii of zinc and boron (2.15 Å)[28] and are therefore consistent with a direct (*i.e.* non-hydrogen-bridged) Zn–B linkage. As such, $[(MeZn)_2B_3H_7]_2$ represents a rare example of a compound containing a Zn–B bond.

Tri-coordinated zinc and cadmium complexes are uncommon and usually incorporate bulky ligands.[29] Furthermore, the coordination geometry at the metal atom is invariably extremely close to trigonal planar {for example, the sum of the angles around the two crystallographically distinct zinc atoms in $[Zn(S\text{-}^tBu_3C_6H_2\text{-}2,4,6)_2]_2$ are 359.5 and 357.9°}.[29] In $[(MeZn)_2B_3H_7]_2$ the sum of the angles at Zn(2) is 346.5° and the carbon atom of the methyl group lies 0.68 Å above the plane described by Zn(2), B(1) and B(2). It seems likely that this deviation from trigonal planar geometry is due to steric factors; the Zn–C bond points in a direction such as to minimize non-bonded interaction with atoms attached to the B_3 ring.

The geometry of the B_3 unit itself is not unusual; the B–B bonds measure 1.76-1.84 Å and are therefore similar in length to those found in both $[Mn_2(CO)_6(\mu\text{-}Br)(B_3H_8)]$[26] and $[H_2B(NH_3)_2][B_3H_8]$,[30] with small differences reflecting the replacement of one of the bridging hydrogens by a methylzinc unit.

4.5 Vibrational Spectra of $[(MeZn)_2B_3H_7]_2$

In order to corroborate the hydrogen atom positions indicated in Figure 4.1, the infrared and Raman spectra of $[(MeZn)_2B_3H_7]_2$ were measured. The extreme sensitivity of the compound to laser damage meant that initial experiments performed using conventional Raman techniques merely resulted in decomposition of the sample. Subsequent experiments using the FT-Raman technique, a very low laser power (< 80 mW) and a sample cooled to -196°C allowed satisfactory spectra to be measured. However, even with such methods, it was possible to collect only a small number of scans prior to sample decomposition; consequently the signal-to-noise ratio was somewhat poorer than normal.

The infrared and FT-Raman spectra of solid $[(MeZn)_2B_3H_7]_2$ are illustrated in Figures 4.3 and 4.4, respectively, and assignments of the principal features listed in Table 4.7. These spectra corroborate the crystal structure (which displays a centre of inversion)

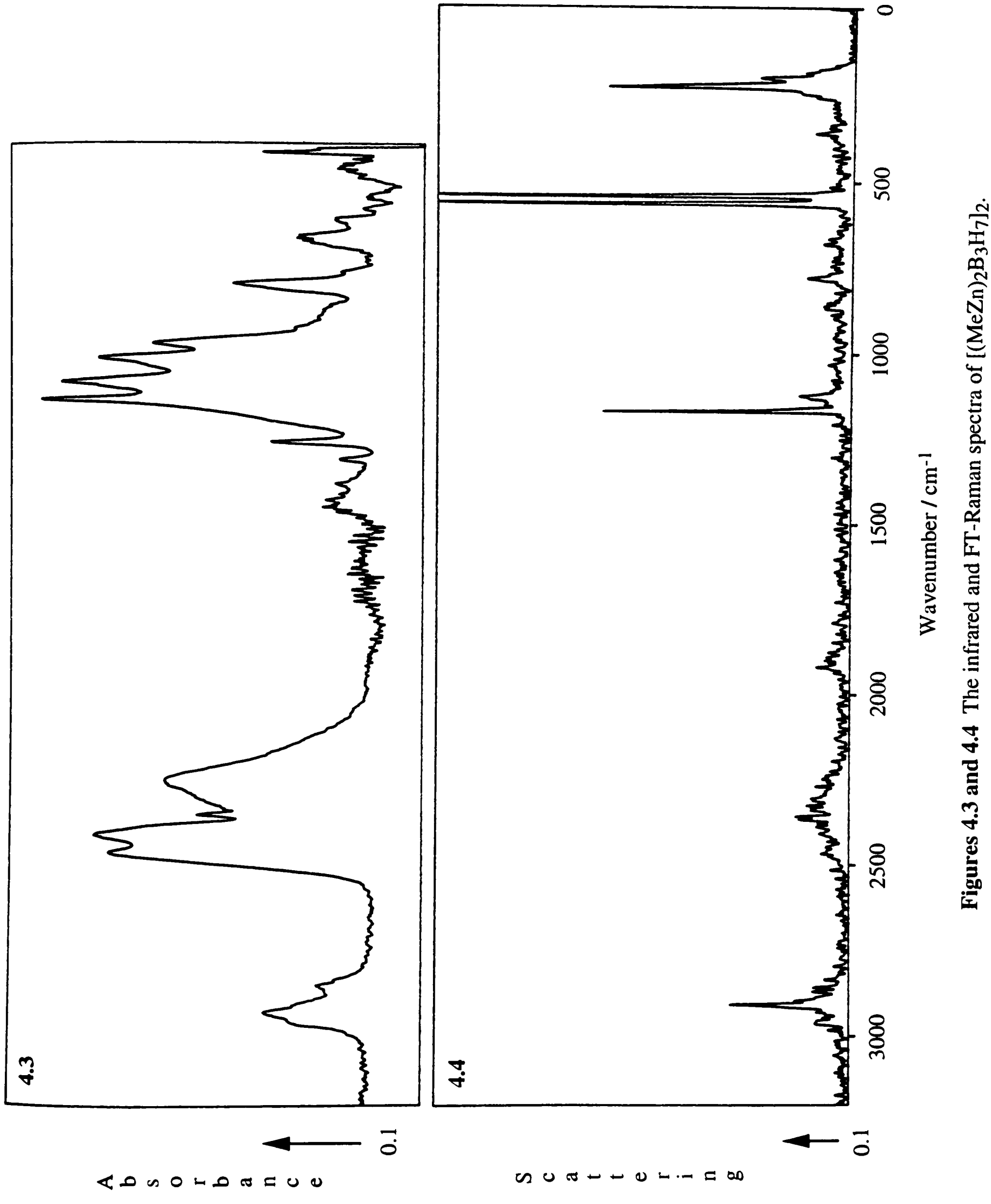

Figures 4.3 and 4.4 The infrared and FT-Raman spectra of $[(MeZn)_2B_3H_7]_2$.

Table 4.7 Assignments of the infrared and Raman spectra of $[(MeZn)_2B_3H_7]_2$.

Wavenumber / cm^{-1}		Assignment[a]
Infrared	Raman	
2933 w		ν_a(C–H)
	2907 m	ν_s(C–H)
2853 w		2 x $\delta_a(CH_3)$
2465 s		$\nu_a(B–H_t)$
2413 s		$\nu_s(B–H_t)$
	2362 w,br	$\nu(B–H_b)$
2257 m,br		$\nu(B–H_b)$
	1919 w	$\nu(B–H_b)$
1384 vw		$\delta_a(CH_3)$
1311 w		Ring stretching
1261 w		Ring stretching
	1166 ms	$\delta_s(CH_3)$
1140 vs		BH_2 twisting
	1123 w	BH_2 twisting
1090 s		$\delta(BH_2)$
1020 s		$\delta(BH_2)$
976 ms		$\rho(BH_2)$
802 mw		Ring breathing
	778 w	BH_2 wagging
667 w		$\rho(CH_3)$
	563 vs	ν(Zn–C)
	539 vs	ν(Zn–C)
420 w		ν(Zn–B)
	226 s	ν(Zn–B)
	203 w,sh	Zn–Me bending

[a] Assignments based upon analogies with (i) compounds containing a methylzinc unit, notably $[MeZnBH_4]$[6] and $[Me_2Zn]$;[31] (ii) species containing a B_3 unit, *e.g.* $[CsB_3H_8]$[32] and $[(H)(OC)_3Fe(B_3H_8)]$;[33] (iii) species containing a terminal BH_2 group, *e.g.* $[MeZn(\mu\text{-}H)_2BH_2]$,[6] $[Me_2Ga(\mu\text{-}H)_2BH_2]$[22] and $[CsB_3H_8]$;[32] and (iv) species containing Zn···B unit, *e.g.* $[MeZn(\mu\text{-}H)_2BH_2]$,[6] solid $[MeZnBH_4]$[6] and $[Me_4N]_2[Zn(B_{10}H_{12})_2]$.[5]

in so far as no vibrational transitions are observed to be active in both infrared absorption and Raman scattering. The spectra are now examined in more detail.

4.5.1 Vibrational Features Attributable to a BH_2 Group

The vibrational spectra provide persuasive evidence for the existence of a BH_2 group. Thus, the infrared spectrum shows *two* bands (at 2465 and 2413 cm^{-1}) in the region characteristic of $\nu(B-H_t)$ fundamentals (t = terminal),[34] with wavenumbers and splitting similar to the bands attributed to the corresponding modes of the apical BH_2 group in solid $[CsB_3H_8]$ (2465 and 2415 cm^{-1}).[32] Furthermore, bands attributable to the twisting, deformation, rocking and wagging modes of a BH_2 group are also in evidence;[35] these can be found at 1140, 1090/1020, 976 and 778 cm^{-1}, respectively. The assignments are made by analogy with corresponding features in the infrared spectra of compounds containing a $B(H_t)_2$ group, notably $[MeZn(\mu\text{-}H)_2BH_2]$[6] and $[Me_2Ga(\mu\text{-}H)_2BH_2]$.[22] The analogous bands in the spectra of these compounds appear at 1126 (1146), 1116 (1095), 953 (970) and 713 (730) cm^{-1}, respectively {wavenumbers of bands due to $[Me_2Ga(\mu\text{-}H)_2BH_2]$ appear in parentheses}. The vibrational spectra thus endorse the existence of two terminal hydrogen atoms attached to B(1) and make it unlikely that either hydrogen is involved in bonding to Zn(2) *via* a Zn–H–B linkage.

4.5.2 Vibrational Features Attributable to the B_3H_7 Fragment

Bands attributable to the stretching of bridging B–H bonds in B–H–Zn (2257 cm^{-1}) and B–H–B units (1919 cm^{-1}) find counterparts in the spectra of solid $[MeZnBH_4]$ (2257 cm^{-1})[6] and $[(H)(OC)_3FeB_3H_8]$ (1915 cm^{-1}).[33] The second feature provides strong evidence for the existence of a hydrogen atom bridging one edge of the B_3 unit [H(13) bridges B(1) and B(3)]. The existence of a feature assigned to the stretching of B–H bonds in a B–H–Zn unit is entirely consistent with the linkage of basal boron

atoms of the B_3 unit to Zn(1) and Zn(1A) *via* bridging hydrogens. Such a linkage is also consistent with the observed Zn···B distances [2.41(2) and 2.45(2) Å].

4.5.3 Vibrational Features Attributable to Zn–C and Zn–B Units

Prominent in the FT-Raman spectrum are two equally intense bands at 563 and 539 cm^{-1} arising from ν(Zn–C) modes {*cf.* 557 cm^{-1} for solid $[MeZnBH_4]$[6] and 558 cm^{-1} (mean of ν_s and ν_a) for $[Me_2Zn]$[31]}. Such a finding is consistent with the presence of the two distinct methylzinc environments in $[(MeZn)_2B_3H_7]_2$ implied by the structure depicted in Figure 4.1. Given the similarity in the coordination geometries of Zn(1) and the Zn atom in solid $[MeZnBH_4]$, it is likely that the feature at 563 cm^{-1} has its origins in a vibration which involves mainly stretching of the Zn(1)–C(1) unit.

The feature at 420 cm^{-1} is assigned to a motion involving stretching of a hydrogen-bridged Zn···B unit, by analogy with similar features in the spectra of solid $[MeZnBH_4]$ (443 cm^{-1})[6] and solid $[Me_2GaBH_4]$ (395 cm^{-1}).[22]

Intense scattering observed in the Raman spectrum at 226 cm^{-1} probably originates in a Zn–B stretching motion involving the ZnB_2 unit, in keeping with the vibrational assignments proposed for compounds of the type $[Me_4N]_2[M(B_{10}H_{12})_2]$ (M = Zn, Cd or Hg).[5] Bands found at 286, 244 and 228 cm^{-1}, respectively, can be associated with antisymmetric M–B stretching modes involving the central MB_4 unit.[5]

4.6 NMR Spectra of $[(MeZn)_2B_3H_7]_2$

^{11}B and ^{1}H NMR spectra of $[(MeZn)_2B_3H_7]_2$ were measured for $[^2H_8]$toluene, $[^2H_2]$dichloromethane and $[^2H_8]$tetrahydrofuran solutions at temperatures in the range -60 to +20°C. As a result of the slightly lower solubility of $[(MeZn)_2B_3H_7]_2$ in $[^2H_8]$toluene and its tendency to form viscous oils with the retention of solvent molecules when recovered from ether solvents, $[^2H_2]$dichloromethane was the solvent of choice for NMR

studies. Typical $^{11}B[^1H]$ spectra at -20 to 20°C and the ^1H spectrum at -20°C for $[^2H_2]$dichloromethane solutions are illustrated in Figures 4.5 and 4.6, respectively.

4.6.1 ^{11}B NMR Spectra

The $^{11}B[^1H]$ NMR spectrum of $[(MeZn)_2B_3H_7]_2$ in $[^2H_2]$dichloromethane solution at -20°C shows five distinct resonances at δ_B -25.6, -34.2, -36.7, -55.0 and -57.6. Warming the sample causes the relative intensities of the signals to change. The features at δ_B -25.6, -34.2 and -55.0 are observed to become more intense with respect to those at δ_B -36.7 and -57.6. With the solution at 20°C, only three signals of equal intensity remain (at δ_B -25.5, -34.1 and -55.0). In the absence of ^1H decoupling the first two appear to be broad singlets and the third a 1:2:1 triplet [$J(^{11}B-^1H)$ = 84.1 Hz]. Cooling the sample back to -20°C causes the original spectrum to be reproduced. These observations imply that solutions of $[(MeZn)_2B_3H_7]_2$ in $[^2H_2]$dichloromethane solution feature an equilibrium between more than one species.

The signals observed with the sample at 20°C are consistent with a species along the lines illustrated in Figure 4.1 incorporating three distinct boron atoms, one bound to two equivalent terminal hydrogen atoms and the other two bearing no such atoms. Coupling to bridging hydrogens appears not to be resolved, the linewidths typically being large in comparison with the coupling constants expected for bridging hydrogens.[36] The relative ordering of the ^{11}B chemical shifts for atoms B(1), B(2) and B(3) is in line with the empirical rules proposed by Teixidor *et al.* for boranes and heteroboranes,[37] and by Rath and Fehlner for metal-rich metallaboranes.[38] That B(1) has a higher coordination number (6) than either B(2) or B(3) (both 5) and is attached to two terminal hydrogen atoms implies that it would have a more negative chemical shift.[37,38] Of the two basal boron atoms, B(2) and B(3), B(2) would be expected to have the more positive chemical shift (*i.e.* would be assigned to the signal at δ_B -25.6) as a result of the deshielding effect of the directly bonded metal atom.[38]

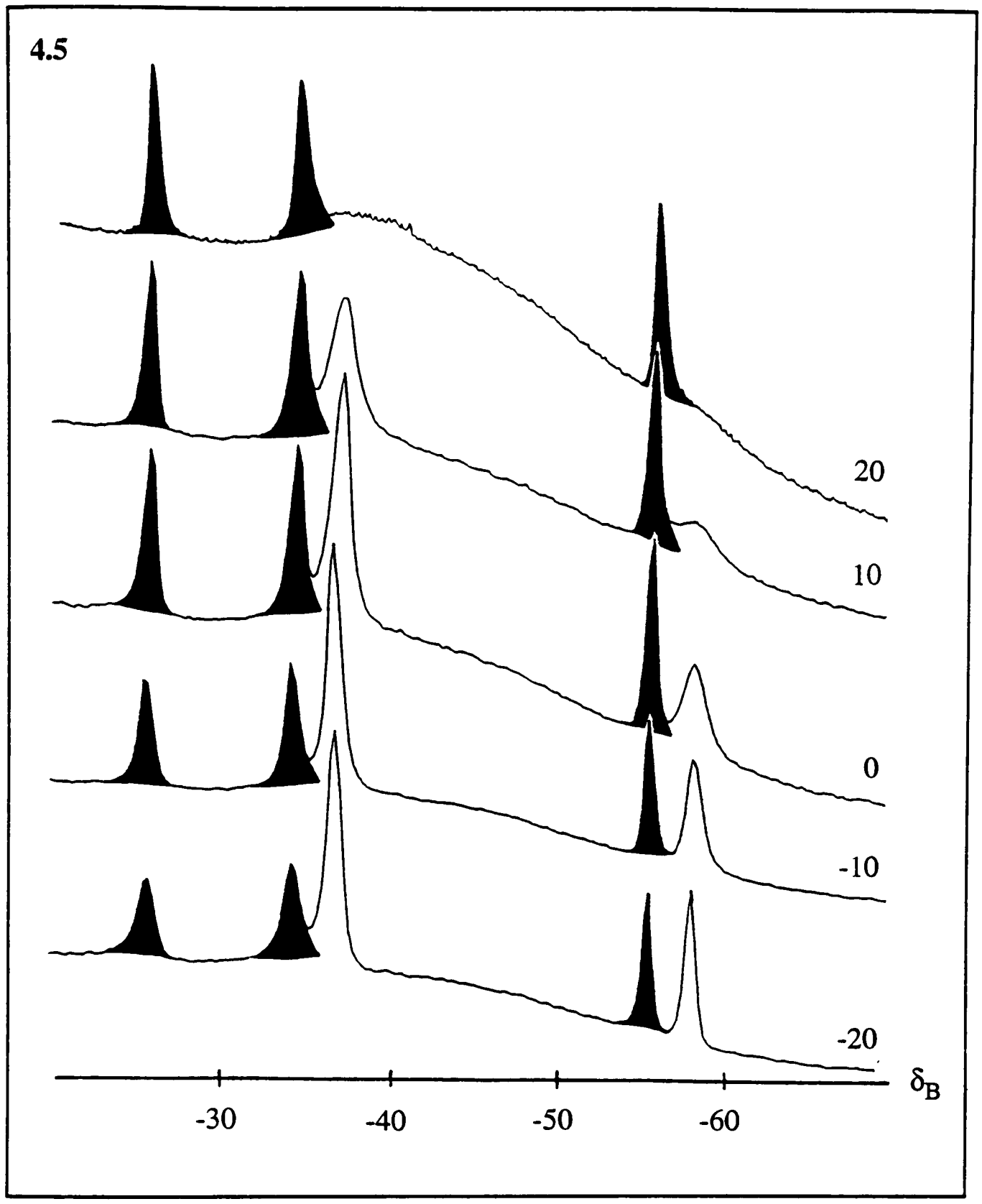

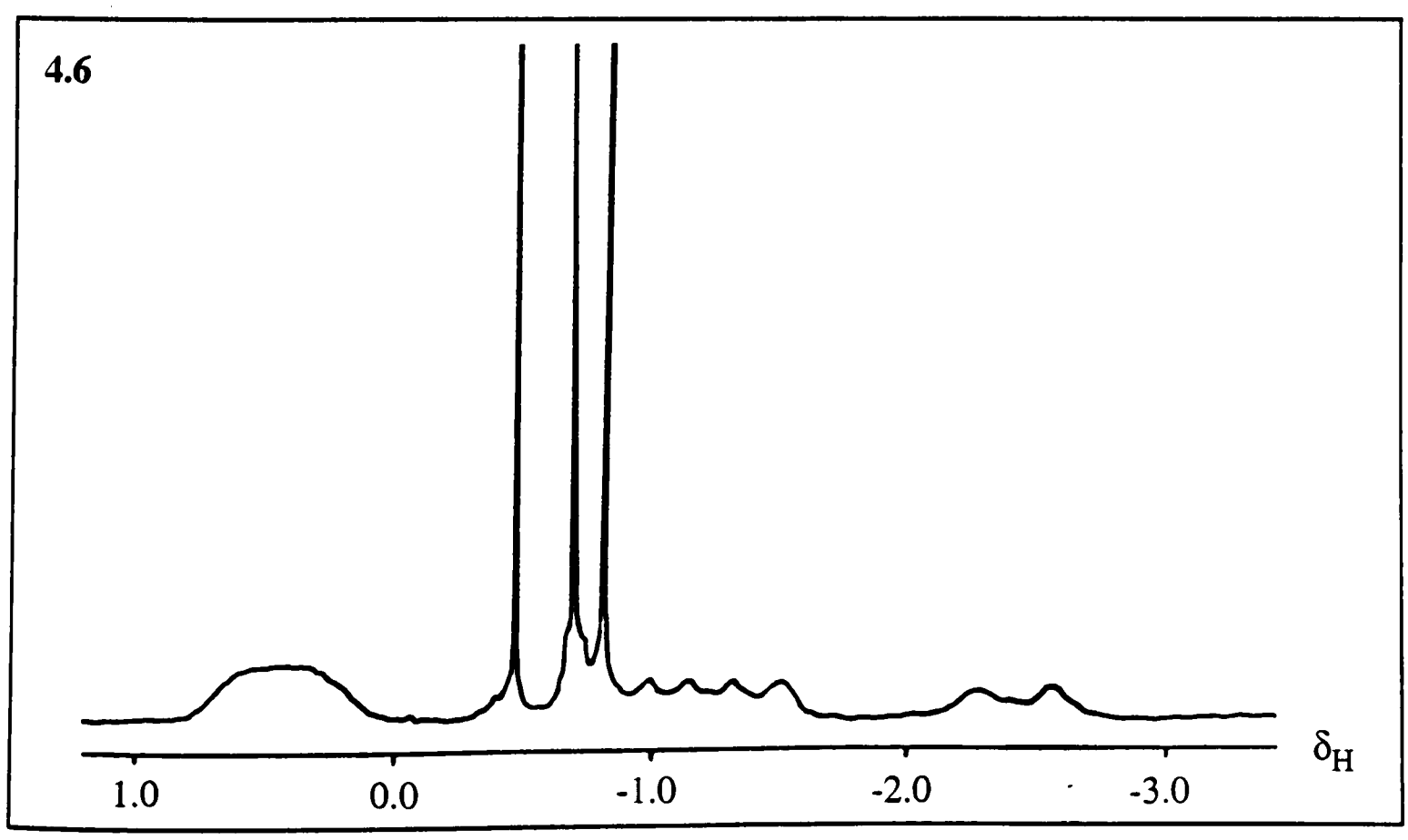

Figures 4.5 and 4.6 The ^{11}B and ^{1}H NMR spectra of $[(MeZn)_2B_3H_7]_2$ in $[^2H_2]$dichloromethane.

The additional signals present in the ^{11}B spectrum of the sample at -20°C consist of a broad singlet at δ_B -36.7 (relative intensity 2) and a 1:2:1 triplet at δ_B -57.6 (relative intensity 1). The similarity in chemical shift and coupling pattern of the signals at δ_B -57.6 and -55.0 implies that the first arises from a boron atom similar in its environment to B(1), being attached to two terminal hydrogens. The remaining signal at δ_B -36.7 must be due to two boron atoms rendered equivalent by a fluxional process that is rapid even at -20°C.

One possible explanation for these observations is that in $[^2H_2]$dichloromethane solution $[(MeZn)_2B_3H_7]$ exists as a mixture of species in equilibrium, possibly involving different states of aggregation of the $(MeZn)_2B_3H_7$ fragment. The signals observed with the sample at 20°C are consistent with the static, dimeric structure $[(MeZn)_2B_3H_7]_2$ illustrated in Figure 4.1; the additional signals appearing at lower temperatures could possibly be attributed to a more highly aggregated species, $[(MeZn)_2B_3H_7]_n$, in which B(2) and B(3) are rendered equivalent by a fluxional process such as that thought to occur in $Me_2MB_3H_8$ (M = Ga or Al)[14] and involving an intermediate incorporating monodentate coordination of the B_3H_8 ligand.

Attempts to confirm the existence of an equilibrium featuring species of the type $[(MeZn)_2B_3H_7]_n$ by vapour pressure depression or other colligative measurements were frustrated by the sparing solubility of the compound in suitable, weakly coordinating solvents at room temperature, and by its thermal instability at significantly higher temperatures.

4.6.2 ^1H NMR Spectra

The ^1H NMR spectrum of the $[^2H_2]$dichloromethane solution at 20°C shows a somewhat broad singlet at δ_H -0.27 attributable to methyl protons of the methylzinc moieties. The broadness of the signal probably results from the existence of two unresolved resonances due to the two different methyl environments implicit in a species such as that illustrated in Figure 4.1. Signals due to protons bound to boron are broad and difficult to distinguish from the baseline at this temperature.

With the sample at -20°C the spectrum (Figure 4.6) shows at least three signals attributable to methyl protons. This is consistent with the presence of more than one species in equilibrium. The spectrum also shows three broad signals attributable to protons bound to boron at δ_H (i) 0.45 [extremely broad resonance, linewidth *ca.* 200 Hz], (ii) -1.24 [1:1:1:1 quartet] and (iii) -2.41, with intensities in the ratio 4:2:1. With reference to the numbering scheme of Figure 4.1, these are assigned, respectively, (i) to the bridging protons H3, H4, H5 and H6, (ii) to the protons of the BH_2 group (H1 and H2), and (iii) to the bridging proton of the B–H–B group (H13). The position of the resonance attributed to the Zn–H–B protons (δ_H 0.45) is somewhat unusual. Protons bridging between boron and metal atoms usually resonate at lower (*i.e.* more negative) chemical shifts than do terminal hydrogens or those bridging between two boron atoms.[39]

4.7 *Ab Initio* Calculations

In view of the unusual structure of $[(MeZn)_2B_3H_7]_2$ as determined by X-ray diffraction, it was thought that *ab initio* calculations might prove useful not only by probing possible molecular geometries, but also by providing further endorsement of the poorly defined hydrogen atom locations. To this end, geometry optimizations were obtained for $[MeZnB_3H_8]$ and for the B_3H_7ZnMe ligand. The former calculations were intended to provide a comparison with the hydrogen-bridged linkage of the B_3H_7ZnMe ligand to Zn(1) and Zn(1A), the latter to provide a comparison with the geometry of the unusual B_3H_7ZnMe unit itself. All calculations were carried out by the group of Professor P.v.R. Schleyer at the University of Erlangen-Nürnberg.

4.7.1 Discussion

The final geometries optimized for $[MeZnB_3H_8]$ and for the B_3H_7ZnMe ligand at the HF/tzp level of theory are illustrated in Figures 4.7 and 4.8, respectively. Comparisons of the calculated bond lengths and angles for both species with the

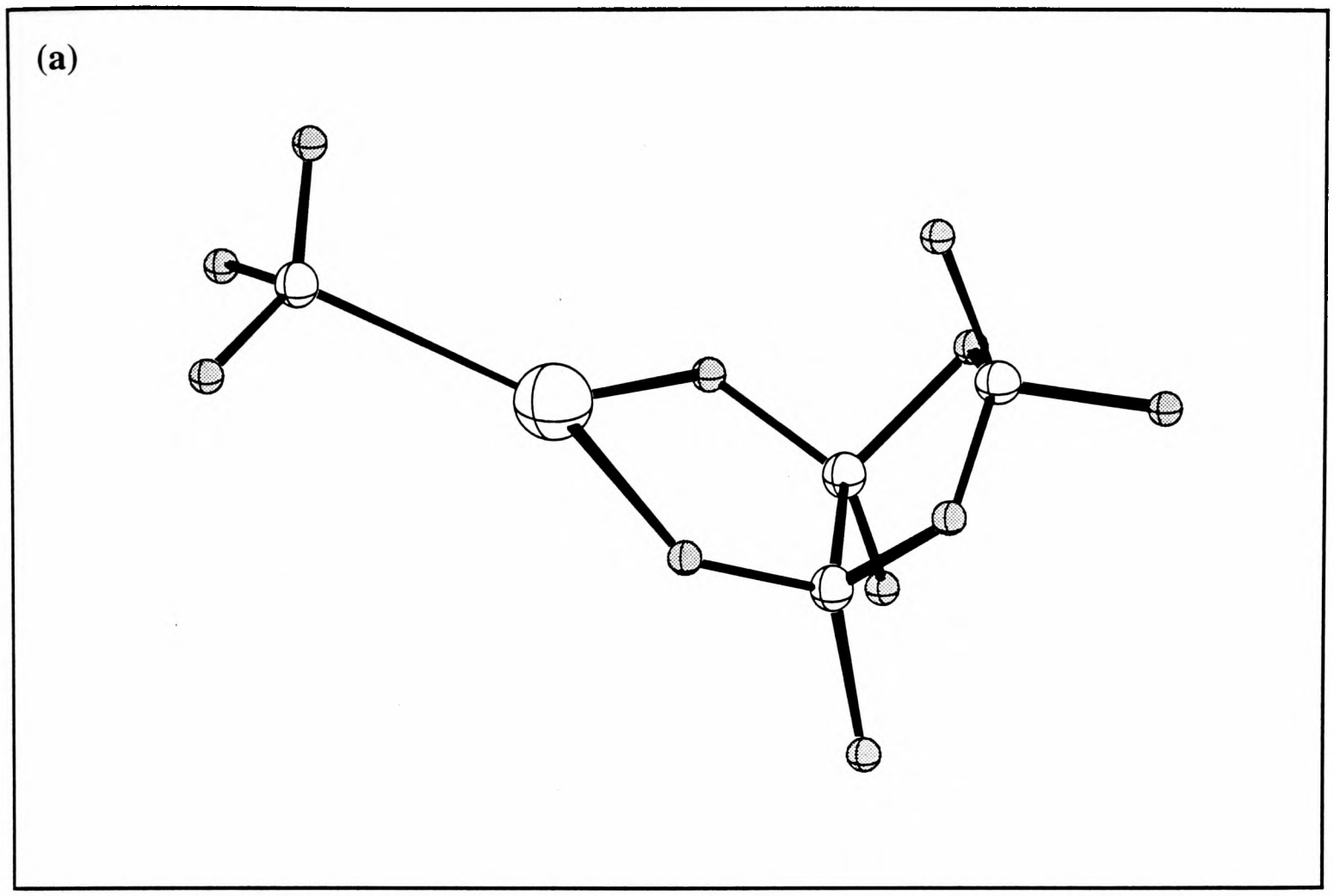

Figure 4.7 (a) Perspective and (b) plan views of the final geometry optimization of $[MeZnB_3H_8]$ at the HF/tzp level of theory.

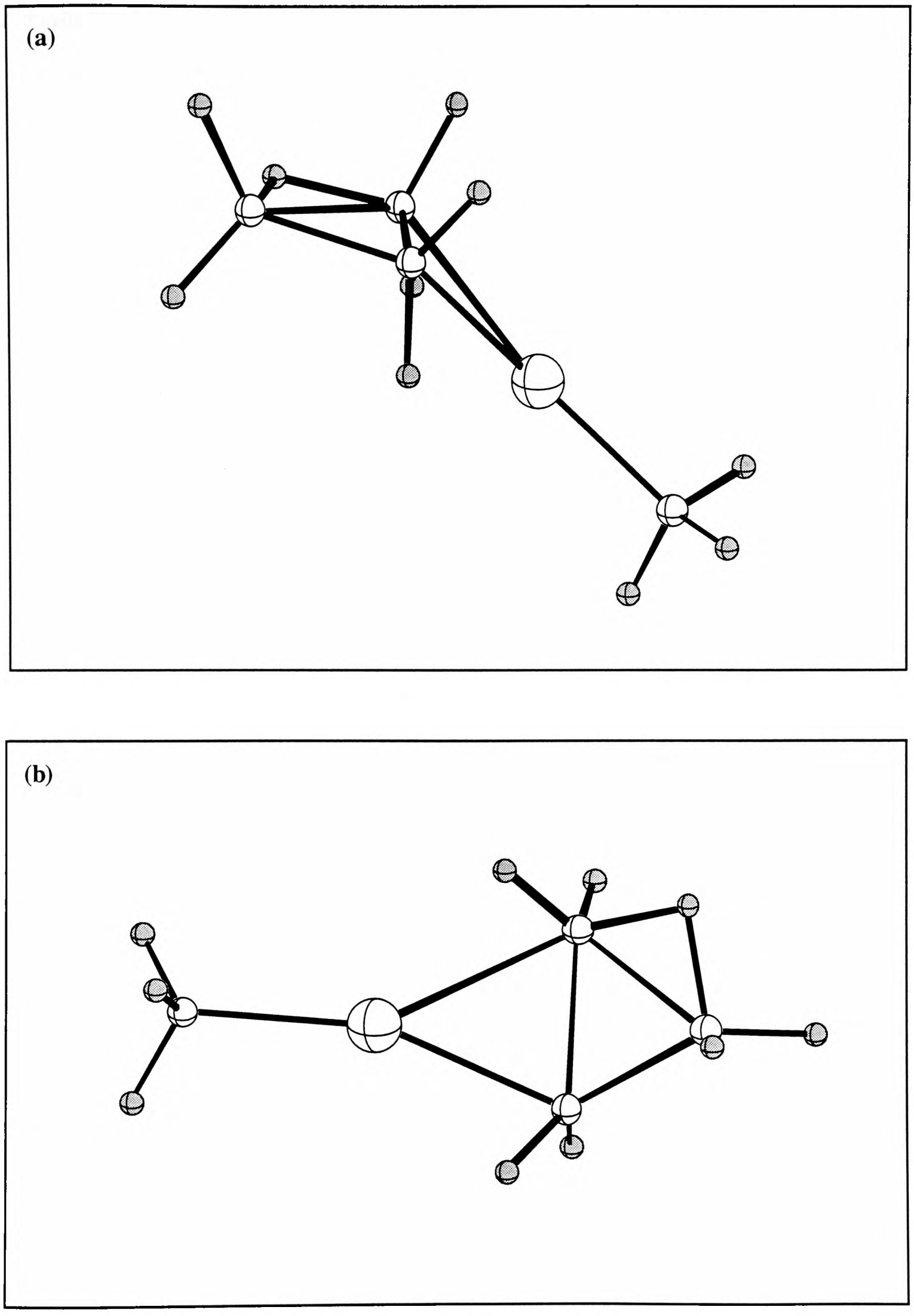

Figure 4.8 (a) Perspective and (b) plan views of the final geometry optimization of B_3H_7ZnMe at the HF/tzp level of theory.

Table 4.8 Comparison of calculated bond lengths (Å) and angles (°) for $MeZnB_3H_8$ with corresponding values in $[(MeZn)_2B_3H_7]_2$.

Parameter[a]	Experimental	HF/svp	HF/tzp
Zn(1)–C(1)	1.951(14)	2.003	1.989
Zn(1)–B(2)	2.41(2)	2.414	2.352
Zn(1)–B(3)	2.45(2)	2.414	2.352
B(2)–B(3)	1.76(2)	1.829	1.822
B(1)–B(3)	1.84(3)	1.872	1.864
B(1)–B(2)	1.78(3)	1.872	1.864
Zn(1)–H(5)	1.90(2)	1.876	1.858
B(3)–H(5)	1.25	1.258	1.249
B(3)–H(13)	1.19	1.258	1.249
B(2)–Zn(1)–B(3)	42.5(6)	44.54	45.61
Zn(1)–B(2)–B(3)	70.2(8)	67.73	67.20
Zn(1)–B(3)–B(2)	67.3(8)	67.73	67.20
B(1)–B(2)–B(3)	62.7(10)	60.74	60.72
B(1)–B(3)–B(2)	59.1(10)	60.74	60.72
B(2)–B(1)–B(3)	58.3(10)	58.50	58.55
Sum of angles at Zn(1)	299.7	360	359.1
Torsional angle[b]	149.6(10)	107.90	120.46

[a] The numbering scheme is consistent with that used in Table 4.6 for the structure determined by X-ray diffraction. [b] Defined as the angle between the planes described by atoms Zn(1), B(2), B(3) and B(1), B(2), B(3).

Table 4.9 Comparison of calculated bond lengths (Å) and angles (°) for the B_3H_7ZnMe ligand with corresponding values in $[(MeZn)_2B_3H_7]_2$.

Parameter[a]	Experimental	HF/tzp
Zn(2)–C(2)	1.92(2)	2.006
Zn(2)–B(1)	2.21(2)	2.360
Zn(2)–B(2)	2.15(2)	2.188
B(1)–B(2)	1.78(3)	1.798
B(1)–B(3)	1.84(3)	1.869
B(2)–B(3)	1.76(2)	1.798
B(1)–H(1)	1.36	1.228
B(1)–H(2)	1.37	1.203
B(1)–H(13)	1.19	1.332
B(3)–H(13)	1.17(2)	1.332
B(1)–Zn(2)–B(2)	48.1(7)	46.38
Zn(2)–B(1)–B(2)	64.0(9)	61.73
Zn(2)–B(2)–B(1)	67.9(9)	71.89
B(1)–B(2)–B(3)	62.7(10)	62.60
B(1)–B(3)–B(2)	59.1(10)	58.70
B(2)–B(1)–B(3)	58.3(10)	58.70
Sum of angles at Zn(2)	346.4(22)	359.46
Torsional angle[b]	157.2(11)	146.95

[a] The numbering scheme is consistent with that used in Table 4.6 for the structure determined by X-ray diffraction. [b] Defined as the angle between the planes described by atoms Zn(2), B(1), B(2) and B(1), B(2), B(3).

experimental values found for $[(MeZn)_2B_3H_7]_2$ are made in Tables 4.8 and 4.9. Fuller details of the *ab initio* calculations can be found in Appendix 5.

(a) $MeZnB_3H_8$. Several different starting geometries for $[MeZnB_3H_8]$ at both the HF/svp and the HF/tzp levels of theory were used. These included (i) a methylzinc unit bridging a B–B bond of the B_3H_8 unit (*via* two bridging hydrogen atoms), giving a species of overall C_s symmetry and incorporating a bidentate B_3H_8 ligand, and (ii) a methylzinc unit sitting above the B_3 ring with possible interaction to three terminal hydrogen atoms and thereby involving tridentate ligation of the B_3H_8 ligand (again C_s symmetry). Both of these starting geometries optimized to a structure with zinc coordinated to a single B–B bond *via* two bridging hydrogens such that the zinc atom lies in the H–B–B–H plane.

Comparison of the calculated bond lengths and angles with those found in $[(MeZn)_2B_3H_7]_2$ reveals close agreement in most cases. In particular, the similarity of the Zn(1)···B(2,3) distances lends considerable weight to the positioning of intervening hydrogen atoms. The observed and calculated distances from both Zn(1) and B(2,3) to the bridging hydrogen atoms are also pleasingly close. The geometry of the B_3 ring itself is reasonably reproduced by the calculations, with small differences reflecting the replacement of one bridging hydrogen atom by a methylzinc unit in $[(MeZn)_2B_3H_7]_2$.

The largest differences between the observed and calculated dimensions occur for the torsional angle and for the sum of the angles at Zn(1). In the latter case, the calculated angles imply trigonal coordination of Zn(1), the difference from the observed value (299.7°) merely reflecting the change in coordination geometry on dimerization {Zn(1) being coordinated to a methyl group and *four* bridging hydrogen atoms in $[(MeZn)_2B_3H_7]_2$}. The discrepancies for the torsional angle [*i.e.* the angle between the Zn(1)B(2)B(3) and B(1)B(2)B(3) planes] are also likely to reflect changes which occur on dimerization. Coordination of a second pair of bridging hydrogen atoms to Zn(1) would be expected to cause the methyl group to move out of the $Zn(\mu\text{-}H)_2B_2$ plane and come into closer contact with the B_3 unit. Opening out of the torsional angle to compensate for this is therefore to be expected.

(b) B_3H_7ZnMe ligand. The calculated bond lengths and angles for the B_3H_7ZnMe ligand (at the HF/tzp level of theory) are compared with the observed dimensions of $[(MeZn)_2B_3H_7]_2$ in Table 4.9 and again show a reasonable level of agreement. In particular, the much shorter Zn–B distances [Zn(2)–B(1,2)] observed for non hydrogen-bridged linkages are reproduced. Similarly, the tight B(1)–Zn(2)–B(2) angle [48.1(7)°] expected for a ZnB_2 three-centre, two-electron bond is also predicted by the *ab initio* calculations (46.38°). Furthermore, the variation in B–B bond lengths within the B_3 ligand [B(1)–B(2) and B(1)–B(3)] accompanying the replacement of a bridging hydrogen atom by a methylzinc unit is also reproduced by the calculations. The greatest discrepancy between the observed and calculated values occurs for bonds to the relatively poorly located H1, H2 and H13 atoms.

Interestingly, although the predicted torsional angle [reflecting the angular displacement of Zn(2) from the plane of the B_3 ring] is reasonably similar to that determined experimentally for $[(MeZn)_2B_3H_7]_2$, the observed deviation from trigonal coordination at the zinc atom is not reproduced.

4.8 Conclusions and Suggestions for Further Research

The reaction between $[B_4H_{10}]$ and a three-fold excess of $[Me_2Zn]$ in the gas phase at ambient temperatures affords not the expected product $[MeZnB_3H_8]$ but colourless acicular crystals of $[(MeZn)_2B_3H_7]_2$ in yields of *ca.* 10% based on reaction (9) and the amount of $[B_4H_{10}]$ taken. This compound is involatile, extremely air- and

$$3Me_2Zn + B_4H_{10} \longrightarrow [(MeZn)_2B_3H_7] + BMe_3 + MeH + ZnH_2 \qquad (9)$$

moisture-sensitive, and decomposes *in vacuo* over a period of *ca.* 48 h at room temperature. Heating to 150°C to ensure complete decomposition affords a solid residue containing only zinc and boron, together with hydrogen gas and a mixture of the methylboranes, $[BMe_3]$ and $[MeBH_2]_2$.

Single crystals were loaded into capillaries fused directly to the reaction vessel which were then sealed off *in vacuo* and held at 150 K for the collection of X-ray diffraction data. The crystal structure revealed that the product is in fact a dimer, $[(MeZn)_2B_3H_7]_2$, with an unprecedented structure featuring two distinct zinc environments; two B_3H_7ZnMe ligands, formally derived from B_3H_8 by replacement of a μ_2-H by a μ_2-ZnMe unit, each function in a *bis*(bidentate) manner linking together two other MeZn centres through pairs of Zn–H–B bridges. Further characterization of the compound was achieved by measurement of its infrared, Raman and NMR spectra, and by elemental analysis. Comparison with optimized structures calculated using *ab initio* methods for $[MeZnB_3H_8]$ and for the B_3H_7ZnMe ligand reveals pleasing agreement between observed and calculated dimensions, and provides persuasive support for the hydrogen atom positions.

The chemistry of $[(MeZn)_2B_3H_7]_2$ warrants further investigation. In particular, given the reaction between $[Me_2S]$ and $[MeZnBH_4]$ (which yields the molecular adduct $[MeZnBH_4{\cdot}SMe_2]$ in which the sulphur ligand is coordinated to the zinc atom), it would be interesting to see if a similar reaction involving $[(MeZn)_2B_3H_7]_2$ leads to the break-up of the dimeric structure with the formation of species of the type $[(MeZn)_2B_3H_7{\cdot}nSMe_2]$. In view of the unusual structure of $[(MeZn)_2B_3H_7]_2$, it would also be interesting to investigate the reaction of B_4H_{10} with a range of other methylmetal and metal hydride derivatives, such as $[Me_3Al]_2$, $[Me_3Ga]$, $[Me_3In]$,[40] $[Me_2Cd]$ and even $[Me_3N{\cdot}AlH_3]$. Whether any of these reactions represent viable routes to derivatives containing the B_3H_8 group remains to be seen.

In addition, the structure and properties of methylzinc derivatives of higher boranes, such as the compound $[MeZnB_6H_9]$ formed by the reaction between $[Me_2Zn]$ and $[B_6H_{10}]$,[3] would offer worthwhile comparisons with those of $[(MeZn)_2B_3H_7]_2$.

References for Chapter 4

1. G.D. Barbaras, C. Dillard, A.E. Finholt, T. Wartik, K.E. Wilzbach and H.I. Schlesinger, *J. Am. Chem. Soc.*, 1951, **73**, 4585.
2. H. Nöth, E. Wiberg and L.P. Winter, *Z. Anorg. Allg. Chem.*, 1971, **386**, 73.
3. D.L. Denton and S.G. Shore, Abstracts of 162nd meeting of A.C.S., Washington, D.C., 1961, INORG, 4.
4. N.N. Greenwood and N.F. Travers, *J. Chem. Soc., A*, 1968, 15.
5. N.N. Greenwood and N.F. Travers, *J. Chem. Soc., A*, 1971, 3257; N.N. Greenwood, J.A. McGinnety and J.D. Owen, *J. Chem. Soc., A*, 1971, 809.
6. Chapter 3, this thesis; S. Aldridge, A.J. Blake, A.J. Downs, S. Parsons and C.R. Pulham, *J. Chem. Soc., Dalton Trans.*, in press; J.W. Nibler and T.H. Cook, *J. Chem. Phys.*, 1973, **58**, 1596.
7. G.A. Koutsantonis, F.C. Iee and C.L. Raston, *J. Chem. Soc., Chem. Commun.*, 1994, 1975.
8. D.F. Gaines, J.L. Walsh, J.H. Morris and D.F. Hillenbrand, *Inorg. Chem.*, 1976, **17,** 1516.
9. C.R. Pulham and A.J. Downs, unpublished results.
10. D. Ridley, Ph.D. Thesis, University of Durham, 1965.
11. N.N. Greenwood and N.F. Travers, *J. Chem. Soc., A*, 1967, 880.
12. N.N. Greenwood, J.A. McGinnety and J.D. Owen, *J. Chem. Soc., Dalton Trans.*, 1972, 989.
13. F.M. Miller and D.M. Ritter, *Inorg. Chem.*, 1970, **9**, 1284.
14. J.J. Borlin and D.F. Gaines, *J. Am. Chem. Soc.*, 1972, **94**, 1367; C.J. Dain, A.J. Downs and D.W.H. Rankin, *J. Chem. Soc., Dalton Trans.*, 1981, 2467.
15. W.J. Lehmann, C.O. Wilson, Jr., and I. Shapiro, *J. Chem. Phys.*, 1958, **28**, 777.
16. K. Nakamoto, *Infrared and Raman Spectra of Inorganic and Coordination Compounds,* 4th edn., Wiley, 1986.

17. G.E. Ryschkewitsch and K.C. Nainan, *Inorg. Synth.*, 1974, **15**, 111.

18. R.W. Parry and S.G. Shore, *J. Am. Chem. Soc.*, 1958, **80**, 8.

19. R. Schaeffer, F. Tebbe and C. Phillips, *Inorg. Chem.*, 1964, **3**, 1475.

20. H.D. Johnson, II, and S.G. Shore, *J. Am. Chem. Soc.*, 1970, **92**, 7586.

21. W.J. Lehmann, C.O. Wilson, Jr., and I. Shapiro, *J. Chem. Phys.*, 1960, **33**, 590.

22. A.J. Downs and P.D.P. Thomas, *J. Chem. Soc., Dalton Trans.*, 1978, 809.

23. J. Cosier and A.M. Glazer, *J. Appl. Crystallogr.*, 1986, **19**, 105.

24. SIR92, A. Altomare, G. Cascarano, C. Giacovazzo and A. Guagliardi, *J. Appl. Crystallogr.*, 1993, **26**, 343.

25. SHELXL-93, G.M. Sheldrick, University of Göttingen, Germany, 1993.

26. M.W. Chen, D.F. Gaines and L.G. Hoard, *Inorg. Chem.*, 1980, **19**, 2989.

27. N.N. Greenwood and J.A. Howard, *J. Chem. Soc., Dalton Trans.*, 1976, 177.

28. J.E. Huheey, E.A. Keiter and R.L. Keiter, *Inorganic Chemistry: Principles of Structure and Reactivity*, 4th edn., Harper Collins, 1993.

29. See, for example, M. Bochmann, K.J. Webb, M.B. Hursthouse and M. Mazid, *J. Chem. Soc., Dalton Trans.*, 1991, 2317; B.L. Benac, A.H. Cowley, R.M. Jones, C.M. Nunn and T.C. Wright, *J. Am. Chem. Soc.*, 1989, **111**, 4986; M. Bochmann, G. Burembya, R. Grinter, J. Lu, K.J. Webb, D.J. Williamson, M.B. Hursthouse and M. Mazid, *Inorg. Chem.*, 1993, **32**, 532; S.S. Al-Juaid, N.H. Buttrus, C. Eaborn, P.B. Hitchcock, A.T.L. Roberts, J.D. Smith and A.C. Sullivan, *J. Chem. Soc., Chem. Commun.*, 1986, 908.

30. C.R. Peters and C.E. Nordman, *J. Am. Chem. Soc.*, 1960, **82**, 5758.

31. A.M. Coats, D.C. McKean, H.G.M. Edwards and V. Fawcett, *J. Mol. Struct.*, 1994, **320**, 159.

32. J. Tomkinson, C.J. Ludman and T.C. Waddington, *Spectrochim. Acta*, 1979, **35A**, 117.

33. D.F. Gaines and S.J. Hildebrandt, *Inorg. Chem.*, 1978, **17**, 794.

34. T.J. Marks and J.R. Kolb, *Chem. Rev.*, 1977, **77**, 263.

35. See, for example, *Gmelin Handbook of Inorganic Chemistry*, 8th edn., 'Boron Compounds', 2nd Supplement, Vol. 1, Springer-Verlag, 1983, p. 72.

36. See, for example, A.R. Siedle, *Annu. Rep. N.M.R. Spectrosc.*, 1982, **12**, 177.

37. F. Teixidor, C. Vinas and R.W. Rudolph, *Inorg. Chem.*, 1986, **25**, 3339.

38. N.P. Rath and T.P. Fehlner, *J. Am. Chem. Soc.*, 1988, **110**, 5345.

39. See, for example, C.E. Housecoft, *Boranes and Metallaboranes: Structure, Bonding and Reactivity*, 2nd edn., Ellis Horwood, 1994.

40. Chapter 6, this thesis.

Chapter Five
Studies of Some Aluminium Tetrahydroborate Derivatives

5.1 Introduction

5.1.1 Previous Work in this Area

In contrast to the corresponding derivatives of Group 12 elements, aluminium tetrahydroborates have attracted numerous structural investigations.[1] Since an initial report by Schlesinger *et al.* of its synthesis *via* the reaction of trimethylaluminium with diborane [reaction (1)][2] and its subsequent synthesis from aluminium trichloride and lithium tetra-

$$Al_2Me_6 + 4B_2H_6 \longrightarrow 2Al(BH_4)_3 + 2BMe_3 \qquad (1)$$

hydroborate [reaction (2)],[3] aluminium *tris(*tetrahydroborate) has been the subject of

$$AlCl_3 + 3LiBH_4 \longrightarrow Al(BH_4)_3 + 3LiCl \qquad (2)$$

several structural studies.[1] Analysis of the electron-diffraction pattern of the gaseous molecule by Haaland *et al.*[4] confirmed the bidentate ligation of the BH_4 groups implied by infrared measurements,[5] but failed to differentiate between a trigonal prismatic (D_{3h}) structure and one conforming to D_3 symmetry in which the plane of the $Al(\mu\text{-}H)_2B$ unit is no longer perpendicular to the AlB_3 plane.

X-ray diffraction has yielded the structures of the crystalline adducts $[Al(BH_4)_3{\cdot}NMe_3]$[6] and $[Ph_3MeP]^+[Al(BH_4)_4]^-$,[7] the aluminium centres displaying pentagonal bipyramidal and distorted dodecahedral coordination, respectively. In each case, the bonding of all BH_4 ligands to the aluminium centre occurs *via* two bridging hydrogens. Indeed, recent *ab initio* calculations have shown that the $Al(\eta^2\text{-}BH_4)_3$

structure lies 9.1 kJ mol^{-1} below $Al(\eta^3\text{-}BH_4)(\eta^2\text{-}BH_4)_2$ and 58.4 kJ mol^{-1} below $Al(\eta^1\text{-}BH_4)(\eta^2\text{-}BH_4)_2$, these species incorporating a single BH_4 group bonded to the aluminium in a tridentate and monodentate fashion, respectively.[8]

Alkylaluminium tetrahydroborates have been prepared by exchange between aluminium *tris*(tetrahydroborate) and the appropriate trialkylaluminium species, according to reactions (3) and (4).[9,10] In the cases of $[Me_2AlBH_4]$[11] and $[MeAl(BH_4)_2]$,[12]

$$Al(BH_4)_3 + Al_2R_6 \longrightarrow 3R_2AlBH_4 \qquad (3)$$

$$4Al(BH_4)_3 + Al_2R'_6 \longrightarrow 6R'Al(BH_4)_2 \qquad (4)$$

[where R = Me or Et and R' = Me, Et, ^{n}Pr or ^{i}Bu]

structures have been determined for the gaseous molecules by electron diffraction. Hence the BH_4 groups are found to exhibit bidentate ligation, the coordination numbers of the aluminium centre being four and five, respectively. Examination of the infrared and Raman spectra of $[Me_2AlBH_4]$ in both the solid and vapour phases by Thomas led him to conclude that there are significant structural differences between the two phases.[13] In particular, the pattern of bands associated with B–H stretching vibrations was found to be very similar to that observed for solid beryllium *bis*(tetrahydroborate)[14] and methylzinc tetrahydroborate.[15] On this basis, a "semi-ionic" $[Me_2Al]^+[BH_4]^-$ or polymeric structure was proposed for solid $[Me_2AlBH_4]$.

The vibrational spectra of $[MeAl(BH_4)_2]$ also show a number of changes when the compound passes from the vapour to the solid phase;[13] most striking of these is the appearance of a strong band at 2235 cm^{-1}. The changes were tentatively ascribed to a switch in the mode of ligation from bidentate to tridentate of one of the BH_4 groups.[13]

Hydridoaluminium tetrahydroborates of the types $H_nAl(BH_4)_{3-n}$ and $H_nAl(BH_4)_{3-n}\cdot NMe_3$ (where n = 1 or 2) have also been synthesized,[16,17] although no definitive structural data for any of these compounds has been forthcoming.

5.1.2 Aims of the Present Research

In view of the unusual structure of solid methylzinc tetrahydroborate and the interesting structural changes accompanying condensation implied by the vibrational spectra of $[Me_2AlBH_4]$ and $[MeAl(BH_4)_2]$,[13] it was decided to investigate further the structures of these two compounds in the solid phase. This was to be accomplished by X-ray diffraction of suitable crystals grown from the liquid at low temperature.

In addition, the structure of solid $[Al(BH_4)_3]$ was to be investigated using similar techniques in order (i) to enable comparisons to be made with the molecular structure deduced by electron diffraction of the vapour,[4] and (ii) to establish trends in structure and bonding for the series $Me_nAl(BH_4)_{3-n}$ (where $n = 0,1$ or 2).

5.2 Synthesis of Aluminium Tetrahydroborates

Aluminium *tris*(tetrahydroborate) was prepared from $[AlCl_3]$ and $[LiBH_4]$ by the method of Schlesinger *et al.*[3] The exact experimental details are set out in Table 2.4. The purity of samples was established by comparison of the infrared spectrum of the vapour with that of an authentic sample.[5]

Dimethylaluminium tetrahydroborate and methylaluminium *bis*(tetrahydroborate) were prepared *via* reactions (3) and (4), respectively.[9,10]

(a) Dimethylaluminium tetrahydroborate. In a typical reaction $[Me_6Al_2]$ (250 mg, 1.73 mmol) and $[Al(BH_4)_3]$ (124 mg, 1.73 mmol) were co-condensed in a Pyrex glass ampoule equipped with a constriction and a breakseal, as illustrated in Figure 2.2. After sealing the constriction, the ampoule was maintained at room temperature for *ca.* 4 h. The reaction being assumed to be complete, the ampoule was attached to the vacuum line *via* a train of all-glass traps cooled successively to -31, -45 and -196°C. $[Me_2AlBH_4]$ collected as a white crystalline solid in the trap held at -45°C; it is a colourless liquid at room temperature, freezing in the range 10-13°C, and forming long acicular crystals upon controlled cooling. The purity of samples was assessed by comparison of the infrared

spectra of both solid films at low temperature and the vapour with those of authentic samples.[9,13]

(b) Methylaluminium bis(tetrahydroborate). [$MeAl(BH_4)_2$] was prepared using apparatus and procedures similar to those outlined above, although 163 mg (1.13 mmol) of [Me_6Al_2] and 320 mg (4.5 mmol) of [$Al(BH_4)_3$] were used in a typical experiment. Fractionation *in vacuo* through a trap held at -63°C left [$MeAl(BH_4)_2$] as a glassy solid involatile at -126°C. The purity of samples was assessed by measurement of the infrared spectra of a solid film and of the vapour and by reference to the ^{11}B and ^{1}H NMR spectra of solutions in [$^2H_8$]toluene.[9,13]

Samples of all three compounds were loaded into Pyrex capillaries each of *ca.* 0.5 mm internal diameter for the purpose of attempted crystal growth. Invariably, the first step involved rigorous pre-conditioning of the capillary by exposure to the sample vapour for 1-2 h prior to re-evacuation, this serving to scavenge any residual moisture adsorbed on the glass surfaces. A small quantity (*ca.* 0.01 cm^3) of the compound was then transferred from the storage ampoule and condensed in the neck of the vessel; with careful warming the material was caused to melt and run down to the bottom of the capillary. Typically a depth of 1.5-2 cm of liquid compound was required. Once this was achieved, the sample was cooled to -196°C, and the capillary sealed such that its total length did not exceed 3 cm.

5.3 Growth of Crystals for X-ray Diffraction

Crystals were grown from the liquid using the method illustrated in Figure 2.5 and outlined in Section 2.3.7.1.

(a) Dimethylaluminium tetrahydroborate. A single crystal of [Me_2AlBH_4] was grown from the solid/liquid phase boundary by slow cooling of the liquid (at 5 K h^{-1}) from 287 K.

(b) Methylaluminium bis(tetrahydroborate). It proved impossible to obtain single crystals of [$MeAl(BH_4)_2$] using either the slow cooling or the zone-refining techniques.

Solid [$MeAl(BH_4)_2$] appears to be an amorphous glass and it proved difficult even to detect a well defined melting point.

(c) Aluminium tris(tetrahydroborate). Initially, a single crystal of [$Al(BH_4)_3$] was grown from the solid/liquid phase boundary by slow cooling of the liquid (at 5 K h^{-1}) from 210 K. The sample was then cooled to 180 K and an oscillation photograph taken in order to establish the quality of the crystal. A random peak search then yielded sufficient strong reflections to obtain a provisional unit cell and to begin data collection. However, over a period of 30-45 min the intensities of the standard reflections declined steadily. Investigation by oscillation photography of further crystals grown in this manner confirmed that these, too, lost crystallinity over a period of 1 h at 180 K. Cooling the crystal to 110 rather than 180 K resulted in much more rapid loss of crystallinity. These findings suggest that a phase change may have been taking place in the temperature range 180-210 K, with the β-phase formed by cooling the liquid changing slowly to the low-temperature α-form. In order to investigate this possibility further, crystals were subsequently cooled only to 195 K, conditions which would allow the collection of a data set for the β-phase if the transition temperature lies in the range 195-180 K. In the event, this proved to be the case.

A crystal of the low temperature phase was grown using the zone-refining technique (Section 2.3.7.1) at 150 K. The quality of the crystal, as determined by oscillation photography, was found to be markedly inferior to those of the β-phase grown by the slow cooling technique.

5.4 The Crystal Structure of Dimethylaluminium Tetrahydroborate at 150 K

5.4.1 Crystal Data

$C_2H_{10}AlB$, M = 143.78, orthorhombic, *Pbca*, a = 10.029(6), b = 12.401(4), c = 17.947(9) Å, U = 2232(2) $Å^3$, λ = 0.71073 Å, Z = 8, D_c = 0.856 g cm^{-3}, $F(000)$ =

640, T = 150 K; colourless crystal, 0.80 x 0.40 x 0.40 mm.

5.4.2 Data Collection

Data were collected on a Stoë Stadi-4 four circle diffractometer with graphite-monochromated Mo-Kα radiation; ω-2θ mode, ω half width $(1.32 + 0.35\tan\theta)^{o}$. Of the 1746 reflections measured ($\theta_{max} = 24.97^{o}$; $0 \leq h \leq 10$, $0 \leq k \leq 14$, $0 \leq l \leq 21$), 1699 were unique.

5.4.3 Structure Solution and Refinement

The crystal structure of dimethylaluminium tetrahydroborate was solved by Dr. S. Parsons using direct methods (SIR92) and refined by full-matrix least-squares methods with anisotropic displacement parameters for all non-hydrogen atoms (SHELXTL). Methyl hydrogens were located in a difference synthesis performed about the loci of possible hydrogen atom positions; in subsequent cycles of least-squares refinement the methyl groups were treated as rigid rotating groups [r(C–H) = 0.96 Å]. All hydrogen atoms attached to boron were located in difference syntheses and allowed to refine freely. Other structure solution and refinement details are listed in Appendix 6.

5.4.4 Discussion of Results

The structure of $[Me_2AlBH_4]$ at 150 K is illustrated in Figure 5.1 and a packing diagram shown in Figure 5.2. Bond distances and angles are listed in Table 5.1; fractional atomic coordinates (including those for the hydrogen atoms) and anisotropic displacement parameters are listed in Appendix 6.

The structural results show that solid dimethylaluminium tetrahydroborate consists of helical polymers in which dimethylaluminium units are linked by BH_4 groups exhibiting bidentate ligation with respect to each of the adjacent metal atoms. In this respect, the

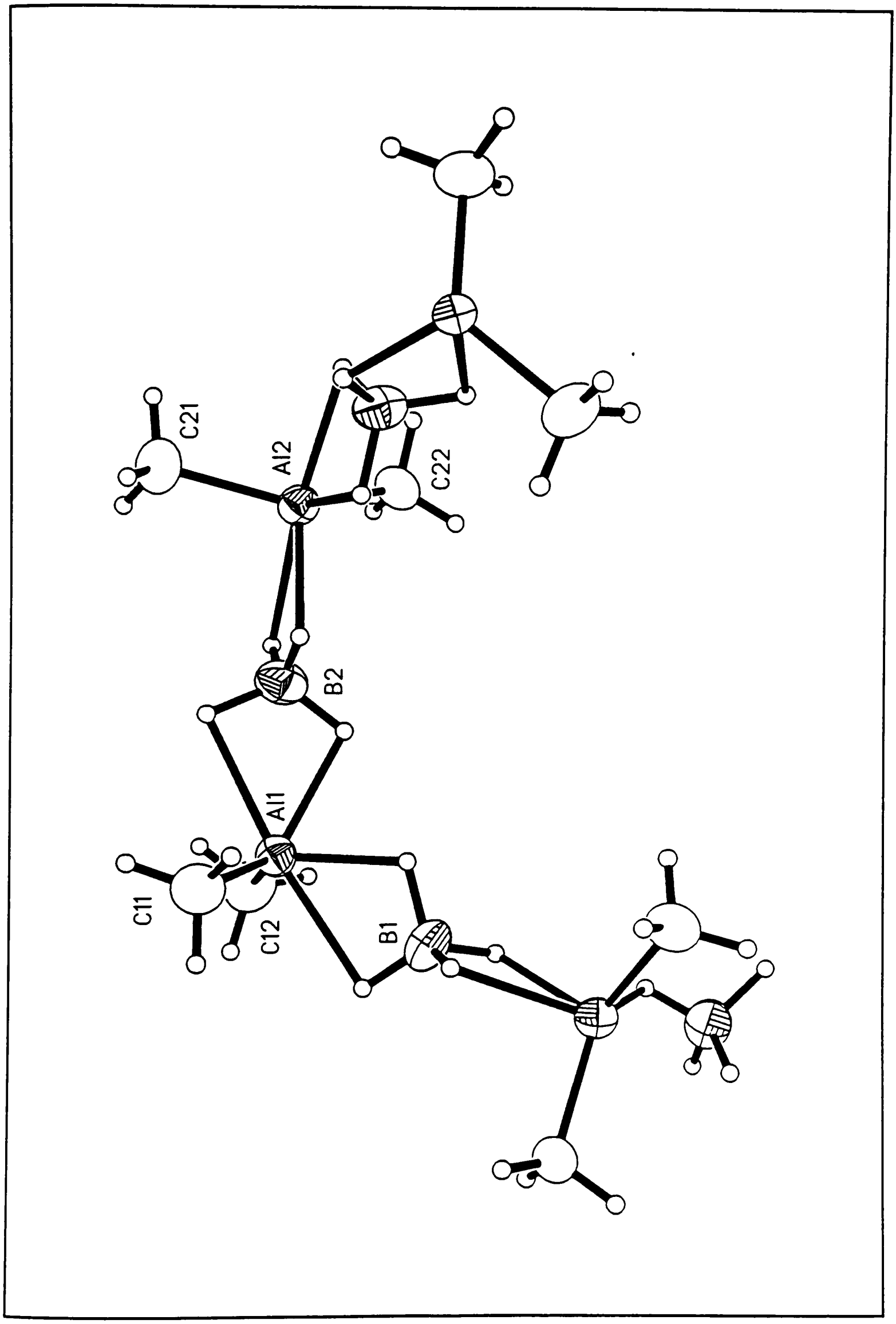

Figure 5.1 The crystal structure of $[Me_2AlBH_4]$ at 150 K.

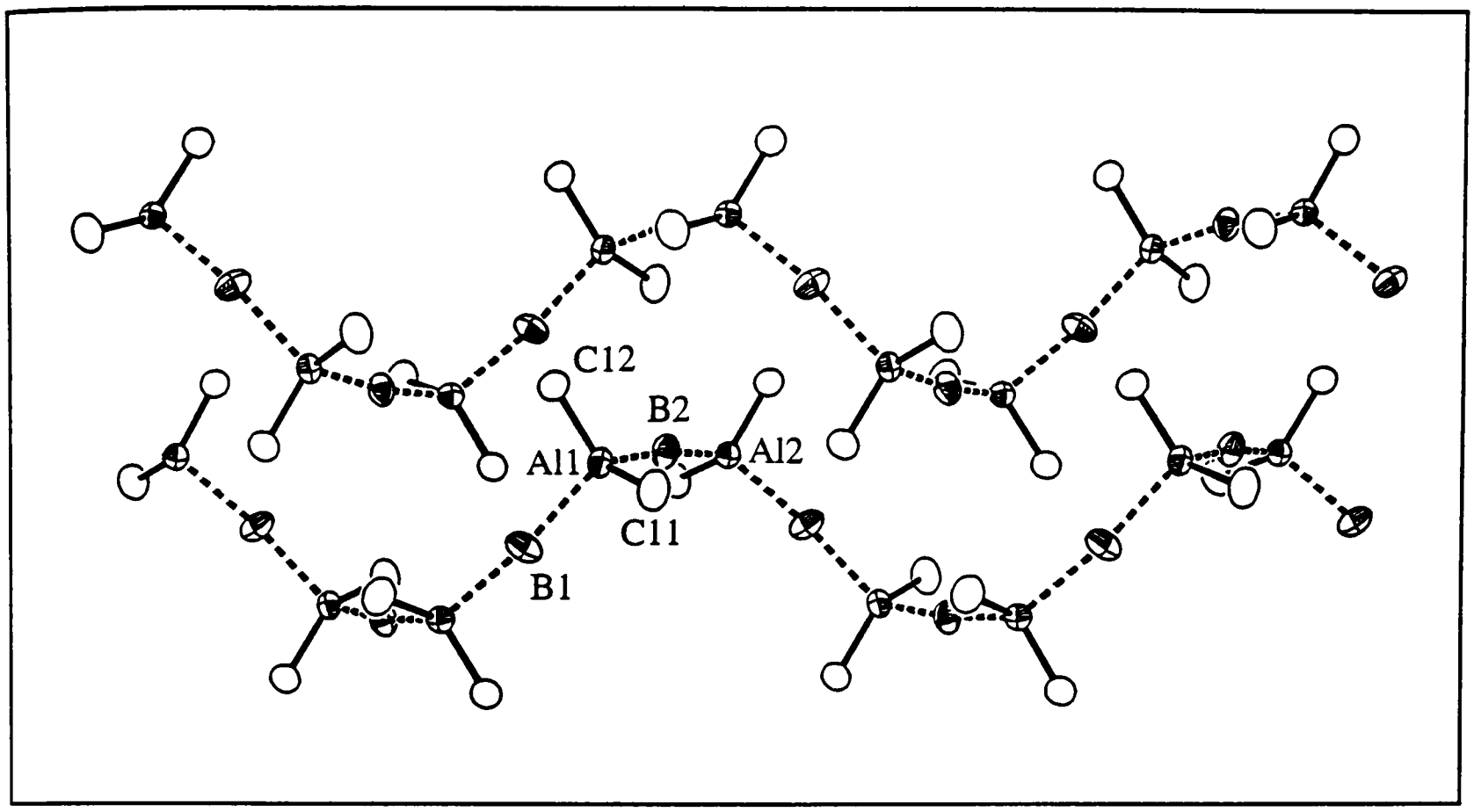

Figure 5.2 Packing of the polymeric chains in crystalline $[Me_2AlBH_4]$ at 150 K.

Table 5.1 Bond distances (Å) and angles (°) for crystalline [Me_2AlBH_4] at 150 K.[a]

Al(1)–C(12)	1.912(5)	Al(1)–H(21)	1.97(5)
Al(1)–C(11)	1.926(5)	B(1)–H(11)	1.12(5)
Al(1)–B(1)	2.419(6)	B(1)–H(12)	1.17(4)
Al(1)–B(2)	2.392(6)	B(1)–H(13)	1.16(5)
Al(2')–B(1)	2.423(6)	B(1)–H(14)	1.07(5)
Al(1)–H(12)	1.82(4)	C(11)–H(11A)	0.98
C(12)–Al(1)–C(11)	130.5(2)	Al(1)–B(1)–H(12)	46(2)
C(12)–Al(1)–B(2)	99.3(2)	Al(2')–B(1)–H(12)	127(2)
C(11)–Al(1)–B(2)	106.9(2)	Al(1)–B(1)–H(13)	127(2)
C(12)–Al(1)–B(1)	105.7(2)	Al(2')–B(1)–H(13)	47(2)
C(11)–Al(1)–B(1)	96.5(2)	Al(1)–B(1)–H(14)	122(2)
C(11)–Al(1)–H(12)	102.7(14)	Al(2')–B(1)–H(14)	63(2)
C(11)–Al(1)–H(21)	123.7(14)	H(11)–B(1)–H(12)	109(3)
B(1)–Al(1)–H(21)	95.1(14)	H(11)–B(1)–H(13)	111(3)
B(2)–Al(1)–H(12)	93(2)	H(11)–B(1)–H(14)	113(4)
H(12)–Al(1)–H(21)	69(2)	H(12)–B(1)–H(13)	108(3)
B(1)–Al(1)–B(2)	119.9(2)	H(12)–B(1)–H(14)	108(3)
Al(1)–B(1)–Al(2')	171.8(3)	H(13)–B(1)–H(14)	109(3)
Al(1)–B(1)–H(11)	63(2)	Al(1)–C(11)–H(11A)	109.5(2)
Al(2')–B(1)–H(11)	123(2)	H(11A)–C(11)–H(11B)	109.5

[a] Symmetry operations: single prime: $-x, y - 1/2, -z + 1/2$.

structure resembles closely those of beryllium *bis*(tetrahydroborate)[18] and methylzinc tetrahydroborate.[15] Comparative parameters for these three compounds are set out in Table 5.2. The beryllium atom in $[Be(BH_4)_2]$ is bonded to six bridging hydrogen atoms, these being arranged such that the coordination of the central metal atom is trigonal prismatic.[18] The aluminium centre in $[Me_2AlBH_4]$ is also *hexa*-coordinated being bonded to four bridging hydrogen atoms and two methyl groups. In this case, however, the arrangement of the ligands is best described in terms of a distorted octahedral geometry, the planes of the bridging $Al(\mu\text{-}H)_2B$ groups being virtually at 90° to that of the AlC_2

Table 5.2 Comparison of selected bond lengths (Å) and angles (°) for $[Me_2AlBH_4]$, $[Be(BH_4)_2]$ and $[MeZnBH_4]$.

Parameter	$[Me_2AlBH_4]$		$[Be(BH_4)_2]^a$	$[MeZnBH_4]$
	solid	vapour	solid	solid
B–H	1.07(5)-1.17(4)	1.207(17)-1.230(17)	1.08(2)-1.17(3)	1.32(4)-1.36(5)
M···B	2.419(6), 2.392(6)	2.128(8)	2.001(4), 1.999(5)	2.30(2)-2.32(2)
M–H	1.82(4), 1.97(5)	1.770(32)	1.59(2)-1.65(2)	1.81(5), 1.82(5)
Covalent radius of metal atom[b]	1.26	1.26	1.06	1.31
H–B–H	108(3)-113(4)	112.5(3.7) 116.2[c]	109(2)-112(2)	103(3)-115(4)
M–B–M	171.8(3)	*d*	175.4(7)	171.9(3)
B–M–B	119.9(2)	*d*	111.7	98.6(7)
Reference	This work	11	18	15

[a] Parameters relate to the BH_4 units within the helical chain. [b] See reference 19. [c] Fixed. [d] Not applicable.

unit. Distortion from idealized octahedral geometry occurs by closing up the AlC_2 angle [from 180 to 130.5(2)°] and consequent bending of the $Al(\mu\text{-}H)_2B$ units away from the AlC_2 plane, as shown in Figure 5.3. Distortion of the $Al(H_b)_4$ unit from the planar geometry implicit in octahedral coordination is small. Hence the coordination geometry of the aluminium centre contrasts with that found in $[Al(BH_4)_3]$, which shows a trigonal prismatic arrangement of ligands in both the vapour [4] and solid phases (*vide infra*).

It is noteworthy that, whereas the helical polymeric skeletons of solid $[Be(BH_4)_2]$ and $[MeZnBH_4]$ spiral around 4_1 and 3_1 axes, respectively, the analogous unit in $[Me_2AlBH_4]$ is disposed around a 2_1 crystallographic screw axis. In all three compounds

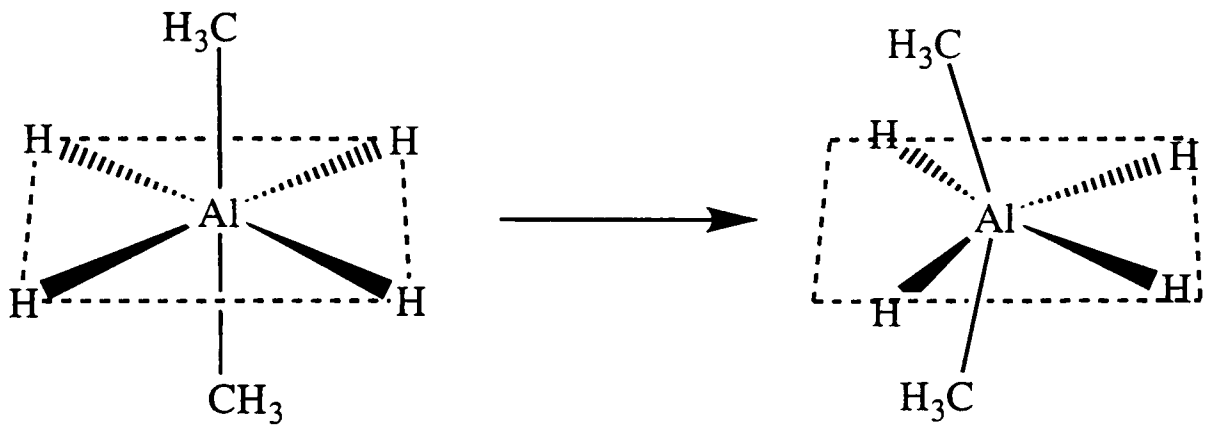

Figure 5.3 Distortion from octahedral geometry of the aluminium centre in $[Me_2AlBH_4]$.

the M–B–M angle is close to 180° and the departure from linearity probably reflects contrasting coordination geometries at the metal atom. The B–M–B angles are 119.9(2), 111.7 and 98.6(7)° for $[Me_2AlBH_4]$, $[Be(BH_4)_2]$ and $[MeZnBH_4]$, respectively.

Further examination of the crystal structure of $[Me_2AlBH_4]$ reveals that the degree of interaction between the metal centre and the BH_4 ligand is considerably less than in $[MeZnBH_4]$[15] but similar to that associated with the more ionic formulation prevailing in $[Be(BH_4)_2]$.[18] Thus, the B–H distances in $[Me_2AlBH_4]$ and $[Be(BH_4)_2]$ are 1.07(5)-1.17(4) and 1.08(2)-1.17(3) Å, respectively, whereas those in $[MeZnBH_4]$ are found to be 1.32(4) and 1.36(5) Å.[15,18] Furthermore, the H–B–H angles show smaller distortions from the idealized tetrahedral values than do those in $[MeZnBH_4]$,[15] although the experimental errors in each case are in the order of 3°. In addition, the Al–H and

Al···B distances [1.82(4), 1.97(5) and 2.392(6), 2.419(6) Å] are also indicative of weaker M···BH_4 interactions. The corresponding values for [$MeZnBH_4$] are 1.81(5) and 2.30(2) Å, respectively, despite the fact that the covalent radius of zinc (1.31 Å) is slightly larger than the covalent radius of aluminium (1.26 Å).[19]

Comparison of the structure of the gaseous molecule[11] with that of solid [Me_2AlBH_4] reveals several differences consistent with the change from a discrete molecular structure to a polymer incorporating alternate $[Me_2Al]^+$ and $[BH_4]^-$ ions. Thus, the Al···B and Al–H distances are appreciably longer in the solid phase [2.392(6), 2.419(6) and 1.82(4), 1.97(5) Å] than in the vapour [2.128(8) and 1.77(3) Å] and the C–Al–C angle opens up from 118.4(7)° (for the vapour) to 130.5(2)° (for the solid). The increase in the M···B distance on condensation is 0.16 Å for [$MeZnBH_4$] (Zn···B distance for the monomer calculated using DFT),[15] 0.211 Å for $[Be(BH_4)_2]$[18] and 0.264 Å for [Me_2AlBH_4]. This implies that the structural differences between the solid and vapour phases are greatest for [Me_2AlBH_4], *i.e.* that the degree of charge separation, $R_nM^+ BH_4^-$ is greatest for solid [Me_2AlBH_4]. Such a situation may reflect greater inductive stabilization of the "isolated" Me_2Al^+ cation (as compared with $MeZn^+$, for example) made possible by the presence of *two* methyl groups.

The crystal structure of solid [Me_2AlBH_4] shows some of the features predicted by Thomas on the basis of his infrared and Raman measurements.[13] For example, the opening out of the C–Al–C angle with the switch from the vapour to the solid, predicted on the basis of the relative intensities in infrared absorption of the symmetric and antisymmetric Al–C stretching vibrations, is observed to be the case. Furthermore, a strong band at 2194 cm^{-1} in the infrared spectrum of solid [Me_2AlBH_4] can be attributed to the stretching of B–H bonds within the semi-ionic polymer backbone. The position of such a band could be explained either in terms of the antisymmetric B–H stretching vibration of a slightly distorted BH_4^- ion or in terms of an antisymmetric B–H_b stretching vibration of an Al(μ-H)$_2$B(μ-H)$_2$Al unit. The extent of interaction between the metal centre and BH_4 group can be elucidated only by examination of the bond lengths and angles deduced from the crystal structure.

Given that structures in which the metal centre is *hexa*-coordinated are common in aluminium chemistry,[20] it is of little surprise that $[Me_2AlBH_4]$ adopts a polymeric structure in the solid phase. This makes possible an increase in the coordination number of the aluminium centre from four (for the monomer present in the vapour) to six. However, the structure of the solid is highly unusual in featuring a BH_4 group bridging two Group 13 metal centres. The only other compound exhibiting a similar structural unit is solid $[H_2GaBH_4]$, although the GaH_2 units here are bridged by *bis*(monodentate) $(\mu\text{-H})B(H)_2(\mu\text{-H})$ units.[21] Bridging between gallium and boron atoms *via* a single hydrogen atom gives rise to a somewhat longer M···B distance (2.46-2.49 Å[21]) than is found in $[Me_2AlBH_4]$ [2.419(6), 2.392(6) Å], despite the extremely similar covalent radii of aluminium and gallium.[19] It is interesting to note that, whereas the aluminium centre in solid $[Me_2AlBH_4]$ exploits all four hydrogens of the BH_4 ligand in order to increase its coordination number to six, the gallium centre in solid $[H_2GaBH_4]$ retains the approximately tetrahedral, four-coordinate geometry seen in the vapour phase, with the consequence that each BH_4 ligand bears two terminal hydrogen atoms.[21] This difference in coordination geometries is consistent with the structural properties of many other aluminium and gallium compounds, for example solid $[AlCl_3]$ and $[GaCl_3]$.[20]

5.5 The Crystal Structures of Aluminium *Tris*(tetrahydroborate) at 195 and 150 K

5.5.1 Crystal Data

(a) α form. AlB_3H_{12}, M = 71.51, monoclinic, $C2/c$, a = 21.917(4), b = 5.986(1), c = 21.787(4) Å, β = 111.90(3)°, U = 2652.1(9) Å^3, λ = 0.71073 Å, Z = 16, D_c = 0.716 g cm^{-3}, T = 150 K, colourless crystal.

(b) β form. AlB_3H_{12}, M = 71.51, orthorhombic, ~~$Pna2(1)$~~ $Pna2_1$, a = 18.021(3), b = 6.138(2), c = 6.199(1) Å, U = 685.7(3) Å^3, λ = 0.71073 Å, Z = 4, D_c = 0.693 g cm^{-3},

T = 195 K, colourless crystal.

5.5.2 Data Collection

Data for both phases were collected on a Stoë Stadi-4 four circle diffractometer with graphite-monochromated Mo-Kα radiation; ω-2θ mode, ω half width (1.32 + 0.35tanθ)°.

(a) α form. Of the 1477 reflections measured (θ_{max} = 20.00°; -17 ≤ h ≤ 26, -6 ≤ k ≤ 0, -19 ≤ l ≤ 23), 1233 were unique.

(a) β form. Of the 767 reflections measured (θ_{max} = 22.47°; -1 ≤ h ≤ 19, -1 ≤ k ≤ 6, -1 ≤ l ≤ 6), 598 were unique.

5.5.3 Structure Solution and Refinement

The crystal structure of the high temperature (β) phase was solved by Dr. S. Parsons using direct methods (SIR92), while that of the low temperature (α) phase was solved for the aluminium atom using Patterson methods (SHELXTL). Both structures were refined by full-matrix least-squares methods with anisotropic displacement parameters for all non-hydrogen atoms (SHELXTL). Methyl hydrogens were located in a difference synthesis performed about the loci of possible hydrogen atom positions; in subsequent cycles of least-squares refinement the methyl groups were treated as rigid rotating groups [r(C–H) = 0.96 Å]. All hydrogen atoms attached to boron were located in difference syntheses; in the β phase the positional parameters were refined freely and common isotropic thermal parameters refined for chemically similar atoms whereas in the α phase similarity restraints were applied to chemically equivalent bonds. Other structure solution and refinement details are listed in Appendices 7 and 8.

5.5.4 Discussion of Results

The molecular structure of $[Al(BH_4)_3]$ at 195 K (that is, for the β phase) is illustrated in Figure 5.4 and a packing diagram shown in Figure 5.5. The arrangement of the molecular units in the more dense α phase at 150 K is illustrated in Figure 5.6 and the view along the *b*-axis for this form shown in Figure 5.7. Bond distances and angles for both phases are listed in Tables 5.3 and 5.4; fractional atomic coordinates and anisotropic displacement parameters are listed in Appendices 7 and 8 (for the α and β phases, respectively).

The crystal structures of both phases of aluminium tetrahydroborate are made up of discrete molecular $Al(BH_4)_3$ units. The geometry of the $Al(BH_4)_3$ molecule itself varies little between the two phases, the most significant differences affecting (i) the angle between the Al B(1) B(2) and Al H(1A) B(1) planes (which is 89.1° for the β phase and 78.2° for the α phase), and (ii) the $B(H_t)_2$ angles, which appear to be less uniform in the more densely packed α phase. The poorer quality of the results obtained for this phase is reflected in the larger standard deviations quoted, particularly for parameters involving bonds to hydrogen atoms.

The principal difference between the α and β phases relates to the *packing* of the molecular units. In the β phase the closest intermolecular Al···H distances are 3.6 Å. These distances are too long to permit any secondary interaction between $Al(BH_4)_3$ molecules, rather they characterize the packing of molecular units. In the β phase there are two 'nearest neighbour' molecules positioned above and below the triangular faces of the trigonal prismatic $Al(\mu\text{-}H)_6$ unit. In the denser α phase the shortest Al···H distance is 3.25 Å and again this rules out any significant secondary interaction between $Al(BH_4)_3$ molecules. The closest approach of a terminal hydrogen to a second molecular unit occurs for the $Al(BH_4)_3$ located below the triangular face of the trigonal prismatic $Al(\mu\text{-}H)_6$ unit. In contrast to the β phase there is only one such 'nearest neighbour', with the molecular units spiralling around a 2_1 axis as shown in Figure 5.7. Interestingly, although the existence of any secondary interaction can be ruled out, the spiralling of $Al(BH_4)_3$ units

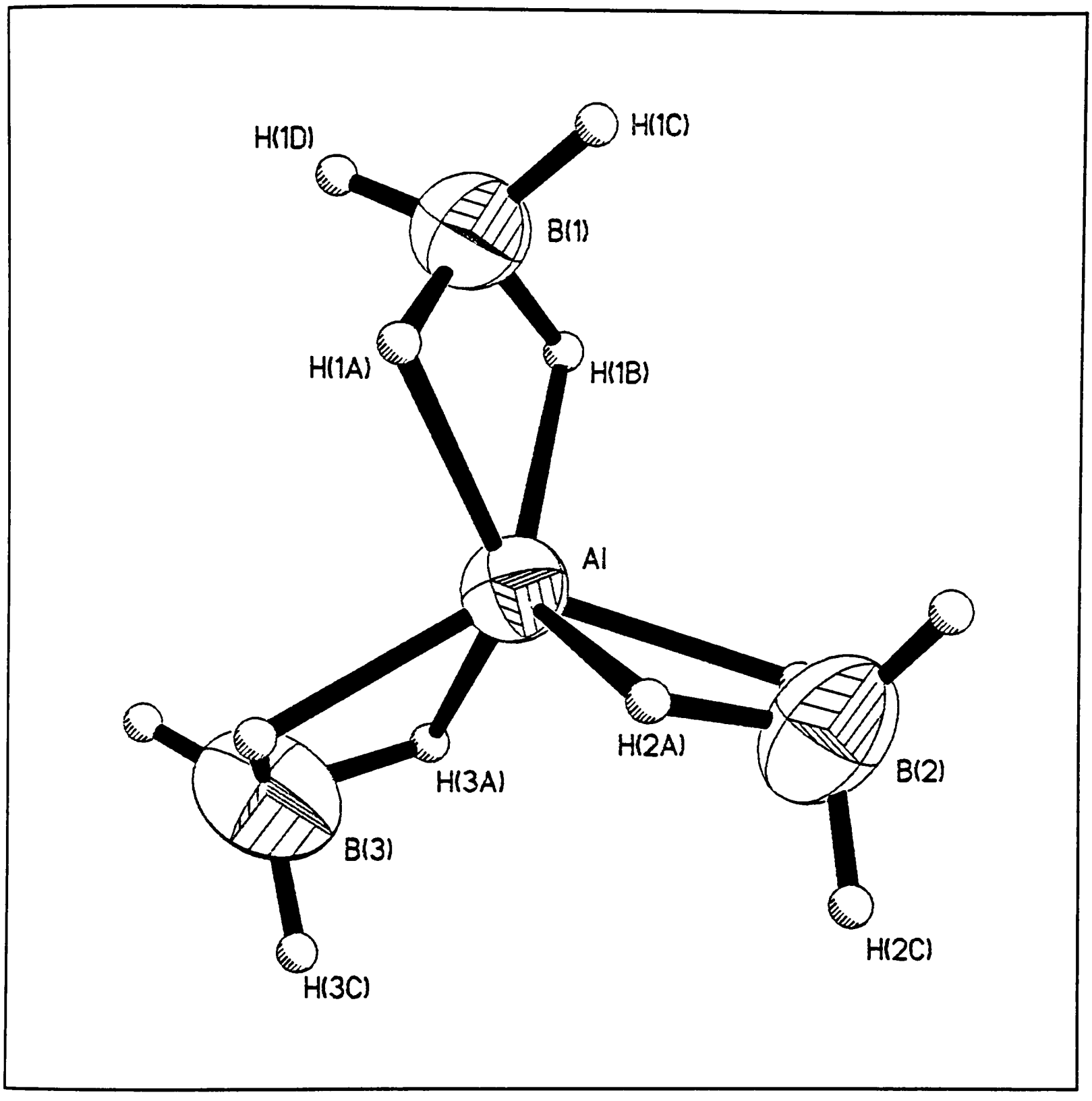

Figure 5.4 The molecular structure of $[Al(BH_4)_3]$, as determined by X-ray diffraction of a crystalline sample of the β phase at 195 K.

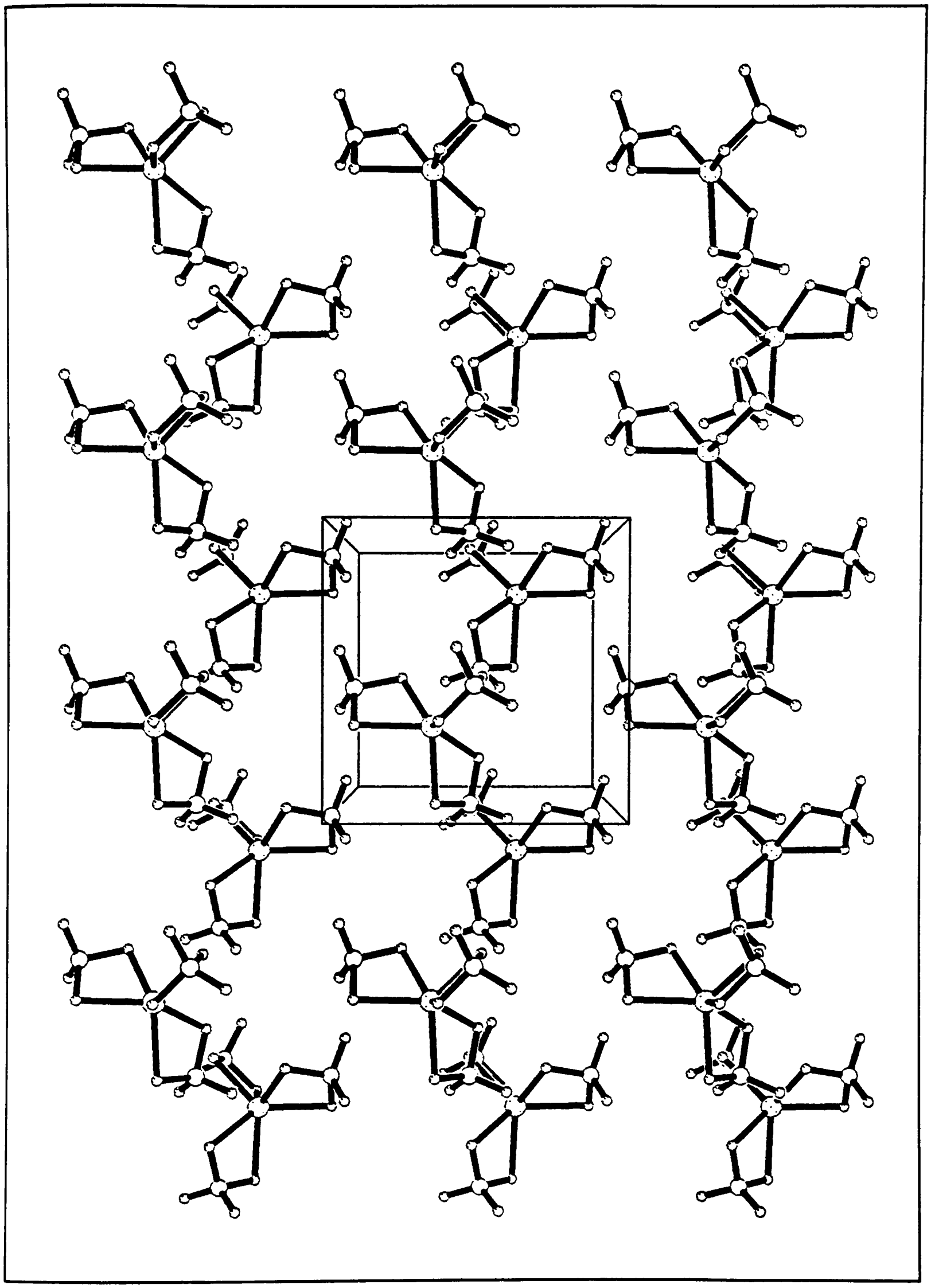

Figure 5.5 Packing of the $Al(BH_4)_3$ units in the β phase of solid aluminium *tris*(tetrahydroborate) at 195 K.

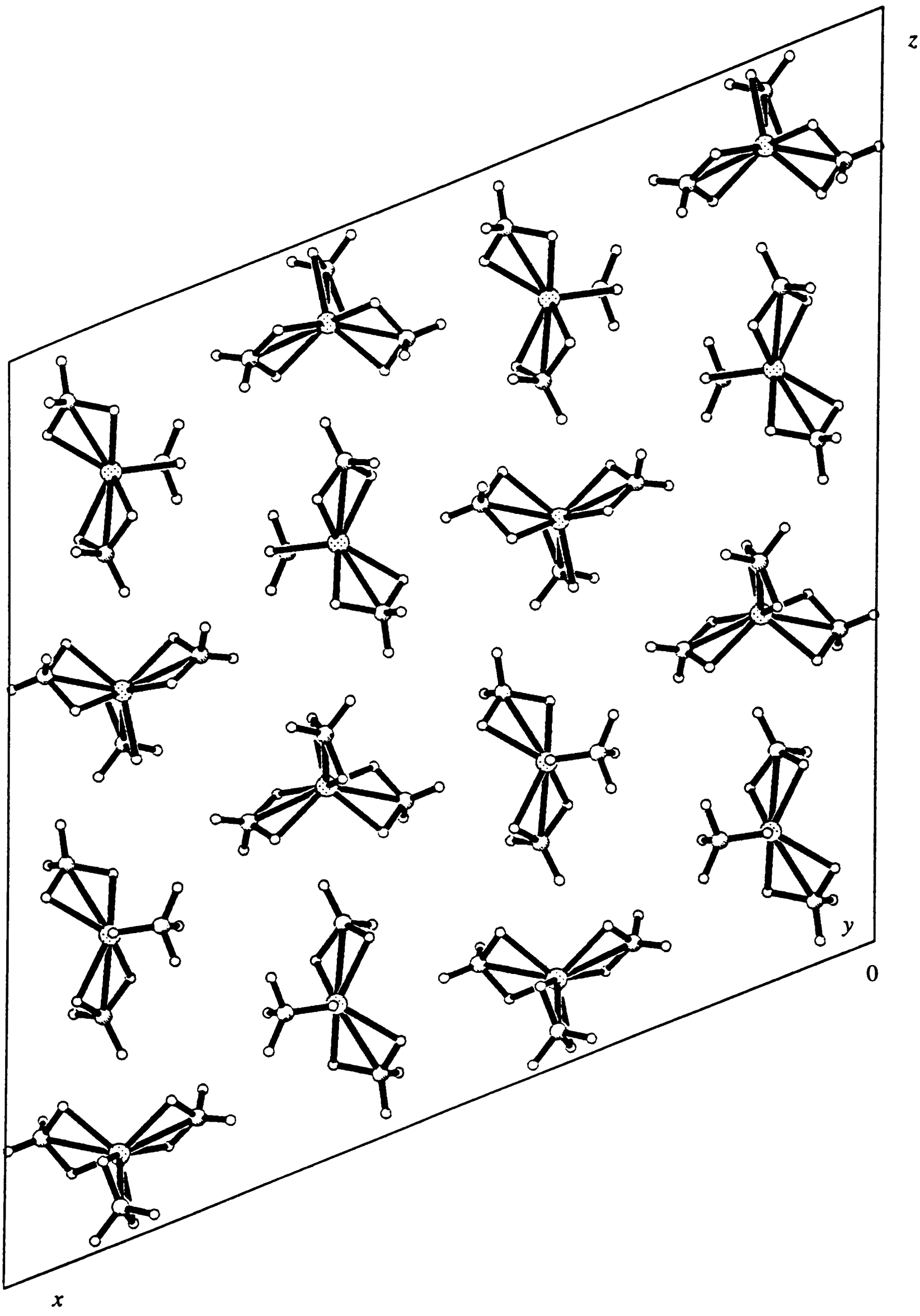

Figure 5.6 Packing of the $Al(BH_4)_3$ units in the α phase of solid aluminium *tris*(tetrahydroborate) at 150 K.

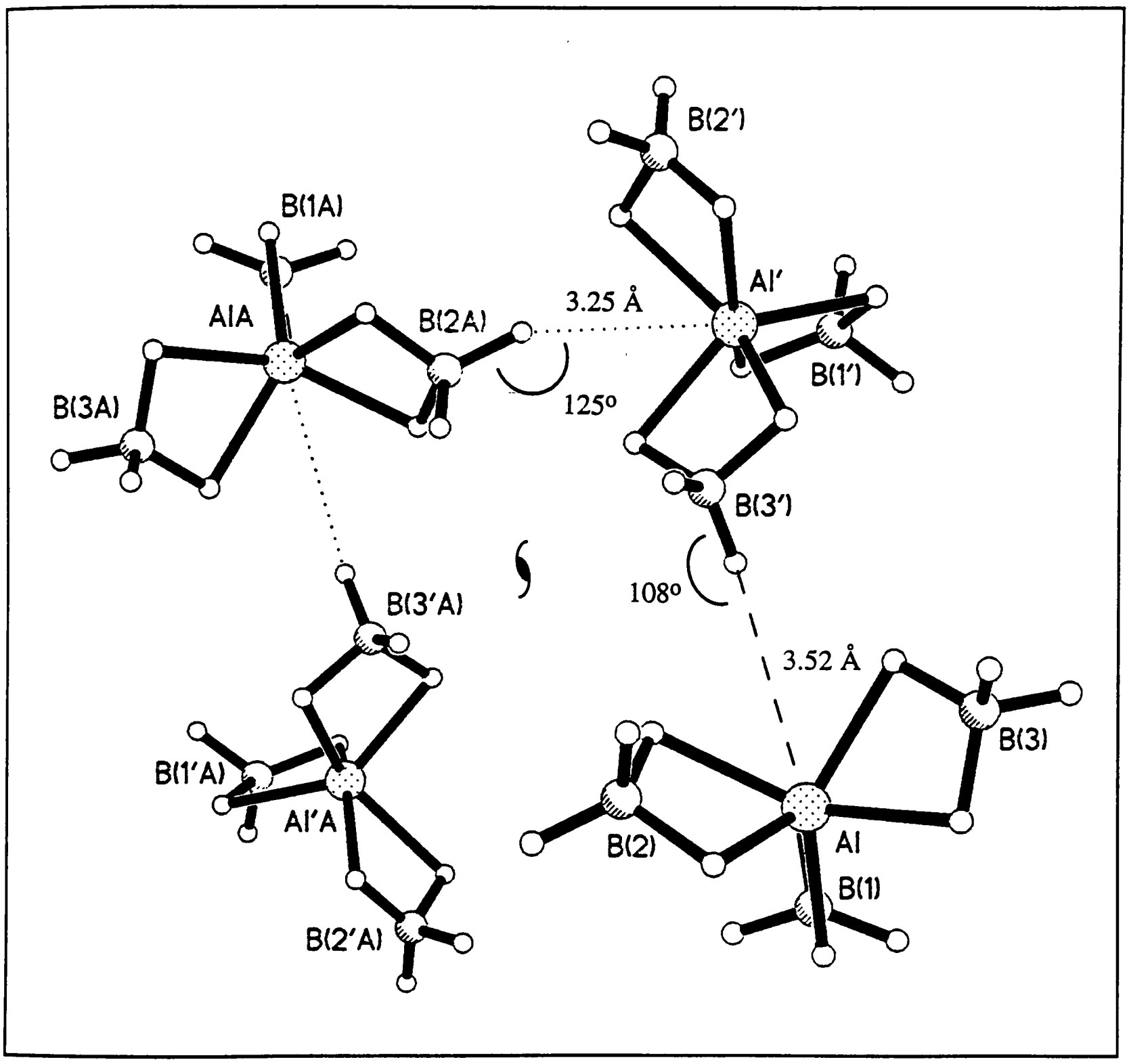

Figure 5.7 View along the *b*-axis of the α phase of solid $Al(BH_4)_3$.

Table 5.3 Comparison of the bond lengths (Å) obtained for the α- and β-phases of solid $[Al(BH_4)_3]$ by X-ray diffraction with those deduced for the gaseous molecule by electron diffraction and those calculated by *ab initio* methods.

Parameter[a]	X-ray diffraction		Electron diffraction[b]	*Ab initio* calculation (MP2 level)[c]
	α-phase	β-phase		
Al–B(1)	2.10(2)	2.103(8)		
Al–B(2)	2.11(2)	2.121(9)	2.143(3)	2.149
Al–B(3)	2.14(2)	2.128(9)		
Al–H(1A)	1.74(4)	1.67(5)		
Al–H(1B)	1.73(4)	1.70(4)		
Al–H(2A)	1.75(4)	1.73(4)	1.801(6)	1.752
Al–H(2B)	1.74(4)	1.75(4)		
Al–H(3A)	1.75(4)	1.74(4)		
Al–H(3B)	1.76(4)	1.71(4)		
B(1)–H(1A)	1.13(4)	1.14(3)	1.283(12)	1.270
B(1)–H(1B)	1.14(4)	1.12(3)		
B(1)–H(1C)	0.99(4)	0.99(3)	1.196(12)	1.194
B(1)–H(1D)	1.01(4)	0.99(3)		

[a] Numbering scheme taken from the structure obtained for the α-phase by X-ray diffraction. [b] From reference 4. [c] From reference 8.

Table 5.4 Comparison of the bond angles (°) obtained for the α- and β-phases of solid $[Al(BH_4)_3]$ by X-ray diffraction with those deduced for the gaseous molecule by electron diffraction and those calculated by *ab initio* methods.

Parameter[a]	X-ray diffraction		Electron diffraction[b]	*Ab initio* calculations (MP2 level)[c]
	α-phase	β-phase		
B(1)–Al–B(2)	119.2(7)	118.7(4)		
B(1)–Al–B(2)	121.1(7)	118.7(4)	120	120
B(1)–Al–B(2)	119.7(7)	122.5(4)		
H(1A)–Al–H(1B)	65(2)	65(2)		
H(2A)–Al–H(2B)	65(2)	63(2)	73.4(8)	72.4
H(3A)–Al–H(3B)	65(2)	65(2)		
H(1A)–B(1)–H(1B)	111(4)	106(3)		
H(2A)–B(2)–H(2B)	109(4)	109(3)	114.0(2)	109.2
H(3A)–B(3)–H(3B)	112(3)	108(3)		
H(1C)–B(1)–H(1D)	123(10)	123(4)		
H(2C)–B(2)–H(2D)	114(10)	124(5)	116.2(22)	121.2
H(3C)–B(3)–H(3D)	102(9)	129(5)		
H(1A)–B(1)–H(1C)	120(8)	108(5)	*d*	*d*
H(1A)–B(1)–H(1D)	101(8)	108(5)		
θ[e]	78.2(8)	89.1(6)	72.8(24)	66.8

[a] Numbering scheme taken from the structure obtained for the α-phase by X-ray diffraction. [b] From reference 4. [c] From reference 8. [d] Not given. [e] Taken as the angle between the planes defined by Al, B(1), B(2) and Al, H(1A), B(1).

around a crystallographic screw axis mirrors the behaviour of compounds such as $[MeZnBH_4]$,[15] $[Be(BH_4)_2]$[18] and $[Me_2AlBH_4]$.

Electron diffraction of $[Al(BH_4)_3]$ in the vapour phase[4] confirmed the planar AlB_3 skeleton and bidentate coordination of the BH_4 ligands implied by vibrational spectroscopy.[5] Haaland *et al.* were unable, however, to differentiate conclusively between D_{3h} and D_3 models. For the D_3 model, an angle, θ, of 72.8 ± 2.4^o between the AlB_3 and $Al(\mu\text{-}H)_2B$ planes was found to give the best agreement between the experimental and calculated scattering (see Figure 5.8). Subsequent *ab initio* calculations have suggested

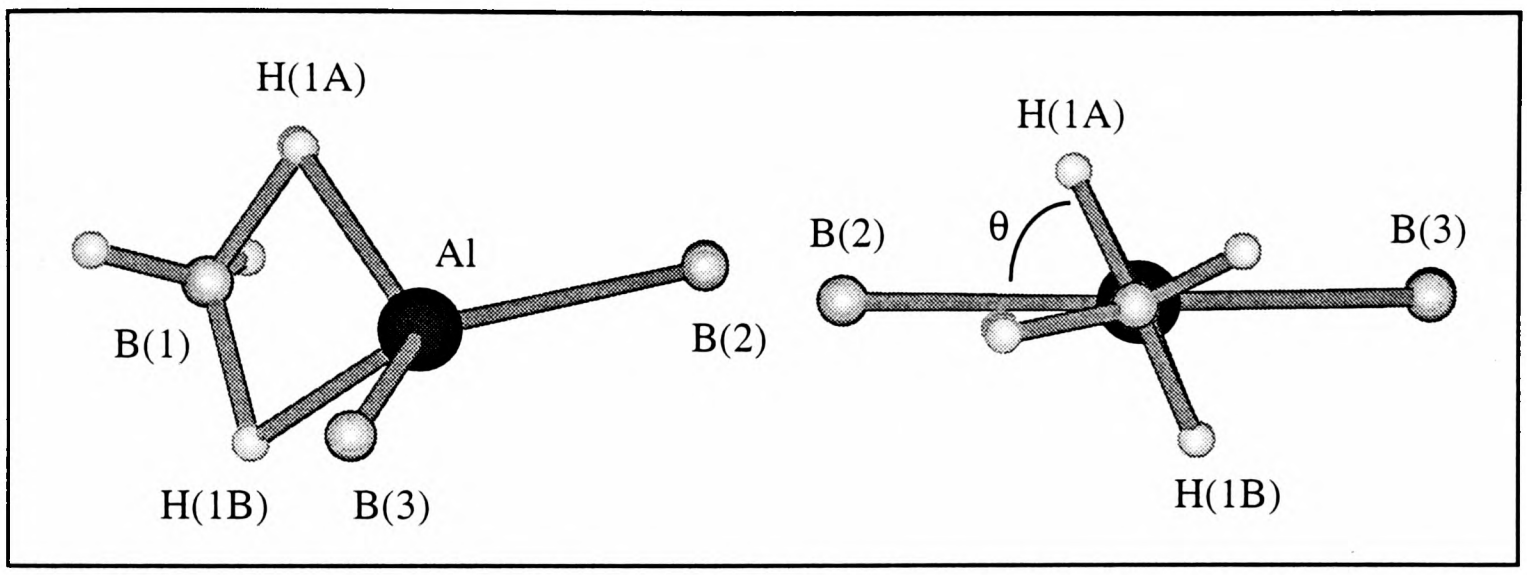

Figure 5.8 Representation of the angle, θ, between the AlB_3 and $Al(\mu\text{-}H)_2B$ planes.

that the D_{3h} structure is a transition state between two minima corresponding to configurations of D_3 symmetry, with the energy minimum occurring for $\theta = 66.8^o$.[8,22] Interestingly, whereas the corresponding angle in the α phase is 78.2^o, that in the β phase is 89.1^o. The change in angle between the solid phases implies that crystal packing forces play a relatively important rôle in fixing this structural parameter Indeed, given the extremely low barrier predicted for synchronous rotation of the three BH_4 groups (0.8-3.7 kJ mol^{-1} [8]), such a variation could easily be accounted for by small changes in molecular interactions in the solid state.

The other major differences between the molecular structure determined by X-ray diffraction and those deduced by electron diffraction and *ab initio* methods concern the bond lengths to hydrogen. The bridging and terminal B–H bonds appear typically to be

0.2-0.25 Å shorter than those in the gaseous molecule. The Al–B distances, on the other hand, show close levels of agreement, and it seems likely that the apparent discrepancy in bond lengths involving hydrogen atoms is an artifact resulting from the involvement in bonding of the single hydrogen 1s electron, such that the centre of electron density no longer coincides with the hydrogen nucleus (see reference 1 and Section 2.2.3).

The $B–H_b$ and $B–H_t$ bond lengths are very similar to those found in the $[Al(BH_4)_4]^-$ ion [0.95(5)-1.22(5) and 0.80(5)-1.07(5) Å, respectively[7]], the greater spread of bond lengths for this species reflecting the distorted dodecahedral coordination geometry of the bridging hydrogens.[7] The Al–H and Al···B distances for $[Al(BH_4)_3]$ [1.67(5)-1.75(4) and 2.103(8)-2.128(9) Å] are somewhat shorter than the corresponding parameters for $[Al(BH_4)_4]^-$, although this is more likely to signal the effects of charge and greater steric congestion at the aluminium centre in $[Al(BH_4)_4]^-$ than any unusual bonding in the parent compound.

The $Al(\mu\text{-}H)_2B$ bridges in both α and β forms of solid $Al(BH_4)_3$ are symmetrical, in that both $Al–H_b$ and both $B–H_b$ distances are, to within one standard deviation, the same. This contrasts with the situation in $[Al(BH_4)_4]^-$, in which one of the two bridging hydrogens shows a significantly longer $B–H_b$ bond [1.22(5) compared with 0.95(5) Å] and a markedly shorter $Al–H_b$ bond than the other. This too almost certainly reflects the more regular arrangement of the boron atoms around the aluminium centre and the less sterically crowded coordination sphere in $[Al(BH_4)_3]$.

The molecular structure of $[Al(BH_4)_3{\cdot}NMe_3]$ elucidated by Wallbridge *et al.* in 1966 contains *hepta*-coordinate aluminium, the NMe_3 ligand and six bridging hydrogens adopting a distorted pentagonal bipyramidal geometry.[6] The Al···B distances in the trimethylamine complex (2.23 ± 0.01 Å) are similar to those observed for both phases of $[Al(BH_4)_3]$ and also for $[Al(BH_4)_4]^-$, although the Al–H (1.97 ± 0.11 Å), $B–H_b$ (1.43 ± 0.11 Å) and $B–H_t$ bond lengths (1.19 ± 0.11 Å) are significantly longer than those displayed by either $[Al(BH_4)_3]$ or $[Al(BH_4)_4]^-$.[7] Such lengthening of the bonds to hydrogen may reflect the fact that the aluminium centre in $[Al(BH_4)_3{\cdot}NMe_3]$ is less electron deficient than that in $[Al(BH_4)_3]$ and that the degree of interaction with the BH_4

ligands is therefore lessened {although such an argument does not explain the discrepancy between the bond lengths in $[Al(BH_4)_4]^-$ and $[Al(BH_4)_3{\cdot}NMe_3]$}. However, given the fact that the structure of $[Al(BH_4)_3{\cdot}NMe_3]$ was solved by photographic methods, there must be doubts concerning the reliability of the estimated lengths of bonds to hydrogen atoms.

Given the disposition of $[Me_2AlBH_4]$ to form a polymeric, semi-ionic structure in the solid state and that of $[Al(BH_4)_3]$ to remain as discrete molecular units, the structure of the intermediate compound $[MeAl(BH_4)_2]$ would be of considerable interest. Vibrational studies carried out by Thomas led him to conclude that $[MeAl(BH_4)_2]$ undergoes a significant change of structure with the transition from the vapour to the solid phase.[13] Indeed, a strong band found at 2235 cm^{-1} in the infrared spectrum of the solid[13] is reminiscent of features attributable to the stretching motions of B–H bonds within the polymeric chains of $[Me_2AlBH_4]$, $[MeZnBH_4]$[15] and $[Be(BH_4)_2]$.[14] That the volatilities of $[MeAl(BH_4)_2]$[13] and $[Al(BH_4)_3]$[23] should be similar (compared with the much lower volatility of $[Me_2AlBH_4]$) tends, on the other hand, to argue against a structure for $[MeAl(BH_4)_2]$ in the solid state involving significant aggregation of the molecular units. It is unfortunate, therefore, that the solid monomethylaluminium compound is a glass with no definite melting point, although this fact in itself implies that there are only small energy differences beween various possible structures.

5.6 Conclusions and Suggestions for Further Research

The structure of dimethylaluminum tetrahydroborate in the solid phase has been shown by X-ray diffraction to consist of helical polymeric chains in which dimethylaluminium and tetrahydroborate units alternate. The BH_4 groups exhibit bidentate ligation with respect to each of the adjacent metal atoms. Examination of the B–H, Al–H and Al···B bond lengths and H–B–H angles reveals that the degree of interaction between the metal centre and the BH_4 group is considerably less than in $[MeZnBH_4]$,[15] and that

there is polarization in the sense of the ionic formulation $[Me_2Al]^+[BH_4]^-$ akin to that found in $[Be(BH_4)_2]$.[18]

Solid aluminium *tris*(tetrahydroborate) exhibits two phases. The more dense α phase crystallizes in a monoclinic space group, whereas the β phase, stable at higher temperatures, displays orthorhombic symmetry. The transition temperature is in the range 180-195 K. The crystal structures show that each phase is made up of discrete $Al(BH_4)_3$ units, the principal differences between the two relating to the packing of the individual molecules. The molecular structure determined by X-ray diffraction for the β phase conforms, within the limits of experimental error, to D_{3h} symmetry. In contrast, the molecular units present in the α phase display an angle, θ, between the AlB_3 and $Al(\mu\text{-}H)_2B$ planes of 78.2° and are therefore more in keeping with with the results of *ab initio* calculations, which predict D_3 symmetry and θ = 66.8° for the isolated $Al(BH_4)_3$ molecule.

Given the success of slow cooling methods in growing crystals of $[Me_2AlBH_4]$ and $[Al(BH_4)_3]$ suitable for X-ray diffraction, this technique could be applied to several other compounds which are liquid at room temperature, but which promise to show unusual or noteworthy structures in the solid state. The vibrational spectra of solid $[Me_2GaBH_4]$, for example, show marked changes from those of the vapour,[13,24] and further investigation of the solid phase using X-ray diffraction techniques could prove rewarding. Other hydride derivatives which might warrant similar studies include $[HGa(BH_4)_2]$,[25] $[GaH_3]_n$,[26] $[Me_2GaH]_n$,[27] $[H_2GaB_3H_8]$[28] and $[Me_2GaB_3H_8]$.[29] Studies are currently in progress to investigate the structure of $[Me_2AlB_3H_8]$[29] in the solid state.

References for Chapter 5

1. See, for example, T.J. Marks and J.R. Kolb, *Chem. Rev.*, 1977, **77**, 263.
2. H.I Schlesinger, R.T. Sanderson and A.B. Burg, *J. Am. Chem. Soc.*, 1939, **61**, 536.
3. H.I Schlesinger, H.C. Brown and E.K. Hyde, *J. Am. Chem. Soc.*, 1953, **75**, 209.
4. A. Almenningen, G. Gundersen and A. Haaland, *Acta Chem. Scand.*, 1968, **22**, 328.
5. D.A. Coe and J.W. Nibler, *Spectrochim. Acta*, 1972, **29A**, 1789.
6. N.A. Bailey, P.H. Bird and M.G.H. Wallbridge, *J. Chem. Soc., Chem. Commun.*, 1965, 438; N.A. Bailey, P.H. Bird and M.G.H. Wallbridge, *J. Chem. Soc., Chem. Commun.*, 1966, 286.
7. D. Dou, J. Liu, J.A. Krause Bauer, G.T. Jordan, IV, and S.G. Shore, *Inorg. Chem.*, 1994, **33**, 5443.
8. I. Demachy and F. Volatron, *Inorg. Chem.*, 1994, **33**, 3695.
9. P.R. Oddy and M.G.H. Wallbridge, *J. Chem. Soc., Dalton Trans.*, 1976, 869.
10. P.R. Oddy and M.G.H. Wallbridge, *J. Chem. Soc., Dalton Trans.*, 1976, 2076.
11 M.T. Barlow, A.J. Downs, P.D.P. Thomas and D.W.H. Rankin, *J. Chem. Soc., Dalton Trans.*, 1979, 1793.
12. M.T. Barlow, C.J. Dain, A.J. Downs, P.D.P. Thomas and D.W.H. Rankin, *J. Chem. Soc., Dalton Trans.*, 1980, 1374.
13. P.D.P. Thomas, D.Phil. Thesis, University of Oxford, 1977.
14. J.W. Nibler, D.F. Shriver and T.H. Cook, *J. Chem. Phys.*, 1971, **54**, 5257.
15. J.W. Nibler and T.H. Cook, *J. Chem. Phys*, 1973, **58**, 1596; Chapter 3, this thesis; S. Aldridge, A.J. Blake, A.J. Downs, S. Parsons and C.R. Pulham, *J. Chem. Soc., Dalton Trans.*, in press.
16. P.R. Oddy and M.G.H. Wallbridge, *J. Chem. Soc., Dalton Trans.*, 1978, 572.
17. A.J. Downs and L.A. Jones, *Polyhedron*, 1994, **13**, 2401.

18. D.S. Marynick and W.N. Lipscomb, *J. Am. Chem. Soc.*, 1971, **93**, 2322; D.S. Marynick and W.N. Lipscomb, *Inorg. Chem.*, 1972, **11**, 820.

19. L. Pauling, *The Chemical Bond*, 3rd edn., Cornell, New York, 1967, p. 148.

20. See, for example, A.J. Downs (ed.), *Chemistry of Aluminium, Gallium, Indium and Thallium*, Blackie, Glasgow, 1993.

21. P.F. Souter, A.J. Downs and S. Parsons, unpublished results; P.F. Souter, D.Phil. Thesis, University of Oxford, 1995.

22. C.W. Bock, C. Roberts, K. O'Malley, M. Trachtman and G.J. Mains, *J. Phys. Chem.*, 1992, **96**, 4859.

23. D.R. Lide (ed.), *Handbook of Chemistry and Physics,* 75th edn., C.R.C. Press, Boca Raton, FL, 1994-1995.

24. A.J. Downs and P.D.P Thomas, *J. Chem. Soc., Dalton Trans.*, 1978, 809.

25. A.J. Downs and P.D.P Thomas, *J. Chem. Soc., Chem. Commun.*, 1976, 825.

26. A.J. Downs, M.J. Goode and C.R. Pulham, *J. Am. Chem. Soc.*, 1989, **111**, 1936; C.R. Pulham, D. Phil. Thesis, University of Oxford, 1991.

27. P.L. Baxter, A.J. Downs, M.J. Goode, D.W.H. Rankin and H.E. Robertson, *J. Chem. Soc., Chem. Commun.*, 1986, 805.

28. C.R. Pulham, A.J. Downs, D.W.H. Rankin and H.E. Robertson, *J. Chem. Soc., Chem. Commun.*, 1990, 1520.

29. J.J. Borlin and D.F. Gaines, *J. Am. Chem. Soc.*, 1972, **94**, 1367.

Chapter Six
The Synthesis, Characterization and Structure of Dimethylindium Octahydrotriborate

6.1 Introduction

6.1.1 Background

The comparative weakness of In–H bonds has meant that until relatively recently few well characterized indium hydrides have been prepared.[1] These have included compounds of the types $M[R_2InH_2]$ and $M[RInH_3]$,[2] where M = an alkali metal and R = Me, Et or Me_3SiCH_2. Subsequently, use of the large *tris*(trimethylsilyl)methyl (*tsi*) group has enabled the synthesis and characterization of the complex $[Li(THF)_2][(tsi)H_2In(\mu\text{-}H)InH_2(tsi)]$.[3] The structure of the anion, determined by X-ray diffraction, features indium centres apparently linked by a single bridging hydrogen atom in a manner similar to that found in $Na[Me_3Al(\mu\text{-}H)AlMe_3]$.[4]

The very recent synthesis of dimethylindium tetrahydroborate, $[Me_2InBH_4]$, *via* the reaction between trimethylindium and gaseous diborane at ambient temperatures [reaction (1)][5] has provided fresh impetus for exploration of indium hydride chemistry by

$$Me_3In + B_2H_6 \longrightarrow Me_2InBH_4 + 1/2[MeBH_2]_2 \qquad (1)$$

offering obvious parallels with $[Me_2GaBH_4]$, the synthesis of which was one of the initial steps in the development of gallium hydride chemistry.[6] Spectroscopic studies of the solid hint, however, at a formulation coming closer to an ion pair, $[Me_2In]^+[BH_4]^-$, than to a molecule with a significant In–H bonding interaction.

The octahydrotriborate derivatives $[Me_2AlB_3H_8]$ and $[Me_2GaB_3H_8]$ are known to have structures in the vapour phase incorporating bidentate ligation of the B_3H_8 group,

being formally derived from tetraborane(10) by replacement of an apical BH_2 by an Me_2M unit (M = Al or Ga).[7,8] The NMR properties of these two compounds in [$^2H_8$]toluene solution at room temperature imply the presence of more fluxional molecules, and, given the greater tendency in indium chemistry towards formation of the $[Me_2M]^+$ ion,[9] investigation of the species $[Me_2InB_3H_8]$ would be of considerable interest, both from a spectroscopic and a structural viewpoint.

Earlier work by Ward suggested that dimethylindium octahydrotriborate could be prepared by the reaction of thallium(I) octahydrotriborate with dimethylindium chloride in monoglyme solution at -40°C, according to reaction (2).[10] The product was characterized

$$Me_2InCl + TlB_3H_8 \xrightarrow[-40^oC]{\text{monoglyme}} Me_2InB_3H_8 + TlCl \qquad (2)$$

by its infrared and ^{11}B and ^1H NMR spectra, although no chemical analysis was attempted. However, the presence of monoglyme in crystalline samples, as indicated by characteristic signals in the ^1H NMR spectrum, together with properties (physical state and thermal stability) which are at odds with the results to be presented here, suggest that the compound was unlikely to be $[Me_2InB_3H_8]$, but may well have been a solvated adduct of the type $[(Me_2InB_3H_8)_n \cdot \text{monoglyme}]$.

6.1.2 Aims of the Present Research

Comparison with the preparative routes giving access to the aluminium and gallium compounds[7] suggests that an analogous reaction [equation (3)] may be be used to synthesize $[Me_2InB_3H_8]$.

$$Me_2InCl + [^nBu_4N][B_3H_8] \longrightarrow Me_2InB_3H_8 + [^nBu_4N]Cl \qquad (3)$$

However, given the known reactivity of tetraborane(10) towards methylmetal compounds,[11,12] and the propensity of trimethylindium and trimethylthallium to react with

higher boranes [for example *via* reactions (4) and (5)[13,14]], the reaction of trimethylindium

$$2Me_3In + B_{10}H_{14} \longrightarrow [Me_2In]^+[B_{10}H_{12}InMe_2]^- + 2MeH \quad (4)$$

$$Me_3In + B_{10}H_{14} \longrightarrow MeInB_{10}H_{12} + 2MeH \quad (5)$$

with tetraborane(10) also invites investigation. Accordingly, it was decided to study both of these reaction pathways as potential routes to $[Me_2InB_3H_8]$ and, if either of them proved successful, to attempt a detailed structural and spectroscopic characterization of the product.

6.2 Synthesis of Dimethylindium Octahydrotriborate

6.2.1 Experiments with Dimethylindium Chloride and Tetra-*n*-butylammonium Octahydrotriborate

Dimethylindium chloride was prepared from indium trichloride and methyllithium by the method of Clark and Pickard.[15] Typically, 4.9 cm^3 of a 1.84 M methyllithium solution in diethyl ether were added dropwise to 1.0 g (4.5 mmol) of indium trichloride in *ca.* 30 cm^3 of diethyl ether at -78°C. The mixture was then allowed to warm to room temperature and stirred vigorously for 48 h. Volatile species were then removed *in vacuo* and the product purified by sublimation at 120°C with condensation on a cold finger held at -20°C. Yields were typically 0.45 g (56 %) based on reaction (6) and the amount of

$$InCl_3 + 2MeLi \longrightarrow Me_2InCl + 2LiCl \quad (6)$$

indium trichloride taken. The purity of a sample was assessed by comparing the infrared spectrum with that of an authentic sample[15] and by chemical analysis.

The reaction of dimethylindium chloride with freshly recrystallized tetra-*n*-butylammonium octahydrotriborate was investigated by mixing the two solids *in vacuo* at

-196°C and allowing them to warm to room temperature. As with the analogous reactions used to prepare $[Me_2AlB_3H_8]$ and $[Me_2GaB_3H_8]$,[7,8] an excess of the octahydrotriborate was used. Typically, 0.158 g (0.88 mmol) of dimethylindium chloride and 0.315 g (1.12 mmol) of tetra-*n*-butylammonium octahydrotriborate were taken. After *ca.* 30 min at room temperature droplets of a colourless, viscous liquid were observed to form in the reaction vessel. Further liquid continued to form on standing for 3-4 h. The reaction vessel was then attached to a train of traps leading to the main vacuum line and attempts were made to isolate the liquid by fractionation *in vacuo*. However, despite several attempts, the liquid proved to be insufficiently volatile to permit separation from the residual solids; warming to *ca.* 60°C brought about decomposition of the sample rather than volatilization. In these circumstances, it was decided to investigate the alternative synthetic route from trimethylindium and tetraborane(10), since the co-products were likely to be volatile in this case, and the problem of separating $[Me_2InB_3H_8]$ from a mixture containing involatile solids was likely to be alleviated, and possibly avoided altogether.

6.2.2 Synthesis from Trimethylindium and Tetraborane(10)

In a typical reaction, trimethylindium (0.138 g, 0.86 mmol) and tetraborane(10) (0.069 g, 1.129 mmol) were co-condensed in a 100 cm^3 bulb equipped with a constriction and a break-seal, and the mixture was allowed to warm to room temperature. After *ca.* 1 h, droplets of a colourless, viscous liquid were observed to form and, after a further 12 h at this temperature, the reaction appeared to proceed no further. The reaction vessel was then attached to a train of traps leading to the main vacuum line, these being cooled to 0, -15 and -196°C, respectively. The viscous liquid was observed to evaporate slowly from the trap held at 0°C and to be involatile at -15°C. On the basis of these distillation properties, the pure liquid was estimated to have a vapour pressure in the range 0.5-1 Torr at room temperature. Examination of the contents of the trap cooled to -196°C by infrared and ^1H NMR measurements revealed a mixture of dimethyldiborane, $[MeBH_2]_2$, and unchanged tetraborane(10).[16-19]

6.2.3 Elemental Analysis of Dimethylindium Octahydrotriborate

A sample of the viscous liquid was sealed in a break-seal ampoule, cooled to -78°C and sent to the Analytische Laboratorien, Gummersbach, Germany. The sample was cooled to -78°C for transportation and until immediately prior to analysis because of its tendency to decompose over periods of 48-72 h at room temperature. The results of elemental analysis are summarized in Table 6.1.

		Carbon	Hydrogen	Indium	Boron	Total
Experimental	Percentage by mass	12.21	6.99	62.70	16.68	98.58
	Ratio	1	6.82	0.54	1.52	-
Calculated for $InB_3C_2H_{14}$	Percentage by mass	12.96	7.61	61.94	17.49	100
	Ratio	1	7	0.5	1.5	-

Table 6.1 Elemental analysis of $[Me_2InB_3H_8]$.

Analysis of the viscous liquid to confirm the formula $Me_2InB_3H_8$, together with identification of dimethyldiborane as the only more volatile co-product, implies that the reaction of trimethylindium with tetraborane(10) is best written as in equation (7). Hence

$$Me_3In + B_4H_{10} \longrightarrow Me_2InB_3H_8 + 1/2[MeBH_2]_2 \qquad (7)$$

the reaction parallels that of trimethylindium with diborane in that it effectively brings about replacement of an apical BH_2 unit in the parent borane by an Me_2In group. Interestingly, in contrast to the reaction of tetraborane(10) with dimethylzinc [reaction (8)],

$$3Me_2Zn + B_4H_{10} \longrightarrow [(MeZn)_2B_3H_7] + BMe_3 + MeH + ZnH_2 \qquad (8)$$

there appears to be no tendency towards incorporation of a second methylmetal fragment into the borane skeleton.[11]

Yields of dimethylindium octahydrotriborate were typically 100-110 mg (63-69%) based on equation (7) and the amount of trimethylindium taken.

6.2.4 Growth of Crystals for X-ray Diffraction

Samples of $[Me_2InB_3H_8]$ were loaded in Pyrex capillaries each 0.3-0.6 mm in internal diameter for the purpose of attempted crystal growth. Invariably, the first step involved rigorous pre-conditioning of the capillary by exposure to the sample vapour for 1-2 h prior to re-evacuation, this serving to scavenge any residual moisture adsorbed on the glass surfaces. A small quantity (*ca.* 0.01 cm^3) of the compound was then transferred from the storage ampoule and condensed in the neck of the vessel; with careful warming, the material was caused to melt and run down to the bottom of the capillary. Typically, a depth of 1.5-2 cm of liquid compound was required. Once this was achieved, the sample was cooled to -196°C, and the capillary sealed such that its total length did not exceed 3 cm.

Crystals were grown from the liquid using the method illustrated in Figure 2.5 and outlined in Section 2.3.7.1. A single crystal of $[Me_2InB_3H_8]$ was grown from the solid/liquid phase boundary using the slow cooling method employed previously to grow single crystals of $[Me_2AlBH_4]$ and the β phase of $[Al(BH_4)_3]$. In this instance, a suitable crystal was grown by cooling the liquid (at 5 K h^{-1}) from 247 K.

6.3 The Crystal Structure of Dimethylindium Octahydrotriborate at 150 K

6.3.1 Crystal Data

$C_2H_{14}InB_3$, M = 185.38, monoclinic, $P2_1/c$, a = 11.718(4), b = 9.578(4),

c = 14.994(5) Å, β = 105.31(4)°, U = 1623.1(10) Å^3, λ = 0.71073 Å, Z = 8, D_c = 1.517 g cm^{-3}, F(000) = 720, T = 150 K, colourless crystal.

6.3.2 Data Collection

Data were collected on a Stoë Stadi-4 four circle diffractometer with graphite-monochromated Mo-Kα radiation; ω-2θ mode, ω half width (1.32 + 0.35tanθ)°. Of the 3179 reflections measured (θ_{max} = 25.04°; $-13 \leq h \leq 13$, $0 \leq k \leq 11$, $0 \leq l \leq 17$), 2850 were unique.

6.3.3 Structure Solution and Refinement

The crystal structure of dimethylindium octahydrotriborate was solved by Dr. S. Parsons using direct methods (SIR92) and refined by full-matrix least-squares methods with anisotropic displacement parameters for all non-hydrogen atoms (SHELXTL). Methyl hydrogens were located in a difference synthesis performed about the loci of possible hydrogen atom positions; in subsequent cycles of least-squares refinement the methyl groups were treated as rigid rotating groups [r(C–H) = 0.96 Å]. All hydrogen atoms attached to boron were located in difference syntheses and allowed to refine freely. Other structure solution and refinement details are listed in Appendix 9.

6.3.4 Discussion of Results

The molecular structure of [$Me_2InB_3H_8$] at 150 K is depicted in Figure 6.1 and a diagram illustrating the interaction between molecular units shown in Figure 6.2. Bond distances and angles are listed in Table 6.2; fractional atomic coordinates and anisotropic displacement parameters are given in Appendix 9.

The structure of [$Me_2InB_3H_8$] shows that the B_3H_8 ligand is linked to the indium centre *via* two bridging hydrogen atoms and, superficially at least, is therefore similar to

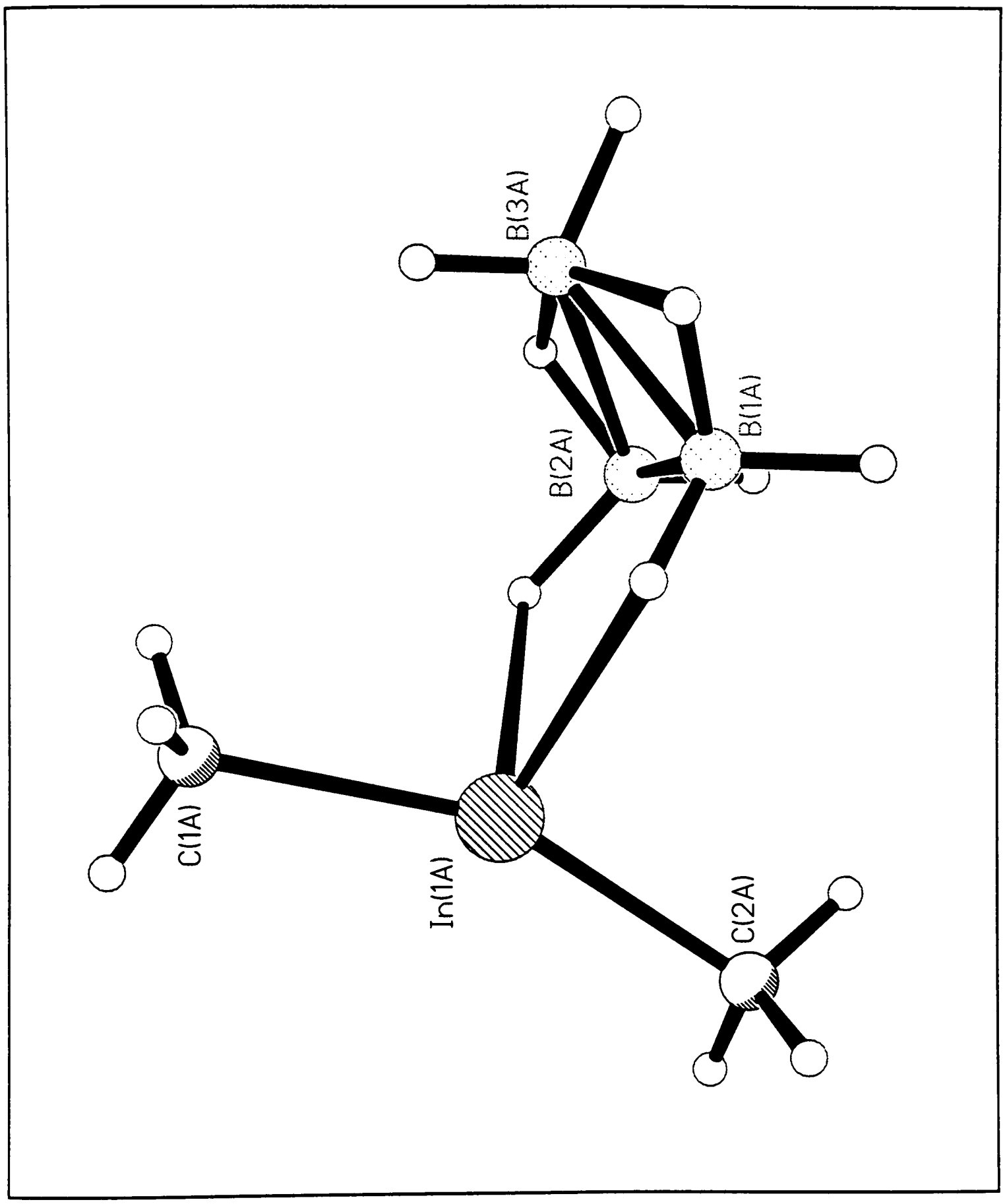

Figure 6.1 The molecular structure of $[Me_2InB_3H_8]$ at 150 K.

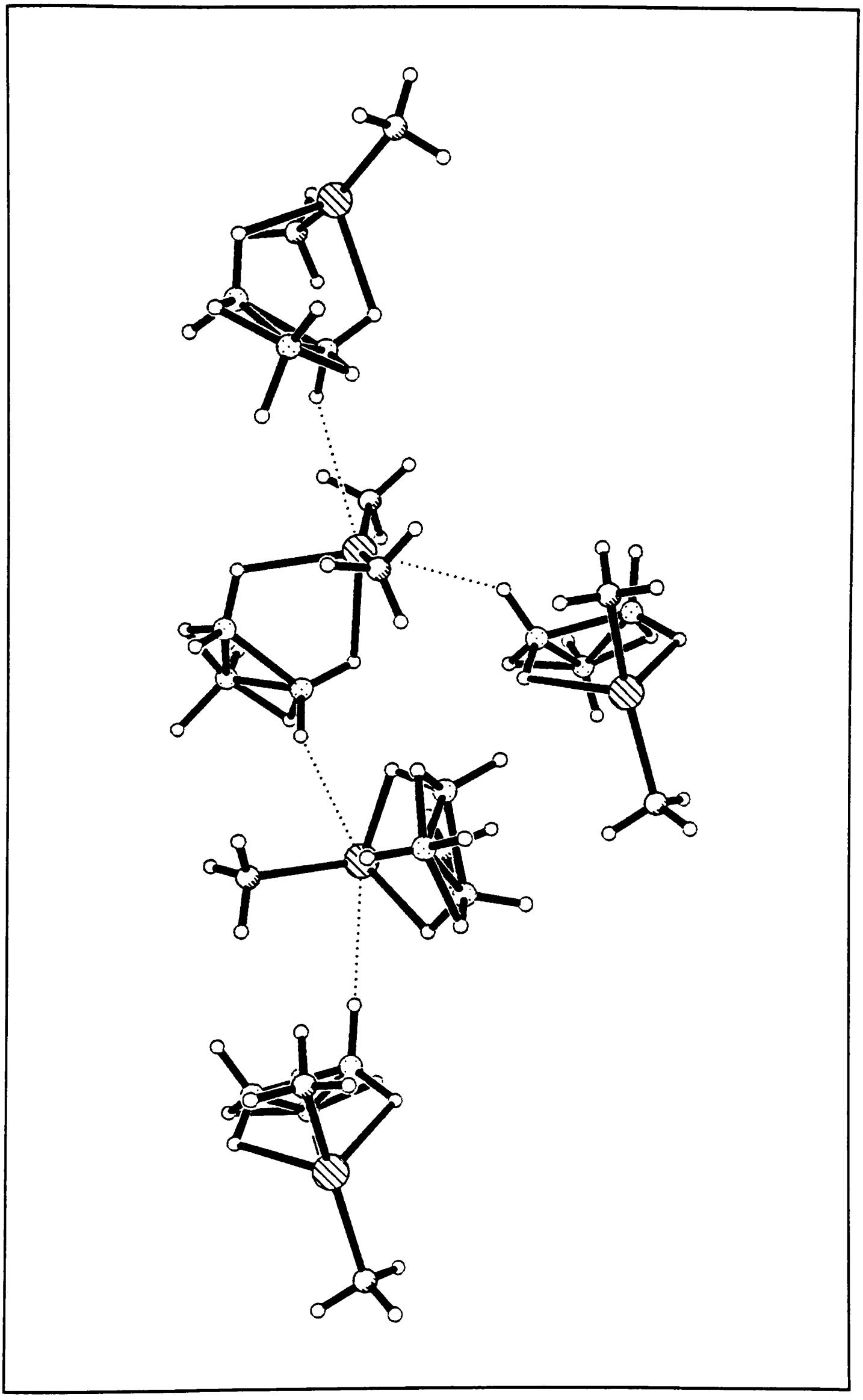

Figure 6.2 Intermolecular interactions in solid dimethylindium octahydrotriborate.

Table 6.2 Bond distances (Å) and angles (°) for crystalline $[Me_2InB_3H_8]$ at 150 K.

In(1A)–C(1A)	2.105(5)	B(1A)–H(2A)	1.07(4)
In(1A)–C(2A)	2.103(5)	B(1A)–H(13A)	1.11(6)
In(1A)–H(1A)	2.22(4)	B(2A)–H(3A)	1.20(4)
In(1A)–H(3A)	2.16(4)	B(2A)–H(4A)	1.09(4)
C(1A)–H(1A1)	0.98[a]	B(2A)-H(23A)	1.14(5)
B(1A)–B(2A)	1.779(7)	B(3A)–H(5A)	0.95(9)
B(1A)–B(3A)	1.790(8)	B(3A)–H(6A)	1.14(4)
~~B(1A)–B(2A)~~ B(2A)–B(3A)	1.809(8)	B(3A)–H(13A)	1.49(6)
B(1A)–H(1A)	1.11(4)	B(3A)–H(23A)	1.39(6)
C(1A)–In(1A)–C(2A)	158.6(2)	H(5A)–B(3A)–H(13A)	109(4)
C(1A)–In(1A)–H(1A)	98.2(10)	H(5A)–B(3A)–H(23A)	99(4)
C(1A)–In(1A)–H(3A)	94.0(11)	H(6A)–B(3A)–H(13A)	98(3)
H(1A)–In(1A)–H(3A)	81(2)	H(6A)–B(3A)–H(23A)	102(4)
H(1A1)–C(1A)–H(1A2)	109.5[a]	H(1A)–B(1A)–H(2A)	108(3)
B(2A)–B(1A)–B(3A)	60.9(3)	H(1A)–B(1A)–H(13A)	103(3)
B(1A)–B(2A)–B(3A)	59.8(3)	H(2A)–B(1A)–H(13A)	101(4)
B(1A)–B(3A)–B(2A)	59.2(3)	H(3A)–B(2A)–H(4A)	112(3)
B(1A)–In(1A)–B(2A)	37.6(2)	H(3A)–B(2A)–H(23A)	97(3)
H(13A)–B(3A)–H(23A)	136(3)	H(4A)–B(2A)–H(23A)	111(4)
H(5A)–B(3A)–H(6A)	115(4)		

[a] Fixed.

the molecular structures of $[Me_2AlB_3H_8]$ and $[Me_2GaB_3H_8]$ in the vapour phase as determined by electron diffraction.[8] Bond lengths involving hydrogen atoms are typically up to 0.3 Å shorter for $[Me_2InB_3H_8]$ reflecting not only the differing nature of the parameter involved (r_α, as opposed to r_a),[20] but also shrinkage effects inherent in the location of hydrogen atoms by X-ray diffraction,[21] a phenomenon also encountered in the case of $[Al(BH_4)_3]$.[22,23] Asymmetric bridging of the B(1)–B(3) and B(2)–B(3) bonds by H(13) and H(23) [which are typically 0.3-0.35 Å closer to the basal boron atoms, B(1) and B(2), than to the apical boron atom, B(3)] mirrors the situation in other compounds containing a bidentate B_3H_8 group {*viz.* $[Me_2AlB_3H_8]$,[8] $[Me_2GaB_3H_8]$,[8] $[Be(B_3H_8)_2]$,[24] $[(Ph_3P)_2CuB_3H_8]$[25] and $[B_4H_{10}]$[26]}. A comparison of other structural parameters of $[Me_2InB_3H_8]$ with the corresponding values for related derivatives containing one or more bidentate B_3H_8 groups is made in Table 6.3.

Closer examination of the structures of $[Me_2MB_3H_8]$ (M = Al, Ga or In) reveals a tendency towards a more ionic formulation in solid $[Me_2InB_3H_8]$ akin to that implied by vibrational spectroscopy for solid $[Me_2InBH_4]$. Firstly, the M···B distance [2.735(6), 2.754(6) Å] is somewhat longer than would have been predicted on the basis of the corresponding values for $[Me_2AlB_3H_8]$ and $[Me_2GaB_3H_8]$ [2.307(8) and 2.344(9) Å, respectively], even when allowance is made for the larger tetrahedral covalent radius of indium [1.44 Å for indium; 1.26 Å for both aluminium and gallium[27]].

Secondly, the C–In–C angle [158.6(2)°] is significantly larger than that found in either of the aluminium or gallium compounds [126.8 and 130.3°, respectively]. Indeed, the angle is very similar to that determined by X-ray diffraction for the compound $[Me_2In][O_2CMe]$ [152.2(6)°][28] and akin to those obtained from spectroscopic measurements for species such as $[Me_2In][O_3SMe]$[29] and $[Me_2In][SbCl_6]$[30] in solution; such compounds are believed to dissolve in polar solvents (such as nitromethane) yielding solvated $[Me_2In]^+$ and X^- ions (where X = O_3SMe or $SbCl_6$). In $[Me_2In][O_2CMe]$ the indium centre effectively increases its coordination number from four to six by interaction with oxygen atoms of other $[O_2CMe]$ units, as illustrated in Figure 6.3. A similar situation arises in solid $[Me_2InB_3H_8]$. A degree of secondary interaction between indium

Parameter[a]	$Me_2InB_3H_8$	$Me_2GaB_3H_8$[b]	$Me_2AlB_3H_8$[b]	$Be(B_3H_8)_2$[c]	$[(H_3N)_2BH_2]^+[B_3H_8]^-$ [d]	$(Ph_3P)_2CuB_3H_8$[e]	B_4H_{10}[f]
B(1)–B(3)	1.790	1.856[g]	1.856[g]	1.834	1.77	1.82	1.845
B(1)–B(2)	1.779	1.705[g]	1.705[g]	1.766	1.80	1.76	1.705
B(2)–B(3)	1.809	1.856[g]	1.856[g]	1.834	1.77	1.82	1.845
B–H_t	0.95-1.14	1.22-1.25	1.18-1.21	1.045-1.137	1.05-1.20	1.0-1.3	1.03-1.17
B(1,2)–H_b	1.11, 1.14	1.270	1.272	1.188, 1.058	1.2	1.15	1.21
B(3)–H_b	1.39, 1.49	1.440	1.447	1.306, 1.378	1.5	1.52	1.37
B(1,2)–H_m	1.11, 1.20	1.270	1.277	1.190, 1.158	[h]	1.21	1.21
M···B	2.735, 2.754	2.334	2.307	1.981, 1.973	[h]	2.30	1.856
M–H_m	2.22, 2.16	1.906	1.989	1.494, 1.515	[h]	1.85	1.37

[a] Numbering scheme consistent with that used for $[Me_2InB_3H_8]$. [b] These are r_a values obtained from electron-diffraction measurements reported in reference 8. [c] From reference 24. [d] From reference 31. [e] From reference 25. [f] From reference 26. [g] Fixed equal to the corresponding values in gaseous B_4H_{10}. [h] Unavailable or not symmetry-related to $[Me_2InB_3H_8]$.

Table 6.3 (a) Comparison of selected bond lengths (Å) for compounds containing the B_3H_8 unit.

Parameter[a]	$Me_2InB_3H_8$	$Me_2GaB_3H_8$[b]	$Me_2AlB_3H_8$[b]	$Be(B_3H_8)_2$[c]	$[(H_3N)_2BH_2]^+[B_3H_8]^-$ [d]	$(Ph_3P)_2CuB_3H_8$[e]	B_4H_{10}[f]
B(1)–B(3)–B(2)	59.8	54.7[g]	54.7[g]	57.5	61.1	58.5	56.6
H(13)–B(1)–H(1)	103	[h]	[h]	100.6, 98.1	[h]	100	95.6
H(6)–B(3)–B(5)	111	122.0[g]	122.0[g]	122.2	[h]	110	125.1
H(13)–B(3)–H(23)	136	[h]	[h]	132.6	145.3	144	134.7
H(1)–M–H(3)	81	[h]	[h]	125.2	[h]	103	134.7

[a] Numbering scheme consistent with that used for $[Me_2InB_3H_8]$. [b] These are r_a values obtained from electron-diffraction measurements reported in reference 8. [c] From reference 24. [d] From reference 31. [e] From reference 25. [f] From reference 26. [g] Fixed equal to the corresponding values in gaseous B_4H_{10}. [h] Unavailable or not symmetry-related to $[Me_2InB_3H_8]$.

Table 6.3 (b) Comparison of selected angles (°) for compounds containing the B_3H_8 unit.

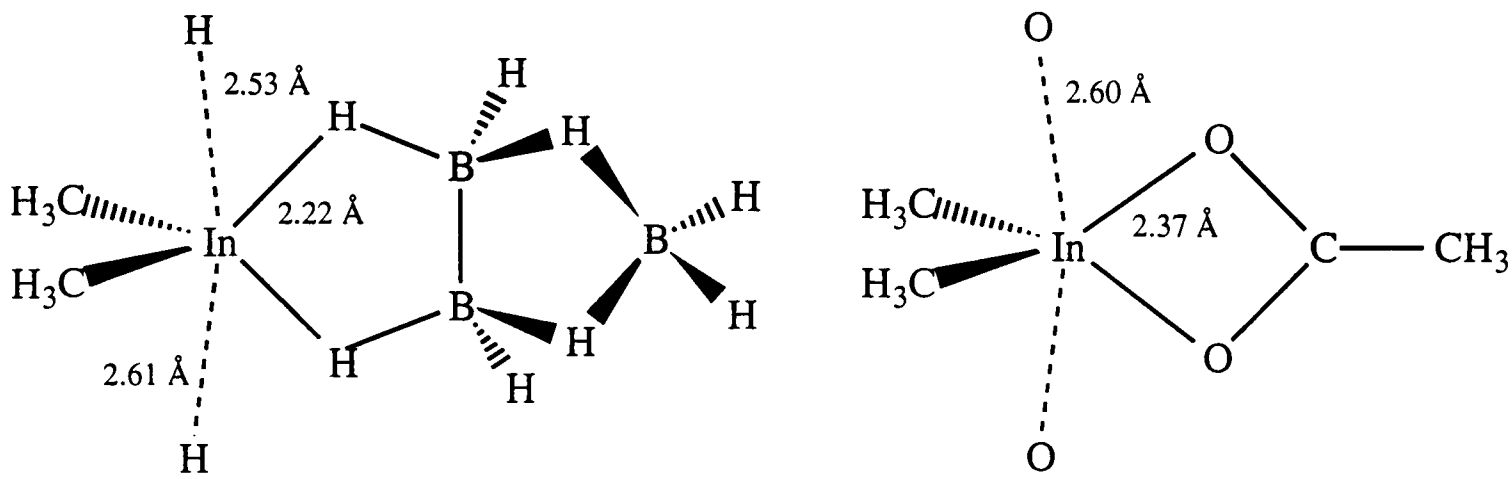

Figure 6.3 Secondary interactions in solid $[Me_2InB_3H_8]$ and $[Me_2InO_2CMe]$.[28]

centres and the terminal hydrogen atoms H(2) and H(4) attached to the basal boron atoms [B(1) and B(2)] is implied by In···H distances as short as 2.53 Å. Furthermore, the angle between the indium centre and the two bridging hydrogen atoms [∠H(1)–In–H(3), 81(2)°] is substantially smaller than the corresponding values in $[Be(B_3H_8)_2]$,[24] $[(Ph_3P)_2CuB_3H_8]$[25] or B_4H_{10}[26] [125.2(11), 103(2) and 134.7(35)°, respectively], reflecting the increased crowding of the indium coordination sphere.

It appears, therefore, that solid dimethylindium octahydrotriborate contains $[Me_2InB_3H_8]$ units in which there is some degree of charge separation $[Me_2In]^+[B_3H_8]^-$, coordination at each indium centre being augmented *via* secondary interactions with terminal hydrogens of adjacent B_3H_8 units. Such behaviour is not without precedent in indium chemistry {consider, for example, $[Me_2In][ReO_4]$,[32] $[Me_2In][InI_4]$,[33] and $[Me_2In][O_2CMe]$,[28]}.

$[Me_2InB_3H_8]$ represents a rare example of a structurally authenticated compound containing an In–H bond. The anion $[(tsi)H_2In(\mu\text{-}H)InH_2(tsi)]^-$ is thought to contain both In–H and In–H–In linkages on the basis of infrared measurements, although the quality of the X-ray data was not sufficient to permit location of the hydrogen atoms. The crystal structure of $K[H(InR_3)_2]$ (R = CH_2CMe_3), which has been determined by Beachley *et al.*,[34] contains the $[R_3In–H–InR_3]^-$ anion in which the two indium centres are linked by a single bridging hydrogen atom. The In–H bond lengths, at 1.950(23) and 1.933(15) Å, are considerably shorter than those in $[Me_2InB_3H_8]$; this, too, is consistent with a significant degree of charge separation $[Me_2In]^+[B_3H_8]^-$ in the octahydrotriborate.

6.4 Spectroscopic Characterization of Dimethylindium Octahydrotriborate

6.4.1 NMR Spectroscopy

NMR spectroscopy has often proved to be a useful tool in differentiating between various possible structures open to B_3H_8 derivatives in solution [see Section 2.2.2(b)]. Accordingly, ^{11}B and ^{1}H NMR spectra were measured for solutions of $[Me_2InB_3H_8]$ in $[^2H_8]$toluene solution at temperatures in the range -90 to 40°C. The ^{1}H NMR spectrum at room temperature is shown in Figure 6.4; ^{11}B spectra at temperatures in the range -10 to 40°C are shown in Figure 6.5.

The ^{1}H NMR spectrum at room temperature shows a sharp singlet at δ_H -0.22 (relative intensity 3) and a broad resonance centred at δ_H 0.85 (relative intensity 4). Cooling the solution causes some sharpening of both signals, although, even at -90°C, no fine structure can be resolved for either signal, and there is no sign of any other resonances in the range δ_H = -5 to 10 ppm.

The ^{11}B spectrum at -20°C shows a single, broad unresolved hump centred at δ_B -32.1. Upon warming the solution to 0°C, some fine structure can be detected, while at 40°C it is possible to resolve all nine lines of a nonet [$J(^{11}B–^{1}H)$ = 33.4 Hz]. Cooling the solution from -20°C, on the other hand, results in little change in the spectrum, there being no sign of any other resonance in the range δ_B = -60 to 100 ppm.

The sharp ^{1}H singlet is assigned to the protons of the methyl groups, its position being consistent with that found for other methylindium compounds {*e.g.* $[Me_2InBH_4]$[5] and $[Me_3In]$[35]}. The broad ^{1}H resonance at δ_H 0.85 is assigned to all eight hydrogen atoms attached to boron, having a chemical shift similar to those of the corresponding signals for $[C_5H_5BeB_3H_8]$,[36] $[Me_2AlB_3H_8]$[7] and $[Me_2GaB_3H_8]$.[7] These results indicate that both methyl groups are equivalent, as are all eight boron-bound hydrogen atoms under the conditions of the experiment. Similar conclusions may be drawn from an analysis of the ^{11}B spectrum at room temperature; the nine-line multiplet has a chemical shift and

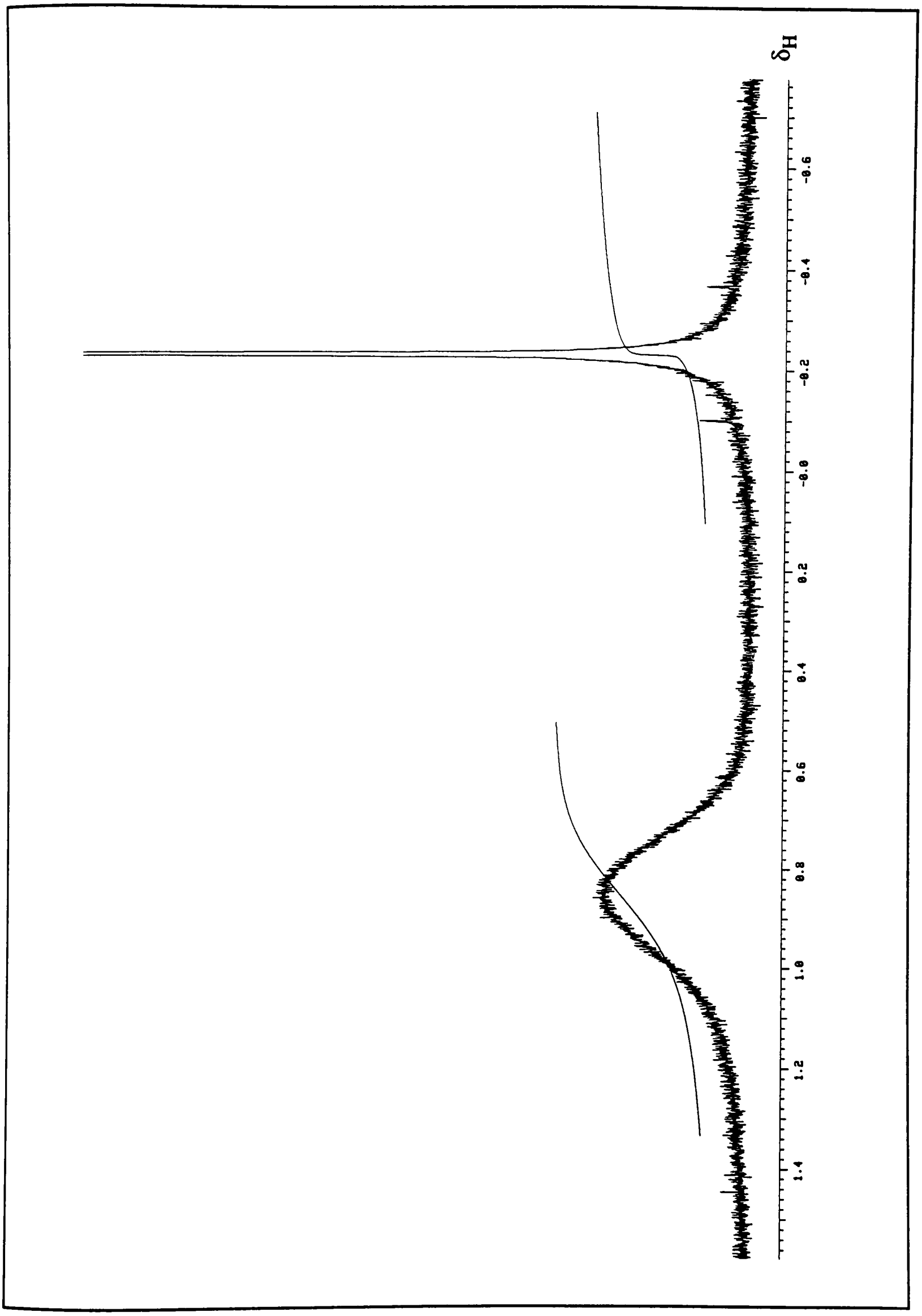

Figure 6.4 The ^{1}H NMR spectrum of dimethylindium octahydrotriborate in $[^{2}H_{8}]$toluene solution at room temperature.

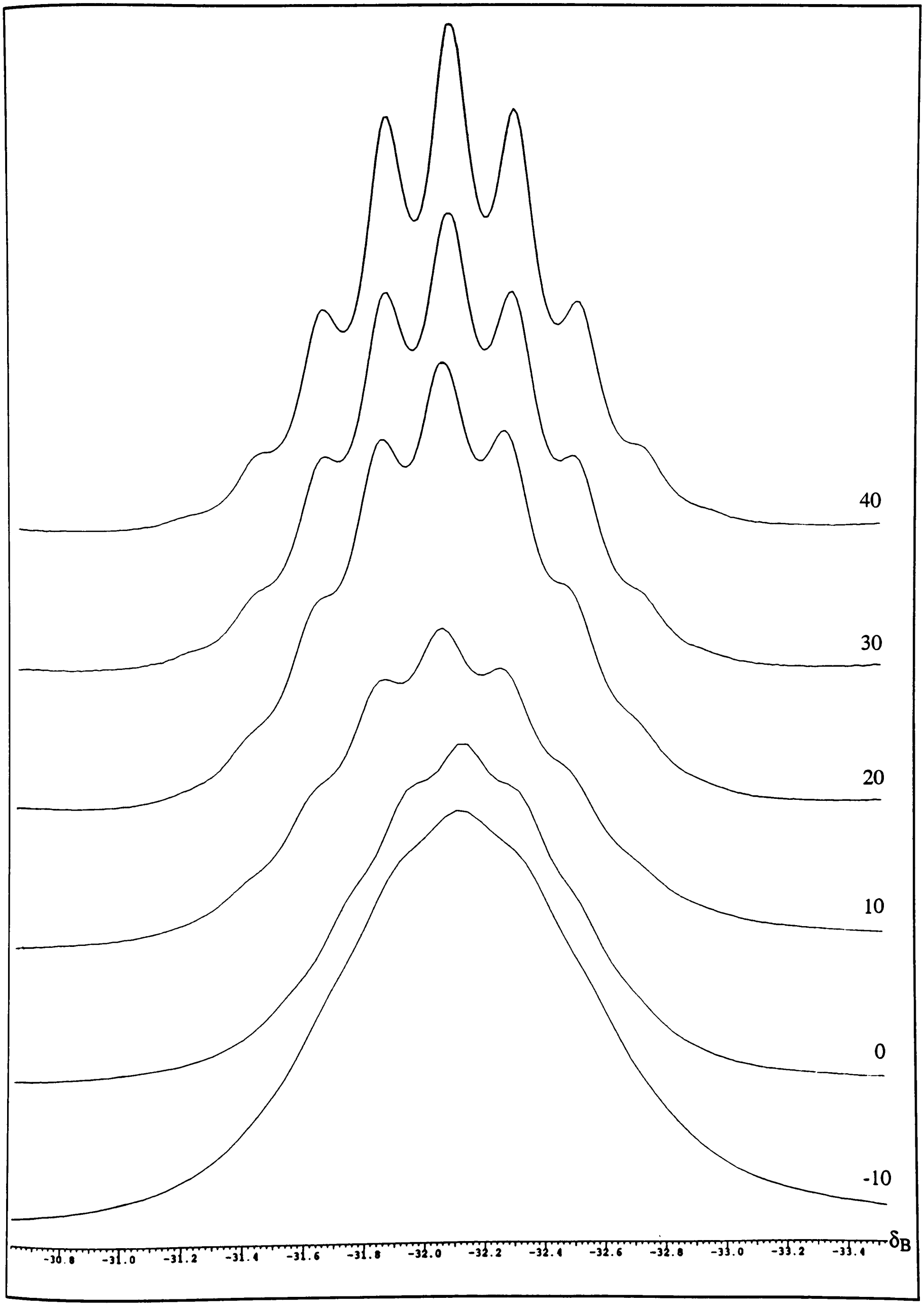

Figure 6.5 The ^{11}B NMR spectra of dimethylindium octahydrotriborate in [$^{2}H_8$]toluene solution at temperatures in the range -10 to 40°C.

coupling constant similar to those observed for $[Me_2GaB_3H_8]$[7] and $[C_5H_5BeB_3H_8]$,[36] indicating that all three boron atoms, as well as all eight boron-bound hydrogen atoms, are equivalent.

The spectra at room temperature are very similar to those observed for solutions of $[Me_2AlB_3H_8]$ and $[Me_2GaB_3H_8]$ under comparable conditions.[7] The fluxionality of these two molecules has been explained in terms of a mechanism in which the initial step involves cleavage of one of the M–H bonds, leaving the B_3H_8 ligand bound to the methylmetal fragment in a monodentate fashion.[7] Further intermediate species are then proposed to facilitate exchange of hydrogen atoms around the B_3H_8 moiety.

In distinct contrast to the corresponding spectra of the aluminium and gallium analogues,[7] the ^1H and ^{11}B NMR spectra of $[Me_2InB_3H_8]$ show no sign of any other resonances on cooling to -90°C. Indeed, the only discernible changes are the collapse of the multiplet structure of the ^{11}B resonance and eventual "washing-out" of the B–H coupling as a result of "correlation time decoupling." [37] In the cases of the aluminium and gallium compounds, distinct resonances were observed in both the ^1H and ^{11}B spectra at temperatures below -70°C, corresponding to the different proton and boron atom environments implicit in a static structure such as **I**.[7,8]

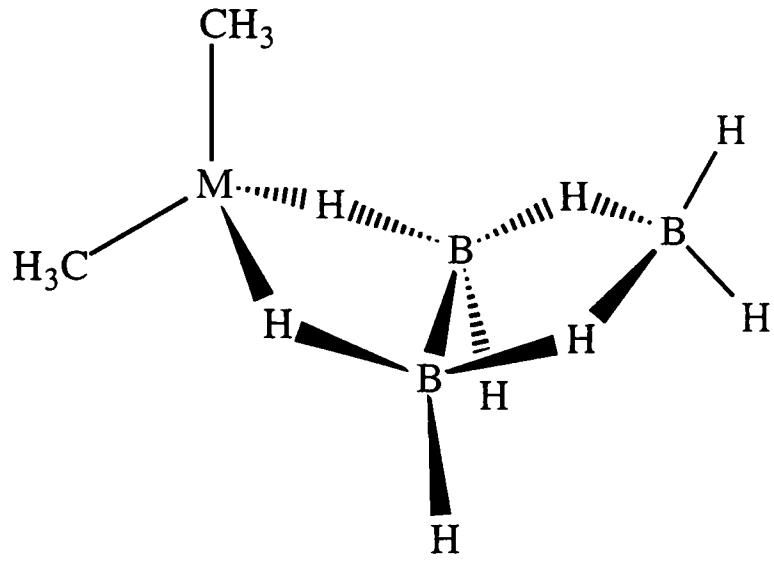

I

The fact that all the boron atoms and all the boron-bound hydrogens in $[Me_2InB_3H_8]$ remain equivalent implies that the structure is fluxional, even at -90°C. This in turn is indicative of much weaker interaction in solution between the Me_2M and B_3H_8

fragments for M = In. Indeed, the spectra for $[Me_2InB_3H_8]$ are similar to those reported for dichloromethane solutions of $Na[B_3H_8]$[38] and $[^nBu_4N][B_3H_8]$,[39] in which the interaction between the cation and $[B_3H_8]^-$ fragment is largely coulombic.[39]

6.4.2 Infrared Spectroscopy

Vibrational spectroscopy has proved to be an extremely useful technique for establishing the mode of coordination of a B_3H_8 group to a metal centre in both the solid and vapour phases [see Section 2.2.1(b)]. Thus, for example, the tetraborane(10)-like structure of $[H_2GaB_3H_8]$, incorporating bidentate ligation of the B_3H_8 group in both the solid and vapour is evident from a survey of its infrared and Raman spectra.[40]

Access to the infrared spectrum of $[Me_2InB_3H_8]$ in the vapour phase was precluded by its low vapour pressure and by its tendency to react with the caesium iodide windows and halocarbon wax of the infrared cell. Consequently, spectra were measured for the matrix-isolated species; bands of a molecule are typically shifted by only a few wavenumbers from the gas-phase frequencies by interaction of the trapped molecule with the host lattice.[41] The best spectra were obtained using nitrogen as the matrix gas and with the vapour sampled above the compound at -23°C. The principal aim of such measurements was to obtain information regarding the structure of $[Me_2InB_3H_8]$ in the vapour phase. To this end, analogous spectra were also measured for $[Me_2AlB_3H_8]$, which has been shown by electron-diffraction measurements to have a tetraborane(10)-like structure (**I**) in the vapour phase.[8] It was hoped that comparison of the spectra of matrix-isolated $[Me_2InB_3H_8]$ and $[Me_2AlB_3H_8]$ would allow some inferences to be drawn concerning the structure of gaseous $[Me_2InB_3H_8]$. The aluminium compound was made according to the method of Borlin and Gaines, and shown to be pure on the basis of ^1H and ^{11}B NMR measurements.[7]

Infrared spectra were also measured for a solid film of $[Me_2InB_3H_8]$. It was hoped that changes in the spectra with the transition from the vapour to the solid phase might shed some light on any structural changes occurring on condensation. In addition,

the spectrum of solid [$Me_2AlB_3H_8$] was measured, with an eye to comparing it with the spectrum of the solid indium compound and so gaining some information about the (unknown) structure of the solid aluminium compound.

The infrared spectrum of matrix-isolated [$Me_2InB_3H_8$] is reproduced in Figure 6.6 and that of the solid in Figure 6.7. The corresponding spectra for the aluminium compound are shown in Figures 6.8 and 6.9, respectively. Wavenumbers and proposed assignments are listed in Table 6.4.

6.4.2.1 Discussion of Results

(a) Spectra of matrix-isolated species. It is evident from a survey of the infrared spectra of matrix-isolated [$Me_2InB_3H_8$] and [$Me_2AlB_3H_8$] that the patterns of bands for the two compounds are very similar. Gaseous [$Me_2AlB_3H_8$] has been shown by electron diffraction to consist of a molecular species with a structure similar to **I**. Reference to the vibrational spectra of compounds containing terminal Me_2In units {e.g. $[Me_2InCl]_2$,[15] $[Me_3In]$[42] and $[Me_2InBH_4]$[5]} and doubly hydrogen-bridged octahydrotriborate ligands {e.g. $[H_2GaB_3H_8]$[40] and $[B_4H_{10}]$[17]} and comparison with the spectra of the matrix-isolated aluminium compound leave little doubt that [$Me_2InB_3H_8$] also exists in the vapour phase as a molecular species in which a dimethylmetal unit has formally replaced one of the apical BH_2 groups of tetraborane(10). Such a molecule featuring bidentate ligation of the B_3H_8 group and *tetra*-coordinated indium, has C_s symmetry, with 54 vibrational modes spanning the *a*' and *a*" symmetry classes. The low symmetry of the molecule, combined with the similarity in energy of many of the vibrational modes, means that there will inevitably be considerable mixing of some of the normal coordinates. In the absence (i) of Raman measurements, (ii) of experiments involving selective deuteriation of the CH_3 and B_3H_8 fragments and (iii) of subsequent normal coordinate analysis calculations, it is not possible to complete a full assignment of all the vibrational modes of this molecule. Comparisons with the vibrational spectra of related compounds do, however, allow some tentative assignments to be made.

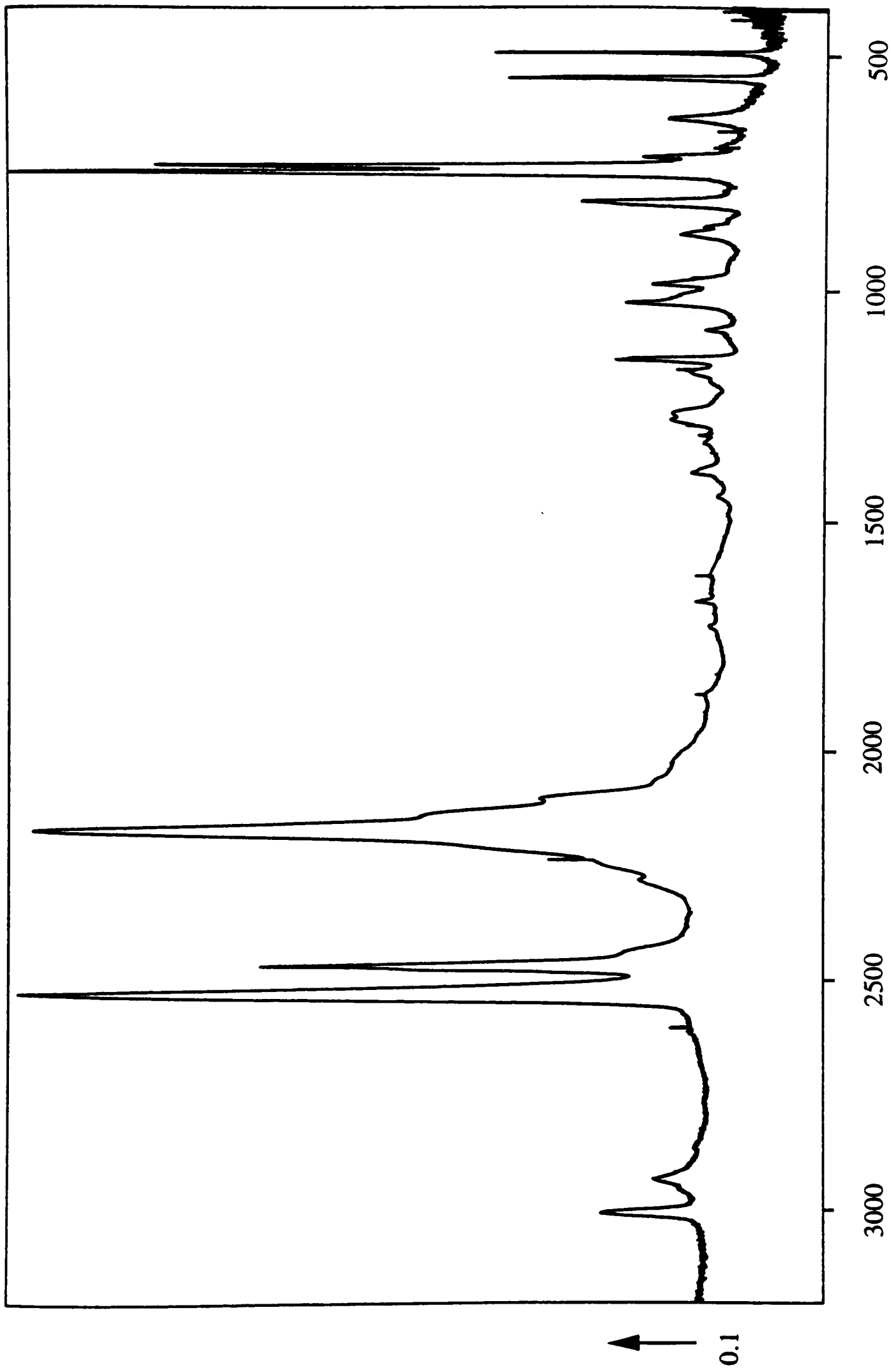

Figure 6.6 The infrared spectrum of dimethylindium octahydrotriborate isolated in a nitrogen matrix at 14 K.

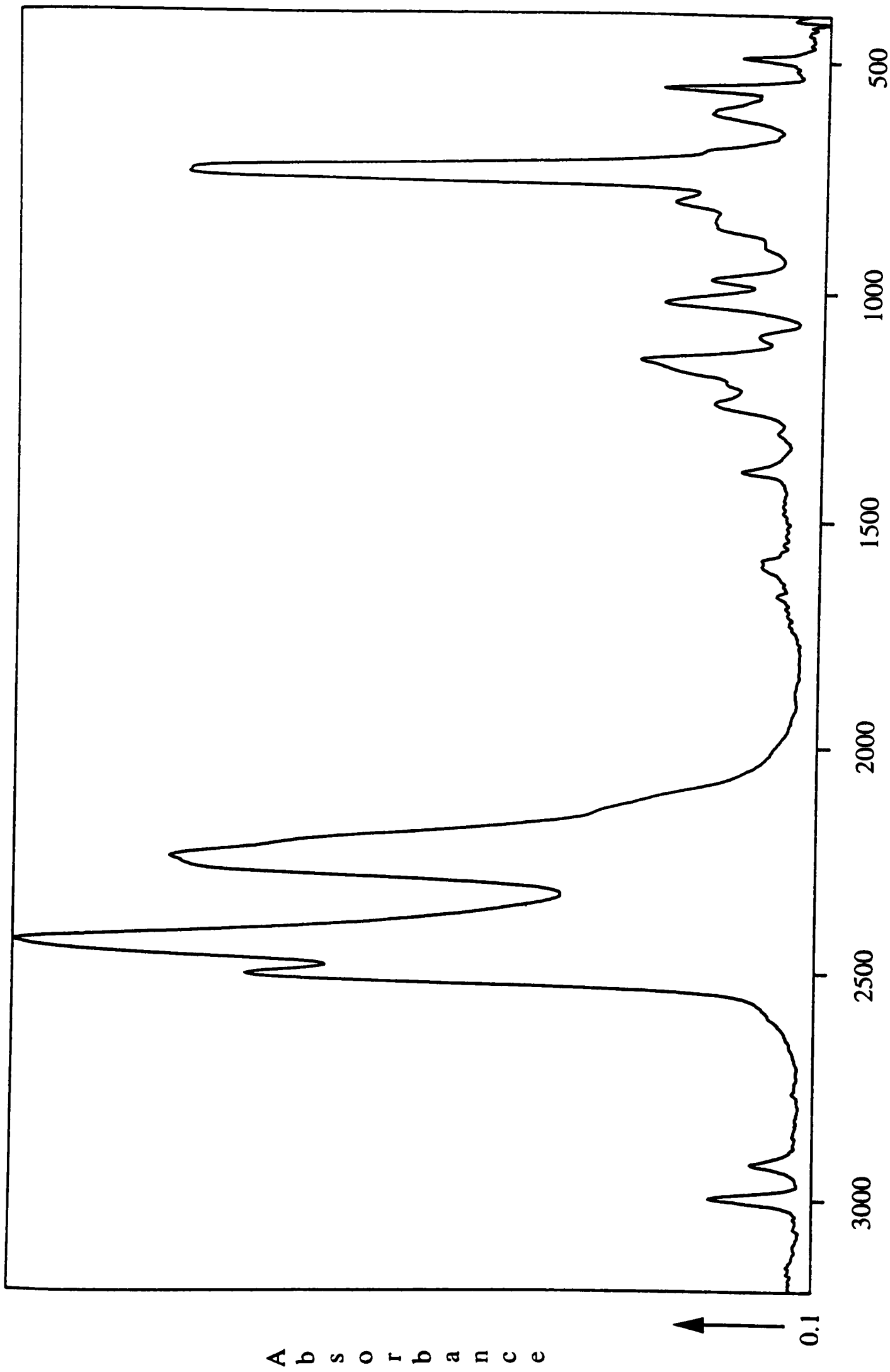

Figure 6.7 The infrared spectrum of an annealed solid film of dimethylindium octahydrotriborate at -196°C.

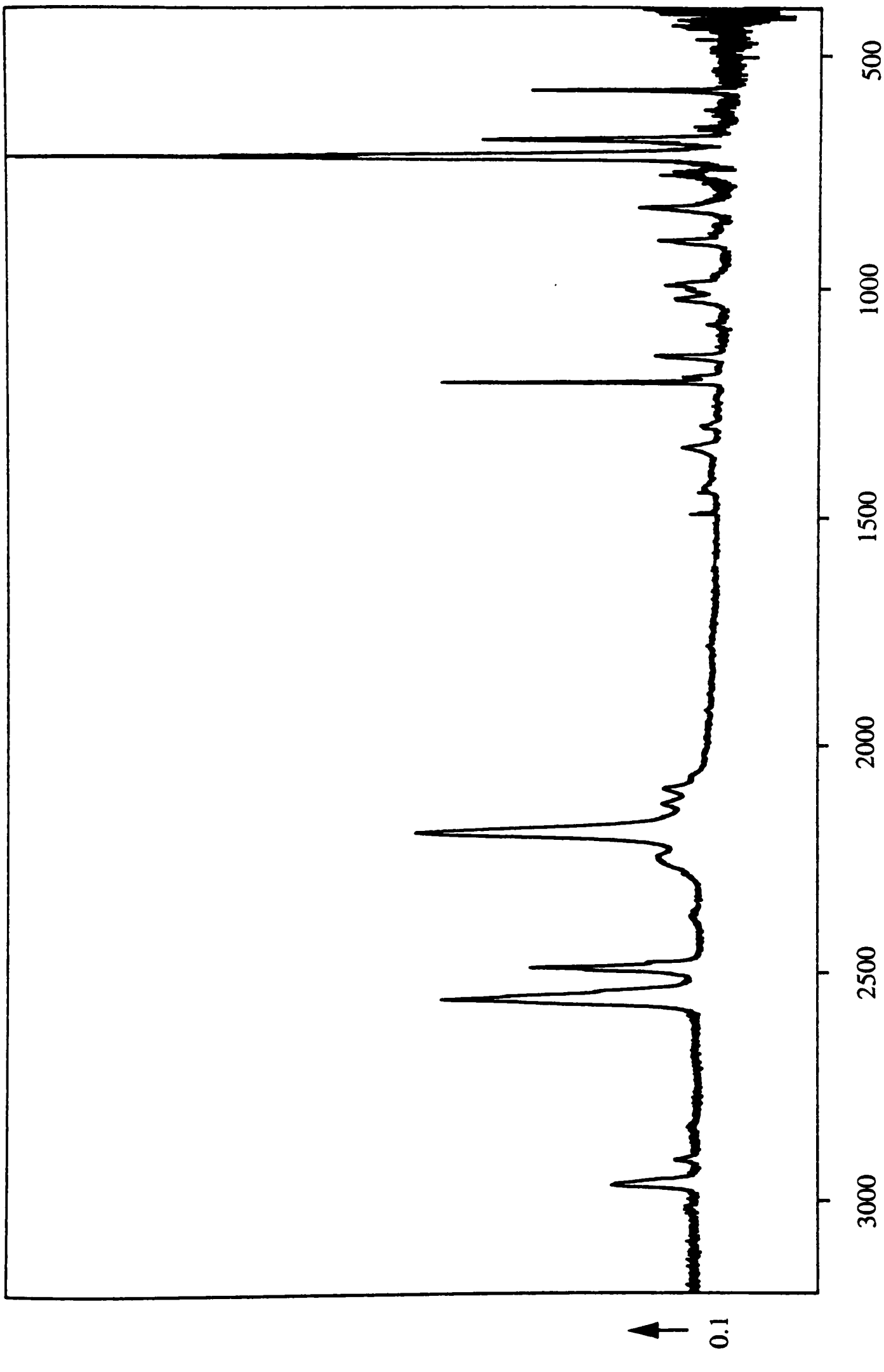

Figure 6.8 The infrared spectrum of dimethylaluminium octahydrotriborate isolated in a nitrogen matrix at 14 K.

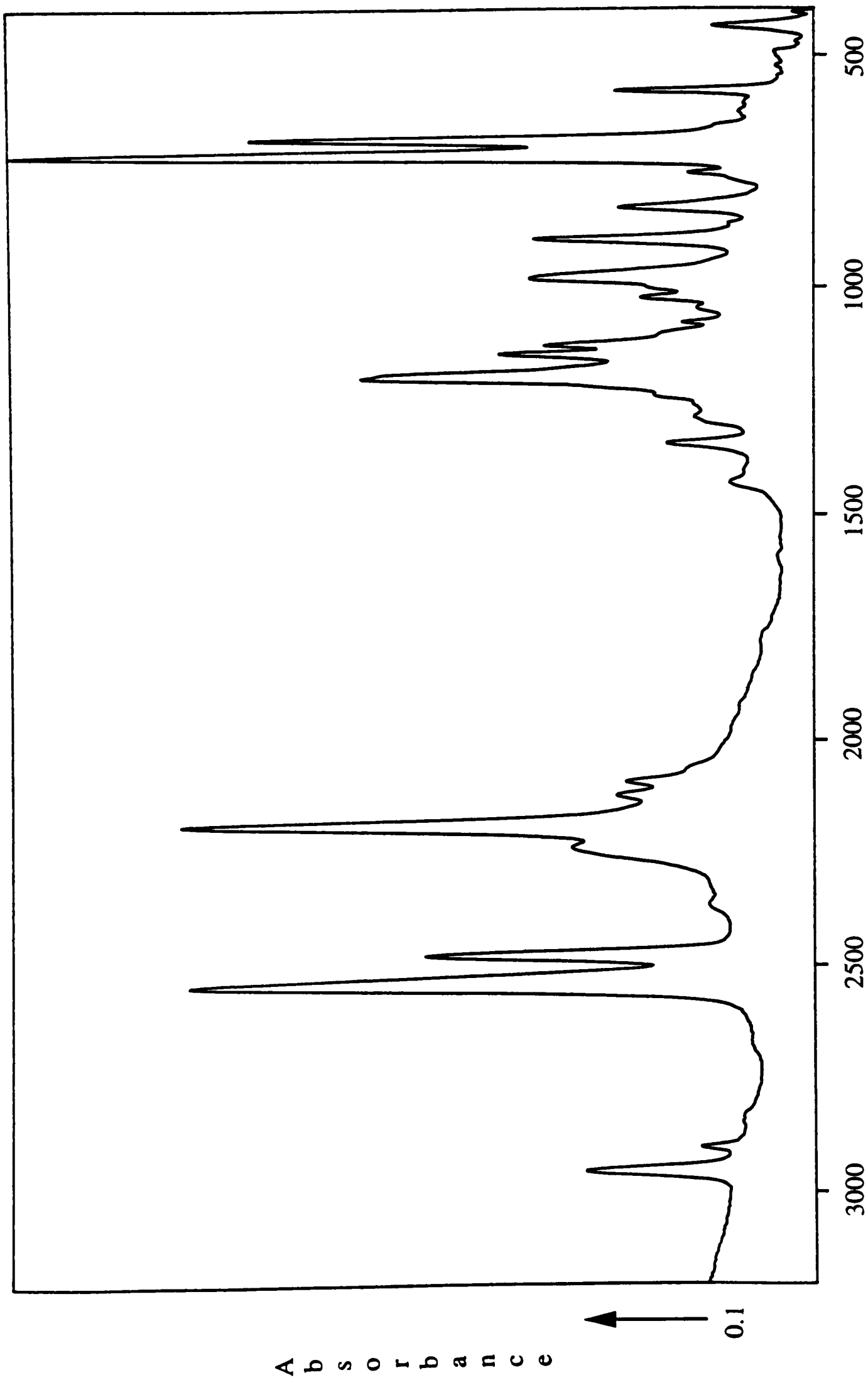

Figure 6.9 The infrared spectrum of an annealed solid film of dimethylaluminium octahydrotriborate at -196°C.

Table 6.4 The vibrational spectra of dimethylindium and dimethylaluminium octahydrotriborates.

$Me_2InB_3H_8$		$Me_2AlB_3H_8$[a]		Assignment[b]
matrix	solid	matrix	solid	
3005	2998	2965	2951	ν_a(C–H)
2955 2933	2924	2911	2901	ν_s(C–H)
2602				1313 + 1279
2528	2506	2567	2540	ν_a(B–H_t)
2466 2434	2434	2487	2475	ν_s(B–H_t)
2173 2138 2104	2268 2244 2205 2126	2190 2129 2096	2236 2187 2120 2091	ν(B–H_b)
1444 1394	1390	1435	1429	$\delta_a(CH_3)$
1313 1279 1265	1306 1242	1348 1301	1341 1285	ν(M–H_b) + out-of-phase δ(B–H)
1176	1198 1167	1205 1194	1200	$\delta_s(CH_3)$
1148	1146	1148	1146 1127	$\delta(BH_2)$
1088	1094	1080	1076	ρ(B–H)
1026 986	1020 970	1025 993	1022 982	$\delta(BH_2)$
881 865	851	899	897	BH_2 twisting
811	804	828	828	Bridge deformation
751 737	743	759	754	$\rho(CH_3)$

Table 6.4 (cont.) The vibrational spectra of dimethylindium and dimethylaluminium octahydrotriborates.

$Me_2InB_3H_8$		$Me_2AlB_3H_8$[a]		Assignment[b]
matrix	solid	matrix	solid	
717	693	717	718	$\rho(CH_3)$
635	612			$\rho(CH_3)$
551	559	683	683	$\nu_a(M–C)$
498	496	578	577	$\nu_s(M–C)$

[a] A provisional assignment of the bands in the infrared spectrum of gaseous $[Me_2AlB_3H_8]$ in the range 2000-3000 cm^{-1} was made by Borlin and Gaines (see reference 7). [b] Assignments made by reference to the vibrational spectra of compounds containing terminal Me_2M units (M = In or Al), *e.g.* $[Me_2InCl]_2$,[15] $[Me_3In]$,[42] $[Me_2InBH_4]$,[5] $[Me_2AlCl]_2$[15] and $[Me_3Al]_2$[43] and doubly hydrogen-bridged octahydrotriborate ligands, *e.g.* $[H_2GaB_3H_8]$[40] and $[B_4H_{10}]$.[17]

The infrared spectra of matrix-isolated [$Me_2InB_3H_8$] and [$Me_2AlB_3H_8$] each show a pattern of bands at high wavenumber characteristic of bidentate coordination of the B_3H_8 group.[7,17,40] The strong bands at 2528 (2567) and 2466 (2487) cm^{-1} {values for [$Me_2AlB_3H_8$] are given in parentheses} are identified as the antisymmetric and symmetric B–H_t stretching modes, respectively, while the B–H_b stretching modes give rise to one or more absorptions near 2173 (2190) cm^{-1}. Features assigned to the deformation, rocking and twisting modes of the terminal BH_2 group are to be found at 1148 (1148), 1026 (1025) and 986 (993), and 881 (899) cm^{-1}.

Of the methyl group vibrations, the symmetric deformation, $\delta_s(CH_3)$, at 1176 (1205) cm^{-1}, is much weaker in the spectrum of the indium compound than in that of its aluminium counterpart, whereas the methyl rocking mode, $\rho(CH_3)$, gives rise to the strongest band in the spectrum of both compounds. Finally, examination of the relative intensities of the bands attributed to the symmetric and antisymmetric In–C stretching vibrations allows an estimate of the C–In–C angle, θ, in matrix-isolated [$Me_2InB_3H_8$] to be made. Determination of the value for the ratio I_{as}/I_s from the measured infrared spectrum (1.93) and use of the approximate relationship[44]

$$I_{as} / I_s = \tan^2(\theta/2)\left\{\frac{m_M + 2m_{Me}\sin^2(\theta/2)}{m_M + 2m_{Me}\cos^2(\theta/2)}\right\}$$

(where *m* denotes the mass of the relevant unit)

yields an angle of 107°. A similar analysis for [$Me_2AlB_3H_8$] yields I_{as}/I_s = 2.08 and consequently an angle of 105°, compared with the value of 126.8° determined by electron diffraction. Such a discrepancy is not unduly surprising given the approximations implicit in this method.[45] However, despite such uncertainties, it appears that the angle determined for the indium compound is significantly smaller than that found in the solid [158.6(2)°]. Such narrowing of the C–In–C angle is consistent with the change from a solid structure featuring significant secondary In···H interactions and a degree of charge separation, $[Me_2In]^+[B_3H_8]^-$, to a more tightly bound molecular species in the vapour.

(b) Spectra of solid samples. At first glance, the infrared spectra of solid [$Me_2InB_3H_8$] and [$Me_2AlB_3H_8$] differ little from those of the matrix-isolated molecules, the principal changes being simply the broadening of bands by the increased intermolecular interactions in the pure solids. This implies that the molecular unit present in the vapour persists without major structural change in the solid.

The spectrum of solid [$Me_2InB_3H_8$] does, however, show two significant changes from that of the matrix-isolated species.

(i) The position of the broad band associated with the stretching of bridging B–H bonds moves to higher wavenumber (2173 to 2268 cm^{-1}).

(ii) The intensity of the band associated with the antisymmetric In–C stretching mode increases with respect to that of the symmetric stretching mode {$I_{as}/I_s = 4.3$ for the solid implying a value of θ in the order of 128° to be compared with a $I_{as}/I_s = 1.93$ for the matrix-isolated [$Me_2InB_3H_8$] molecule}.

These spectral changes are consistent with a solid phase structure incorporating weaker interactions between the indium centre and the bridging hydrogen atoms, and in which the C–In–C angle is significantly wider than in the gaseous molecule.

The changes in the spectra of [$Me_2AlB_3H_8$] accompanying the switch from the vapour to the solid phase are less marked, although here too the intensity ratio for the absorptions due to the antisymmetric and symmetric Al–C stretching modes ($I_{as}/I_s = 4.8$) implies an opening up of the C–Al–C angle in the solid. Clearly, further investigation, for example by X-ray crystallography, is required before any firm conclusions can be reached concerning the detailed structure of solid [$Me_2AlB_3H_8$].

6.5 Conclusions and Suggestions for Further Research

The viscous, slightly volatile liquid [$Me_2InB_3H_8$], a hitherto unknown compound, has been synthesized by the reaction between trimethylindium and tetraborane(10) at room temperature, and isolated by fractionation *in vacuo* in all-glass apparatus. Elemental

analysis and identification of the more volatile co-product as $[MeBH_2]_2$ enables the primary reaction to be formulated as

$$Me_3In + B_4H_{10} \longrightarrow Me_2InB_3H_8 + 1/2[MeBH_2]_2 \qquad (7)$$

The structure of this compound in the solid and vapour phases and in toluene solution has been investigated. The infrared spectra of the vapour isolated in a solid nitrogen matrix is consistent with a monomeric structure featuring bidentate ligation of the B_3H_8 group and *tetra*-coordinated indium, similar to the structures of gaseous $[Me_2AlB_3H_8]$ and $[Me_2GaB_3H_8]$ as determined by electron diffraction.[8] A single crystal grown by slow cooling of the liquid and maintained at 150 K was characterized by X-ray diffraction. The structure revealed evidence of a significant degree of charge separation $[Me_2In]^+[B_3H_8]^-$ and of some secondary interaction between the terminal hydrogen atoms of two B_3H_8 ligands and the indium centre of an adjacent $[Me_2InB_3H_8]$ unit. The ^1H and ^{11}B NMR spectra argue for weakened interaction between the dimethylindium and octahydrotriborate fragments and for a rapidly fluxional B_3H_8 unit when the compound is dissolved in toluene, the ^{11}B NMR spectrum at 40°C showing the nonet expected for coupling of each boron to eight equivalent protons.[37]

Given the success achieved in growing single crystals of $[Me_2InB_3H_8]$ suitable for X-ray diffraction and the dearth of information concerning the structures of $[Me_2AlB_3H_8]$ and $[Me_2GaB_3H_8]$ in the solid phase, there would clearly be merit in attempting to grow crystals of these two compounds using similar techniques. Structural parameters obtained from such studies may prove useful in view of the problems of extensive correlation encountered in the electron-diffraction study,[8] although there are clear signs of structural perturbation of the $[Me_2AlB_3H_8]$ molecule accompanying condensation. In the case of the aluminium compound, such studies are already under way.

Further investigation of the structure of gaseous $[Me_2InB_3H_8]$, notably by electron diffraction, could also prove to be rewarding, although given the relatively low vapour pressure of the compound and its tendency to decompose on heating to temperatures in

excess of 50°C, such experiments could be problematic. Measurements of the Raman spectra of matrix-isolated and solid $[Me_2InB_3H_8]$ would also be useful in providing a fuller basis for analysis of the vibrational properties of the compound.

Given the known reaction of dimethylaluminium chloride with $[^nBu_4N][B_3H_8]$ [reaction(9)],[7] the analogous reaction of methylaluminium dichloride with two equivalents

$$Me_2AlCl + [^nBu_4N][B_3H_8] \longrightarrow Me_2AlB_3H_8 + [^nBu_4N]Cl \qquad (9)$$

of $[^nBu_4N][B_3H_8]$ might be expected to proceed in accordance with reaction (10), yielding

$$MeAlCl_2 + 2[^nBu_4N][B_3H_8] \longrightarrow MeAl(B_3H_8)_2 + 2[^nBu_4N]Cl \qquad (10)$$

the hitherto unknown compound $[MeAl(B_3H_8)_2]$. Aluminium trichloride has been shown to react with $[^nBu_4N][B_3H_8]$ and the compound $[Al(B_3H_8)_3]$ may be one of the products, although side-reactions and difficulties preventing the reaction from proceeding to completion frustrated detailed analysis.[46]

The reaction of trimethylthallium with tetraborane(10) would also warrant investigation as a potential route to dimethylthallium octahydroborate, $[Me_2TlB_3H_8]$, which may be expected to come closest of all to the ionic formulation $[Me_2Tl]^+[B_3H_8]^-$.

References for Chapter 6

1. See, for example, A.J. Downs (ed.), *Chemistry of Aluminium, Gallium, Indium and Thallium*, Blackie, Glasgow, 1993.
2. D.G. Tuck, in *Comprehensive Organometallic Chemistry*, eds. G. Wilkinson, F.G.A. Stone and E.W. Abel, Vol. 1, Pergamon, Oxford, 1982, p. 683.
3. A.G. Avent, C. Eaborn, P.B. Hitchcock, J.D. Smith and A.C. Sullivan, *J. Chem. Soc., Chem. Commun.*, 1986, 988.
4. J.L. Atwood, D.C. Hrncir, R.D. Rogers and J.A.K. Howard, *J. Am. Chem. Soc.*, 1981, **103**, 6787.
5. C.R. Pulham and A.J. Downs, unpublished results.
6. A.J. Downs and P.D.P. Thomas, *J. Chem. Soc., Dalton Trans.*, 1978, 809; A.J. Downs and C.R. Pulham, *Adv. Inorg. Chem.*, 1994, **41**, 171.
7. J.J. Borlin and D.F. Gaines, *J. Am. Chem. Soc.*, 1972, **94**, 1367.
8. C.J. Dain, A.J. Downs and D.W.H. Rankin, *J. Chem. Soc., Dalton Trans.*, 1981, 2465.
9. See, for example, K. Wade and A.J. Bannister in *Comprehensive Inorganic Chemistry*, eds. A.F. Trotman-Dickenson, H.J. Emeléus and R.S. Nyholm, Vol. 1, Pergamon, Oxford, 1973, p. 1112.
10. I.M. Ward, Ph.D. Thesis, University of Leeds, 1975.
11. Chapter 4, this thesis; S. Aldridge, A.J. Blake, A.J. Downs and S. Parsons, *J. Chem. Soc., Chem. Commun.*, 1995, 1363.
12. F.M. Miller and D.M. Ritter, *Inorg. Chem.*, 1970, **9**, 1284.
13. N.N. Greenwood, B.S. Thomas and D.W. Waite, *J. Chem. Soc., Dalton Trans.*, 1975, 299.
14. N.N. Greenwood and J.A. Howard, *J. Chem. Soc., Dalton Trans.*, 1976, 177.
15. H.C. Clark and A.L. Pickard, *J. Organomet. Chem.*, 1967, **8**, 427.
16. W.J. Lehmann, C.O. Wilson, Jr., and I. Shapiro, *J. Chem. Phys.*, 1960, **33**, 590.

17. A.J. Dahl and R.C. Taylor, *Inorg. Chem.*, 1971, **10**, 2508.

18. J.B. Leach, C.B. Ungermann and T.P. Onak, *J. Magn. Resonance*, 1972, **6**, 74.

19. J.B. Leach, T.P. Onak, J. Spielman, R.R. Rietz, R. Schaeffer and L.G. Sneddon, *Inorg. Chem.*, 1970, **9**, 2170.

20. See, for example, E.A.V. Ebsworth, D.W.H. Rankin and S. Cradock, *Structural Methods in Inorganic Chemistry*, 2nd edn., Blackwell Scientific Publications, Oxford, 1991.

21. See, for example, T.J. Marks and J.R. Kolb, *Chem. Rev.*, 1977, **77**, 273.

22. Chapter 5, this thesis.

23. A. Almenningen, G. Gundersen and A. Haaland, *Acta Chem. Scand.*, 1968, **22**, 328.

24. J.C. Calabrese, D.F. Gaines, S.J. Hildebrandt and J.H. Morris, *J. Am. Chem. Soc.*, 1976, **98**, 5489.

25. S.J. Lippard and K.M. Melmed, *Inorg. Chem.*, 1969, **8**, 2755.

26. C.J. Dain, A.J. Downs, G.S. Laurenson and D.W.H. Rankin, *J. Chem. Soc., Dalton Trans.*, 1981, 472.

27. L. Pauling, *The Chemical Bond*, 3rd edn., Cornell University Press, New York, 1967, p. 148.

28. F.W.B. Einstein, M.M. Gilbert and D.G. Tuck, *J. Chem. Soc., Dalton Trans.*, 1973, 248.

29. H. Olapinski, J. Weidlein and H.D. Hausen, *J. Organomet. Chem.*, 1974, **64**, 193.

30. H.J. Widler, H.D. Hausen and J. Weidlein, *Z. Naturforsch.*, 1975, **30b**, 645.

31. C.R. Peters and C.R. Nordman, *J. Am. Chem. Soc.*, 1960, **82**, 5758.

32. H. Schmidbaur and D. Koth, *Naturwissenschaften*, 1976, **63**, 42.

33. J.S. Poland and D.G. Tuck, *J. Organomet. Chem.*, 1972, **42**, 315.

34. O.T. Beachley, Jr., S.-H.L. Chao, M.R. Churchill and R.F. See, *Organometallics*, 1992, **11**, 1486.

35. N. Muller and A.L. Otermat, *Inorg. Chem.*, 1963, **2**, 1075.

36. D.F. Gaines, J.L. Walsh, J.H. Morris and D.F. Hillenbrand, *Inorg. Chem.*, 1978, **17**, 1516.

37. H. Beall and C.H. Bushweller, *Chem. Rev.*, 1973, **73**, 465.

38. R.E. Williams, *J. Inorg. Nucl. Chem.*, 1961, **20**, 265.

39. G.E. Ryschkewitsch and K.C. Nainan, *Inorg. Synth.*, 1974, **15**, 111.

40. C.R. Pulham, A.J. Downs, D.W.H. Rankin and H.E. Robertson, *J. Chem. Soc., Dalton Trans.*, 1992, 1509.

41. See, for example, A.J. Downs and S.C. Peake in *Molecular Spectroscopy,* Chemical Society Specialist Periodical Reports, Vol. 1, 1973, Chapter 9; M.J. Almond and A.J. Downs, *Adv. Spectrosc.*, 1989, **17**, 1.

42. J.R. Hall, L.A. Woodward and E.A.V. Ebsworth, *Spectrochim. Acta*, 1964, **20**, 249.

43. G.E. Coates, M.L.H. Green and K. Wade, *Organometallic Compounds*, 3rd edn., Vol. 1, *The Main Group Elements*, Methuen, London, 1967.

44. See, for example, I.R. Beattie, J.S. Ogden and D.D. Price, *J. Chem. Soc., Dalton Trans.*, 1982, 505.

45. W.M.A. Smit, *J. Mol. Struct.*, 1973, **19**, 789.

46. L.A. Jones, D.Phil. Thesis, University of Oxford, 1993.

Appendix One
The Crystal Structure of Methylzinc Tetrahydroborate

Crystal data

Empirical formula	CH_7BZn
Crystal size (mm)	1.00 x 0.10 x 0.05
Crystal system	Trigonal
Space group	*R*3*c*
Unit cell dimensions	$a = 15.831(10)$ Å
	$b = 15.831(10)$ Å
	$c = 8.36(2)$ Å
Volume	1814(4) $Å^3$
Z	18
Formula Weight	95.25
Density (calc.)	1.569 g cm^{-3}
Absorption coefficient	5.837 mm^{-1}
F(000)	864

Data Collection

Diffractometer used	Stöe Stadi-4
Radiation used	Mo-Kα (λ = 0.71073 Å)
Temperature (K)	150
Monochromator	Highly orientated graphite crystal
θ range	2.57 to 22.52°
Scan type	ω - 2θ
Standard reflections	3 measured every 60 minutes

Index ranges	$-9 \leq h \leq 16, -16 \leq k \leq 8, -8 \leq l \leq 8$
Reflections collected	1693
Independent reflections	502 ($R_{int} = 0.0846$)
Absorption correction	Based on Ψ scan data ($T_{min} = 0.731$, $T_{max} = 0.938$)

Solution and Refinement

Refinement method	Full-matrix least-squares on F^2
Data/restraints/parameters	502/16/41
Goodness of fit	1.018
Final R indices [$I > 2\sigma(I)$]	$R = 7.20\%$, $wR = 17.47\%$
R indices (all data)	$R = 7.65\%$, $wR = 17.86\%$
Absolute structure parameter	0.2(2)
Largest difference peak	0.659 e Å^{-3}
Largest difference hole	-0.631 e Å^{-3}

Table A.1.1 Atomic coordinates (x 10^{-4}) and equivalent isotropic displacement parameters (Å^2 x 10^3).

	x	y	z	U(eq)[a]
Zn(1)	9444(1)	1807(1)	9337(1)	33(1)
C(1)	8872(11)	404(11)	9247(24)	41(4)
B(1)	9122(14)	2751(12)	11052(24)	37(4)

[a] U(eq) is defined as one third of the trace of the orthogonalized U_{ij} tensor.

Table A.1.2 Anisotropic displacement parameters.[a]

	U_{11}	U_{22}	U_{33}	U_{23}	U_{13}	U_{12}
Zn(1)	28(1)	25(1)	45(1)	0(1)	0(1)	13(1)
C(1)	32(9)	18(8)	70(12)	7(7)	10(9)	10(8)
B(1)	45(10)	27(9)	47(11)	5(8)	1(8)	24(9)

[a] The anisotropic displacement factor exponent takes the form :
$-2\pi(h^2a^{*2}U_{11} + ... + 2hka^*b^*U_{12})$

Table A.1.3 Hydrogen atom coordinates (x 10^{-4}) and isotropic displacement parameters (Å^2 x 10^3).

	x	y	z	U(eq)[a]
H(1A)	9208(56)	236(12)	8431(94)	49
H(1B)	8179(22)	104(12)	8984(138)	49
H(1C)	8940(74)	163(14)	10291(43)	49
H(1)	8626(54)	2275(68)	9752(87)	44
H(2)	9775(62)	2460(73)	11221(81)	44
H(3)	8582(62)	2610(35)	12341(86)	44
H(4)	9552(72)	3730(35)	10845(88)	44

[a] U(eq) is defined as one third of the trace of the orthogonalized U_{ij} tensor.

Appendix Two
Density Functional Theory Calculations for [MeZnBH4]

Table A.2.1 Atomic coordinates of the final geometry optimization.

Centre number	Atom	*x*	*y*	*z*
1	Dummy atom	0.000000	0.000000	0.000000
2	Zn	0.000000	0.000000	1.000000
3	B	2.148263	0.000000	1.000000
4	C	-1.944528	0.000000	1.035019
5	H	-2.342206	0.000000	0.017728
6	H	-2.323775	-0.885399	1.548905
7	H	-2.323775	0.885399	1.548905
8	H	1.436357	-1.054683	0.938788
9	H	1.436357	1.054683	0.938788
10	H	2.818552	0.000000	0.009445
11	H	2.689080	0.000000	2.068056

Table A.2.2 Harmonic frequencies (cm^{-1}), infrared intensities ($kM\ mol^{-1}$) and force constants ($mDyne\ Å^{-1}$).

ν	Symmetry type	Harmonic frequency	Infrared intensity	Force constant
1	a'	70.0331	9.5334	0.0056
2	a"	96.0555	2.0244	0.0066
3	a"	121.1677	6.8754	0.0196

Table A.2.2 (cont.) Harmonic frequencies (cm^{-1}), infrared intensities ($kM\ mol^{-1}$) and force constants (mDyne $Å^{-1}$).

ν	Symmetry type	Harmonic frequency	Infrared intensity	Force constant
4	a'	246.9462	1.1138	0.0485
5	a'	444.8142	36.4363	0.4348
6	a'	579.5720	37.0195	0.9342
7	a"	646.4146	8.3777	0.2827
8	a'	712.2180	37.8279	0.3627
9	a"	741.0123	22.8266	0.3827
10	a'	971.1036	0.5583	0.6582
11	a'	1136.5465	52.7863	0.8665
12	a"	1179.3603	0.5213	0.8279
13	a'	1229.1518	0.1566	1.0754
14	a'	1299.7691	10.7375	1.0685
15	a"	1437.3627	113.8172	1.2565
16	a"	1453.6695	1.9086	1.3143
17	a'	1455.7117	2.4698	1.3178
18	a"	2073.6805	98.2724	2.7671
19	a'	2074.8307	288.2835	2.6106
20	a'	2535.6378	71.4018	3.9787
21	a'	2610.8498	92.7417	4.5081
22	a'	3032.7358	12.3631	5.5912
23	a'	3109.8198	9.2394	6.2695
24	a"	3114.2201	9.7691	6.2910

Table A.2.3 Distance matrix (Å)

	1	2	3	4	5
1	0.000000				
2	1.000000	0.000000			
3	2.369606	2.148263	0.000000		
4	2.202829	1.944844	4.092941	0.000000	
5	2.342273	2.539840	4.596648	1.092259	0.000000
6	2.929670	2.546597	4.591770	1.091714	1.768835
7	2.929670	2.546597	4.591770	1.091714	1.768835
8	2.014150	1.783038	1.273976	3.542881	4.029671
9	2.014150	1.783038	1.273976	3.542881	4.029671
10	2.818568	2.987547	1.196030	4.872242	5.160765
11	3.392345	2.893423	1.196030	2.747367	5.433018

	6	7	8	9	10
6	0.000000				
7	1.770799	0.000000			
8	3.813069	4.274898	0.000000		
9	4.274898	3.813069	2.109365	0.000000	
10	5.440349	5.440349	1.971420	1.971420	0.000000
11	5.116851	5.116851	1.989200	1.989200	2.062678

	11
11	0.000000

Appendix Three

Ab Initio Calculations for $[MeZnBH_4]_2$

Table A.3.1 Atomic coordinates of the final geometry optimization at the HF/tzp level.

Centre number	Atom	*x*	*y*	*z*
1	Dummy atom	0.000000	0.000000	0.000000
2	Dummy atom	0.000000	0.000000	1.098800
3	Zn	1.706110	0.000000	0.482192
4	Zn	-1.706110	0.000000	0.482192
5	C	3.459956	0.000000	1.432701
6	C	-3.459956	0.000000	1.432701
7	H	4.284451	0.000000	0.724899
8	H	-4.284451	0.000000	0.724899
9	H	3.564439	0.879027	2.061880
10	H	3.564439	-0.879027	2.061880
11	H	-3.564439	0.879027	2.061880
12	H	-3.564439	-0.879027	2.061880
13	H	-0.982656	1.325821	-0.659174
14	H	0.982656	1.325821	-0.659174
15	H	-0.982656	-1.325821	-0.659174
16	H	0.982656	-1.325821	-0.659174
17	B	0.000000	1.715072	0.000000
18	B	0.000000	-1.715072	0.000000
19	H	0.000000	1.214773	1.136851
20	H	0.000000	-1.214773	1.136851
21	H	0.000000	2.902995	0.092809
22	H	0.000000	-2.902995	0.092809

Table A.3.2 Harmonic frequencies (cm^{-1}), infrared intensities ($kM\ mol^{-1}$) and force constants ($mDyne\ Å^{-1}$).

ν	Symmetry type	Harmonic frequency	Infrared intensity	Force constant
1	a_2	14.9264	0.0000	0.0001
2	b_1	19.8298	0.0157	0.0002
3	a_2	43.5327	0.0000	0.0040
4	a_1	61.9205	0.7369	0.0073
5	b_2	84.6891	5.8015	0.0198
6	b_1	95.4437	7.4904	0.0137
7	a_1	111.3753	5.3132	0.0652
8	a_2	146.1148	0.0000	0.0262
9	a_1	179.6833	20.7773	0.0753
10	b_1	223.7472	41.7577	0.0455
11	b_2	240.0588	86.4488	0.0896
12	a_2	293.8901	0.0000	0.0574
13	b_1	370.8976	77.3886	0.1797
14	a_1	410.4739	2.8391	0.3467
15	b_2	418.6231	37.5859	0.1146
16	a_2	505.9144	0.0000	0.1591
17	a_1	519.4961	1.6081	0.1763
18	b_2	546.4200	27.8954	0.4904
19	a_1	557.4821	10.7666	0.7294
20	b_2	576.8191	36.8101	0.2352
21	a_1	714.1727	52.9749	0.3585
22	b_2	718.5648	22.2710	0.3599
23	a_2	726.0304	0.0000	0.3728
24	b_1	732.0919	112.3476	0.3807
25	b_1	1115.4078	57.8763	0.8463
26	a_1	1138.4745	5.5798	0.8581
27	a_2	1205.4848	0.0000	1.0349
28	b_2	1222.3931	138.4712	1.0444
29	b_1	1282.0761	1.7247	1.0156
30	a_1	1308.2059	7.0418	1.0649

Table A.3.2 (cont.) Harmonic frequencies (cm^{-1}), infrared intensities (kM mol^{-1}) and force constants (mDyne $Å^{-1}$).

ν	Symmetry type	Harmonic frequency	Infrared intensity	Force constant
31	b_2	1318.4195	0.5897	1.2379
32	a_1	1319.1080	1.8867	1.2336
33	b_1	1436.1388	114.1417	1.3185
34	a_1	1453.5794	46.9865	1.3383
35	a_2	1472.1319	0.0000	1.2997
36	b_2	1501.5295	157.3992	1.3503
37	a_2	1571.8561	0.0000	1.5390
38	b_2	1572.0863	0.1960	1.5408
39	a_1	1572.1370	0.9536	1.5411
40	b_1	1572.2382	1.0160	1.5392
41	a_2	2223.4398	0.0000	3.1581
42	b_1	2261.9851	17.0086	3.3029
43	b_1	2302.7337	407.5940	3.1988
44	b_2	2304.7187	1107.9843	3.3977
45	a_1	2316.9217	16.2854	3.2966
46	a_1	2351.7240	196.6594	3.4944
47	b_1	2684.2573	262.1147	4.6324
48	a_1	2685.5173	0.0334	4.6368
49	b_2	3145.3347	59.3783	6.0182
50	a_1	3145.5726	11.0415	6.0190
51	b_2	3215.5180	9.1899	6.6991
52	a_1	3215.5874	40.3098	6.6992
53	a_2	3221.7855	0.0000	6.7316
54	b_1	3221.8416	47.8059	6.7317

Appendix Four
The Crystal Structure of $[(MeZn)_2B_3H_7]_2$

Crystal data

Empirical formula	$C_2H_{13}B_3Zn_2$
Crystal size (mm)	0.65 x 0.15 x 0.11
Crystal system	Monoclinic
Space group	*P*2(1)/*c*
Unit cell dimensions	a = 10.038(2) Å
	b = 7.814(2) Å
	c = 11.076(2) Å
	β = 111.92(3)°
Volume	806.0(3) $Å^3$
Z	2
Formula Weight	400.59
Density (calc.)	1.651 g cm^{-3}
Absorption coefficient	5.842 mm^{-1}
F(000)	400

Data Collection

Diffractometer used	Stöe Stadi-4
Radiation used	Mo-Kα (λ = 0.71073 Å)
Temperature (K)	150
Monochromator	Highly orientated graphite crystal
θ range	3.28 to 24.95°
Scan type	ω - 2θ

Standard reflections	3 measured every 60 minutes
Index ranges	$-11 \leq h \leq 10, -8 \leq k \leq 8, 0 \leq l \leq 11$
Reflections collected	1735
Independent reflections	1077 ($R_{int} = 0.1081$)

Solution and Refinement

Refinement method	Full-matrix least-squares on F^2
Data/restraints/parameters	1069/13/70
Goodness of fit	1.016
Final R indices [$I > 2\sigma(I)$]	$R = 6.23\%$, $wR = 12.11\%$
R indices (all data)	$R = 13.36\%$, $wR = 15.61\%$
Extinction coefficient	0.0015(11)
Largest difference peak	1.064 e Å^{-3}
Largest difference hole	-0.616 e Å^{-3}

Table A.4.1 Atomic coordinates (x 10^{-4}) and equivalent isotropic displacement parameters (Å^2 x 10^3).

	x	y	z	U(eq)[a]
Zn(1)	-766(2)	1688(2)	9875(2)	31(1)
Zn(2)	3429(2)	2942(2)	10660(2)	43(1)
C(1)	-1759(17)	3856(16)	9785(15)	38(4)
C(2)	5249(17)	3838(24)	11786(16)	59(5)
B(1)	2336(19)	1490(24)	8852(18)	44(5)
B(2)	1679(17)	1154(20)	10105(17)	31(4)
B(3)	516(18)	686(22)	8507(14)	30(4)

[a] U(eq) is defined as one third of the trace of the orthogonalized U_{ij} tensor.

Table A.4.2 Anisotropic displacement parameters.[a]

	U_{11}	U_{22}	U_{33}	U_{23}	U_{13}	U_{12}
Zn(1)	36(1)	24(1)	34(1)	1(1)	14(1)	2(1)
Zn(2)	38(1)	50(1)	38(1)	-4(1)	11(1)	-18(1)
C(1)	40(10)	26(8)	44(11)	-11(8)	11(9)	1(8)
C(2)	44(11)	65(12)	54(13)	1(10)	1(10)	-1(10)
B(1)	30(10)	47(11)	44(12)	-3(10)	1(9)	-16(10)
B(2)	28(10)	29(9)	33(11)	13(8)	8(8)	-6(8)
B(3)	38(11)	35(10)	21(10)	0(8)	15(9)	2(9)

[a] The anisotropic displacement factor exponent takes the form :
$-2\pi(h^2a^{*2}U_{11} + ... + 2hka^*b^*U_{12})$

Table A.4.3 Hydrogen atom coordinates (x 10^{-4}) and isotropic displacement parameters ($Å^2$ x 10^3).

	x	y	z	U(eq)[a]
H(1A)	-2726(36)	3637(17)	9771(82)	46
H(1B)	-1828(81)	4467(51)	8991(45)	46
H(1C)	-1222(50)	4554(47)	10546(45)	46
H(2A)	5124(25)	4484(106)	12495(54)	71
H(2B)	5632(51)	4596(101)	11288(26)	71
H(2C)	5920(36)	2891(25)	12149(77)	71
H(1)	2664(21)	3003(41)	8785(18)	53
H(2)	3403(31)	418(33)	8723(18)	53
H(3)	1306(28)	1150(25)	8018(26)	53
H(4)	2139(19)	-33(24)	10798(20)	37

Table A.4.3 (cont.) Hydrogen atom coordinates (x 10^{-4}) and isotropic displacement parameters (Å^2 x 10^3).

	x	*y*	*z*	*U*(eq)[a]
H(5)	1199(18)	2325(27)	10497(18)	37
H(6)	-531(24)	1604(26)	8286(15)	36
H(13)	79(19)	-846(29)	8454(15)	36

[a] *U*(eq) is defined as one third of the trace of the orthogonalized U_{ij} tensor.

Appendix Five
Ab Initio Calculations for [MeZnB$_3$H$_8$] and the MeZnB$_3$H$_7$ Ligand

Table A.5.1 Atomic coordinates of the final geometry optimization for [MeZnB$_3$H$_8$] at the HF/tzp level.

Centre number	Atom	*x*	*y*	*z*
1	Zn	0.0000	0.0000	0.0000
2	Dummy atom	2.2339	0.0000	0.0000
3	B	2.2339	0.9147	0.0000
4	B	2.2339	-0.9147	0.0000
5	B	2.7359	0.0000	1.5543
6	H	2.6830	1.3759	1.0818
7	H	2.6830	-1.3759	1.0818
8	H	2.9309	1.3404	-0.8757
9	H	1.1259	1.5002	0.0108
10	H	1.1259	-1.5002	0.0108
11	H	2.9309	-1.3404	-0.8757
12	H	1.8790	0.0000	2.4011
13	H	3.8792	0.0000	1.9102
14	C	-2.0031	0.0000	0.0151
15	H	-2.3801	0.0000	1.0429
16	H	-2.3975	0.8869	-0.4895
17	H	-2.3975	-0.8869	-0.4895

Table A.5.2 Atomic coordinates of the final geometry optimization for [$MeZnB_3H_8$] at the HF/svp level.

Centre number	Atom	*x*	*y*	*z*
1	Zn	0.0000	0.0000	0.0000
2	B	2.1680	0.9112	0.0000
3	B	2.1680	-0.9112	0.0000
4	B	2.9921	0.0000	1.4014
5	H	2.7870	1.3656	0.9847
6	H	2.7870	-1.3656	0.9847
7	H	2.6849	1.3498	-0.9754
8	H	1.0861	1.4893	0.2368
9	H	1.0861	-1.4893	0.2368
10	H	2.6849	-1.3498	-0.9754
11	H	2.3859	0.0000	2.4282
12	H	4.1795	0.0000	1.4378
13	C	-1.9824	0.0000	-0.1599
14	H	-2.4471	0.0000	0.8223
15	H	-2.3330	0.8790	-0.6921
16	H	-2.3330	-0.8790	-0.6921

Table A.5.3 Atomic coordinates of the final geometry optimization for the $MeZnB_3H_7$ ligand at the HF/tzp level.

Centre number	Atom	*x*	*y*	*z*
1	B	1.5565	0.0000	0.0000
2	B	0.0000	0.9209	0.0000
3	B	0.0000	-0.9209	0.0000
4	Zn	2.0161	2.0914	0.0000
5	H	-0.9409	0.0000	0.0000
6	H	2.2480	0.0000	-1.0143

Table A.5.3 (cont.) Atomic coordinates of the final geometry optimization for the MeZnB$_3$H$_7$ ligand at the HF/tzp level.

Centre number	Atom	*x*	*y*	*z*
7	H	2.2480	0.0000	1.0143
8	H	-0.2543	1.5190	-1.0138
9	H	-0.2543	1.5190	1.0138
10	H	-0.2543	-1.5190	-1.0138
11	H	-0.2543	-1.5190	1.0138
12	C	2.9060	3.8692	0.0000
13	H	3.9875	3.7676	0.0000
14	H	2.6250	-4.4440	0.8777
15	H	2.6250	-4.4440	-0.8777

Appendix Six

The Crystal Structure of Dimethylaluminium Tetrahydroborate

Crystal data

Empirical formula	$C_2H_{10}AlB$
Crystal size (mm)	0.80 x 0.40 x 0.40
Crystal system	Orthorhombic
Space group	*Pbca*
Unit cell dimensions	a = 10.029(6) Å
	b = 12.401(4) Å
	c = 17.947(9) Å
Volume	2232(2) Å^3
Z	8
Formula Weight	71.90
Density (calc.)	0.856 g cm^{-3}
Absorption coefficient	0.190 mm^{-1}
F(000)	640

Data Collection

Diffractometer used	Stöe Stadi-4
Radiation used	Mo-Kα (λ = 0.71073 Å)
Temperature (K)	150
Monochromator	Highly orientated graphite crystal
θ range	2.85 to 24.97^o
Scan type	ω - 2θ
Standard reflections	3 measured every 60 minutes

Index ranges	$0 \leq h \leq 10, 0 \leq k \leq 14, 0 \leq l \leq 21$
Reflections collected	1746
Independent reflections	1699 ($R_{int} = 0.1332$)
Absorption correction	Based on Ψ scan data ($T_{min} = 0.66$, $T_{max} = 0.744$)

Solution and Refinement

Refinement method	Full-matrix least-squares on F^2
Data/restraints/parameters	1685/0/102
Goodness of fit	1.020
Final R indices [$I > 2\sigma(I)$]	$R = 6.33\%$, $wR = 13.53\%$
R indices (all data)	$R = 11.18\%$, $wR = 16.77\%$
Extinction coefficient	0.0001(11)
Largest difference peak	0.287 e Å^{-3}
Largest difference hole	-0.297 e Å^{-3}

Table A.6.1 Atomic coordinates (x 10^{-4}) and equivalent isotropic displacement parameters (Å^2 x 10^3).

	x	y	z	U(eq)[a]
Al(1)	1478(1)	2159(1)	3713(1)	31(1)
Al(2)	-1872(1)	4915(1)	3475(1)	31(1)
B(1)	1846(7)	1028(4)	2635(3)	42(1)
B(2)	-295(6)	3449(5)	3707(4)	45(1)
C(11)	3120(5)	2957(4)	3641(3)	49(1)
C(12)	834(6)	1212(4)	4480(3)	51(1)
C(21)	-1396(5)	5885(4)	4271(3)	54(2)
C(22)	-3482(4)	4128(4)	3256(3)	41(1)

[a] U(eq) is defined as one third of the trace of the orthogonalized U_{ij} tensor.

Table A.6.2 Anisotropic displacement parameters.[a]

	U_{11}	U_{22}	U_{33}	U_{23}	U_{13}	U_{12}
Al(1)	33(1)	27(1)	33(1)	2(1)	-2(1)	-3(1)
Al(2)	29(1)	33(1)	32(1)	-2(1)	3(1)	1(1)
B(1)	49(4)	37(3)	39(3)	-6(2)	11(3)	-7(3)
B(2)	37(3)	51(4)	46(3)	5(3)	4(3)	6(3)
C(11)	41(3)	39(3)	66(4)	-1(2)	-3(3)	-6(2)
C(12)	66(4)	40(3)	48(3)	5(2)	5(3)	-5(3)
C(21)	64(4)	43(3)	56(3)	-4(2)	-14(3)	-10(3)
C(22)	36(3)	43(3)	44(3)	5(2)	-7(2)	-1(2)

[a] The anisotropic displacement factor exponent takes the form :
$-2\pi(h^2a^{*2}U_{11} + ... + 2hka^*b^*U_{12})$

Table A.6.3 Hydrogen atom coordinates (x 10^{-4}) and isotropic displacement parameters (Å^2 x 10^3).

	x	y	z	U(eq)[a]
H(11)	2356(50)	792(35)	3163(25)	56
H(12)	1165(44)	1771(37)	2751(23)	56
H(13)	1168(46)	337(36)	2420(25)	56
H(14)	2526(51)	1243(33)	2203(24)	56
H(11A)	3212(16)	3427(19)	4077(9)	73
H(11B)	3110(14)	3397(19)	3187(9)	73
H(11C)	3872(5)	2454(4)	3622(18)	73
H(12A)	93(22)	781(19)	4286(6)	77
H(12B)	526(31)	1641(4)	4905(8)	77

Table A.6.3 (cont.) Hydrogen atom coordinates (x 10^{-4}) and isotropic displacement parameters (Å^2 x 10^3).

	x	*y*	*z*	*U*(eq)[a]
H(12C)	1556(10)	732(18)	4640(13)	77
H(21)	-258(46)	2713(39)	3372(26)	60
H(22)	-318(48)	4055(38)	3333(26)	60
H(23)	-1174(49)	3435(37)	4054(26)	60
H(24)	557(49)	3626(36)	4083(26)	60
H(21A)	-544(17)	6235(20)	4155(9)	82
H(21B)	-1310(33)	5479(6)	4737(5)	82
H(21C)	-2090(17)	6435(17)	4327(13)	82
H(22A)	-3324(9)	3642(17)	2834(11)	62
H(22B)	-4195(9)	4636(4)	3129(16)	62
H(22C)	-3746(16)	3705(13)	3693(6)	62

[a] *U*(eq) is defined as one third of the trace of the orthogonalized U_{ij} tensor.

Appendix Seven

The Crystal Structure of the α phase of Aluminium *Tris*(tetrahydroborate)

Crystal data

Empirical formula	$H_{12}AlB_3$
Crystal size (mm)	unknown
Crystal system	Monoclinic
Space group	*C2/c*
Unit cell dimensions	$a = 21.917(4)$ Å
	$b = 5.986(1)$ Å
	$c = 21.787(4)$ Å
	$\beta = 111.90(3)^o$
Volume	2652.1(9) $Å^3$
Z	16
Formula Weight	71.51
Density (calc.)	0.716 g cm^{-3}
Absorption coefficient	0.155 mm^{-1}
F(000)	640

Data Collection

Diffractometer used	Stöe Stadi-4
Radiation used	Mo-Kα (λ = 0.71073 Å)
Temperature (K)	150
Monochromator	Highly orientated graphite crystal
θ range	3.33 to 20.00°

Scan type	ω - 2θ
Standard reflections	3 measured every 60 minutes
Index ranges	$-17 \leq h \leq 26$, $-6 \leq k \leq 0$, $-19 \leq l \leq 23$
Reflections collected	1477
Independent reflections	1233 (R_{int} = 0.2356)

Solution and Refinement

Refinement method	Full-matrix least-squares on F^2
Data/restraints/parameters	1054/36/150
Goodness of fit	0.990
Final R indices [$I > 2\sigma(I)$]	R = 8.56%, wR = 12.92%
R indices (all data)	R = 24.64%, wR = 20.65%
Largest difference peak	0.240 e Å^{-3}
Largest difference hole	-0.310 e Å^{-3}

Table A.7.1 Atomic coordinates (x 10^{-4}) and equivalent isotropic displacement parameters (Å^2 x 10^3).

	x	y	z	U(eq)[a]
Al	3795(2)	5901(7)	8361(2)	33(1)
B(1)	3206(8)	3030(32)	8238(9)	56(5)
B(2)	3866(8)	7476(31)	7508(8)	53(5)
B(3)	4304(8)	7262(30)	9308(8)	54(5)
Al'	3669(2)	1094(7)	5953(2)	34(1)
B(1')	3646(9)	-1707(32)	5379(9)	68(6)
B(2')	3782(7)	2233(28)	6014(7)	43(4)
B(3')	4570(7)	2721(31)	6453(8)	53(5)

[a] U(eq) is defined as one third of the trace of the orthogonalized U_{ij} tensor.

Table A.7.2 Anisotropic displacement parameters.[a]

	U_{11}	U_{22}	U_{33}	U_{23}	U_{13}	U_{12}
Al	30(2)	34(3)	35(3)	0(3)	13(2)	7(3)
B(1)	53(11)	64(13)	51(12)	-8(10)	21(10)	-6(10)
B(2)	57(11)	57(13)	34(10)	22(11)	5(9)	30(10)
B(3)	71(12)	57(12)	34(10)	-7(10)	20(9)	3(10)
Al'	33(2)	42(3)	25(2)	8(3)	9(2)	-1(3)
B(1')	79(15)	60(15)	67(13)	-13(11)	28(12)	-22(11)
B(2')	32(8)	42(11)	47(11)	4(9)	8(8)	4(8)
B(3')	24(8)	66(13)	56(11)	-2(10)	-1(8)	2(10)

[a] The anisotropic displacement factor exponent takes the form :
$-2\pi(h^2a^{*2}U_{11} + ... + 2hka^*b^*U_{12})$

Table A.7.3 Hydrogen atom coordinates (x 10^{-4}) and isotropic displacement parameters (Å^2 x 10^3).

	x	y	z	U(eq)[a]
H(1A)	3757(22)	2993(63)	8366(46)	45(8)
H(1B)	3013(20)	4814(73)	8173(47)	45(8)
H(1C)	3027(47)	2727(183)	8584(38)	70(11)
H(1D)	3046(48)	2249(160)	7796(31)	70(11)
H(2A)	4169(33)	5987(109)	7778(30)	45(8)
H(2B)	3557(34)	8117(91)	7806(28)	45(8)
H(2C)	3642(41)	7334(182)	7017(23)	70(11)
H(2D)	4205(40)	8679(136)	7655(48)	70(11)
H(3A)	3763(23)	7595(127)	9008(25)	45(8)

Table A.7.3 (cont.) Hydrogen atom coordinates (x 10^{-4}) and isotropic displacement parameters (Å^2 x 10^3).

	x	*y*	*z*	*U*(eq)[a]
H(3B)	4537(21)	6121(126)	9038(25)	45(8)
H(3C)	4382(48)	6799(171)	9768(28)	70(11)
H(3D)	4517(46)	8796(97)	9376(49)	70(11)

[a] *U*(eq) is defined as one third of the trace of the orthogonalized U_{ij} tensor.

Appendix Eight

The Crystal Structure of the β phase of Aluminium *Tris*(tetrahydroborate)

Crystal data

Empirical formula	$H_{12}AlB_3$
Crystal size (mm)	unknown
Crystal system	Orthorhombic
Space group	*Pna*2(1)
Unit cell dimensions	a = 18.021(3) Å
	b = 6.138(2) Å
	c = 6.199(1) Å
Volume	685.7(3) $Å^3$
Z	4
Formula Weight	71.51
Density (calc.)	0.693 g cm^{-3}
Absorption coefficient	0.150 mm^{-1}
F(000)	160

Data Collection

Diffractometer used	Stöe Stadi-4
Radiation used	Mo-Kα (λ = 0.71073 Å)
Temperature (K)	195
Monochromator	Highly orientated graphite crystal
θ range	3.51 to 22.47°
Scan type	ω - 2θ

Standard reflections	3 measured every 60 minutes
Index ranges	$-1 \leq h \leq 19$, $-1 \leq k \leq 6$, $-1 \leq l \leq 6$
Reflections collected	767
Independent reflections	598 (R_{int} = 0.0341)

Solution and Refinement

Refinement method	Full-matrix least-squares on F^2
Data/restraints/parameters	598/37/76
Goodness of fit	1.154
Final R indices [$I > 2\sigma(I)$]	R = 4.23%, wR = 7.09%
R indices (all data)	R = 6.59%, wR = 8.30%
Absolute structure parameter	0.4(7)
Extinction coefficient	0.074(8)
Largest difference peak	0.172 e Å^{-3}
Largest difference hole	-0.146 e Å^{-3}

Table A.8.1 Atomic coordinates (x 10^{-4}) and equivalent isotropic displacement parameters (Å^2 x 10^3).

	x	y	z	U(eq)[a]
Al	8677(1)	1592(2)	2035(1)	65(1)
B(1)	7780(5)	40(15)	503(15)	98(3)
B(2)	9113(5)	203(17)	4915(15)	103(3)
B(3)	9122(5)	4460(15)	629(21)	113(3)

[a] U(eq) is defined as one third of the trace of the orthogonalized U_{ij} tensor.

Table A.8.2 Anisotropic displacement parameters.[a]

	U_{11}	U_{22}	U_{33}	U_{23}	U_{13}	U_{12}
Al	66(1)	64(1)	65(1)	-6(2)	3(2)	4(1)
B(1)	103(6)	107(6)	85(6)	18(6)	-20(6)	-24(5)
B(2)	98(6)	125(7)	85(6)	-5(6)	-15(5)	31(6)
B(3)	102(6)	88(5)	149(10)	-6(7)	18(7)	1(5)

[a] The anisotropic displacement factor exponent takes the form :
$-2\pi(h^2a^{*2}U_{11} + ... + 2hka^*b^*U_{12})$

Table A.8.3 Hydrogen atom coordinates (x 10^{-4}) and isotropic displacement parameters (Å^2 x 10^3).

	x	y	z	U(eq)[a]
H(1A)	8398(18)	-226(76)	215(80)	96(7)
H(1B)	7744(19)	1321(67)	1790(80)	96(7)
H(1C)	7576(29)	-1277(74)	1214(93)	151(12)
H(1D)	7568(32)	678(98)	-833(79)	151(12)
H(2A)	9320(23)	-107(69)	3238(56)	96(7)
H(2B)	8667(21)	1458(67)	4853(78)	96(7)
H(2C)	9534(26)	912(84)	5627(93)	151(12)
H(2D)	8887(32)	-1166(69)	5420(101)	151(12)
H(3A)	8716(23)	4427(57)	1979(76)	96(7)
H(3B)	9300(25)	2732(53)	287(83)	96(7)
H(3C)	9542(26)	5038(87)	1428(94)	151(12)
H(3D)	8912(33)	4975(103)	-728(77)	151(12)

[a] U(eq) is defined as one third of the trace of the orthogonalized U_{ij} tensor.

Appendix Nine
The Crystal Structure of Dimethylindium Octahydrotriborate

Crystal data

Empirical formula	$C_2H_{14}B_3In$
Crystal size (mm)	unknown
Crystal system	Monoclinic
Space group	*P*2(1)/*c*
Unit cell dimensions	*a* = 11.718(4) Å
	b = 9.578(4) Å
	c = 14.994(5) Å
	β = 105.31(4)
Volume	1623.1(10) $Å^3$
Z	8
Formula Weight	185.38
Density (calc.)	1.517 g cm^{-3}
Absorption coefficient	2.800 mm^{-1}
F(000)	720

Data Collection

Diffractometer used	Stöe Stadi-4
Radiation used	Mo-Kα (λ = 0.71073 Å)
Temperature (K)	150
Monochromator	Highly orientated graphite crystal
θ range	2.55 to 25.04°
Scan type	ω - 2θ

Standard reflections	3 measured every 60 minutes
Index ranges	$-13 \leq h \leq 13, 0 \leq k \leq 11, 0 \leq l \leq 17$
Reflections collected	3179
Independent reflections	2850 (R_{int} = 0.0314)

Solution and Refinement

Refinement method	Full-matrix least-squares on F^2
Data/restraints/parameters	2841/0/178
Goodness of fit	1.039
Final R indices [$I > 2\sigma(I)$]	R = 2.85%, wR = 6.39%
R indices (all data)	R = 4.43%, wR = 7.56%
Extinction coefficient	0.0020(2)
Largest difference peak	0.794 e Å^{-3}
Largest difference hole	-0.531 e Å^{-3}

Table A.9.1 Atomic coordinates (x 10^{-4}) and equivalent isotropic displacement parameters (Å^2 x 10^3).

	x	y	z	U(eq)[a]
In(1A)	9133(1)	7232(1)	7953(1)	28(1)
C(1A)	7698(4)	8574(5)	7400(3)	38(1)
C(2A)	10422(4)	6148(5)	8957(3)	31(1)
B(1A)	10234(5)	6901(6)	6507(4)	30(1)
B(2A)	9193(5)	5529(5)	6448(4)	26(1)
B(3A)	9070(6)	6679(7)	5470(4)	44(2)
In(1B)	6650(1)	2326(1)	8046(1)	28(1)
C(1B)	6733(5)	2718(6)	6682(3)	41(1)

Table A.9.1 (cont.) Atomic coordinates (x 10^{-4}) and equivalent isotropic displacement parameters (Å^2 x 10^3).

	x	*y*	*z*	*U*(eq)[a]
C(2B)	6605(5)	1132(5)	9217(3)	43(1)
B(1B)	7157(5)	4998(6)	8669(4)	31(1)
B(2B)	5603(5)	4830(6)	8270(4)	32(1)
B(3B)	6246(5)	5458(6)	9432(5)	45(2)

[a] *U*(eq) is defined as one third of the trace of the orthogonalized U_{ij} tensor.

Table A.9.2 Anisotropic displacement parameters.[a]

	U_{11}	U_{22}	U_{33}	U_{23}	U_{13}	U_{12}
In(1A)	29(1)	24(1)	31(1)	1(1)	10(1)	3(1)
C(1A)	36(3)	30(3)	47(3)	1(2)	10(2)	4(2)
C(2A)	37(3)	31(3)	27(2)	1(2)	10(2)	2(2)
B(1A)	32(3)	29(3)	32(3)	1(2)	15(2)	-9(2)
B(2A)	31(3)	21(3)	26(3)	2(2)	8(2)	3(2)
B(3A)	58(4)	41(4)	31(3)	5(3)	6(3)	-3(3)
In(1B)	31(3)	30(3)	25(3)	1(1)	8(1)	-1(1)
C(1B)	49(3)	52(3)	24(2)	4(2)	13(2)	-5(3)
C(2B)	67(4)	39(3)	27(3)	9(2)	16(3)	1(3)
B(1B)	30(3)	29(3)	24(3)	-3(2)	7(2)	-2(2)
B(2B)	23(3)	38(3)	35(3)	0(3)	6(2)	8(2)
B(3B)	30(3)	63(4)	41(4)	-13(3)	10(3)	8(3)

[a] The anisotropic displacement factor exponent takes the form :
$-2\pi(h^2a^{*2}U_{11} + ... + 2hka^*b^*U_{12})$

Table A.9.3 Hydrogen atom coordinates (x 10^{-4}) and isotropic displacement parameters ($Å^2$ x 10^3).

	x	*y*	*z*	*U*(eq)[a]
H(1A1)	7172(15)	8142(16)	6851(13)	57
H(1A2)	7994(4)	9463(13)	7227(21)	57
H(1A3)	7261(17)	8741(27)	7864(8)	57
H(2A1)	11045(14)	6798(8)	9271(15)	47
H(2A2)	10766(20)	5409(21)	8658(4)	47
H(2A3)	10054(7)	5734(27)	9411(12)	47
H(1A)	10227(34)	7770(40)	7000(26)	15(10)
H(2A)	11106(40)	6473(47)	6667(28)	31(12)
H(3A)	8517(35)	5630(45)	6922(27)	26(11)
H(4A)	9665(34)	4536(33)	6554(26)	18(10)
H(5A)	8438(51)	7325(53)	5355(37)	48(16)
H(6A)	9281(44)	6246(65)	4825(35)	53(15)
H(13A)	10202(53)	7451(56)	5852(44)	66(19)
H(23A)	8505(47)	5556(59)	5752(36)	61(17)

[a] *U*(eq) is defined as one third of the trace of the orthogonalized U_{ij} tensor.